



Durham E-Theses

The intensity of cosmic ray muons deep underground

Pattison, J. B. N.

How to cite:

Pattison, J. B. N. (1965) *The intensity of cosmic ray muons deep underground*, Durham theses, Durham University. Available at Durham E-Theses Online: <http://etheses.dur.ac.uk/8821/>

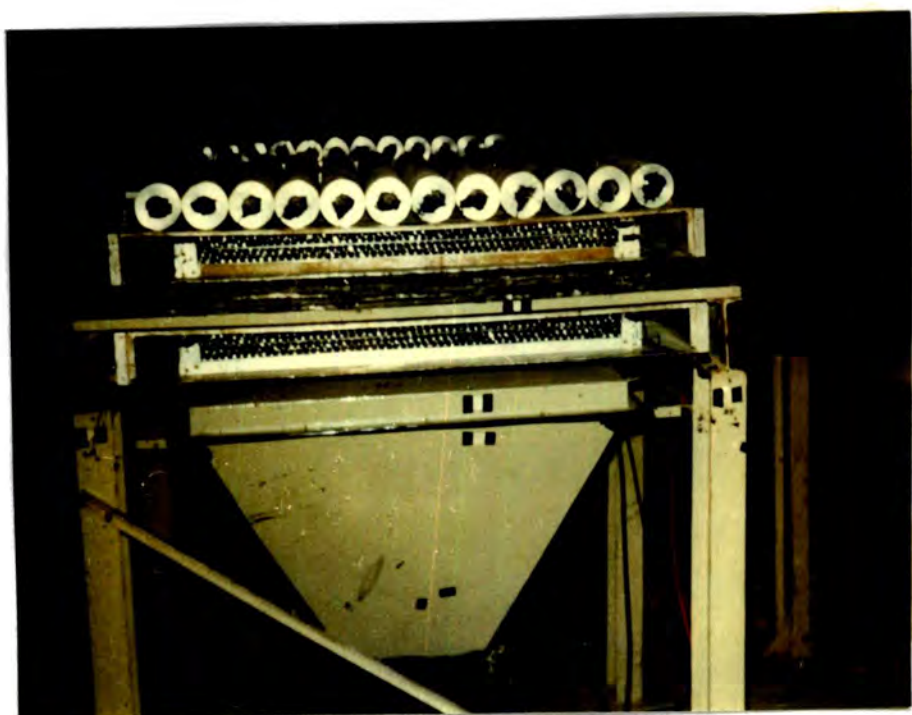
Use policy

The full-text may be used and/or reproduced, and given to third parties in any format or medium, without prior permission or charge, for personal research or study, educational, or not-for-profit purposes provided that:

- a full bibliographic reference is made to the original source
- a [link](#) is made to the metadata record in Durham E-Theses
- the full-text is not changed in any way

The full-text must not be sold in any format or medium without the formal permission of the copyright holders.

Please consult the [full Durham E-Theses policy](#) for further details.



Frontispiece: One of the telescopes in position at 4463 ft. below surface in the Kolar Gold Fields.

THE INTENSITY OF COSMIC RAY MUONS
DEEP UNDERGROUND

By

J.B.M. Pattison, M.Sc.

A thesis submitted to the University of Durham, in
application for the degree of Doctor of Philosophy

December, 1965.



C O N T E N T S .

	<u>Page.</u>
Abstract.	(i)
Preface.	(iii)
Chapter 1. Introduction.	1
1.1 Introduction to Cosmic Rays.	1
1.2 The Underground Component.	3
1.3 Studies of Cosmic Ray Neutrinos.	7
1.4 The Tata-Institute, Bombay, India - Osaka City University, Japan, - Durham University, U.K. - Collaboration.	9
Chapter 2. The Experimental Arrangement for Zenith Angular and Vertical Intensity Studies.	12
2.1 Description of the Apparatus	12
2.2 The Electronic Circuits.	14
2.3 The Plastic Scintillators.	16
2.4 The Neon Flash Tubes.	19
2.5 Description of the Mines.	20
2.6 The Experimental Arrangement	22
2.7 Alignment of the Apparatus.	23
2.8 Operation of the Apparatus.	23
Chapter 3. The Experimental Data.	25
3.1 Operation of the Telescopes	25
3.2 The Measuring Technique.	25
3.3 The Telescope Acceptance Functions.	27
Chapter 4. The Angular Distribution of Muons Underground.	30
4.1 Derivation of the Exponent, n.	30
4.2 Corrections for "noise".	30
4.3 The Theoretical Value of n as a function of Depth.	32
4.4 Measurements of n by other Workers.	35
4.4.1 The Range of Depth to be considered.	35
4.4.2 Barnóthy & Forró (1937-1948)	36
4.4.3 Randall & Hazen (1951,1958)	36
4.4.4 Bollinger (1950-1951)	37
4.4.5 Barrett et al (1952)	38

<u>Contents (Contd.)</u>	<u>Page.</u>
Chapter 5. The Variation of Vertical Intensity with Depth. ...	41
5.1 The Measured Vertical Intensity.	41
5.2 Measurements of Underground Vertical Intensities by Other Workers. ...	42
5.2.1 Barton (1961) ...	42
5.2.2 Miyake et al (1962-3) ...	44
5.2.3 Kitamura et al (1964) ...	45
5.2.4 Castagnoli et al (1964-5).	46
5.2.5 Barton & Stockel (1965)...	47a
5.3 The Best Estimate of the Intensity Vs. Depth Relation.	48
Chapter 6. Interpretation of Results on Single Muons. ...	50
6.1 Propagation of Cosmic Rays Underground. ...	50
6.1.1 Energy Losses due to Ionization & Excitation..	51
6.1.2 Energy Losses due to Direct Pair Production...	54
6.1.3 Energy Losses due to Bremsstrahlung. ...	55
6.1.4 Energy Losses due to Nuclear Interactions. ...	56
6.1.5 The Total Theoretical Rate of Energy Loss. ...	57
6.2 Fluctuations in Energy Losses...	58
6.3 The Angular Distribution of Particles Underground. ...	59
6.4 Implications of the Best Estimate Underground Spectrum....	61
6.4.1 The Sea-Level Energy Spectrum. ...	62
6.5 The Intensity Depth Spectrum ...	62
6.6 The Sea-Level Energy Spectrum...	69
6.7 The K/ π Ratio. ...	73
Chapter 7. The Distribution in Arrival Times of Cosmic Rays far Underground. ...	76
7.1 Introduction. ...	76
7.2 The Experiment of Cowan et al (1964). ...	76
7.3 The Present Experiment. ...	80

<u>Contents (Contd.)</u>		<u>Page.</u>
Chapter 8.	Electromagnetic Interactions....	83
8.1	Introduction.	83
8.2	Classification of Events.	83
8.3	Interpretation of the Electro- magnetic interactions.	84
8.4	Extrapolation to very great depths.	86
8.5	Muons accompanied by Electron Showers.	87
Chapter 9.	Multiple Penetrating Particles..	90
9.1	Introduction.	90
9.2	The Present Experiment.	91
9.2.1	MPP's at 816 m.w.e.	92
9.2.2	MPP's at 1812 m.w.e.	92
9.2.3	MPP's at 4110 m.w.e.	96
9.3	Origin of Particle Bundles.	97
9.4	Comparison with other Workers...	100
Chapter 10.	Neutrino Experiments and Muon Intensities at the Greatest Depths.	101
10.1	Introduction.	101
10.2	The Apparatus.	102
10.3	The Experimental Results.	108
10.4	The Vertical Intensity of Atmos- pheric Muons at 7600 m.w.e....	112
10.5	The South African Neutrino Experiment.	113
10.6	The Experiment of Miyake et al (1962-3) at 8400 m.w.e.	119
10.7	The Experiment of Barton (1961) at 5050 m.w.e.	120
10.8	Conclusion: The Variation of I_V and n at Great Depths.	120
Chapter 11.	Conclusions.	123
Acknowledgments.		
Appendix.		
References.		

A B S T R A C T

The vertical intensity, I_v , and exponent of the angular distribution, n , (where $I_\theta = I_v \cos^n \theta$), of muons underground have been measured using simple telescopes comprising plastic scintillators, geiger counters and neon flash tubes at depths of 816, 1812 and 4110 m.w.e. in the Kolar Gold Fields, India. The observed values of n are 1.92 ± 0.33 , 3.26 ± 0.10 and 5.33 ± 0.50 respectively, and those of I_v are $(2.29 \pm 0.09)10^{-6}$, $(1.98 \pm 0.05)10^{-7}$ and $(4.47 \pm 0.34)10^{-9} \text{ cm}^{-2} \text{ sr}^{-1} \text{ sec}^{-1}$.

These results have been compared with the results of other workers and the intensity-depth relation of Osborne et al (1964). The agreement is quite good at 816 and 4110 m.w.e. but the observed intensity is higher by ~30% at 1812 m.w.e. The integral sea-level muon intensities have been inferred from the range-energy relation, allowing for fluctuations in energy losses. From comparison with γ - ray cascade data it is shown the K/π ratio is sensibly constant at ~30% over the range of primary energy $10^3 - 10^6$ GeV.

No significant non-Poissonian contribution to the distribution of time intervals between the arrival of

successive events underground was noted indicating that the phenomenon of bursts of particles at short time intervals reported by Cowan et al (1964) has not been observed in the present experiment.

The probability of electromagnetic interactions of muons in rock and lead was found to increase (with increasing depth) demonstrating the growing importance of energy losses by bremsstrahlung and direct pair production.

Analysis of multiple penetrating particle events shows that they can be attributed to the production of muons (via pions) in extensive air showers, and to the nuclear interaction of muons in rock.

Several neutrino induced muons and atmospheric muons have been detected in a new experiment, still in operation, at 7600 m.w.e. The vertical intensity of muons has been derived from the latter and compared with that inferred from the South African neutrino experiment at 8500 m.w.e.

Finally, a best estimate of the intensity depth relation is given.

P R E F A C E .

This thesis describes the work done by the author, a member of the Cosmic Radiation Group of the Physics Department in the University of Durham, in the Kolar Gold Fields, India, under the supervision of Professor A.W. Wolfendale.

Together with colleagues from the Tata Institute of Fundamental Research, Bombay, where he was a Visiting Member, the author was responsible for the installation and operation of apparatus detecting cosmic ray muons penetrating the earth's crust in the Kolar Gold Field, India, until relieved by a colleague from Durham University in October 1964.

The apparatus was operated at three depths (816, 1812 and 4110 m.w.e.) underground. The scanning of events was carried out by the technical staff of the University of Durham Physics Department under the supervision of Professor A.W. Wolfendale (during the author's absence in India) and the author after his return. Much of the early analysis and interpretation was the responsibility of the author, and later assistance was given by Mr. D.R. Creed.

The experimental results were presented in the form of two papers at the 9th International Conference on Cosmic Rays, London (September 1965) and an extended paper has been accepted for publication in the Proceedings of the Physical Society (London).

The author has also assisted in the design of the apparatus for the "neutrino" experiment. He has taken part in the installation, maintenance and analysis of events of this experiment during part of 1965. He is responsible for the derivation of the vertical intensity of muons at the depth of operation together with that at 8500 m.w.e., the depth where the Case-Witwatersrand "neutrino" experiment is located in the East Rand Proprietary Mines, Johannesburg. Details of the first results from the neutrino experiment have been published in Physics Letters (Achar et al 1965 b,c) and were also presented at the 9th International Conference on Cosmic Rays, London (September 1965). The composite intensity-depth spectrum given in this thesis is the responsibility of the author.

CHAPTER 1.

INTRODUCTION.

1.1. Introduction to Cosmic Rays.

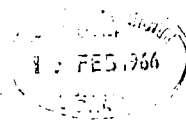
It has been known for some time that the primary flux of the cosmic radiation over a wide energy range consists of 85-88% hydrogen nuclei (i.e. protons), ~ 10% helium nuclei (α -particles) and 1 or 2% of nuclei having atomic number, Z , greater than 2. The primary radiation is almost isotropic, small anisotropies being present only at low energies (≤ 20 GeV) and due to the effect of the earth's magnetic field and some solar effects.

The source of the energetic cosmic ray particles is not known with certainty. That the majority do not come from the sun can be seen from a short calculation. For a particle having charge Ze and energy E eV passing through a magnetic field H gauss, the radius of curvature, ρ , of the particle's orbit is given by the following relation :

$$E/Z = 300 H \rho.$$

If the solar field $H = 10^{-5}$ gauss, and an orbit of radius 10^{15} cm. (equal to twice the distance of Pluto, the outermost planet) is considered, then:

$$E/Z = 3 \times 10^{12} \text{ eV.}$$



Since even for quite a high value of Z , the corresponding energy is many orders of magnitude lower than the most energetic primary particle detected to date ($\sim 10^{20} \text{ eV}$), it is generally accepted that the more energetic primaries are of galactic than solar origin and indeed at the highest energies ($> 10^{18} \text{ eV}$), there is some evidence that there may also be a contribution from outside the galaxy.

On entering the earth's atmosphere the primary cosmic rays interact with the nuclei of oxygen and nitrogen and produce secondary particles of various types. The most abundant secondaries are π -mesons (pions), but significant numbers of K-mesons, nucleons (protons and neutrons) and baryons (Λ , Σ , & Ξ hyperons) are also produced.

The majority of these secondary particles are unstable, decaying with characteristic lifetimes. A study of their decay modes shows that the most common charged particle surviving to sea-level is the μ -meson (muon) which is responsible for about 70% of the intensity. The remaining charged particles at sea-level are electrons, together with a minute contamination ($\lesssim 1\%$) of protons and pions.

It is with the muon component at sea-level and underground that the work described in this thesis is concerned.

1.2. The Underground Component.

As the cosmic rays pass into the earth the electrons lose energy very rapidly through bremsstrahlung, and the protons and pions are lost by nuclear interactions. At depths greater than about 10 metres all the sea-level electrons and nuclear active particles have been absorbed, leaving only the muonic or "hard" component together with a small equilibrium electromagnetic component of electrons and γ -quanta.

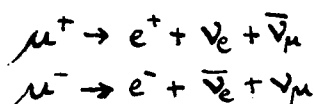
The muon is a member of the lepton class and has the following properties :

(i) Charge: the muon can exist with either positive or negative charge equal in magnitude to that of the electron;

(ii) Mass: $(206.767 \pm 0.002)m_e$, where m_e is the electron mass. (Since mass and energy are inter-convertible, the muon is often quoted as having 'mass' 105.7 MeV);

(iii) Spin: $1/2$, the muon is a fermion obeying Fermi-Dirac statistics;

(iv) Lifetime: the muon decays to an electron and two neutrinos with a lifetime $(2.212 \pm 0.001)10^{-6}$ sec., the exact nature of the decay products depending on the sign of the charge, viz.



$$\pi^+ \rightarrow \mu^+ + \nu_\mu$$

$$K^+ \rightarrow \mu^+ + \nu_\mu \quad (58\%, K_{\mu 2})$$

$$\rightarrow \pi^+ + \pi^0 \quad (26\%, K_{\pi 2})$$

$$\rightarrow \pi^+ + \pi^+ + \pi^- \quad (6\%, K_{\pi 3})$$

$$\rightarrow \pi^+ + \pi^0 + \pi^0 \quad (2\%, K_{\pi 3})$$

$$\rightarrow \mu^+ + \pi^0 + \nu_\mu \quad (4\%, K_{\mu 3})$$

$$K_1^0 \rightarrow \pi^+ + \pi^- \quad (34.5\%)$$

$$K_2^0 \rightarrow \pi^+ + \mu^- + \bar{\nu}_\mu \quad \left. \vphantom{K_2^0} \right\} (16\%)$$

$$\rightarrow \pi^- + \mu^+ + \nu_\mu \quad \left. \vphantom{K_2^0} \right\}$$

$$\rightarrow \pi^+ + e^- + \bar{\nu}_e \quad \left. \vphantom{K_2^0} \right\} (17\%)$$

$$\rightarrow \pi^- + e^+ + \nu_e \quad \left. \vphantom{K_2^0} \right\}$$

$$\rightarrow \pi^+ + \pi^- + \pi^0 \quad (6.5\%)$$

$$\rightarrow \pi^+ + \pi^- \quad (0.2\%)$$

The anti-particles π^- , K^- , \bar{K}_1^0 , \bar{K}_2^0 decay in similar modes to the particles π^+ , K^+ , K_1^0 , K_2^0 respectively, with the appropriate anti-particles as decay products.

Table 1.1 Meson decay schemes giving rise to muons.

where $\nu_e, \bar{\nu}_e$ represent the electron neutrino and anti-neutrino, and $\nu_\mu, \bar{\nu}_\mu$ are the muon neutrino and anti-neutrino respectively; (cf. section 1.3).

(v) Origin: the most important sources of muons are the decay of charged pions and the decay of K-mesons directly to muons or via pion decay (Table 1.1). The contribution to muon production from baryon decay via pion decay is small;

(vi) Interactions: since the muon is a member of the lepton class it interacts weakly with matter, the cross-section for star production being typically $10^{-29} \text{ cm}^2/\text{nucleon}$.

The early experiments below the earth's surface were conducted under water and it is customary to quote depths from the surface in units of "metres of water equivalent" (m.w.e.) where one metre of water equivalent is equal to 100 gm.cm^{-2} . Thus the vertical depth of the atmosphere is 10.30 m.w.e. (1030 gm.cm^{-2}).

Comparison of measurements made on the intensity of the underground component as a function of depth with the sea-level energy spectrum can yield information on the rate of energy loss of muons, this being about 2MeV/gm.cm^{-2} for fast particles. This is one of the reasons for observations being made on the intensity and angular distribution of cosmic rays deep underground. If the

relationship between the range in rock and sea-level energy is assumed, it is possible to extend the sea-level energy spectrum to energies (or, more strictly, momenta) higher than can be measured by conventional magnet spectrographs.

The highest momentum which can be detected by a magnet spectrograph depends on two factors: the strength of the magnetic field and the distance separating the detectors on either side of the magnet. For example, the Durham horizontal solid iron magnet spectrograph was operated at about 16 Kilogauss with two arrays of neon flash tubes separated by a distance of 1.5 metre on each side of the magnet (Pattison, 1963). Even by the most refined measuring technique the maximum detectable momentum was only 370 GeV/c. This spectrograph has recently been modified by inserting a second solid iron magnet and extending the separation between the arrays of flash tubes to about 3 metres on each side of the magnets. For improved track location a further array of flash tubes has been introduced between the magnets. The modified spectrograph has a maximum detectable momentum in the region of 2000 GeV/c. However, by increasing the length of the spectrograph, the solid angle of acceptance is necessarily reduced, and 2000 GeV/c probably represents the practical upper limit for the next decade.

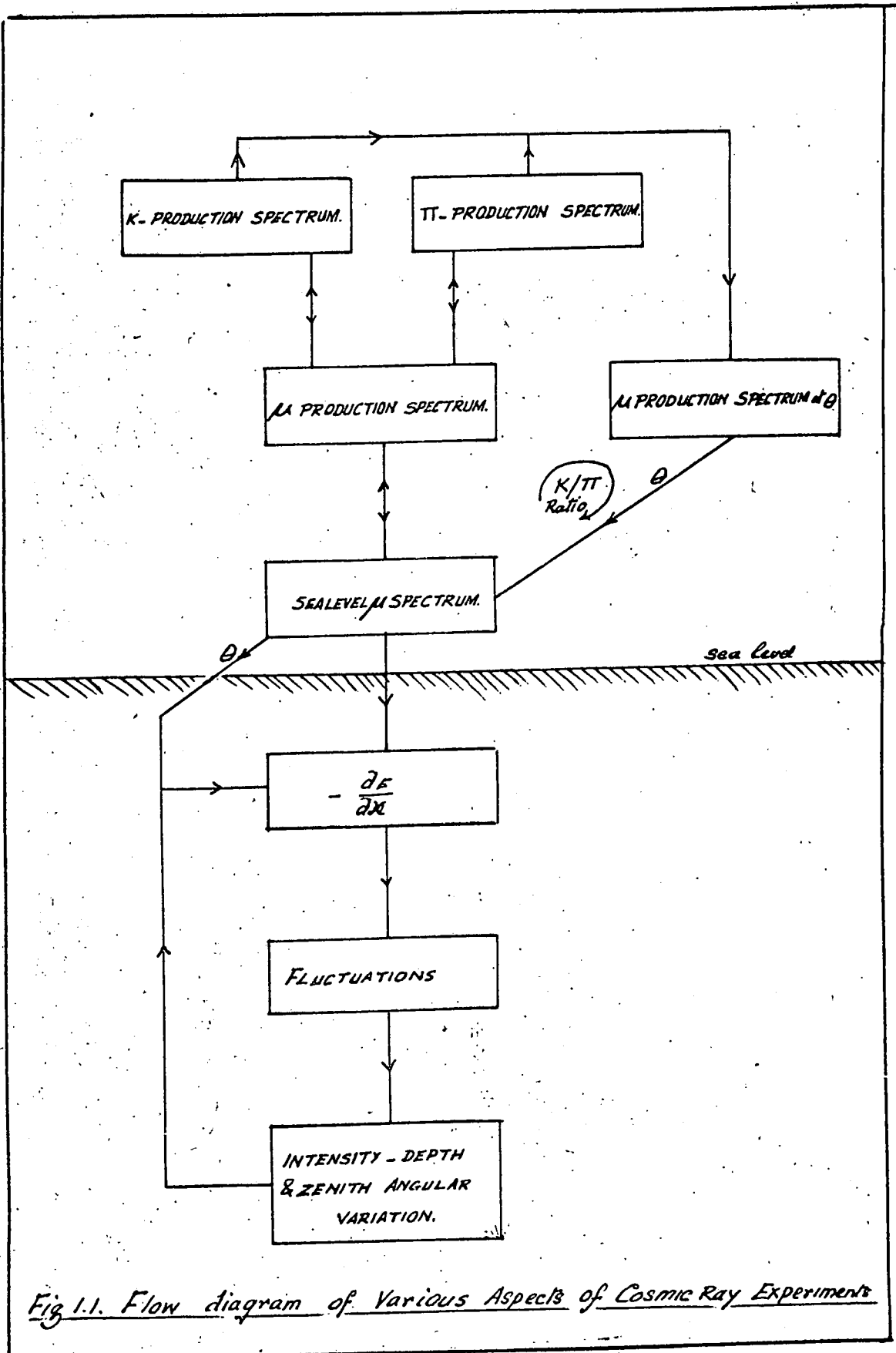


Fig 1.1. Flow diagram of Various Aspects of Cosmic Ray Experiments

In attempts to extend the sea-level energy spectrum to higher energies, several workers have made observations at various depths underground. The instruments used were first calibrated at a fairly shallow depth before being taken to greater depths. A schematic diagram of the various aspects of the study of cosmic ray muons is shown in Fig.1.1. Assuming a range energy relationship for muons, it is possible to construct the sea-level integral energy spectrum from underground measurements. Since direct measurements of energy are not being made telescopes having large areas and solid angles can be used. This is achieved by having the detecting devices parallel and close together. The majority of telescopes operated underground in the past have comprised ionization chambers, geiger counters or scintillation counters. Only a few workers included visual "detectors" (cloud chambers). In recent years the development of the neon flash tube (Conversi tube) and large spark chambers has afforded further means of observing the actual particle tracks.

The use of visual techniques underground is of vital importance for three reasons. Firstly, the zenithal distribution of particles can be easily obtained; secondly, they are necessary at great depths where the

particle rate is low and the rate of chance coincidences with counter devices becomes increasingly important; finally, the nature of the events underground (e.g. single or multiple particles) can be examined.

1.3. Studies of Cosmic Ray Neutrinos.

At very great depths (> 7000 m.w.e.) the vertical muon flux is very small ($\sim 10^{-6}$ times the sea-level flux) and it is possible to search for the products of neutrino induced reactions with such a low background of atmospheric muons. Neutrinos (as its name implies the neutrino is uncharged) interact very weakly with matter and it is estimated that cosmic ray neutrinos can pass through the equivalent of about 10,000 earth diameters of matter without interacting.

The cosmic ray neutrino flux consists basically of two components, of different origins. On the one hand there are the true cosmic neutrinos of galactic or extragalactic origin, whilst on the other there exist neutrinos of atmospheric origin mainly from the decay of K-mesons, pions and muons. It is likely that high energy neutrinos are mainly of atmospheric origin and their flux, energy spectrum and angular distribution can be evaluated.

Experiments have been carried out at accelerators and nuclear reactors studying the interactions of neutrinos

with nucleons in attempts to answer the following questions:

(i) Is the neutrino associated with the muon (ν_μ) in π - μ decay identical with the neutrino involved in beta-decay (ν_e) (i.e. $n \rightarrow p + e^- + \bar{\nu}_e$, $\mu^+ \rightarrow e^+ + \nu_e + \bar{\nu}_\mu$ etc.)?

(ii) What is the cross-section for neutrino-nucleon interactions?

(iii) Do intermediate bosons exist, and if so, what is their mass? (An intermediate boson would affect the cross-section for ν -nucleon interactions); and

(iv) Is there a cut-off momentum for these reactions? (i.e. is there a limit beyond which the cross-section levels off instead of increasing with neutrino energy?).

Experiments so far have yielded the following results for neutrino energies less than 10GeV:

(i) the muon and electron neutrinos are not identical ($\nu_\mu \neq \nu_e$);

(ii) a lower limit of 1.8 GeV has been put to the mass of the intermediate boson; and

(iii) no flattening off of the cross-section for inelastic interactions has been observed.

Since only a lower limit has been put to the mass of the intermediate boson, and the inelastic cross-section is still increasing at machine energies, several cosmic ray experiments have been started in attempts to answer questions (i), (ii) and (iv) because the neutrinos available,

whilst having low fluxes, have much higher energies than those from machines.

1.4. The Tata-Institute, Bombay, India - Osaka City University, Japan - Durham University, U.K. - Collaboration.

In 1963 a series of experiments were proposed by the Durham University Cosmic Ray Group and the Tata Institute of Fundamental Research, Bombay. Two phases of experimentation were suggested, the first phase to be a measurement of the flux and angular distribution of cosmic ray muons at various depths underground in the Champion Reef Mines, Kolar Gold Field, Mysore State, India, and the second phase to be an attempt to search for neutrino induced reactions at a very great depth (7600 ft.) in the same mine. The Osaka City University, Japan, group were invited to also participate in the second phase.

It is mainly with the first phase of this series of experiments that this thesis is concerned, although a survey will be made of the progress in the second phase.

A description of the apparatus for Phase 1 and its operation follows in the next chapter together with a description of the mines and the facilities afforded. The experimental data and the measuring technique are presented in the third chapter as well as details of the determination of the telescope acceptance functions.

In the fourth chapter the results are interpreted with respect to the angular distribution of muons underground. The exponent, n , of the angular distribution is derived as a function of depth, and comparison is made with the results of other workers and with theory.

The variation of the vertical intensity, I_v , with depth is derived in chapter five, and compared with the results of other workers. The best estimate of the depth-intensity variation is also derived.

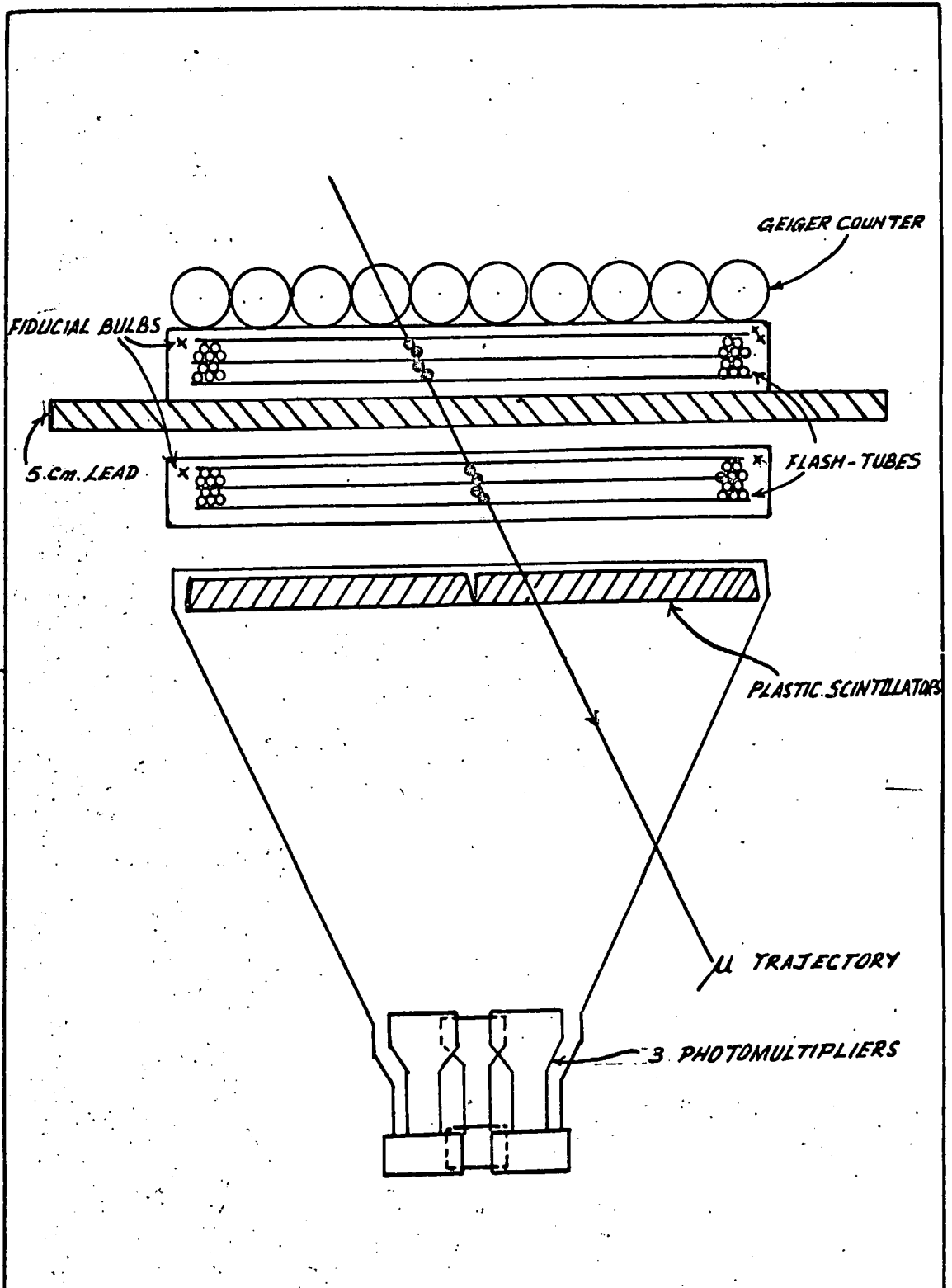
A brief summary of the propagation of muons underground is given in chapter six. The implications of the best estimate of the depth-intensity variation are discussed there, in particular with respect to resolving the problems of the sea-level energy spectrum from the results at shallow depths and the K/π ratio at production from the results at greater depths.

An analysis of arrival times of muons at 1812 m.w.e. and 4110 m.w.e. is made in chapter seven.

The electromagnetic interactions of muons are discussed in chapter eight, and an interpretation is made in the ninth chapter of muon bundles.

Phase 2, the neutrino experiment, is discussed in chapter ten, and the conclusions of the experiments and a discussion of further work are presented in the final chapter.

A geological description of the mines is given in the appendix.



0. 10. 20. 30 cm.

Fig 2.1. The Experimental arrangement.

CHAPTER 2.

THE EXPERIMENTAL ARRANGEMENT FOR ZENITH ANGULAR AND VERTICAL INTENSITY STUDIES.

2.1. Description of the Apparatus.

Since direct measurements of energy are not being made, it is possible to construct for underground use cosmic ray telescopes having large apertures. To demonstrate the difference in apertures between a conventional magnet spectrograph and a typical telescope for underground use, consider the Durham horizontal solid iron magnet spectrograph. Before its present modification began this had an aperture varying between 4 and 18 cm^2 .sr. for high energy particles (> 10 GeV) over the zenith angular range of acceptance (Pattison, 1963). As will be shown in the next chapter the telescopes used in phase one of the series have apertures greater than 10^4cm^2 .sr.

A photograph of one of the telescopes is shown "in situ" at a depth of 4463 ft. below surface in the Champion Reef Mine in the frontispiece, and a scale drawing appears in Fig.2.1. There were two such telescopes.

Each telescope consisted of a layer of plastic

scintillator made up of four square sections each having an area of approximately 0.25 m^2 and thickness 6 cm. The scintillator blocks were positioned so as to form a square of side one metre. The scintillators in each telescope were viewed by three Dumont 6364 (5" diameter) photo-multipliers from a distance of 70 cm. In addition to the scintillators there were ten (twelve at the shallower depth) large geiger counters mounted side by side. These were made of rolled aluminium (1.5 mm thick) and had a sensitive length of 111.5 cm. and internal diameter 10.6 cm. They were manufactured at the Tata Institute of Fundamental Research, Bombay. The end caps of the counters were also made of aluminium with a central glass-to-metal seal for the central anode wire which was made of 4 mil Tungsten wire. The counters were filled with commercial argon and petroleum ether vapour in the ratio 9 : 1 to a pressure of 10 cm.Hg.

A layer of lead 5 cm. thick and area 2.37 m^2 was introduced between the geiger counters and plastic scintillator in order to distinguish between muons and electrons.

The visual detectors comprised two arrays, each of area 1.1 m^2 , of four layers of neon flash tubes. These were introduced into the telescopes between the geiger

counters and plastic scintillator with one array above and the other below the lead. The flash tubes were viewed through a system of mirrors by a single open shutter camera using Ilford HPS, 35 mm. film (ASA 800). This film being red sensitive is most satisfactory in photographing the tracks of particles through the flash tubes. The images found when Kodak Plus-X film (ASA 400) was used were somewhat fainter than those recorded by HPS. The optical path length of the mirror systems was about 6 m. The relevance of this will be discussed in section 2.4.

It should be pointed out that all the components for a particular telescope were used in the same telescope at all depths.

2.2. The Electronic Circuits.

A block diagram of the electronic system is shown in Fig. 2.2. The electronics to the right of the broken line are common to both telescopes.

The photomultiplier pulses were pre-amplified with a gain of about 10 before passing into the main amplifiers where there was a gain of about 1200. The geiger counter pulses were first mixed before entering a pulse shaper and inverter unit.

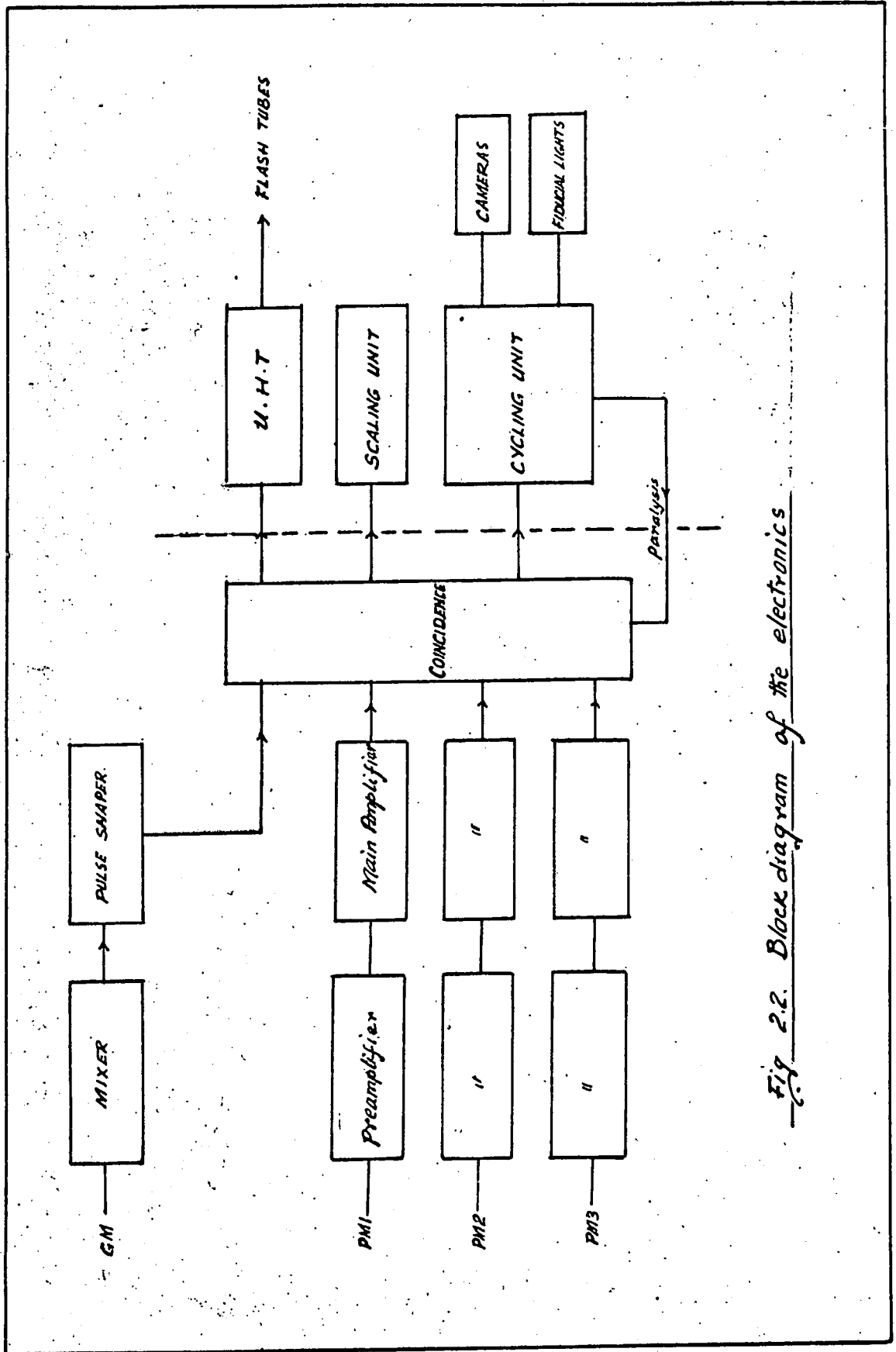


Fig 2.2. Block diagram of the electronics

The output pulses from the amplifiers and pulse shapers passed into separate discriminator and coincidence units, and the requirements for an event to be accepted by a counter telescope were a pulse from the geiger counter inverter unit and simultaneous pulses from the three photomultipliers, (i.e. either $P(1+2+3)+G1$ or $P(4+5+6)+G2$.) When this condition was satisfied a master 4-fold coincidence pulse triggered the high voltage unit (UHT) which comprised an 8 KV hydrogen thyratron (XHS - 100) and pulse transformer (Fig.2.3). The high voltage pulse from this unit was fed to the neon flash tubes in both units and the flashed tubes photographed. At the same time the master pulse triggered a univibrator counting unit which served two purposes; first, it recorded on a message register the number of events accepted (i.e. all 4-fold coincidences) and second, it closed a relay applying the 24 Volt D.C. supply to a cycling motor. This made one revolution (period 7 seconds) for each accepted event during which three switches were operated by means of cams fixed to the motor spindle. Firstly a switch was closed for the whole revolution grounding the inputs to the discriminator units thus preventing any further events to be accepted whilst the apparatus dealt with the triggering particle. The 7 seconds paralysis time was initiated in the first

instance by a second relay in the univibrator circuit for the first 2 seconds. The second cam switch was closed momentarily applying current to fiducial marking lights on each flash tube tray, and bulbs illuminating a clock. The third cam applied power to the camera motor for 3.5 seconds advancing the film. As the cycling motor came to rest the paralysis was released and the apparatus became ready to accept the next particle passing through either telescope.

All the electronic circuits were designed to work on the 220 V., 25 C/s., A.C. mains power available throughout the mines.

2.3. The Plastic Scintillators.

These were made at the Technical Physics Division, Atomic Energy Establishment, Trombay, in a manner similar to that described by Clark et al (1957). It was estimated by Ramanamurthy (1962) that about five photo-electrons on average were released at the photo-cathode of a photomultiplier when a cosmic ray passed through a similar scintillator. Since this number is not very much greater than unity, the noise pulses in the photomultiplier and the cosmic ray induced pulses are not absolutely separated. A typical differential distribution of pulse heights from a single photomultiplier viewing the

scintillators exposed to cosmic radiation at the surface of the mines (870 metres above sea-level) is shown in Fig. 2.4. It can be seen that, although the peak due to cosmic rays is separated from the noise region, there is some overlapping where the pulses due to cosmic radiation are comparable in amplitude to the tail end noise pulses.

The voltages on the photomultipliers and the gains of the amplifiers were set at the surface of the mines such that almost all cosmic rays passing through the telescopes were counted. If then the apparatus is operated underground under the same conditions as at the surface, the pulses from each photomultiplier are then due to :

(i) noise in the photomultipliers,

(ii) radioactivity in the mines, and

(iii) the penetrating component of the cosmic radiation.

The frequency of pulses due to the cosmic radiation were very much smaller compared with the other two sources.

By using fast electronics it is possible, in principle, to have only two photomultipliers viewing the scintillators to record cosmic rays, and demand a fast coincidence pulse ($\lesssim 10^{-8}$ sec.) as indicative of the passage of a cosmic ray. This would virtually eliminate coincidence

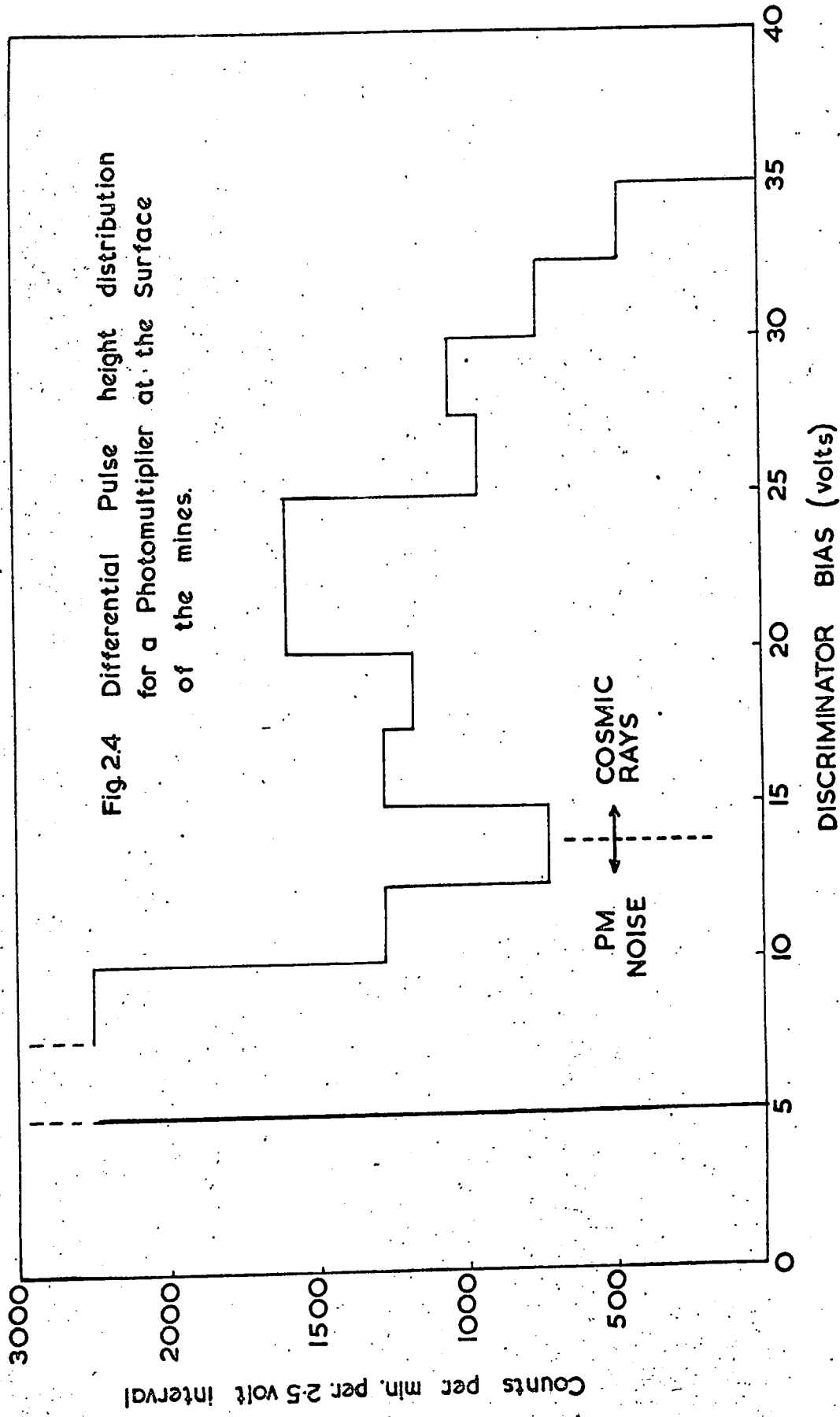


Fig.2.4 Differential Pulse height distribution for a Photomultiplier at the Surface of the mines.

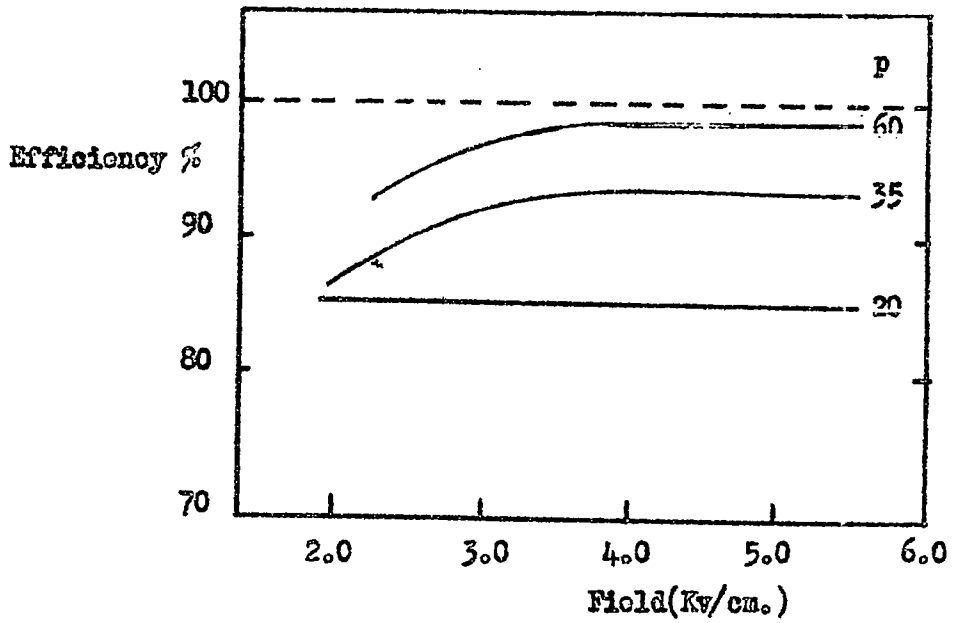


Fig. 2.6(a) The efficiency, field characteristics, with gas pressure (cm.Hg) as parameter. $T_p=3.2\mu\text{sec}$, $T_R=0.5\mu\text{sec}$, $\tau=4\mu\text{sec}$.

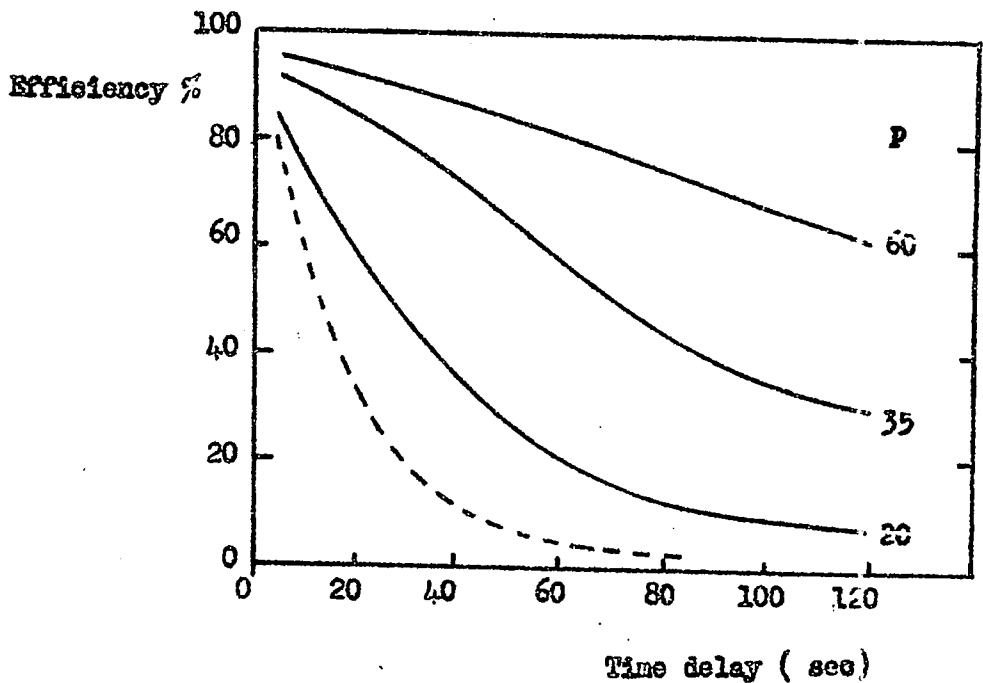


Fig. 2.6(b) The efficiency, time delay characteristics, with gas pressure (cm.Hg) as parameter. $E_{\text{max}}=3.7\text{ Kv/cm}$, $T_R=0.5\mu\text{sec}$, $\tau=4\mu\text{sec}$.
(Dotted line: $p=60\text{ cm.Hg}$, clearing field = 3.6 Kv/cm)

Layer
Efficiency %

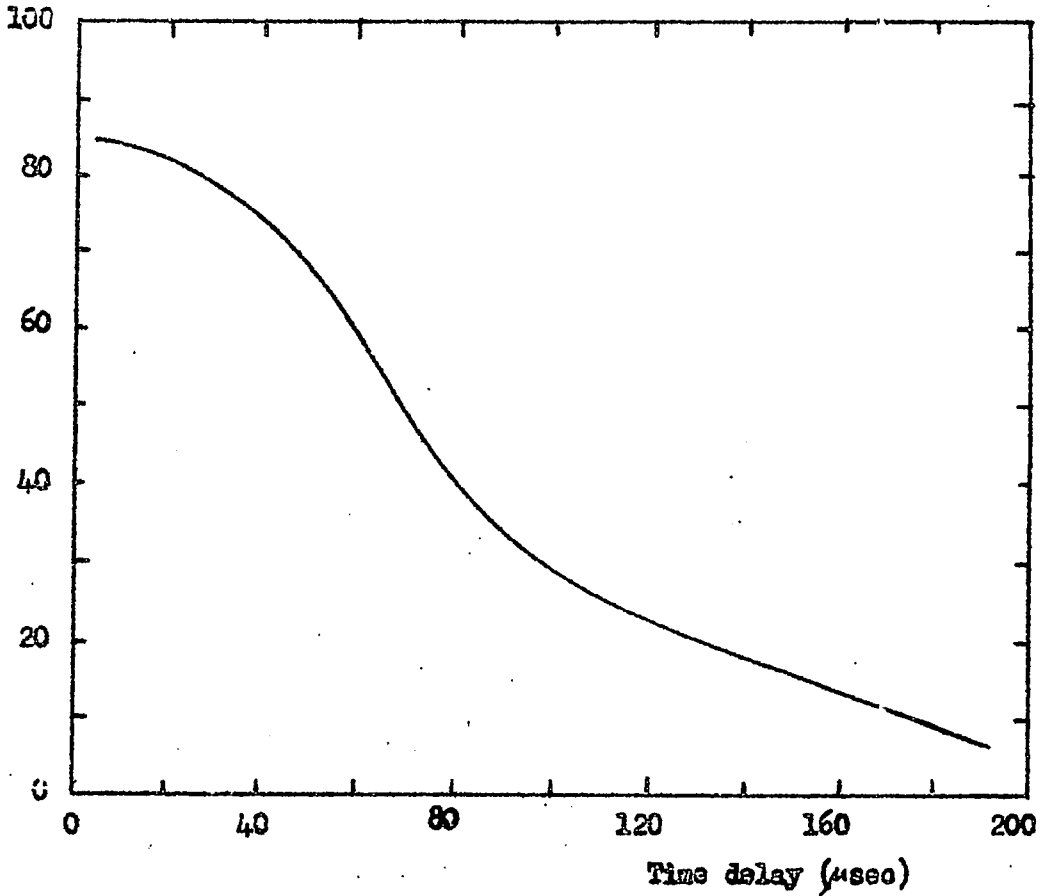


Fig.2.7 (a) -The efficiency, time delay characteristic for the tubes used in the horizontal spectrograph.

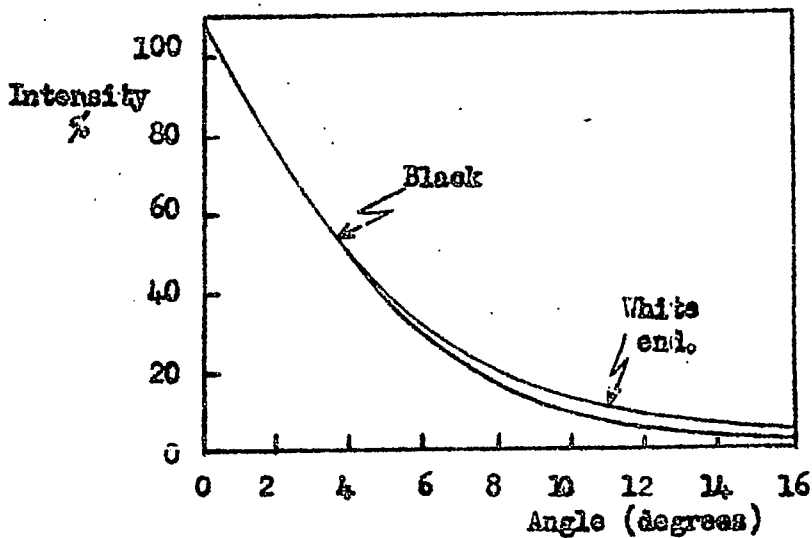


Fig. 2.7 (b) Polar diagram for light output from the flash-tubes.

Table 2.1

Spurious Flashing

The ratios are per tube per 1000 pulses

Field(Kv/cm)	2.1	2.8	3.5	4.2	4.9	5.6
Pressure(cm.Hg)						
60	0.18	0.54	0.37	0.6	0.6	0.6
35	0.0	0.18	0.0	0.18	0.2	0.8
20	0.18	0.18	0.18	0.2	1.2	4.0

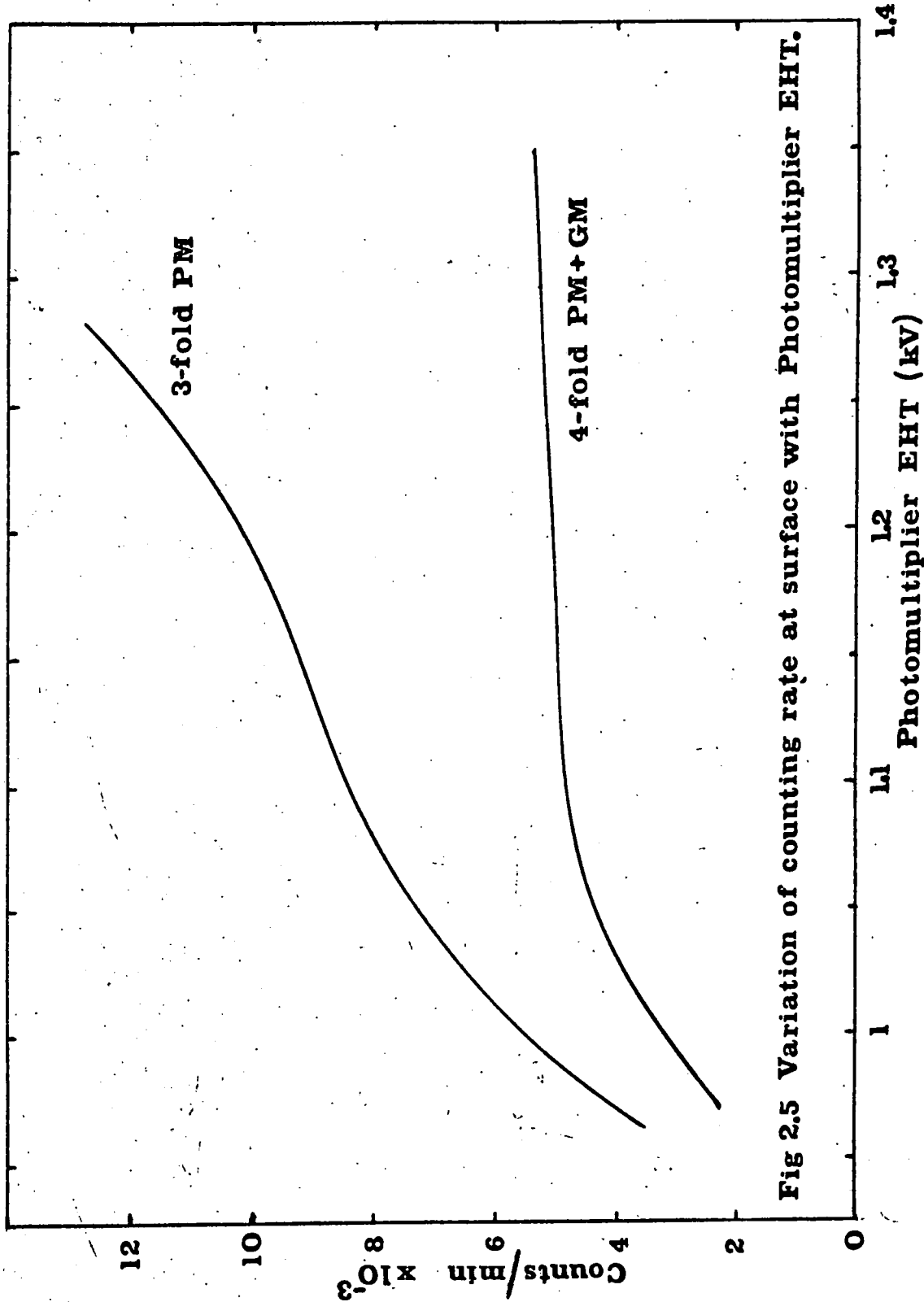


Fig 2.5 Variation of counting rate at surface with Photomultiplier EHT.

pulses due to photomultiplier noise and radioactivity. However, instead of using fast electronics it was decided to have three photomultipliers viewing the scintillators and have a layer of geiger counters above the lead, the triggering requirements to be as mentioned above (Section 2.2.) ($P(1+2+3)+G1$ or $P(4+5+6)+G2$). Because of the random and independent distribution of the spurious pulses in the photomultipliers the number of coincident spurious pulses is a small fraction of the total number of these pulses in each tube.

The method adopted in setting up the photomultiplier voltages and the discriminator bias was to measure the fourfold coincidence rate at the surface as a function of photomultiplier voltages. It was found that there was a plateau region, and the photomultipliers were operated on this plateau. (cf. Fig. 2.5.)

Typical counting rates of two photomultipliers underground were 1473 and 1760 counts per minute. Typical two- and three-fold rates for photomultipliers viewing the same scintillator were 21 and 16 counts per minute respectively. The resolving time of the electronics was $5\mu s$. This was found by measuring the two-fold chance coincidence rate when the photomultipliers were removed from the scintillator cones and covered by black

cloth. The chance four-fold coincidence rate was 1.4 per hour per unit. However, these events appeared as "blanks" on the film, thus demonstrating the advantages of incorporating track recording devices.

2.4. The Neon Flash Tubes.

A brief summary of the characteristics of the neon flash tube is shown in Figs. 2.6 - 2.8 and Table 2.1. (Also cf. Coxell, 1963). The tubes used in the apparatus were 1.1 m. in length, and 1.5 cm. internal diameter and contained neon (98% Ne, 2% He, < 200 vpm A, O₂, N₂) to a pressure of about 60 cm. Hg. They were painted black, except for the plane end window, with a lower white layer over the 20 cm. nearest the window.

For maximum efficiency and visibility the requirements for operation of the tubes are :

- (i) The highest voltage pulse consistent with an insignificant rate of spurious flashing (8 KV/cm);
 - (ii) Short rise time of the applied pulses ($\leq 0.5 \mu s$);
 - (iii) Short delay between the passage of a particle and the application of the pulse ($2 \mu s$);
 - (iv) A direction of photography making the smallest possible angle with the axes of the flash tubes ($\leq 7^\circ$).
- The figures in brackets indicate the actual values of these parameters in the experimental arrangement.

2.5. Description of the Mines.

The Kolar Gold Field (Lat. $12^{\circ}57'N$, Long. $78^{\circ}18' E$) is situated in Mysore State, India, at a distance of 90 Km. from Bangalore. The surface of the area is about 870 m. above sea-level (Madras). Facilities exist in the mines to go down to a maximum depth of 3.18 Km. (~ 9600 m.w.e.) from the surface. Water and electricity (220 V., 25 cycles/second, A.C. mains) are available throughout the mines. The natural temperatures in the mines vary over the range $45^{\circ}-60^{\circ}C$. at depths greater than 1000 metres in places where there is little or no ventilation, and between $20^{\circ}-40^{\circ}C$. in places where air, cooled at the surface and at "spot" coolers underground, circulates. The temperature at the sites chosen for the series of experiments was always less than $30^{\circ}C$. The geological description, chemical composition and densities of rock samples are given in Appendix I. The average density of rocks in the mines is 3.09 gm.cm^{-3} , the average atomic number, Z , is 12.9 and the ratio of atomic number to atomic mass, Z/A , is 0.49.

The depths of the working sites from the 'collars' of the shafts are known correct to the nearest foot. Errors in the estimate of matter above a working site arise mainly from two sources :

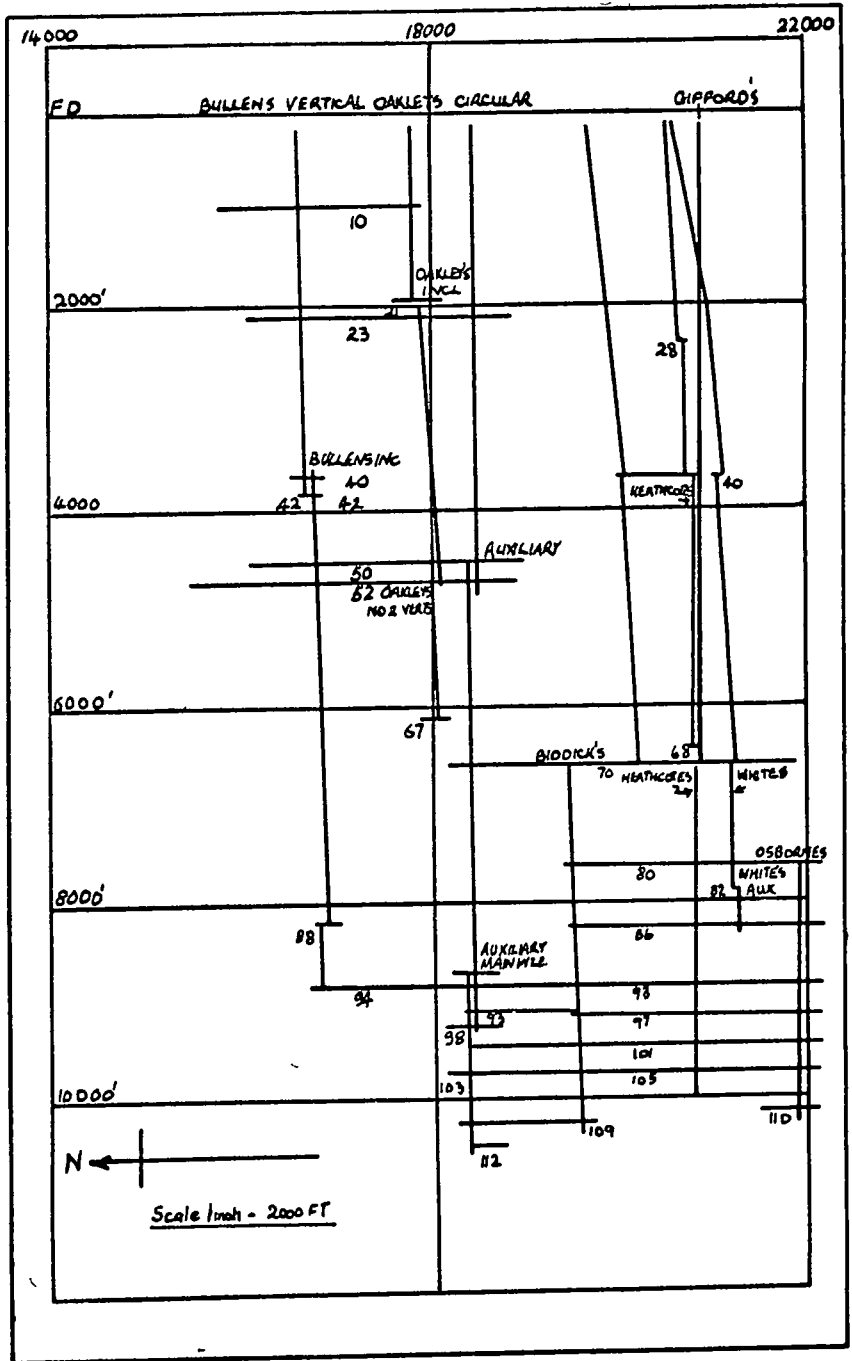


FIG 28 Cross section of Champion Reef Mine

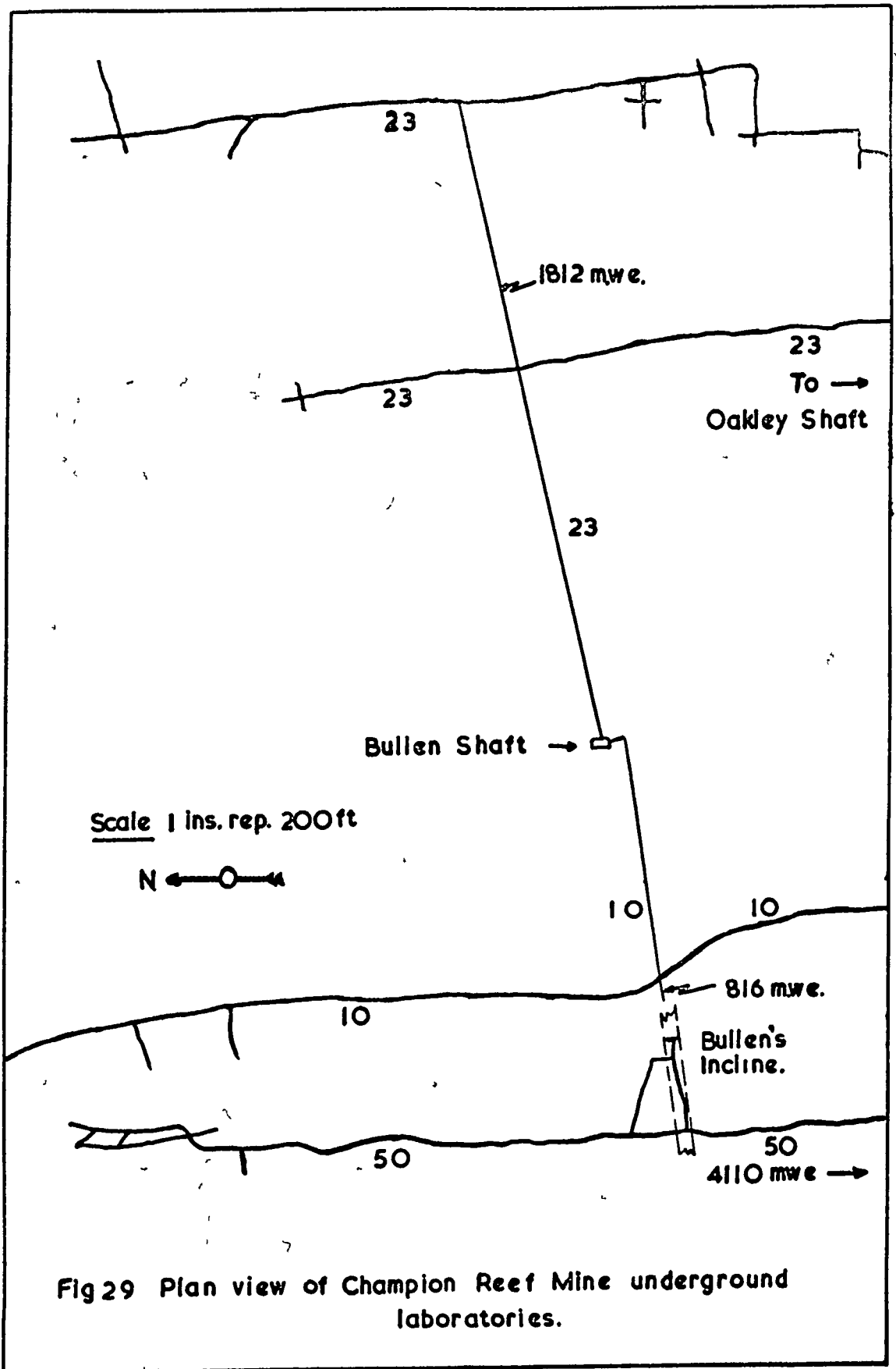


Fig 29 Plan view of Champion Reef Mine underground laboratories.

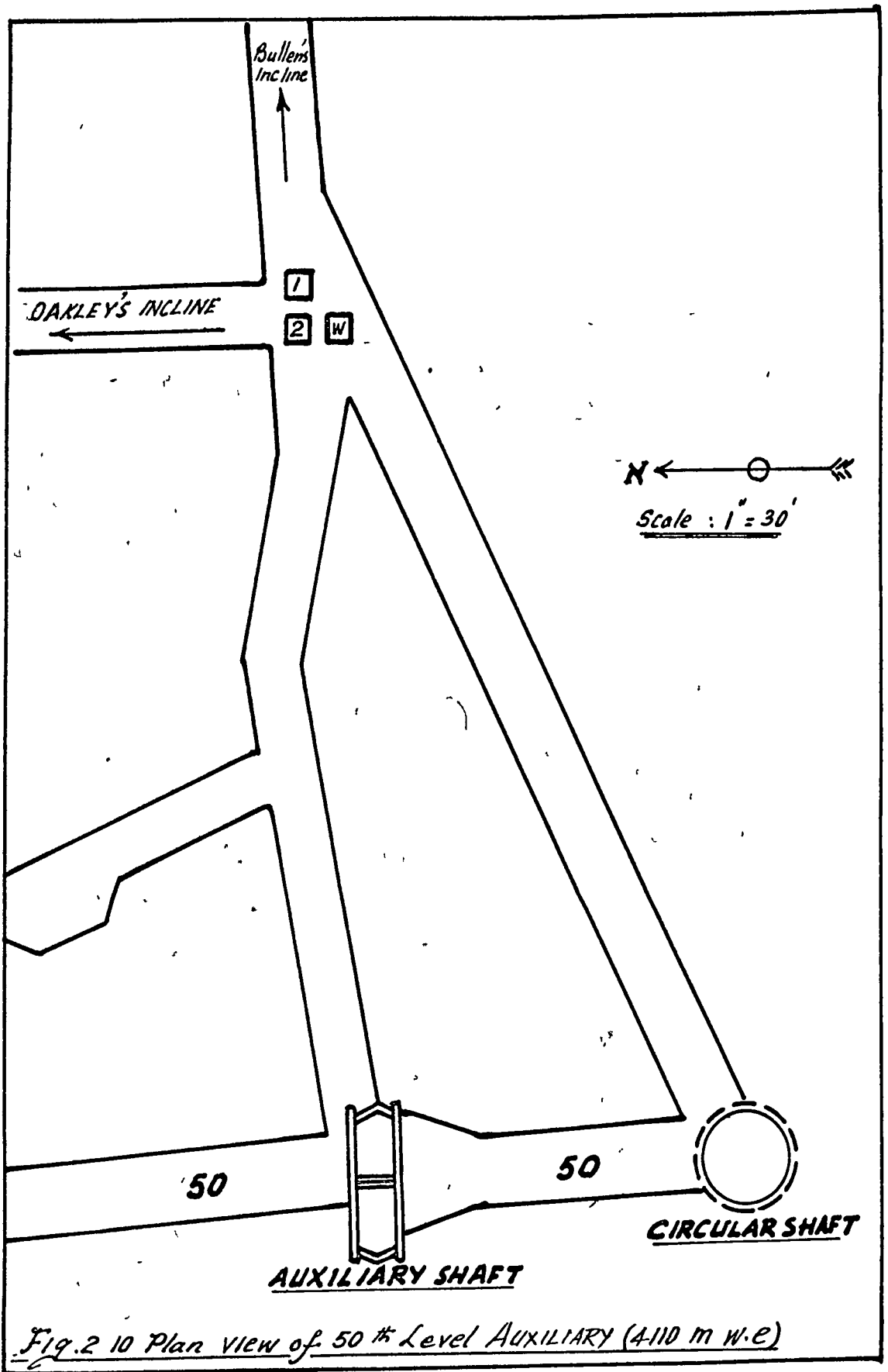


Fig. 2 10 Plan view of 50% Level Auxiliary (4110 m W.E)

(1) A lack of precise knowledge of the composition of the rock and variations in the density of rock samples. The rocks consist mainly of hornblende schist ($> 90\%$ and probably 98% by volume) with auriferous quartz veins and pegmatite dyke intrusions. The densities of rock samples of hornblende schist fluctuate from their mean value of 3.02 gm.cm.^{-3} by about ± 0.04 amounting to a variation of $\pm 1.3\%$ in the density. The density of rocks other than hornblende schist are all $> 2.6 \text{ gm.cm.}^{-3}$; & (ii) Topography of the surface of the mines. This is almost flat over the area under which the experimental sites were located.

The experimental sites selected for the first phase of the series of experiments were 10th level and 23rd level in Bullen Shaft and 50th level Auxiliary Shaft. The second phase (the neutrino experiment) is being conducted at 80th level Heathcote Shaft. In physical units these levels have respective vertical depths (below the top of the atmosphere) 816, 1812, 4110 and 7500 m.w.e. A north-south cross-sectional view of the Champion Reef Mine is shown in Fig. 2.8 and Figs. 2.9 and 2.10 are plan views showing the positions of the sites relative to the shafts in phase 1. At these depths the apparatus was situated at distances of 97 m., 162 m., and 54 m.,

respectively from the nearest vertical shaft. The neutrino laboratory is only about 30 m. away from Heathcote Shaft, but since the telescopes are not arranged to detect vertically moving particles this does not matter. In any case the collar of Heathcote Shaft is about 60 m. above 80th level.

2.6. The Experimental Arrangement.

(i) 816 m.w.e. Since there was only enough space available at this depth for one unit to be "in situ" at a time, and because the cosmic ray rate was expected to be high, the units were operated singly in succession.

(ii) 1812 m.w.e. Here there was sufficient room in the tunnel for the two units to be operated simultaneously. A plan view of the arrangement is shown in Fig. 2.11, and a side elevation showing the optical system for the neon flash tubes is given in Fig. 2.12. Whenever an event was accepted in either unit the high voltage pulse was applied to the flash tubes in both units in a search for electromagnetic interaction products or "bundles" of associated muons.

(iii) 4110 m.w.e. At this depth the arrangement of the two units was the same as at 1812 m.w.e. However, in addition, a third unit (the wing array) containing only two trays of three layers of neon flash tubes

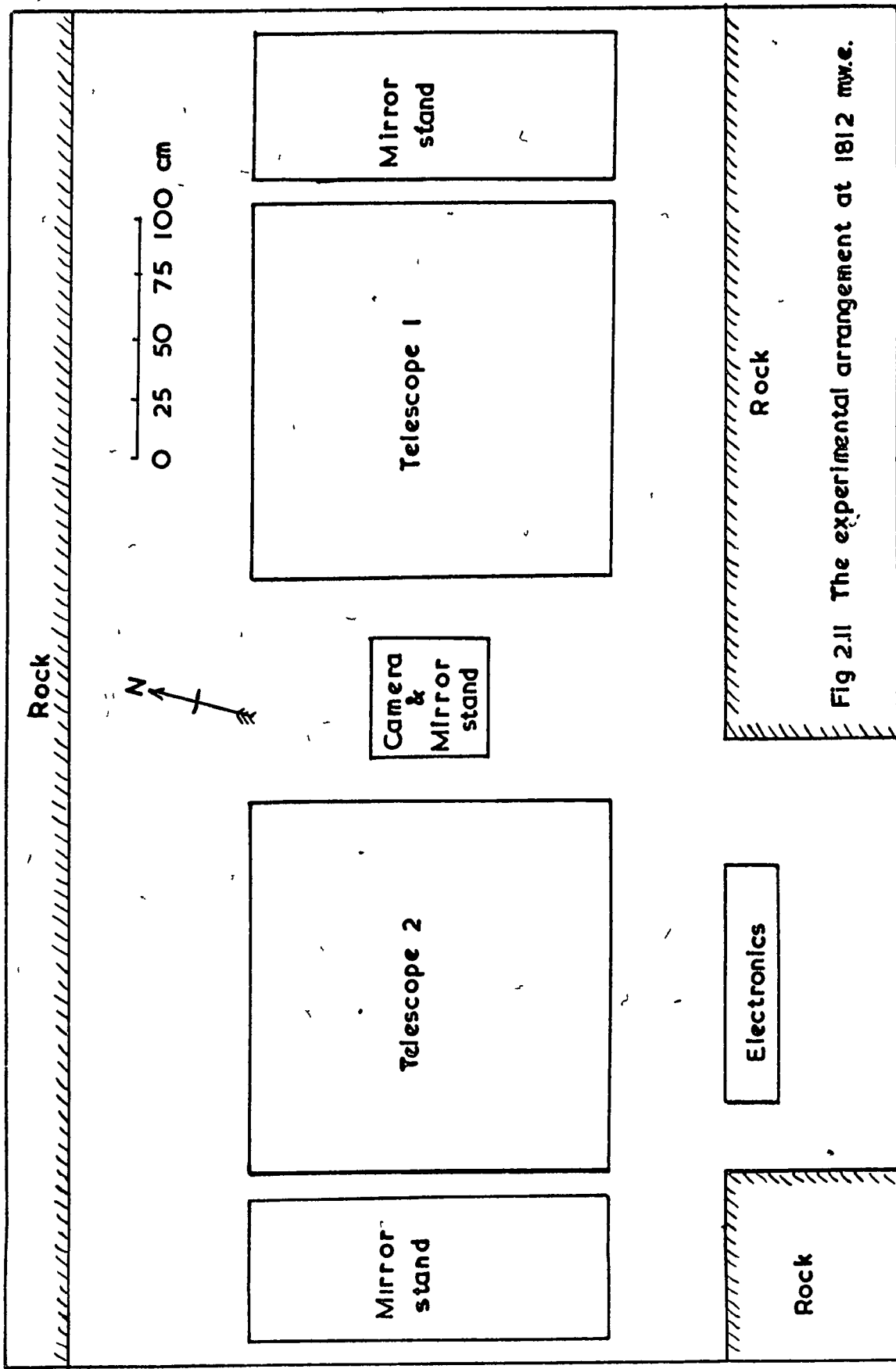


Fig 2.11 The experimental arrangement at 1812 m.w.e.

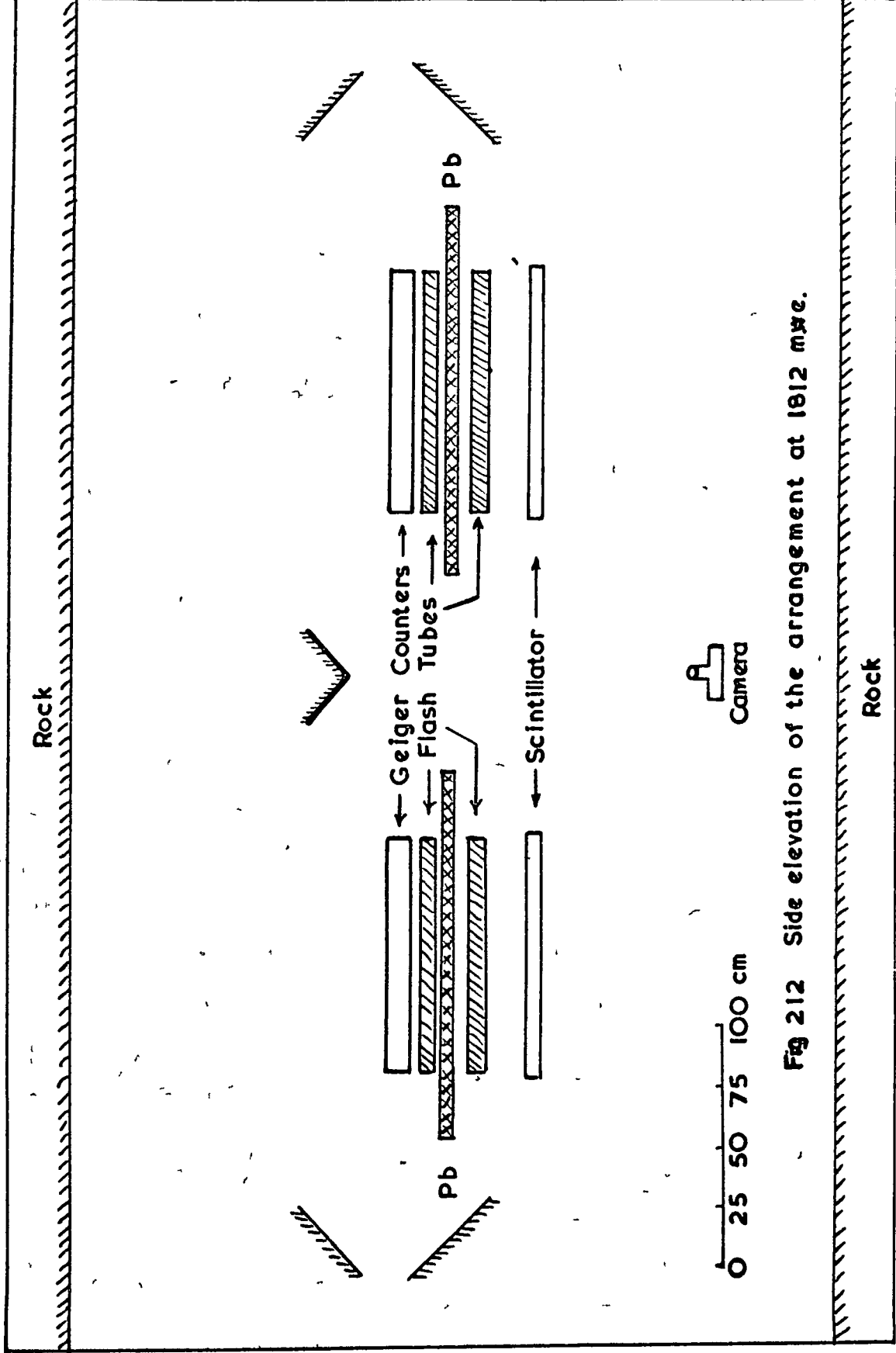


Fig 212 Side elevation of the arrangement at 1812 m.w.e.



Plate I: The experimental arrangement at 4110 m.w.e.
(The wing array can be seen under construction
in the far left.)

separated by 5 cm. of lead. The high voltage pulse was applied to all six neon flash tube trays for each event accepted by either of the detecting units. The wing array, viewed directly by a second camera operated in parallel to the main camera, can be seen in Plate I.

2.7. Alignment of the Apparatus.

At each level the units were positioned such that the plastic scintillators, neon flash tube trays and geiger counters were horizontal. This was achieved using a spirit level, and as a check vertical threads were suspended in front of the flash tubes and a photograph of the threads, flash tubes and fiducial marking lights was taken. It was found that the alignment was accurate to better than one degree.

2.8. Operation of the Apparatus.

The apparatus was checked daily with occasional spot checks. The times of the daily checks were staggered in order that any time variations of the arrival of cosmic rays could be studied.

Daily checks comprised measuring the one-, two- and three-fold coincidence rates for the photomultipliers of each unit, and the total geiger counter rate for each unit. Individual geiger counter rates were checked at frequent intervals. Any serious variations were

investigated and remedied immediately. In addition the univibrator and cycling unit, UHT unit and camera film drive were tested daily. The mains supplies, 300 volt supplies and filament supplies were checked each day.

Immediately before or after a run the apparatus was photographed by illuminating the front of each unit. This was done to ensure that nothing had been left in the optical path which could impede the camera's view. The time of the start and finish of each run was noted as well as the number of four-fold triggers. This was checked with the number of frames on the film for each run. A record was also made of the four-fold coincidence rate in each run (i.e. genuine events plus chance coincidences).

---oOo---

CHAPTER 3.

THE EXPERIMENTAL DATA.

3.1. Operation of the Telescopes.

The apparatus was operated during the period December 1963 to December 1964. After the preliminary testing of the apparatus at the surface of the mines when the voltages for the photomultipliers and geiger counters, the amplifier gains, and discriminator biases were fixed, the apparatus was operated efficiently at 816 m.w.e., 1812 m.w.e. and 4110 m.w.e. for a total of 110 days. During this time some 23,039 photographs were taken of which 9,809 contained tracks of penetrating particles, the difference indicating the number of chance four-fold coincidences. At the three depths the ratio of frames containing a penetrating particle to total frames (chance and genuine events) was 85%, 68% and 4.2% respectively. As mentioned earlier both units were operated simultaneously at the two deeper levels and separately at 816 m.w.e.

3.2. The Measuring Technique.

The photographs were scanned and divided into three categories. The first comprised essentially blank photographs which originated in random coincidences between the geiger counters and photomultipliers and were

Depth (m.w.e.)	816	1812	4110
Total Frames	4273	8411	10355
Total Events	3624	5750	435
Running Time (hours)	49.68	513.55	2061.25
Frame Rate/Hour	$86.0^{\pm 1.3}$	$16.4^{\pm 0.2}$	$5.0^{\pm 0.1}$
Muon Rate/Hour	$72.9^{\pm 1.2}$	$11.2^{\pm 0.2}$	$0.21^{\pm 0.01}$
'Blank' Rate/Hour	$13.0^{\pm 0.5}$	$5.2^{\pm 0.1}$	$4.8^{\pm 0.05}$

TABLE 3.1. - THE MEASURED RATE OF EVENTS.

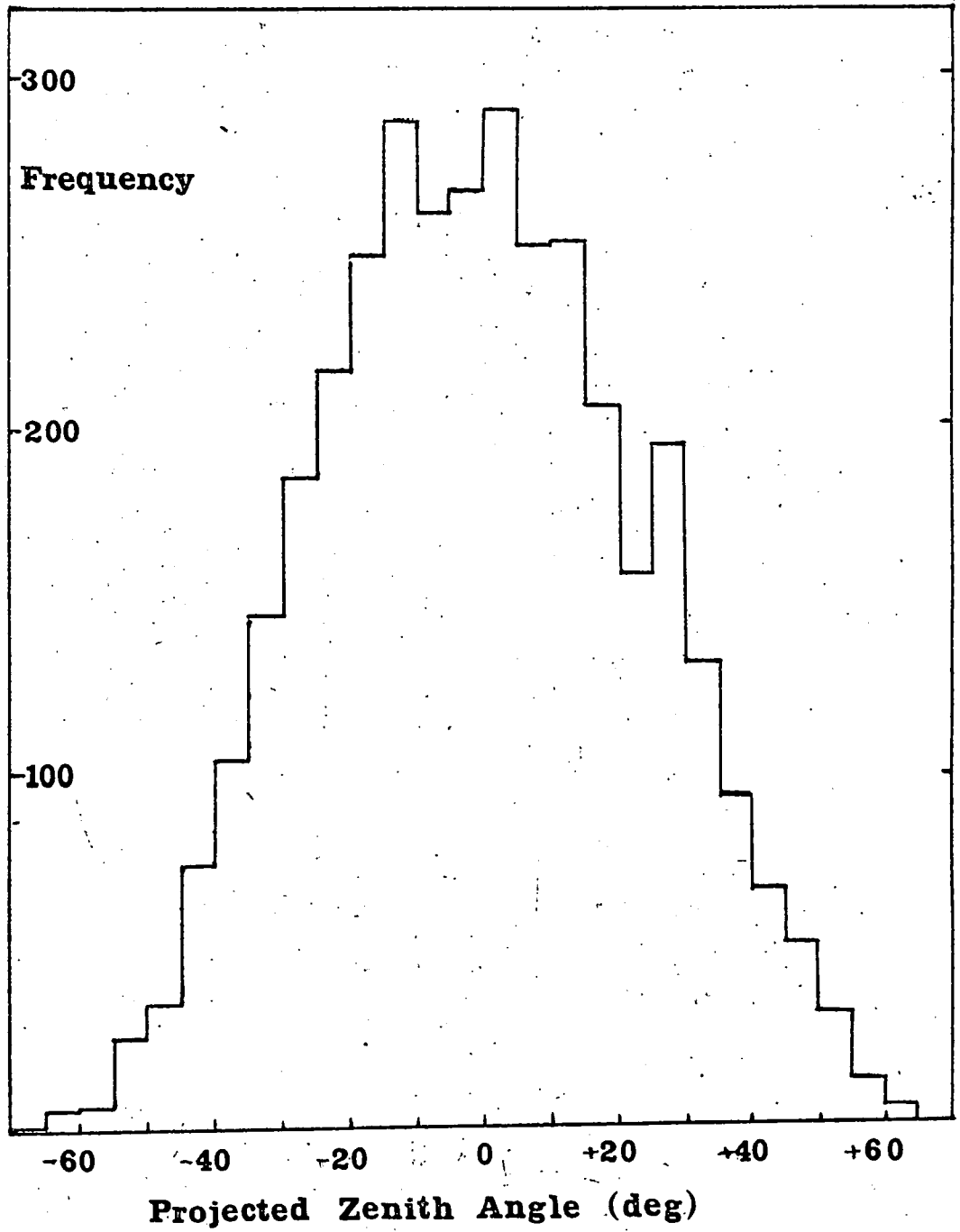


Fig.3.1. The distribution of single muons at 816 m.w.e.

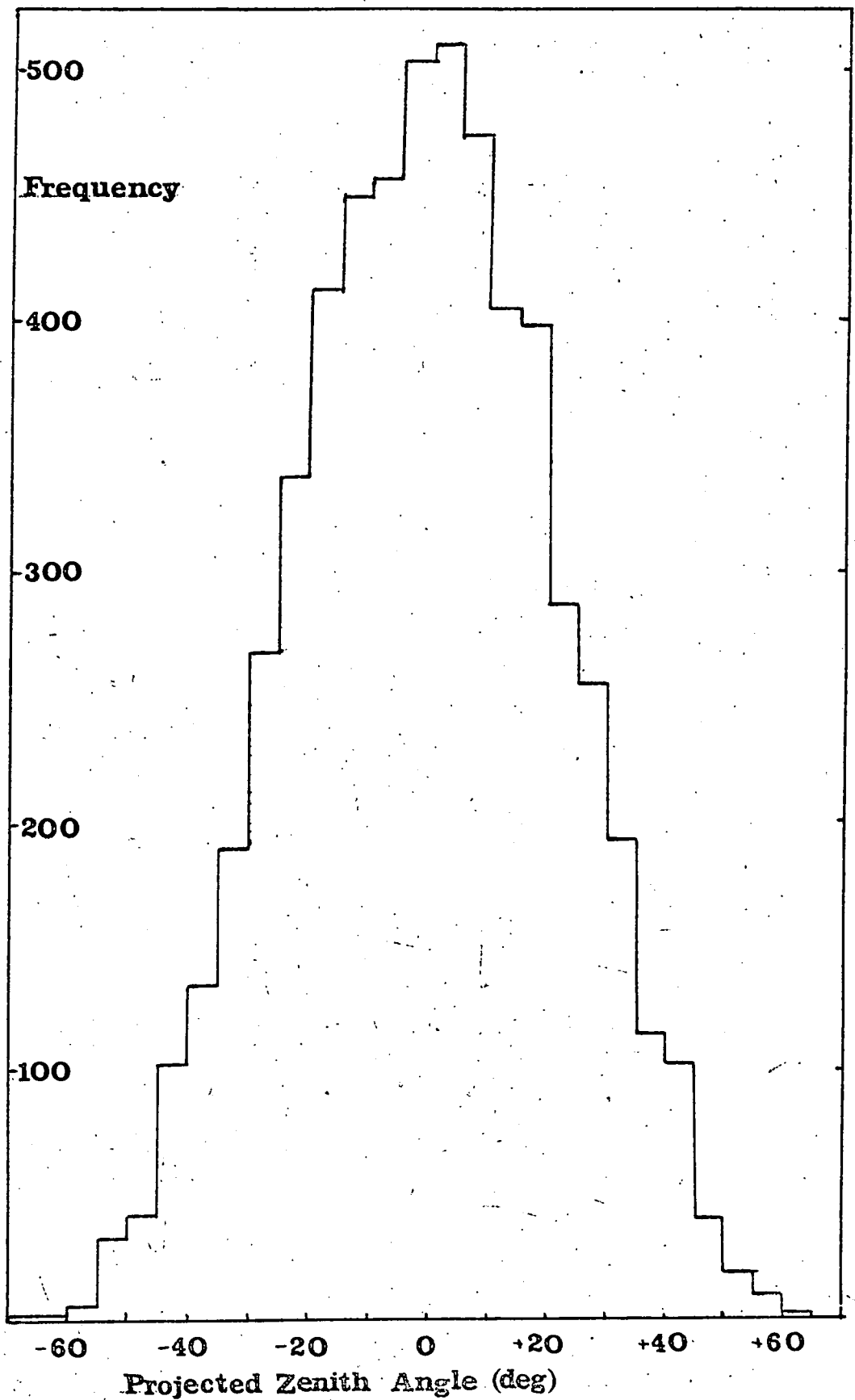


Fig. 3.2. The distribution of single muons at 1812 m.w.e.

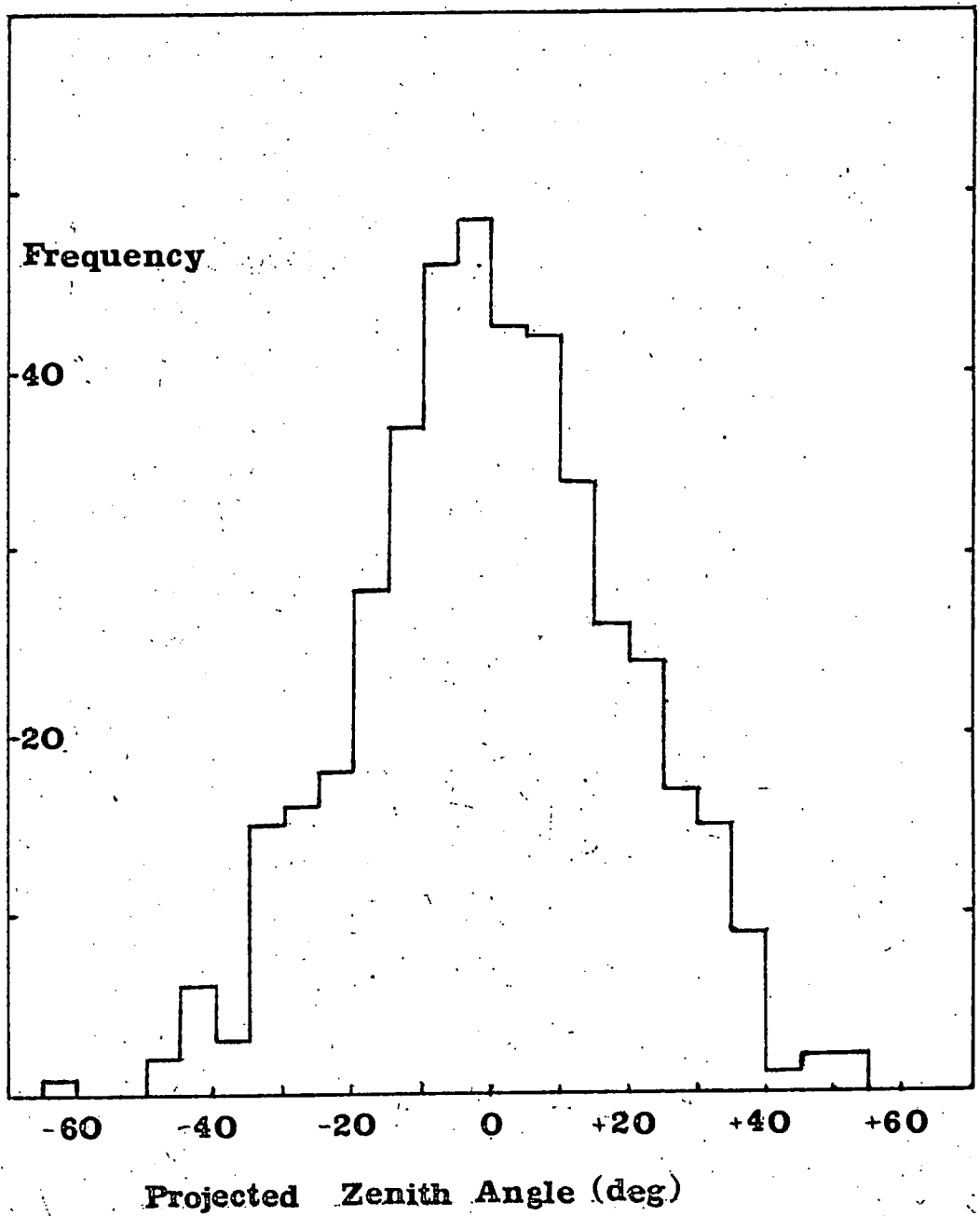


Fig. 3.3. The distribution of single muons at 4110m.w.e.

due largely to noise and the background radioactivity. The number of events in this category increased sharply with depth. The second category comprised events in which single penetrating particles could be resolved and their inclination to the zenith measured. Most of these events consisted of single particles with no other complicating tracks. Where the latter occurred this second category was sub-divided into various groups, viz.

(i) Single penetrating particles accompanied by:

- (a) a knock-on electron from the rock;
- (b) a knock-on shower from the rock;
- (c) a knock-on electron from the lead;
- (d) a knock-on shower from the lead;

and

(ii) Events where more than one penetrating particle was seen to pass through the lead. Dense penetrating showers from which no direction could be determined ($\lesssim 1\%$) were placed in the third category.

The measured rate of events for the three depths are summarized in Table 3.1.

The frequency distributions of single muons (unaccompanied and accompanied) are shown in Figs. 3.1 - 3.3. The telescopes were aligned such that their orientation was the same at each depth (i.e. the geiger

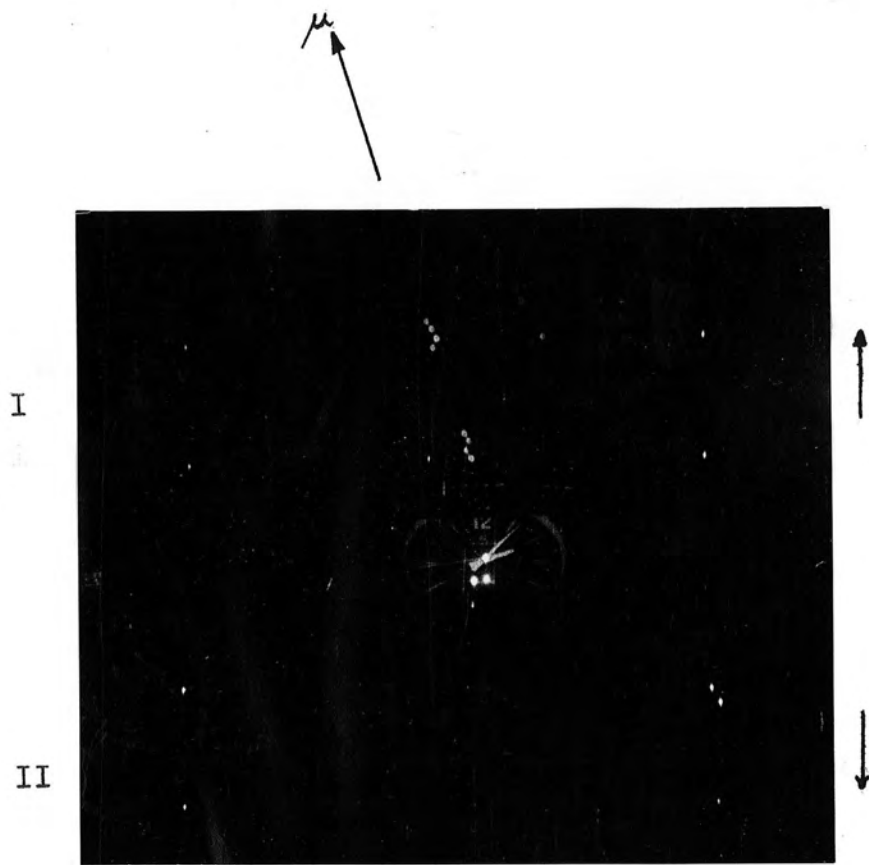


Plate 2 A single penetrating particle in
Unit I.

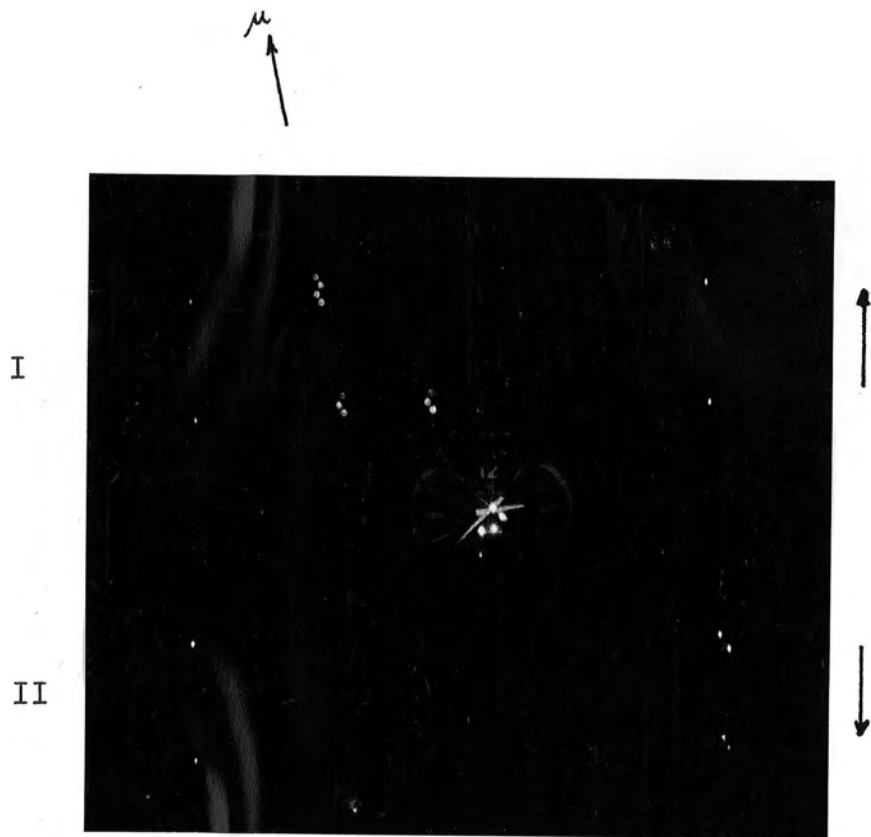


Plate 3 A penetrating particle accompanied
by a secondary electron from the rock.

counter and flash tube axes were approximately parallel to the east-west plane). Thus those particles arriving from north of the zenith were defined as having positive projected zenith angles whilst those from the south were defined negative. The symmetry about the zenith of the distributions indicates that there is no favoured arrival direction for high energy muons.

3.3. The Telescope Acceptance Functions.

In order to convert the observed counting rates into absolute flux values it is necessary to know the differential apertures of the telescopes and the angular distribution of penetrating particles at each level of observation. The method adopted to determine the differential apertures of the telescopes was similar to that used by Lovati et al (1954).

It is conventional and reasonably accurate to represent the angular distribution in spatial angle, ϕ , to the vertical in the form :

$$I(\phi) = I_v \cos^n \phi$$

where I_v is the vertical intensity and $I(\phi)$ the intensity at a zenith angle ϕ . For zenith angles less than about 60° the exponent, n , will be sensibly independent of ϕ at any one depth and will increase slowly with depth, due mainly to the increasing slope of the intensity-depth curve (Barrett et al, 1952).

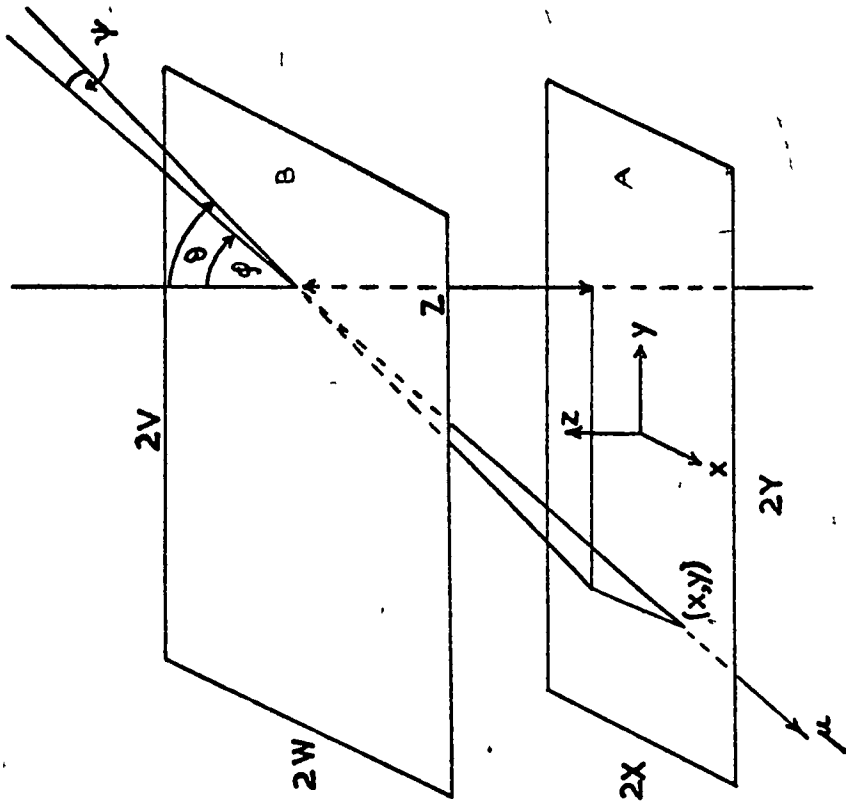


Fig. 3.4 The path of a muon through parallel detectors.

The best fit value of n has been derived by converting the distribution in ϕ to one in projected angle, θ , and finding the value of n which gives the minimum χ^2 -fit for comparison with the observed distribution.

Consider two horizontal rectangular detectors, A and B, having dimensions $2X$ cm. by $2Y$ cm. and $2W$ cm. by $2V$ cm. and placed one above the other at a distance Z cm. (Fig. 3.4) The direction of motion of a particle crossing the detectors is individuated by the angles θ and ψ which are bound to the zenith angle ϕ by

$$\cos \phi = \cos \theta \cdot \cos \psi.$$

With the intensity of the incident particles represented by $I(\phi) = I_v \cos^n \phi$, then the total flux of particles passing through both detectors is

$$\begin{aligned} F_n &= \iiint dx dy \cos \phi \cdot I(\phi) d\omega \\ &= \iiint dx dy \cos \phi \cdot I_v \cos^n \phi d\omega \end{aligned}$$

where $d\omega$ is the elementary solid angle determined by

$$d\omega = \cos \psi \cdot d\psi d\theta.$$

Thus
$$F_n = I_v \iiint dx dy \cos^{n+1} \theta d\theta \cos^{n+2} \psi d\psi$$

which becomes
$$F_n = 2 I_v \int_{\theta_1}^{\theta_2} \cos^{n+1} \theta \cdot d\theta \int_{\psi_1}^{\psi_2} d\psi \int_{x_1}^{x_2} dx \int_{y_1}^{y_2} \cos^{n+2} \psi \cdot d\psi$$

on inverting the order of integration with the limits

$$\theta_1 = 0, \theta_2 = \tan^{-1}\{(Y+V)/Z\}$$

$$Y_1 = -Y, Y_2 = Y - Z \tan \theta$$

$$X_1 = -X, X_2 = X$$

and

$$\psi_1 = -\tan^{-1}\left\{\frac{W+x}{Z} \cdot \cos \theta\right\}, \psi_2 = \tan^{-1}\left\{\frac{W-x}{Z} \cdot \cos \theta\right\}.$$

If $N_n(\theta)$ is the orthogonal projection of the angular distribution on the vertical plane, yz , then

$$F_n = \int N_n(\theta) d\theta$$

Hence
$$N_n(\theta) = 2 I_v \cos^{n+1} \theta (Y+V - Z \tan \theta) \int_{-x}^x dx \int_{\psi_1}^{\psi_2} \cos^{n+2} \psi \cdot d\psi.$$

with the limitation that $Y+V - Z \tan \theta \geq 0$ i.e. $\tan \theta \leq (Y+V)/Z$.

This equation can easily be integrated for integral values of the exponent, n , and the results for integral values of n from zero to 5 are shown in Table 3.2.

Since the solid angle of acceptance is limited by the upper flash tube tray and the plastic scintillator the following dimensions have been used in determining the acceptance functions shown in Figs.3.5.

$$X = 55.0 \text{ cm.}$$

$$Y = 50.0 \text{ cm.}$$

$$W = V = 51.9 \text{ cm.}$$

$$Z = 41.8 \text{ cm.}$$

$$N_0(\theta) = \frac{1}{2} K \cos \theta \left[(X-W) \arctan \left\{ \frac{(W-X) \cos \theta}{Z} \right\} + (W+X) \arctan \left\{ \frac{(W+X) \cos \theta}{Z} \right\} \right]$$

$$N_1(\theta) = \frac{1}{3} K \cos \theta \left[\frac{Z^2 - 2 \{Z^2 + (W-X)^2 \cos^2 \theta\}}{A_+^{1/2}} - \frac{Z^2 - 2 \{Z^2 + (W+X)^2 \cos^2 \theta\}}{A_+^{1/2}} \right]$$

$$N_2(\theta) = \frac{1}{8} KZ^3 \cos^2 \theta \left(A_-^{-1} - A_+^{-1} \right) + \frac{3}{4} \cos^2 \theta \cdot N_0(\theta)$$

$$N_3(\theta) = \frac{1}{15} KZ^4 \cos^3 \theta \left(A_-^{-3/2} - A_+^{-3/2} \right) + \frac{4}{5} \cos^2 \theta \cdot N_1(\theta)$$

$$N_4(\theta) = \frac{1}{24} KZ^5 \cos^4 \theta \left(A_-^{-2} - A_+^{-2} \right) + \frac{5}{6} \cos^2 \theta \cdot N_2(\theta)$$

$$N_5(\theta) = \frac{1}{35} KZ^6 \cos^5 \theta \left(A_-^{-5/2} - A_+^{-5/2} \right) + \frac{6}{7} \cos^2 \theta \cdot N_3(\theta)$$

Where $K = 4 I_V (Y+V - Z \tan \theta)$, $A_+ = Z^2 + (W+X)^2 \cos^2 \theta$.

In general for $n > 1$,

$$N_n(\theta) = \frac{KZ^{n+1} \cos^n \theta}{n(n+2)} \left(A_-^{-n/2} - A_+^{-n/2} \right) + \frac{n+1}{n+2} \cos^2 \theta \cdot N_{n-2}(\theta).$$

TABLE 3.2. - THE TELESCOPE ACCEPTANCE FUNCTIONS AS A FUNCTION OF n .

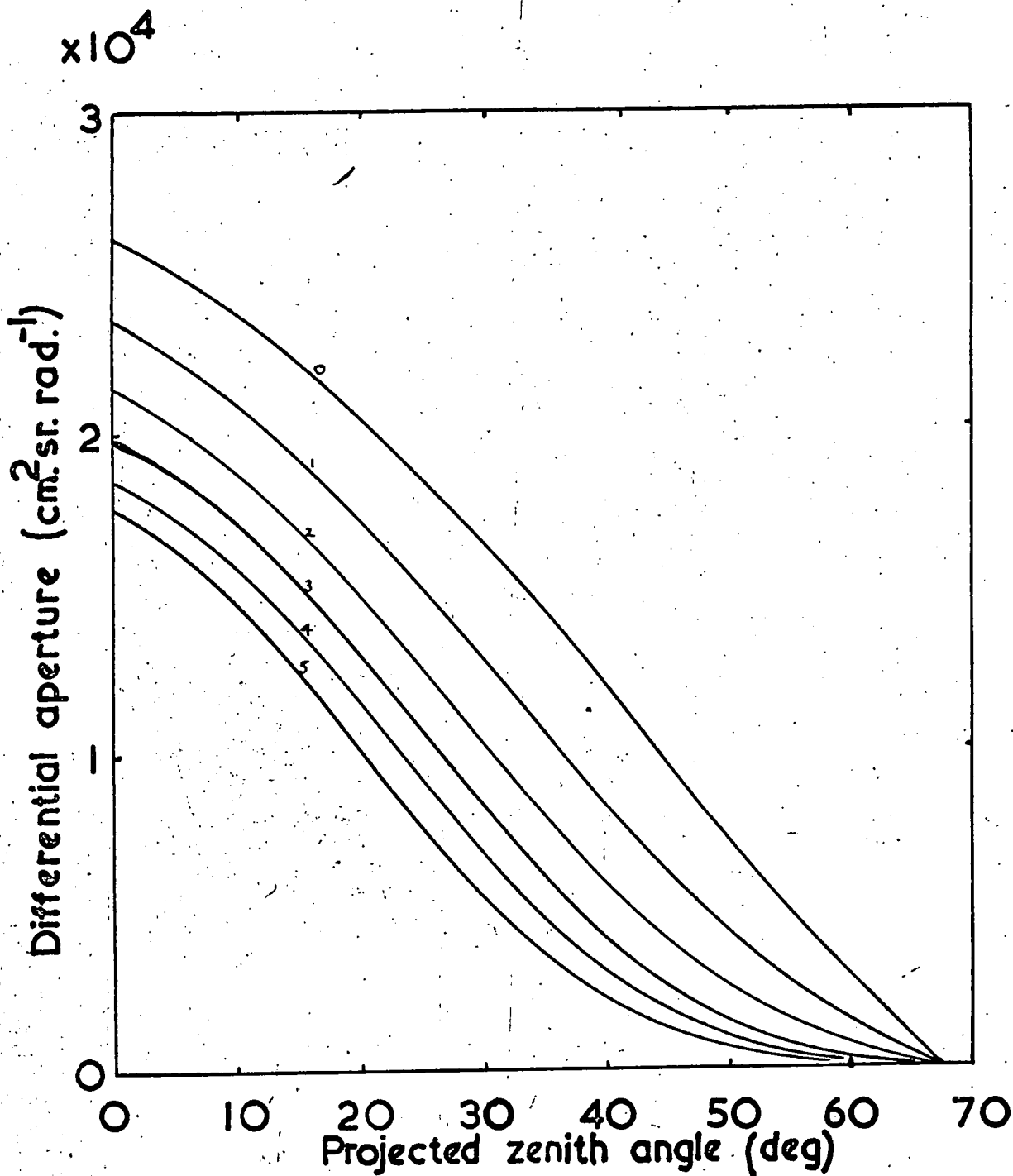


Fig.3.5 The telescope acceptance functions with n as parameter.

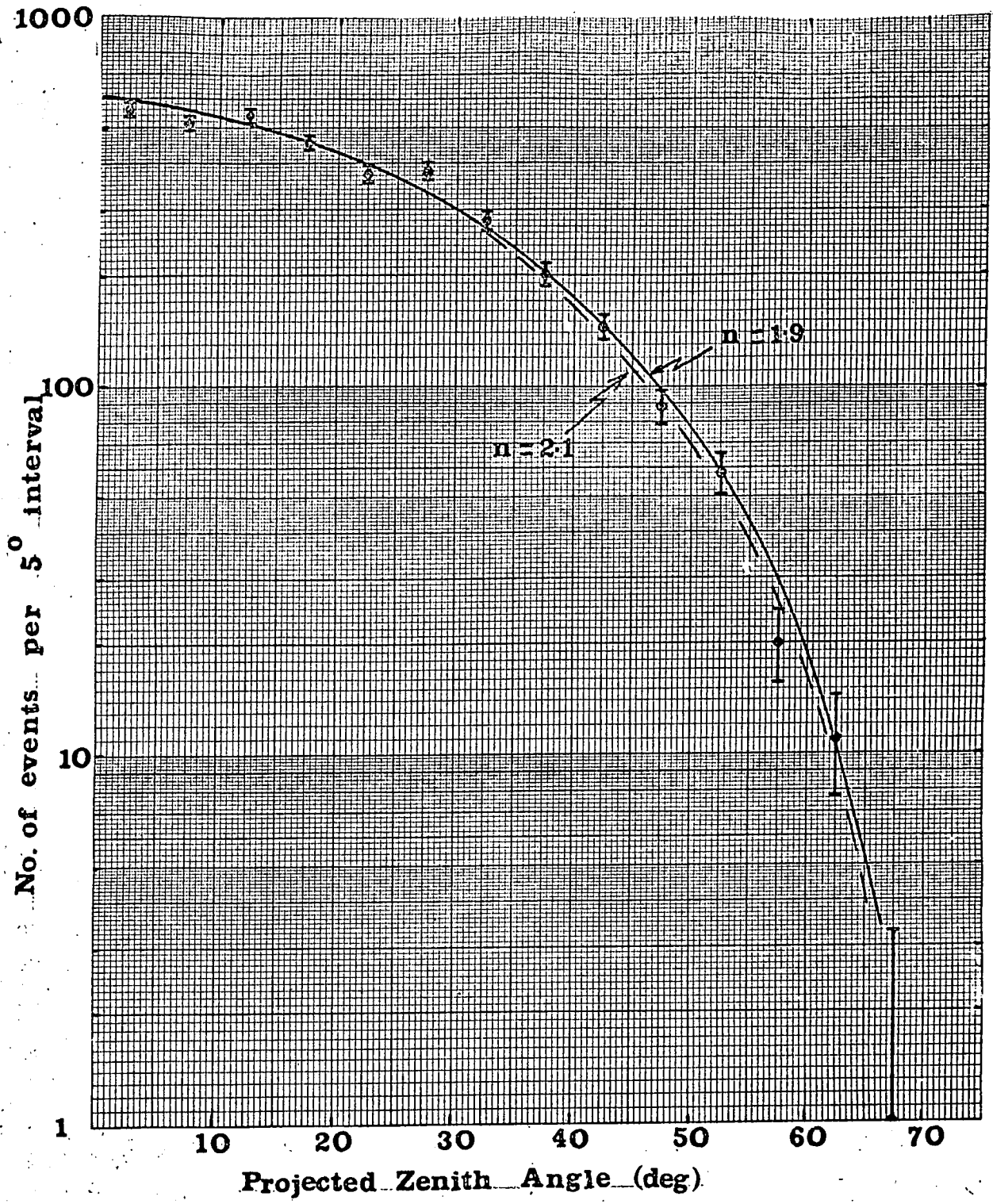


Fig. 4.1. The projected zenith angular distribution of single muons at 816m.w.e.

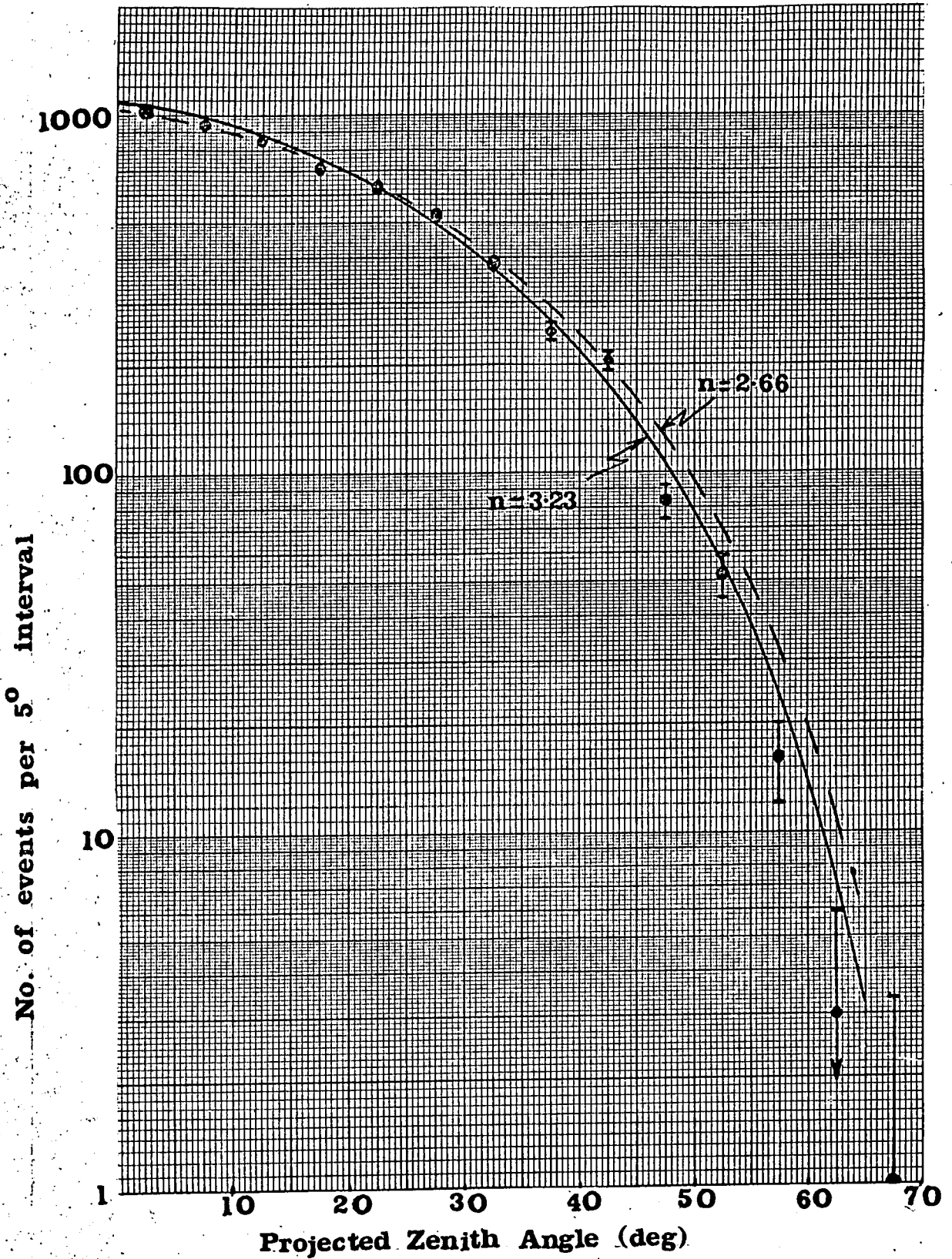


Fig. 4.2. The projected zenith angular distribution of single muons at 1812 m.w.e.

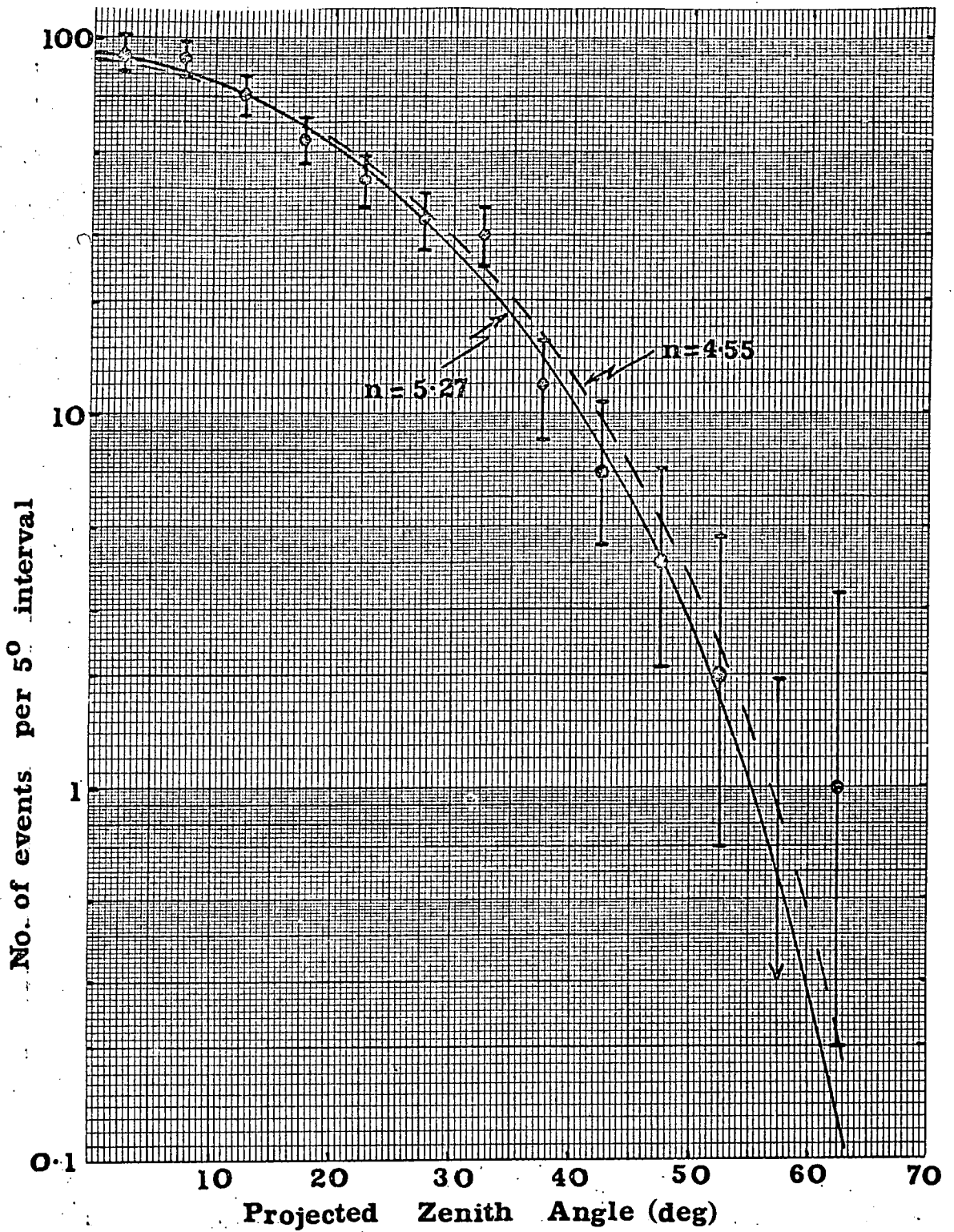


Fig.4.3. The projected zenith angular distribution of single muons at 4110 m.w.e.

CHAPTER 4.

THE ANGULAR DISTRIBUTION OF MUONS UNDERGROUND.

4.1. Derivation of the Exponent, n .

The experimental data shown in Figs.3.1 - 3.3 was folded over in order to obtain the frequency distribution for the projected angles at each depth (Figs.4.1 - 4.3). The Durham Elliott 803 computer was programmed to evaluate the equations for $N_n(\theta)$ shown in Table 3.2, normalize them to the experimental data and derive the relationships between the normalization factor, N^* , and the exponent, n , and between $N_n(\theta)$ and n . Over the range of values of n considered these two relationships are linear of the form $y = ax + b$.

The computer then subjected the experimental data for each depth to a chi-squared test over a selected range of values for the exponent.

4.2. Corrections for "Noise".

In order to allow for errors ("noise") in determining the projected zenith angle a sample of events was rescanned by an independent observer and a histogram plotted of the differences in angle measured by the two observers. This distribution is shown in Fig. 4.4. It was found that the mean total measuring error was $\pm 1.5^\circ$.

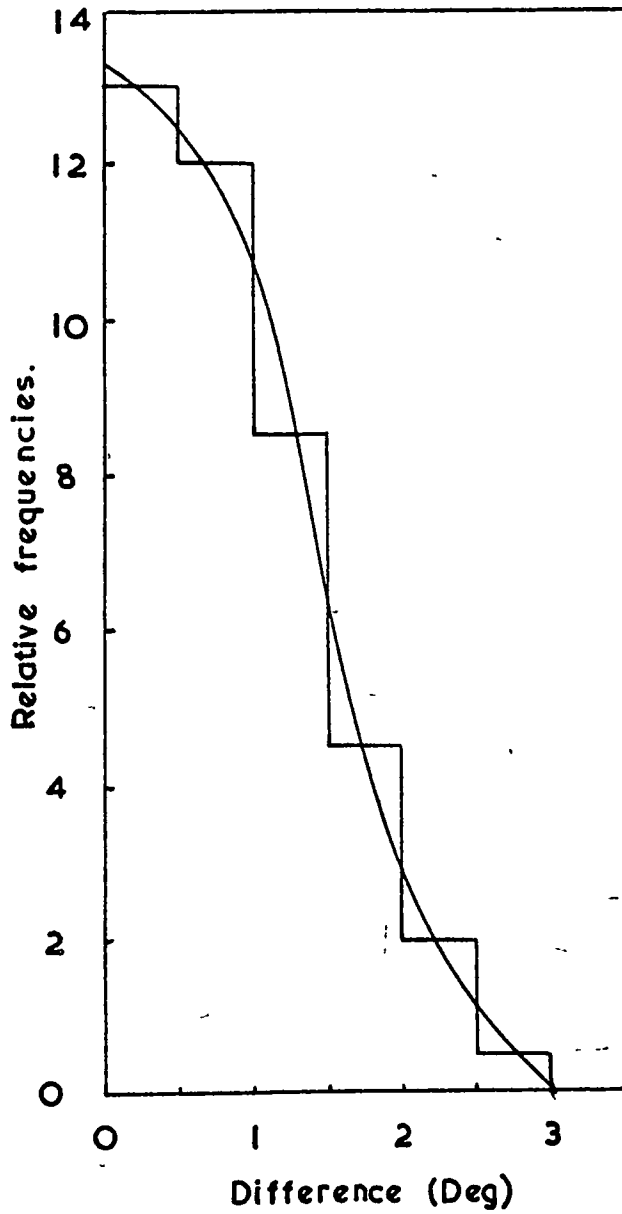


Fig.4.4 Distribution of differences between successive measurements.

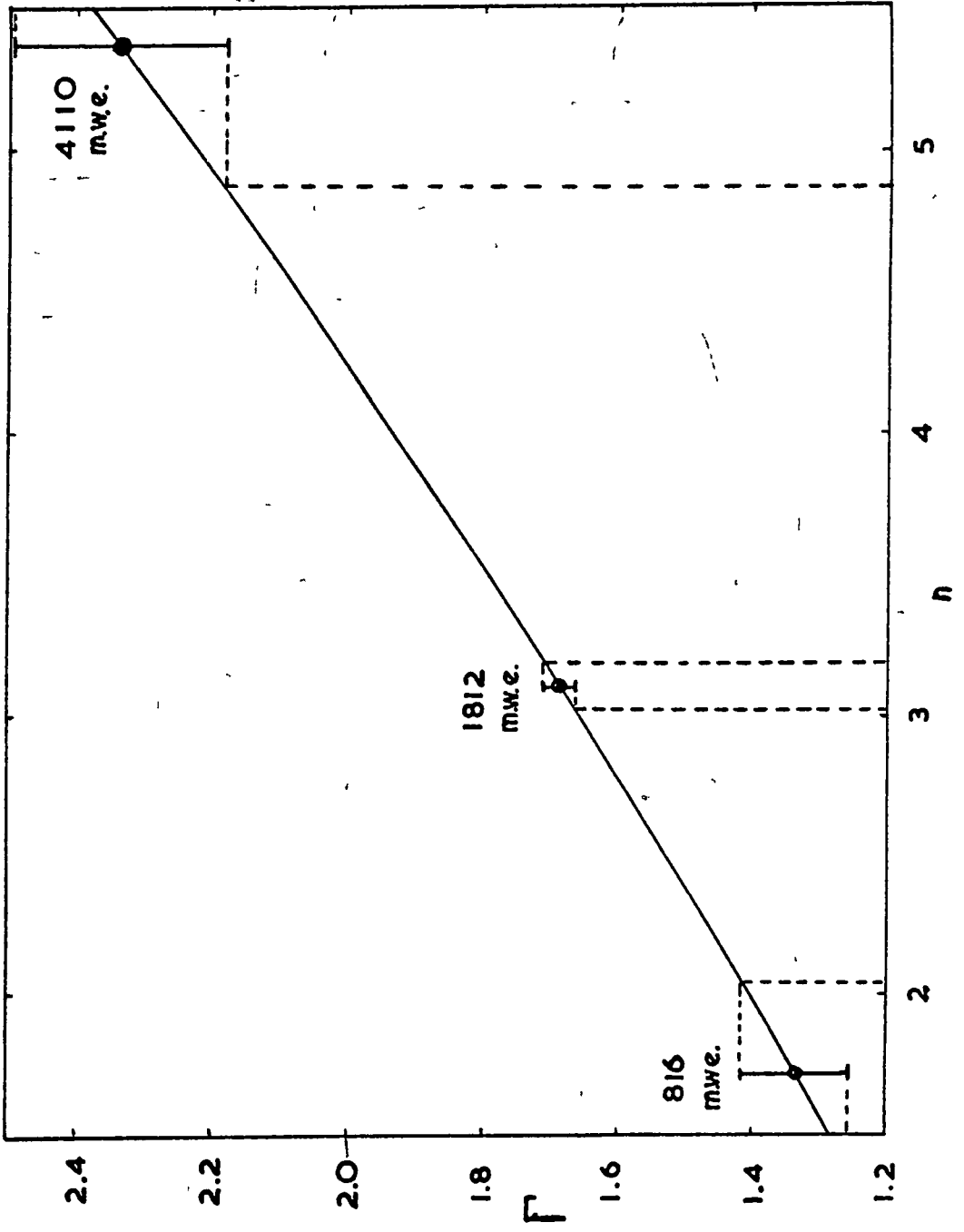


Fig.4.5 The variation of Γ with n

If δ is the error in measurement, then the true standard deviation, σ_0 , is related to the observed standard deviation, σ , by

$$\sigma_0^2 = \sigma^2 - \delta^2$$

For each depth the variation of σ with n was plotted and the slope $\frac{\partial n}{\partial \sigma}$ at the best fit value of n determined. Thus the correction, Δn , to be applied to n for each depth is given by

$$\Delta n = \frac{1}{2} \sigma \left(\frac{\delta}{\sigma} \right)^2 \frac{\partial n}{\partial \sigma}$$

The error in n was calculated from the Γ distribution as a function of n shown in Fig. 4.5 where Γ is the ratio of the predicted number of events having zenith angle less than 20° to the number having angle greater than 20° . The observed values of $\Gamma \pm \delta\Gamma$ were plotted on the theoretical distribution and the points of intersection of the error of the observed value of Γ indicate the error in n . The computed values of n and the values corrected for noise are shown in Table 4.1. The angular distributions for the best fit values of n at the three depths of observation are plotted in Figs. 4.1 - 4.3. The application of the measured values of the angular exponents to the problem of determining the vertical intensity will be considered later.

Depth below top of the atmosphere (m.w.e.)	816	1812	4110
Depth of rock corrected to $Z^2/A = 5.5$ (m.w.e.)	818	1870	4360
Number of events used to evaluate n	3624	5750	435
Number of events used to evaluate the Vertical Intensity (I_v)	3624	4499	435
Corrected running time (sec)	1.496×10^5 (1 unit)	1.324×10^6 (2 units)	7.358×10^6 (2 units)
Cut off angle (θ_c)(deg)	60	60	60
n (uncorrected for noise)	1.90 ± 0.33	3.23 ± 0.10	5.27 ± 0.50
n (corrected for noise)	1.92 ± 0.33	3.26 ± 0.10	5.33 ± 0.50
n ('theoretical')	2.10	2.66	4.55
	$(2.29 \pm 0.09) \times 10^{-6}$		$(4.47 \pm 0.34) \times 10^{-9}$
I_v ($\text{cm}^{-2} \text{sr}^{-1} \text{sec}^{-1}$)		$(1.98 \pm 0.05) \times 10^{-7}$	
I_v (from OPW Spectrum) ($\text{cm}^{-2} \text{sr}^{-1} \text{sec}^{-1}$)	2.09×10^{-6}	1.5×10^{-7}	3.9×10^{-9}

Table 4.1

THE EXPERIMENTAL RESULTS.

<u>Depth (m.w.e.)</u>	<u>Vertical Intensity (cm⁻²sr⁻¹sec⁻¹)</u>
200	6.90 x 10 ⁻⁵
300	2.80 x 10 ⁻⁵
450	1.10 x 10 ⁻⁵
500	8.30 x 10 ⁻⁶
700	3.33 x 10 ⁻⁶
1000	1.22 x 10 ⁻⁶
1500	3.40 x 10 ⁻⁷
2000	1.17 x 10 ⁻⁷
2500	5.20 x 10 ⁻⁸
3000	2.32 x 10 ⁻⁸
4000	6.33 x 10 ⁻⁹
5000	1.90 x 10 ⁻⁹
6000	5.82 x 10 ⁻¹⁰
7000	1.70 x 10 ⁻¹⁰
8000	9.20 x 10 ⁻¹¹

Table 4.2 THE OPW BEST ESTIMATE INTENSITY-DEPTH
SPECTRUM.

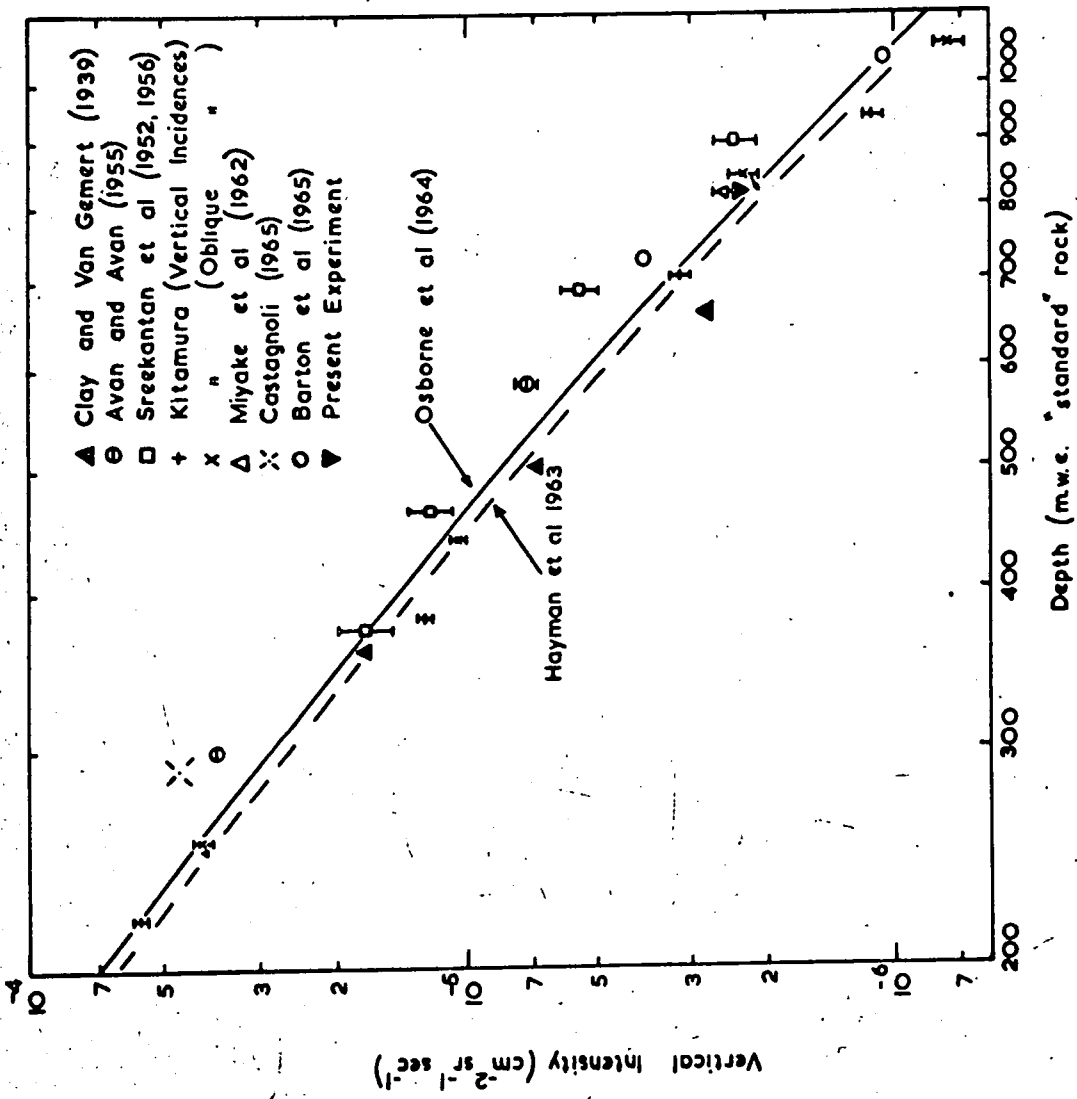
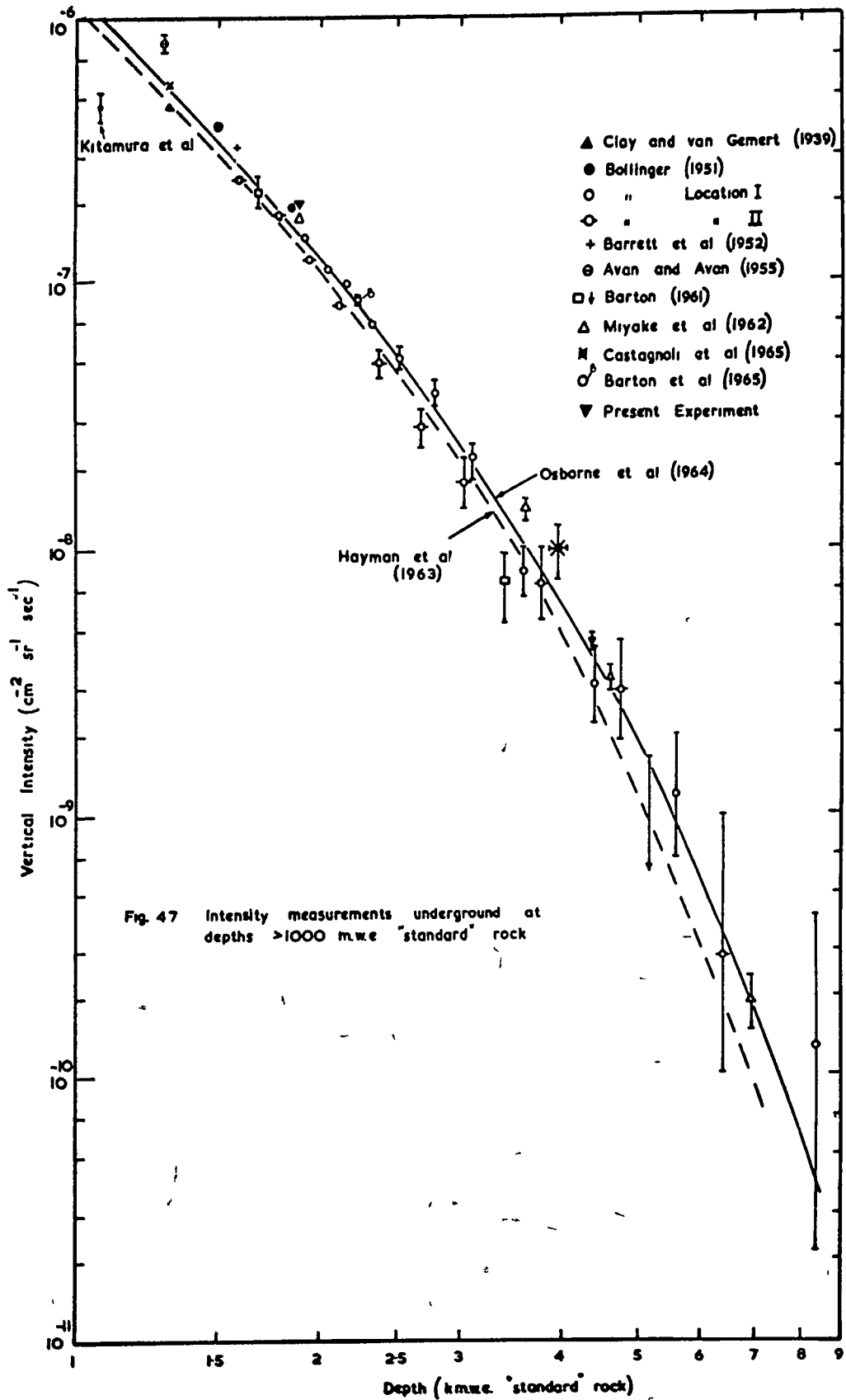


Fig. 4.6 Intensity measurements underground in the range 200 - 1000 m.w.e. "standard" rock



There follows now a comparison with other derivations of n .

4.3. The Theoretical Value of n as a function of Depth.

The variation of n with depth can be predicted from previous measurements of the variation of I_v with depth if allowance is made for the increase in intensity arising from enhanced decay of the parents of muons (pions and kaons, Section 1.2) in the atmosphere. The predicted values of n will be referred to as "theoretical" values.

Following Barrett et al (1952) we can define $n = m - \delta$, where m is the logarithmic derivative of the intensity-depth curve (i.e. $m = - \frac{\partial \ln I}{\partial \ln D}$, where I is the vertical intensity at a depth D), and δ arises from the enhancement factor (which depends on the K/π ratio).

A summary of the best estimate of the integral energy spectrum in the vertical direction at sea-level has been given by Osborne et al (1964). This will be referred to as the OPW spectrum. Taking the results of all previous underground intensity measurements Hayman et al and Osborne et al have given the best estimate of the intensity-depth spectrum for "standard" rock ($Z^2/A = 5.5$) in the range 100 - 10,000 m.w.e. (Figs. 4.6, 4.7 and Table 4.2). The resulting variation

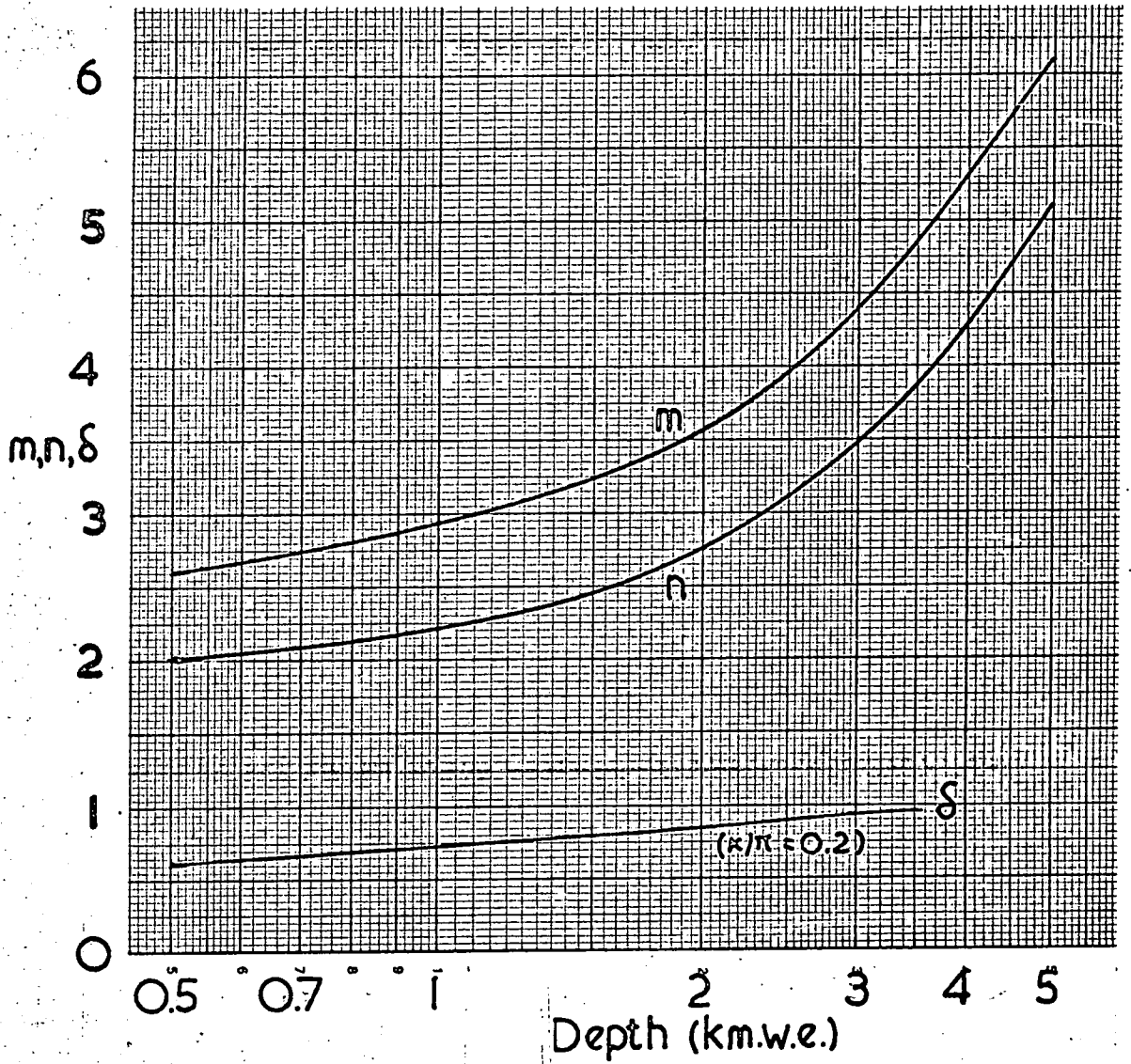


Fig.4.8 The variation of m, n, δ with depth.

of μ with depth is shown in Fig. 4.8. Osborne and Wolfendale (1964) have combined all the available measurements of the energy spectra of electromagnetic cascades in the cosmic radiation to predict the muon spectrum at sea-level on the basis of all pions or all K-mesons as the source of the cascades and muons. They compared these spectra with the muon spectrum measured directly with magnet spectrographs and, at higher energies, inferred from the underground depth-intensity measurements. By interpolation they derived the ratio of production of K-mesons to π -mesons (K/ π ratio) in high energy interactions to be $(20 \pm 20)\%$ at 2×10^4 GeV, through $(10 \pm 15)\%$ at 7×10^4 GeV to $(40 \pm 30)\%$ at 6×10^5 GeV. The best estimate indicated for the K/ π ratio is about 20% over the primary energy range $10^2 - 10^6$ GeV.

The effect of the K/ π ratio on the theoretical value of μ was therefore determined for three values of the ratio, namely zero, 0.2 and infinity. The method adopted in the determination of this effect was as follows.

On the basis that muons are the progeny of pions only, the muon differential energy spectrum at production, $M(\epsilon, \theta)$, at a zenith angle, θ , is given by the following expression:

$$M_{\pi}(E, \theta) = \frac{F_{\pi}(E/r)}{r} \cdot \frac{\lambda_{\pi}}{\lambda_p} \cdot \frac{B_{\pi}(\theta)}{E} \sum_{n=0}^{\infty} \frac{(-\lambda_{\pi}/\lambda')^n}{(n+1) + B_{\pi}(\theta)/E} \quad (4.1)$$

after Barrett et al (1952), where

E is the muon energy at production,

$$r = \frac{\text{mass of muon}}{\text{mass of pion}}$$

$F_{\pi}(E/r)$ is the pion differential energy spectrum at production,

λ_{π}, λ_p are the absorption mean free paths for pion and non-pion producers of pions respectively,

$B_{\pi}(\theta)$ is a function of zenith angle and is given by the relation $B_{\pi}(\theta) = B(x/\rho)_{\theta} / 6.36$ where $\rho \text{ gm.cm}^{-3}$ is the density of the atmosphere at a depth $x \text{ gm.cm}^{-2}$, and

$$(\lambda')^{-1} = \lambda_p^{-1} - \lambda_{\pi}^{-1}$$

If $\lambda_p = \lambda_{\pi}$, a fact which is justified in the reviews by Sitte (1961) and Perkins (1961), the equation 4.1 simplifies to the form

$$M_{\pi}(E, \theta) = F_{\pi}(E/r) \cdot r^{-1} [1 + E/B_{\pi}(\theta)]^{-1} \quad (4.2)$$

The corresponding relation for the vertical muon differential energy spectrum at production is

$$M_{\pi}(E, 0) = F_{\pi}(E/r) \cdot r^{-1} [1 + E/B_{\pi}(0)]^{-1} \quad (4.3)$$

and the ratio, R , of these spectra is given by

$$R = \frac{M_{\pi}(E, \theta)}{M_{\pi}(E, 0)} = \frac{1 + E/B_{\pi}(0)}{1 + E/B_{\pi}(\theta)} \quad (4.4)$$

<u>Depth</u> <u>(m.w.e.)</u>	<u>m</u>	<u>n</u> <u>(K/π = 20%)</u>	<u>δ</u> <u>(K/π = 20%)</u>
500	2.60	2.00	0.60
700	2.75	2.08	0.67
1000	2.93	2.20	0.73
2000	3.56	2.75	0.81
3000	4.41	3.47	0.94
5000	6.10	5.10	1.00

TABLE 4.3. - THE 'THEORETICAL' VALUES OF m, n, δ,
AS A FUNCTION OF DEPTH.

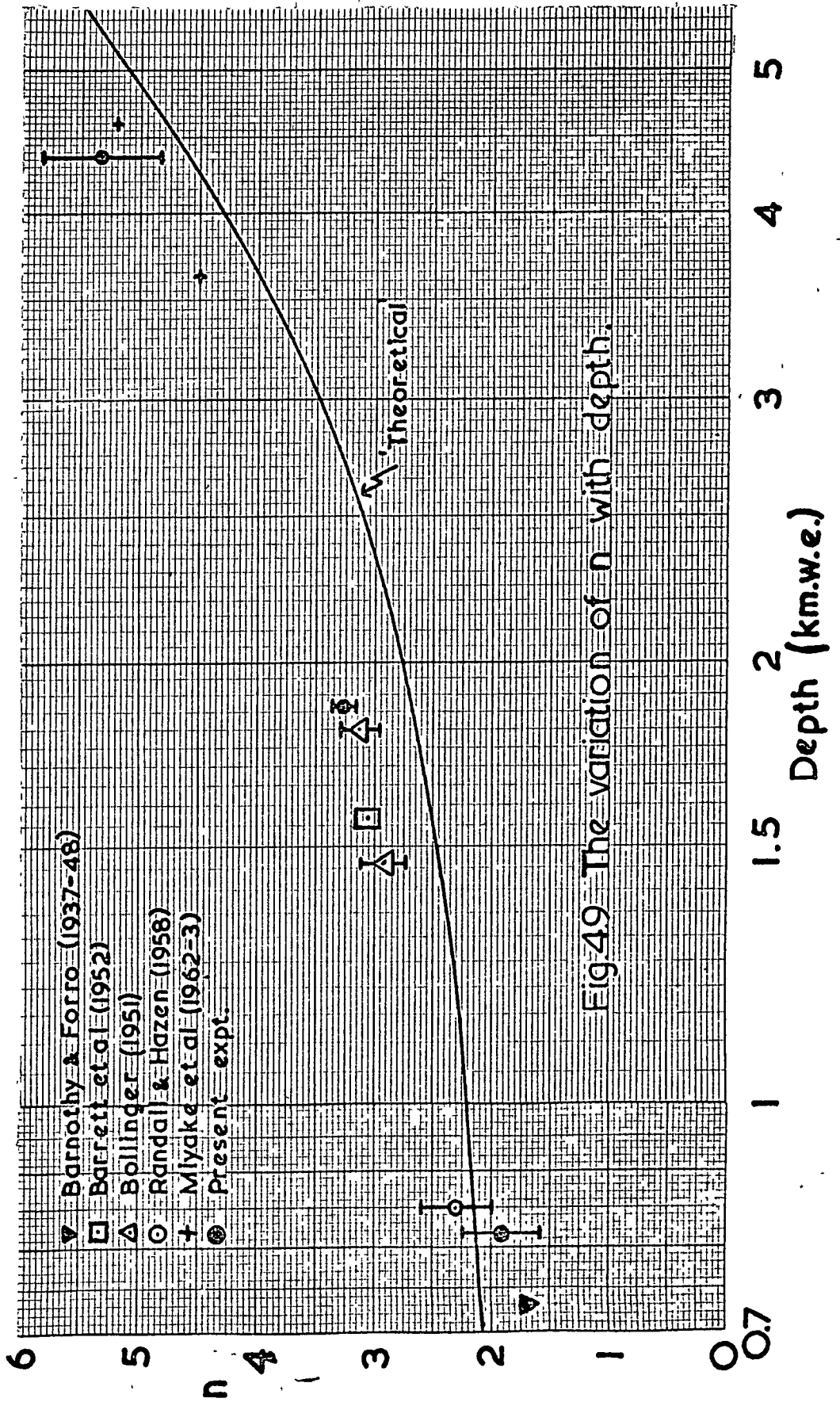


Fig-49 The variation of n with depth.

The ratio, R , was evaluated for various values of zenith angle as a function of the minimum energy a muon required to penetrate to various selected depths. At any depth, in particular the depths of the three observation levels, the value of n is known from the intensity-depth relation (from the OPW spectrum), and hence the function $R \cos^m \theta$ can be determined. The slope of this function gives the theoretical value of n and hence δ . A similar procedure gives the corresponding values of n and δ for $K/\pi = 0.2$ and infinity.

The theoretical variations of n and δ as a function of depth are shown in Fig. 4.8, and are tabulated in Table 4.3 for the three depths of operation. The angular distributions for the predicted values of n are shown in Figs. 4.1 - 4.3. Fig. 4.9 shows the observed values of n and the theoretical variation with depth, together with the results of other workers; the experiments giving these results will be discussed in the next section before a detailed comparison is made.

4.4. Measurements of 'n' by other workers.

4.4.1. The range of depth to be considered.

Only a few workers have measured the angular distribution of muons underground, and discussion will be confined to those measurements at depths greater than about 500 m.w.e.

4.4.2. Barnóthy & Forró (1937 - 1948).

In 1936 these workers operated a 3-fold coincidence geiger counter telescope at a depth of 730 m.w.e. in the Dorog Coal mines near Budapest. The telescope was operated, without any absorbing material present, over the zenith angular range 0° to 90° . Rough corrections were applied for the electron showers by subtracting the rate recorded with the telescope horizontal. Their results approximated a power law, $\cos^n \theta$, with $n = 1.7$. It is generally accepted that the presence of absorbing materials are essential features of underground detectors since the numerous secondary electrons far underground must cause large errors in the measured intensity and the zenith angular variation. Barrett et al. concluded that the results of Barnóthy and Forró would be affected by the presence of secondary electrons giving a reduction in the variation of counting rate with zenith angle and that their results would consequently indicate too low a value of n .

4.4.3. Randall & Hazen (1951, 1958). A geiger counter telescope comprising two layers ($25 \times 70 \text{ cm}^2$) of counters separated by 15 cm. of lead was operated at a depth of 850 m.w.e. in a Detroit Salt Mine. The lower tray of counters was shielded on all sides by lead.

As a means of determining the angular distribution and the absolute intensity the tray separation was varied rather than varying the telescope orientation. It should be pointed out that the 1951 letter seems to have been rescinded in the 1958 paper, (the results published in 1951 gave $n = 2.8 \pm 0.1$ and $\bar{I}_V = (2.17 \pm 0.02)10^{-6}$ $\text{cm}^{-2} \cdot \text{sr}^{-1} \cdot \text{sec}^{-1}$), thus the remainder of this section will be concerned with the 1958 results.

It was found that as the vertical separation of the geiger counter trays was increased (the maximum separation being 61 cm.) the gross two-fold rate and therefore meson flux decreased. The best fit to the relation $I(\theta) = \bar{I}_V \cos^n \theta$ was found to correspond to

$$n = 2.3 \pm 0.3$$

$$\text{and } \bar{I}_V = (2.1 \pm 0.5)10^{-6} \text{ cm}^{-2} \cdot \text{sr}^{-1} \cdot \text{sec}^{-1}.$$

The conclusions regarding parentage of the muons favoured an admixture of K-mesons with pions.

4.4.4. Bollinger (1950-1). Two concentric cylinders of geiger counters separated by a cylinder of lead 6 cm. in radial thickness were operated at depths of 1500 and 1840 m.w.e. (Mean $Z^2/A = 5$). In addition, there was a central core of lead of diameter 20 cm. within the innermost ring of counters. The triggering requirement was that a particle should penetrate both

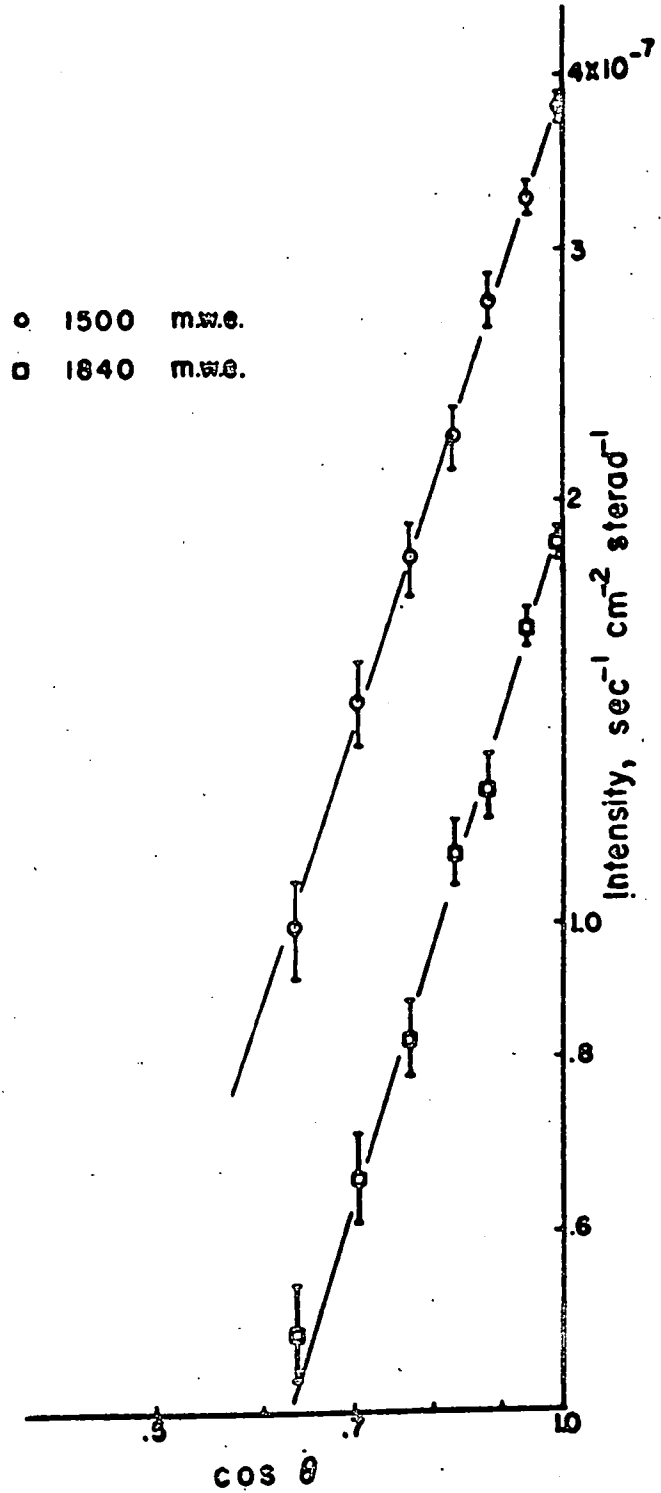


Fig.4.10 The observations of Bollinger (1950-1)

counter arrays and discharge at least two counters in each array. The resulting coincidences were hodoscoped, and the experimental results obtained are shown in Fig. 4.10. The best fit values for n and \bar{I}_V at the two depths of operation are :

Location I (1840 m.w.e.)

$$n = 3.13 \pm 0.17$$

$$\bar{I}_V = 1.91 \times 10^{-7} \text{ cm}^{-2} \cdot \text{sr}^{-1} \cdot \text{sec}^{-1}.$$

Location II (1500 m.w.e.)

$$n = 2.93 \pm 0.19$$

$$\bar{I}_V = 3.90 \times 10^{-7} \text{ cm}^{-2} \cdot \text{sr}^{-1} \cdot \text{sec}^{-1}.$$

In addition, the intensities for greater depths were inferred from the angular distribution. These will be discussed in Chapter 6.

4.4.5. Barrett et al (1952). The apparatus used by the Cornell group at a depth of 1574 m.w.e. is shown in Fig. 4.11. The geiger counter trays B and D were at right angles to the other trays, and a master pulse was generated whenever a four-fold coincidence, ABCD, occurred. This pulse was put in coincidence with each counter in these trays and in E_1 , and a photographic record obtained showing which counters had been discharged. Coincident pulses in E_2 were similarly registered, except that for economy these counters were

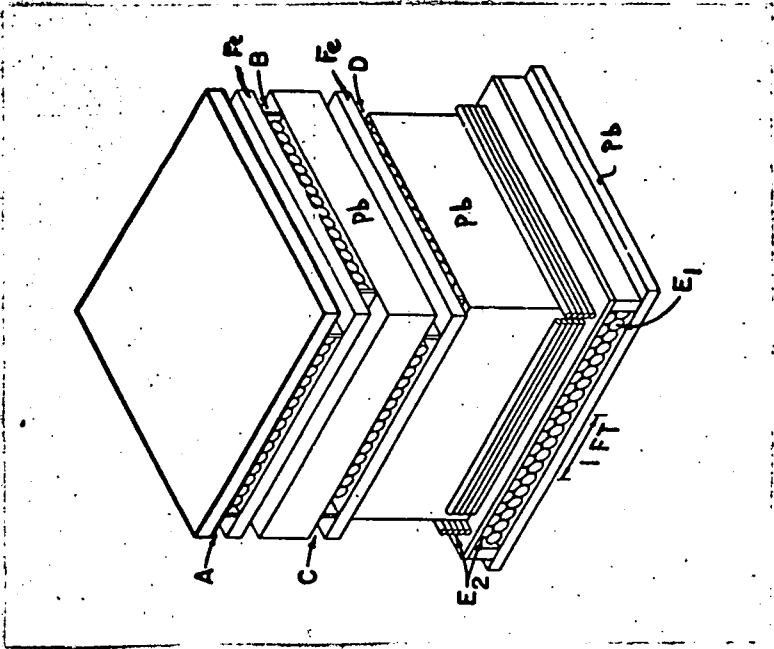


Fig.4.11 The apparatus of Barret et al.

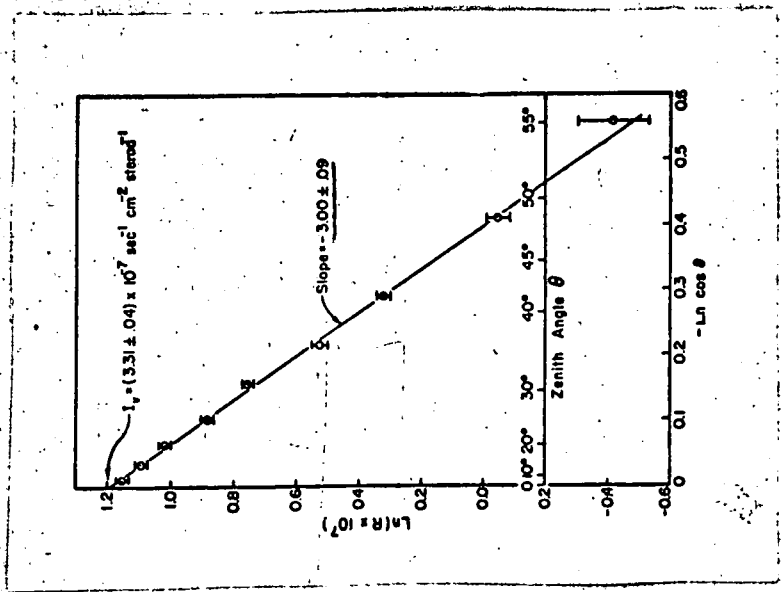


Fig.4.12 The experimental results of Barrett et al. at 1574 m.w.e.

grouped into only thirteen independent channels. The resolving time of the apparatus was such that chance coincidences were negligible. Layers of lead and iron were placed above the top tray and between the first four trays, A-D, in order to absorb the electron component. Electrons generated in a layer immediately above any counter tray would usually remain close to the path of the penetrating particle, thus minimizing errors in the inferred path. The lead under the bottom tray reduced the background counting rate due to gamma-rays from the rock, and protected against electrons scattered up from the floor. The thickness of the lead between D and E was varied during the course of the experiment.

Most of the hodoscope photographs showed simple events in which only one (or occasionally two adjacent) counter was struck in each of trays, A, B, C, & D. In these cases the direction of the track could be determined within about seven degrees. The resolution improved with increasing inclination to the vertical.

Of 18,499 photographs, only 2% could not be classified as to zenith angle. Fig. 4.12 shows the variation with intensity of the penetrating particles at a depth of 1574 m.w.e. It is seen that the experimental points agree well with a straight line expressing

a power law of the form $\bar{I}(\theta) = \bar{I}_v \cos^n \theta$. A least-squares fit yielded the following results :

$$n = 3.00 \pm 0.09$$

$$\bar{I}_v = (3.31 \pm 0.04) 10^{-7} \text{ cm}^{-2} \cdot \text{sr}^{-1} \cdot \text{sec}^{-1}.$$

On correcting for the error due to secondary electrons ($\sim 2\%$ near the vertical direction) and the error due to the effective area decreasing with increasing zenith angle ($\sim 4\%$ near $\theta = 45^\circ$) the following results were obtained :

$$n = 3.06 \pm 0.10$$

$$\bar{I}_v = (3.25 \pm 0.05) 10^{-7} \text{ cm}^{-2} \cdot \text{sr}^{-1} \cdot \text{sec}^{-1}.$$

---o0o---

CHAPTER 5.

THE VARIATION OF VERTICAL INTENSITY WITH DEPTH.

5.1. The Measured Vertical Intensity.

Having determined the best fit value of the angular distribution exponent, n , it is relatively easy to derive the vertical intensity. The following simple expression is used to determine the vertical intensity :

$$I_v = \frac{57.296}{5} \cdot \frac{N_n^*}{\tau \eta} \cdot \frac{1}{u} \text{ cm}^{-2} \text{ sr}^{-1} \text{ sec}^{-1}$$

where 57.296 is the factor converting degrees to radians,

5 takes into account the fact that the angular distributions are plotted as number of particles/ 5° Vs. zenith angle,

N_n^* is the normalization factor used when fitting the acceptance to the observed histograms, and is obtained from the computer analysis,

τ is the running time at a given depth corrected for the inherent dead time of 7 seconds per event,

η is the geiger counter efficiency, and

u represents the number of telescopes operated simultaneously at a given depth. ($u = 1$ for 816 m.w.e., and 2 for 1812 m.w.e. and 4110 m.w.e.)

The geiger counter efficiency was measured at

816 m.w.e. by operating each telescope successively under conditions of three-fold photomultiplier coincidence and normal four-fold coincidence selection. These events were photographed as usual and, correcting for dead time, the efficiency was found to be 93.6%. The calculated values of the vertical intensity are shown in Table 4.1.

5.2. Measurements of Underground Vertical Intensities By Other Workers.

A number of experiments have been carried out during the past thirty years to measure the intensity of cosmic rays at depths greater than 100 m.w.e. Since the review articles by Barrett et al (1952) and George (1952), measurements have been reported by Avan and Avan (1955), Sreekantan et al (1952, 1956), Barton (1961), Miyake et al (and Ramanamurthy) (1962, 1963), Kitamura et al (private communication, 1964) and Castagnoli et al (1964, 1965). A review article on Cosmic Rays Underground has recently (1965) been submitted for publication by Menon and Ramanamurthy. Only the most recent of these experiments will be described here in any detail.

5.2.1. Barton (1961). A block of plastic phosphor scintillator ($53 \times 15 \times 3 \text{ cm}^3$) viewed by two photomultipliers was placed between two layers of four geiger counters of similar total area. A fast

coincidence ($0.1 \mu s$) between the photomultipliers was demanded to obviate spurious counts. The requirement to generate a master pulse was a coincidence ($3 \mu s$) between the fast coincidence from the photomultipliers and the two layers of geiger counters. A ringing coil type pulse height analyser measured the magnitude of the pulses from the last dynodes of the two photomultipliers, and the damped oscillation of a tuned circuit, excited by the incoming pulse, was amplified and passed into a discriminator which triggered once each cycle until the oscillation decayed below a certain fixed level. Thus a chain of pulses whose number was proportional to the logarithm of the height of the original pulse was produced. This number was converted into binary form and, together with the hodoscope data from the geiger counters, was recorded on fourteen tracks on magnetic tape. The width of each channel was proportional to the pulse height accepted by it.

The apparatus was operated at 2000, 3950 and 6075 feet underground in the Lake Shore Gold Mine, Northern Ontario, Canada ($48^{\circ}9'N$, $80^{\circ}3'W$, 320 m.a.s.l.) The rock, mainly syenite-porphry, had density 2.73, $Z = 11.7$, $Z/A = 0.50$ yielding $Z^2/A = 5.85$.

The experimental results are shown in Table 5.1.

Depth ($Z^2/A = 5.85$) (m.w.e.)	Depth Corrected for $Z^2/A = 5.5$ (m.w.e.)	Vertical Intensity ($\text{cm}^{-2} \text{sr}^{-1} \text{sec}^{-1}$)
1660	1675	$(2.22 \pm 0.29) \times 10^{-7}$
3280	3380	$(7.54 \pm 2.30) \times 10^{-9}$
5050	5150	$< 1.64 \times 10^{-9}$

TABLE 5.1. - THE RESULTS OF BARTON (1961).

Comparison of the events recorded at 3950 feet with an earlier 3-fold geiger telescope experiment (Barton and Michaelis, 1961) showed that some events were due to γ -radiation from the surrounding rock. A similar analysis showed that all the events recorded at 6075 feet could be attributed to the effects of γ -radiation and that there was no evidence of cosmic rays in the 21 days that the apparatus was operated at this depth. Thus it was possible to deduce an upper limit to the muon intensity at this depth. Moreover an upper limit to the rate expected from the interactions of anti-neutrinos could also be set (Barton, 1960) but ~~that~~ no definite conclusions about this could be drawn.

5.2.2. Miyake et al (1962,1963). A series of experiments was carried out in 1961-2 by the Bombay group to measure the intensity of cosmic rays underground in the Kolar Gold Field, India, at various depths between 816 m.w.e. and 8400 m.w.e.

The apparatus comprised two layers of plastic scintillator, each having an area 1.62 m^2 and thickness 5 cm., separated by a distance of 34 cm. Between the scintillators, which were each viewed by two Dumont 6364 photomultipliers, there was a layer of lead 5 cm. thick surmounted by a layer of geiger counters. These were used

<u>Depth</u> <u>($Z^2/A=6.33$)</u> <u>(m. w. e.)</u>	<u>Depth corrected</u> <u>for $Z^2/A=5.5$</u> <u>(m. w. e. rock)</u>	<u>n</u>	<u>Vertical Intensity</u> <u>($\text{cm}^{-2} \text{sr}^{-1} \text{sec}^{-1}$)</u>
816	818	2.3	$(2.51 \pm 0.15) \times 10^{-6}$
1812	1870	3.1	$(1.77 \pm 0.07) \times 10^{-7}$
3410	3625	4.5	$(1.42 \pm 0.12) \times 10^{-8}$
4280	4600	5.2	$(3.24 \pm 0.29) \times 10^{-9}$
6380	6900	6.6	$(1.92 \pm 0.45) \times 10^{-10}$
8400	9200	?	$< 10^{-11}$

Table 5.2 THE EXPERIMENTAL RESULTS OF MIYAKE ET AL. (1962 - 64).

only at 6380 m.w.e. and 8400 m.w.e. where it was felt that the chance rate for scintillators alone might have been too high. Consequently the separation of the scintillators was only 25 cm. at depths shallower than 6380 m.w.e.

Each scintillator was viewed by two photomultipliers from a distance of 70 cm., and the selection criterion was a coincidence between the pulses from all four photomultipliers and the geiger counters (where applicable). The resolving time of the apparatus was 2 μ s, and there were two such telescopes, the second one having an area of 1.49 m². Both telescopes were operated side by side at 6380 m.w.e. and 8400 m.w.e.

For each event, a panel, showing the time, date, 4-fold and 5-fold coincidences and the neons of the geiger counter hodoscope, was photographed.

The experimental results are shown in Table 5.2. It is of special interest to note that no counts were recorded in 2880 hours at 8400 m.w.e. Thus only upper limits can be put to the atmospheric muon intensity and the intensity of muons produced locally by neutrino interactions in the surrounding rock.

5.2.3. Kitamura et al (1964). The Osaka City University, Japan, group has recently (October, 1964) concluded a series of intensity measurement under sea

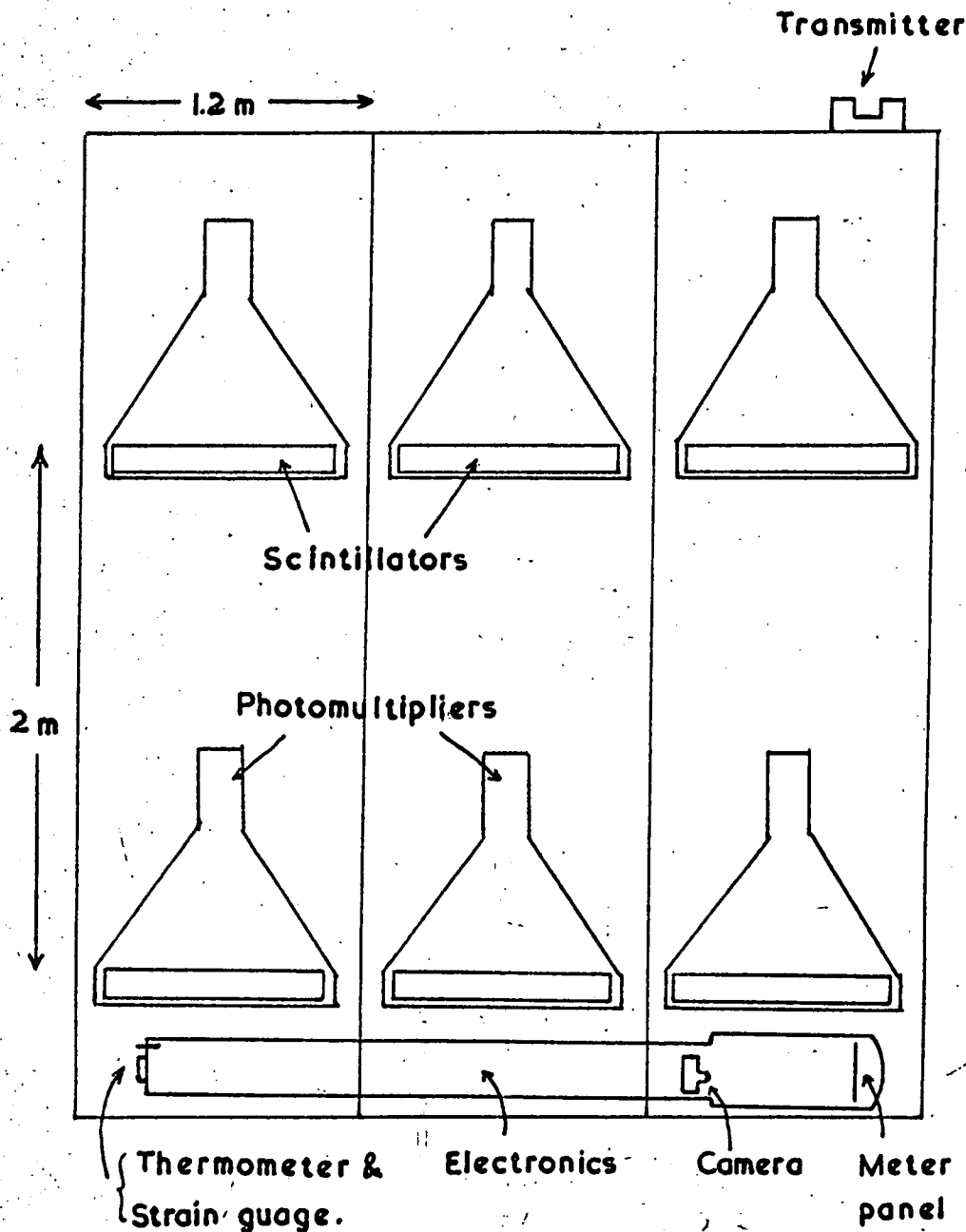


Fig.5.1 The apparatus of Kitamura et al (1964)

Effective Depth (m)	Depth Corrected for $Z_2/A=5.5$ (m.w.e.)	Vertical Incidences ($\text{cm}^{-2} \text{sr}^{-1} \text{sec}^{-1}$)	Oblique Incidences ($\text{cm}^{-2} \text{sr}^{-1} \text{sec}^{-1}$)
220	220	$(5.61 \pm 0.20) 10^{-5}$	$(4.07 \pm 0.20) 10^{-5}$
380	380	$(1.25 \pm 0.05) 10^{-5}$	$(1.04 \pm 0.04) 10^{-5}$
715	705	$(3.20 \pm 0.20) 10^{-6}$	$(2.29 \pm 0.19) 10^{-6}$
960	940	$(1.12 \pm 0.07) 10^{-6}$	$(7.50 \pm 0.60) 10^{-7}$

TABLE 5.3. - THE EXPERIMENTAL RESULTS OF KITAMURA ET AL (1964).

water ($Z = 7.433$, $Z/A = 0.553$, $Z^2/A = 3.76$). The apparatus comprised six plastic scintillators each $100 \times 100 \times 10 \text{ cm}^3$ disposed as shown in Fig.5.1, and was operated at various depths to a maximum of 960 m. The telescope was kept in position underwater by a float above containing oil and by weights below, and the whole was suspended from an anchored beacon ship. Each scintillator was viewed by a single 6364 Dumont photo-multiplier, and two types of two-fold coincidences were recorded :

(i) Vertical coincidences 1+4, 2+5 and 3+6;

& (ii) Oblique coincidences 1+5, 2+6, 3+5 and 2+4.

The coincidences in each channel were recorded by mechanical counters which were photographed after each two-fold pulse. A clock, thermometer, depth and level gauges were also photographed.

The experimental results are shown in Table 5.3. Since these results are not absolute, they have been normalized at 20 m.w.e. to the OPW spectrum (Osborne et al, 1964). The normalized results for depths greater than 200 m.w.e. are also shown in Table 5.3.

5.2.4. Castagnoli et al (1964-5). The completion of the Mt. Blanc road tunnel (1381 m.a.s.l.) has provided an easily accessible deep underground cosmic ray laboratory.

With a view to conducting a neutrino experiment, the vertical intensity of muons has been measured at various depths (to a maximum depth of 4100 m.w.e.) beneath the Mt. Blanc Massif.

The apparatus comprised two plastic scintillators ($70 \times 70 \text{ cm}^2$) separated by a distance of 2.5 m. each viewed by a single photomultiplier (58 AVP) in fast coincidence (resolving time 80 ns). The scintillators were 13 cm. in thickness in order to discriminate in amplitude the radioactive background ($E_{\text{max}} \sim 2 \text{ MeV}$) from the signals due to relativistic particles (energy loss $\sim 26 \text{ MeV}$). To discriminate any electrical noise the pulses from each photomultiplier were displayed on an oscilloscope and photographed at each coincidence. No coincidence pulses which could have been ascribed to electrical noise were observed in a running time of $7.7 \cdot 10^6$ seconds. In order to discriminate against noise due to electrons associated with the muon component a layer of lead of thickness 2 cm. or 6 cm. was placed between the scintillators. The counting rate of each photomultiplier and coincidence circuit was recorded automatically every 100 seconds. There were two such telescopes.

The mean density of the overlying rock is 2.60 gm.cm^{-3} , $Z/A = 0.494$ and $Z^2/A = 5.11$.

$\frac{Z^2}{A} = 5.11$ (m.w.e.)	Depth Corrected for $Z^2/A = 5.5$ (m.w.e.)	n	Vertical Intensity ($\text{cm}^{-2} \text{sr}^{-1} \text{sec}^{-1}$)
140	140	2	$(1.70 \pm 0.04) 10^{-4}$
290	290	2.2	$(4.60 \pm 0.01) 10^{-5}$
1325	1315	3	$(5.60 \pm 0.07) 10^{-7}$
4100 ± 110	3950 ± 100	5-6	$(1.00 \pm 0.23) 10^{-8}$

TABLE 5.4. - THE EXPERIMENTAL RESULTS OF CASTAGNOLI ET AL (1965).

The experimental results are summarized in Table 5.4.

5.2.5 The experiment of Barton et al (1965)

An experiment has been reported recently by these workers concerning measurements of the total intensity at various depths in a coal mine in Kent, England. The apparatus consisted of a combined scintillation and geiger counter telescope. The scintillator, comprising $90 \times 40 \times 4 \text{ cm}^3$ of NE102 plastic phosphor, was viewed from each end by two 2" diameter photomultipliers and was mounted between two layers of geiger counters. Each layer comprised 23 counters of diameter 3.7 cm. and length 40cm. Suitable biasing of the electronics eliminated spurious events due to background γ -radiation.

The experimental results are shown in table 5.5. The rate of events has been corrected for the angular distribution of muons underground, and normalized to unity at 60 m.w.e. The data has been analyzed by the present author in two ways. Firstly, the intensity-depth relation of Menon and Ramanamurthy (1965) has been extrapolated to sea-level and the vertical intensity at 60 m.w.e. rock ($4.95 \times 10^{-4} \text{ cm}^{-2} \text{ sr}^{-1} \text{ sec}^{-1}$) has been used to determine the intensities, $I_v(l)$, at the three greater depths. Secondly,

Depth (m.w.e. 'standard' rock)	60	724	1058	2225
Time (hr.)	0.516	20.42	143.8	1006
Events	4124	1124	2118	1123
Multiples (%)	18	18	23	28
Min. energy (GeV)	12.5	190	300	740
Rel. vertical intensity)	1.0	$(7.2 \pm 0.3)10^{-3}$	$(1.94 \pm 0.06)10^{-3}$	$(1.57 \pm 0.07)10^{-4}$
$I_V(60 \text{ m.w.e.})$		$5.4 \times 10^{-4} \text{ cm}^{-2} \text{ sr}^{-1} \text{ sec}^{-1}$		
$I_V(12.5 \text{ GeV})$		$4.95 \times 10^{-4} \text{ cm}^{-2} \text{ sr}^{-1} \text{ sec}^{-1}$		
$I_V(1) \text{ cm}^{-2} \text{ sr}^{-1} \text{ sec}^{-1}$)		$(3.89 \pm 0.16)10^{-6}$		$(8.48 \pm 0.38)10^{-8}$
)		$(1.05 \pm 0.03)10^{-6}$		
$I_V(2) \text{ cm}^{-2} \text{ sr}^{-1} \text{ sec}^{-1}$)		$(3.56 \pm 0.15)10^{-6}$		$(7.77 \pm 0.35)10^{-8}$
)		$(9.60 \pm 0.30)10^{-7}$		
$I_V(\text{OPW}) \text{ cm}^{-2} \text{ sr}^{-1} \text{ sec}^{-1}$		2.95×10^{-6}	1.00×10^{-6}	8.1×10^{-8}
$I(1)/I(\text{OPW})$		1.32 ± 0.05	1.05 ± 0.03	1.05 ± 0.05
$I(2)/I(\text{OPW})$		1.21 ± 0.05	0.96 ± 0.03	0.96 ± 0.04

Table 5.5 The results of Barton et al. (1965).

the vertical intensity at 12.5 GeV (the energy corresponding to 60 m.w.e.) has been found from the energy spectrum of Osborne et al. (1964). This is $5.4 \times 10^{-4} \text{ cm}^{-2} \text{ sr}^{-1} \text{ sec}^{-1}$ and was used to determine the intensities, $I_V(2)$, at the three greatest depths. $I_V(1)$ and $I_V(2)$ are shown in table 5.5, and compared with the OPW relation in figure 6.5 (Chapter 6) where it is seen that there is good agreement at the two greatest depths for both methods. At 724 m.w.e., however, the two methods give intensities which are 32% and 21% higher than expected. It should be remembered that these are total intensities since some contamination from side showers and secondary electrons is expected, and should therefore be regarded as upper limits to the intensities. The magnitude of this effect is not known, but is thought to be about 5-8%.

5.3 The best estimate of the Intensity vs. Depth relation.

A survey was made by Hayman et al. (1963), referred to as HPW, of the measured underground intensities and a best estimate was made of the intensity-depth curve. However, it was realized that the underground intensity measurements contributing most to the combined data at great depths (Miyake et al. 1962-3) were made under rock having a significantly greater value of Z^2/A than for the

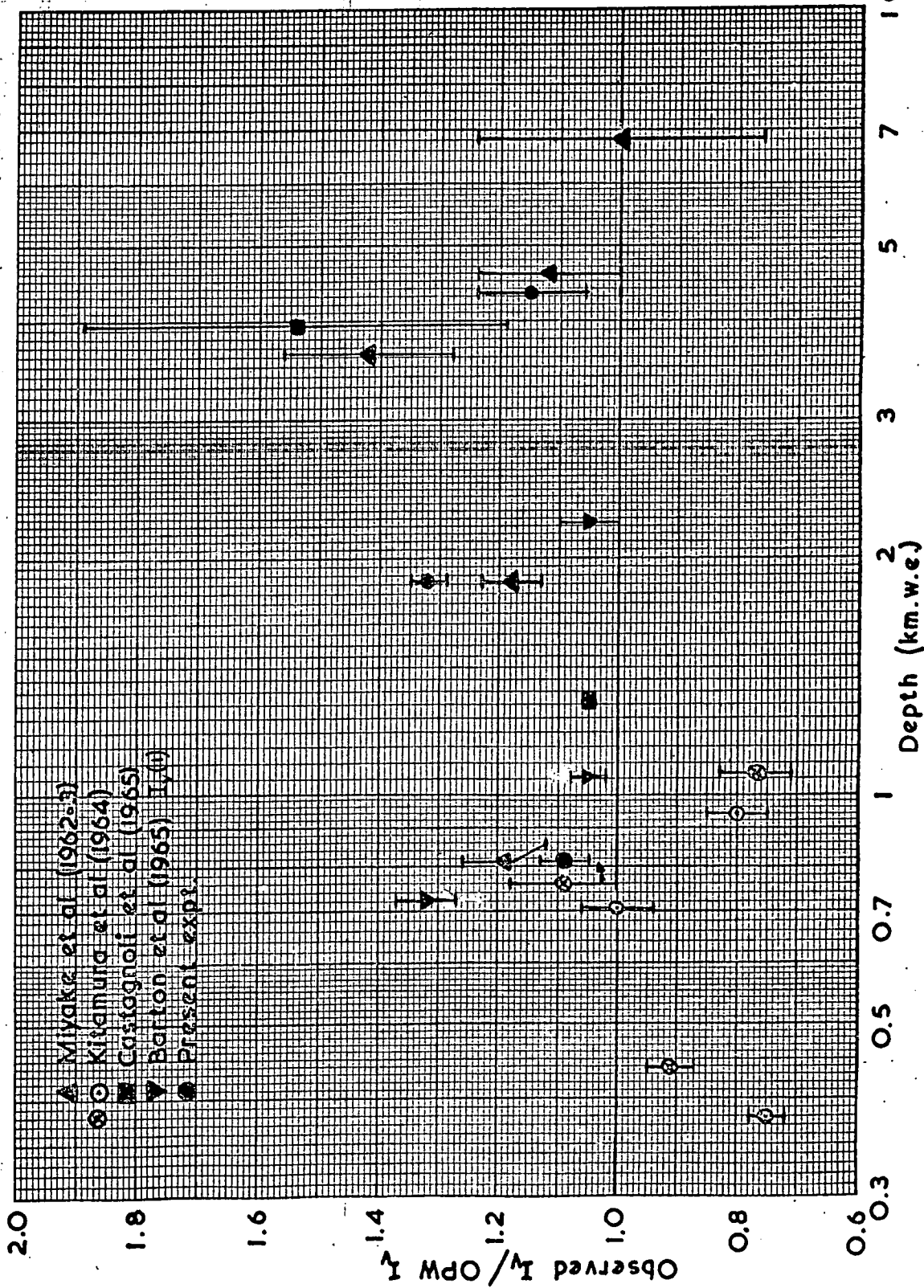


Fig.5.2 Comparison of recent experimental results with the spectrum of Osborne et al.

majority of other measurements: 6.33 compared with 5.5. The result of a more accurate analysis (Osborne et al 1964) allowing for the difference in Z^2/A from one experiment to another is an increase in the effective depth of the observations of Miyake et al. For example, the actual depths of 6370 and 8390 m.w.e. correspond to effective depths of 6900 and 9200 m.w.e. (Said et al, private communication). Similar corrections have been made to the data of Srekantan et al (1956), Bollinger (1950, 1951), Barrett et al (1952) and Barton (1961). The resulting best estimate of the intensity-depth curve was shown in Fig.4.6 and 4.7. The dotted curve is that due to Hayman et al (1963). It is seen that the effect of Z^2/A becomes important at depths in excess of 3000 m.w.e. Corrections have been applied to the results of recent experiments (Miyake et al., Kitamura et al., Castagnoli et al., and the experiment being reported here) for the effect of Z^2/A to the "standard" value of 5.5, and comparison with the OPW intensity-depth spectrum is made in Figs. 4.6, 4.7 and 5.2. Discussion of the implications of the intensity-depth spectrum is deferred until the next chapter.

CHAPTER 6.

INTERPRETATION OF RESULTS ON SINGLE MUONS.

6.1. Propagation of Cosmic Rays Underground.

There is fairly general agreement that the Cosmic ray particles which penetrate to great depths underground are muons. There is no other known particle except the neutrino which is as penetrating as the muon and since the neutrino is uncharged no confusion arises.

It is important to examine the rate of energy loss of high energy muons because of the relevance to electromagnetic processes occurring at small impact parameters and at high energies. Direct measurement of energy loss is difficult, but an indirect method is available using the measured sea-level vertical muon spectrum together with underground intensity measurements. The usual procedure is to relax the assumed relation for the average energy loss until there is agreement between the predicted depth-intensity relation and the measured intensities (e.g. Barrett et al (1952), George (1952), Pine et al (1959), Ashton (1961), Ozaki (1962) and Hayman et al (1963). Such treatments are difficult to carry out because the high-energy sea-level spectrum and the underground intensities are not known very

accurately, and also because of uncertainty in the magnitude of the theoretical cross-sections.

The main processes by which high energy muons lose energy in passing through matter are as follows :

- (i) ionization and excitation,
 - (ii) direct pair production,
 - (iii) bremsstrahlung,
- and (iv) nuclear interaction.

6.1.1. Energy losses due to ionization and excitation. The probability $P(E, E^1)dE^1$ that a muon of mass μc^2 , energy E , and spin 1/2 transfers an energy in the interval $E^1, E^1 + dE^1$ to an electron of mass mc^2 in traversing unit thickness of matter is

$$P(E, E^1)dE^1 = 2C \frac{mc^2}{\beta^2} \frac{dE^1}{(E^1)^2} \left[1 - \beta^2 \frac{E^1}{E_m^1} + \frac{1}{2} \left(\frac{E^1}{E + \mu c^2} \right)^2 \right]$$

where

$$C = \pi N \frac{Z}{A} r_e^2$$

N is Avogadro's number

Z is the atomic number of the medium

A is the atomic weight of the medium

r_e is the classical electron radius

β is the velocity of the muon

and E_m^1 is the maximum transferable energy given by

$$E_m^1 = E^2 \left(E + \frac{\mu^2 c^4}{2mc^2} \right)^{-1}$$

It is convenient to consider distant collisions and close collisions separately. A close collision may be defined as any collision resulting in the ejection of an electron of energy greater than a predetermined value, η . Conversely electrons are ejected with energy less than η in distant collisions. For close collisions the rate of energy loss is given by

$$-\frac{dE}{dx} = \int_{\eta}^{E_m} E' P(E, E') dE'$$

Integration gives the following results for the energy loss per gm.cm⁻² :

Close collision: $-\left(\frac{dE}{dx}\right)_{\text{Coll} > \eta} = 2C \frac{mc^2}{\beta^2} \left[\ln \frac{E_m}{\eta} - \beta^2 + \frac{1}{4} \left(\frac{E_m}{E + mc^2} \right)^2 \right]$

Distant collisions: $-\left(\frac{dE}{dx}\right)_{\text{Coll} < \eta} = 2C \frac{mc^2}{\beta^2} \left[\ln \left\{ \frac{2mc^2 \beta^2 \eta}{(1-\beta^2) I^2(Z)} \right\} - \beta^2 \right]$

where $I(Z)$ the average ionization potential of an atom of medium having atomic number Z is given by $I(Z) = 13.5 Z \text{ eV}$.

For distant collisions in dense materials, however, the screening of the electric field of the muon by the atoms of the medium has to be taken into account. The correction, Δ , due to the density effect according to Fermi (1939-40) and Halpern & Hall (1940, 1948) is given by

$$\Delta = -2C \frac{mc^2}{\beta^2} \left[\ln \left\{ \frac{\epsilon - 1}{1 - \beta^2} \right\} - 1 \right], \text{ for } \beta > \epsilon^{-1/2}.$$

where ϵ is the dielectric constant of the medium relative to vacuum.

$$\text{Thus } -\left(\frac{dE}{dx}\right)_{\text{Coll}} = 2C \frac{mc^2}{\beta^2} \left[\ln \left\{ \frac{2mc^2 \beta^2 E'_m}{(\epsilon-1) I^2(Z)} \right\} - 2\beta^2 + 1 + \frac{1}{4} \left(\frac{E'_m}{E + mc^2} \right)^2 \right]$$

$$\text{with } \epsilon = 1 + N \rho \frac{Z}{A} \cdot \frac{e^2 h^2}{\pi mc^2 I^2(Z)}, \quad \text{for } \beta > \epsilon^{-1/2}$$

where ρ is the density of the medium.

Substituting for the constants in the collision loss equation with $Z = 11$, $A = 22$, $\rho = 2.65 \text{ gm.cm}^{-3}$ ("standard rock"),

$$-\left(\frac{dE}{dx}\right)_{\text{Coll}} = 1.88 + 0.077 \ln \left(\frac{E'_m}{mc^2} \right) \text{ MeV/gm.cm}^{-2}$$

This equation which is valid for $E > 10 \text{ GeV}$ is that given by Barrett et al (1952) and has been confirmed by Sternheimer (1952, 1959) using an aluminium target ($Z = 13$, $A = 27$, $\rho = 2.7 \text{ gm.cm}^{-3}$).

Over a wide range of transferred energies the cross-section for a muon transferring a fraction, ν , of its energy to an electron is given by

$$\sigma(E, \nu) d\nu = \text{const.} \frac{d\nu}{E\nu^2}$$

where the constant is a slowly varying function of E , ν , and the constants of the medium.

6.1.2. Energy losses due to direct pair-production. The mechanism of pair production by a relativistic charged particle can be understood by assuming that the electromagnetic field of the particle is equivalent to a flux of photons. On passing near an atomic nucleus each virtual photon has a certain probability of undergoing materialization. The screening of the Coulomb field of the nucleus by the outer electrons can be important, but the spin of the incident particle is not.

The equations of Bhabha for the probability of pair production have been integrated by Mando and Ronchi (1952), following the calculations of Racah (1937) and Hayakawa and Tomonaga (1949) and give the following result:

$$-\left(\frac{dE}{dx}\right)_{pp} = \frac{N}{A} \frac{m}{\mu} \frac{(\alpha Z r_0)^2}{\pi} E \left[19.3 \ln \frac{E}{mc^2} - 53.7 \right] \times f$$

where α is the fine structure constant

$$\text{and } f = \left[\frac{16}{9} \ln (183 Z^{-1/3}) + 1 \right] \left[\frac{16}{9} \ln \frac{E}{mc^2} - \frac{14}{9} + \ln 2 \right]^{-1}$$

is the factor by which the energy loss is reduced by the effect of screening. For $E < 30 \text{ GeV}$, $f = 1$.

On substitution for the constants,

$$-\left(\frac{dE}{dx}\right)_{p.p.} = 4.16 \times 10^7 E \left[\ln \frac{E}{mc^2} - 2.78 \right] \text{ MeV/gm.cm}^{-2}$$

For $500 \leq E \leq 10^4$ GeV an approximate expression is

$$-\left(\frac{dE}{dx}\right)_{p.p.} = 1.6 \times 10^{-6} E \text{ MeV/gm.cm}^{-2}$$

and the cross-section for complete screening over a wide range of transferred energies is

$$\sigma(E, \nu) d\nu = \text{const.} \frac{d\nu}{E\nu^3}$$

6.1.3. Energy losses due to Bremsstrahlung.

When a charged particle passes close to a nucleus it is accelerated in the Coulomb field of the nucleus and radiation (Bremsstrahlung) is emitted. Following the treatments of Rossi (1952) and Rozental and Streltsov (1959) then the rate of energy loss is given by the following equations:

$$\begin{aligned} \text{for } E < E_0, \quad -\left(\frac{dE}{dx}\right)_B &= 4 \alpha N r_e^2 \frac{Z^2}{A} \left(\frac{m}{\mu}\right)^2 E \left[\ln\left(\frac{12}{5} \frac{EZ^{-1/3}}{\mu c^2}\right) - \frac{1}{3} \right] \\ &= 1.80 \times 10^{-7} E \left[\ln \frac{E}{\mu c^2} - 0.257 \right] \text{ MeV/gm.cm}^{-2} \end{aligned}$$

$$\begin{aligned} \text{and for } E > E_0, \quad -\left(\frac{dE}{dx}\right)_B &= 4 \alpha N r_e^2 \frac{Z^2}{A} \left(\frac{m}{\mu}\right)^2 E \left[\ln\left(183 \frac{\mu}{m} Z^{-1/3}\right) + \frac{1}{18} \right] \\ &= 1.76 \times 10^{-6} E \text{ MeV/gm.cm}^{-2} \end{aligned}$$

where E_0 is the energy above which screening is effective

$$\text{and } E_0 = \frac{2\pi}{\alpha Z^3} \frac{\mu c^2}{mc^2} \nu$$

and ν is the fractional photon energy. For $\nu = 1/2$, then

$E_0 = 4300$ GeV. The cross-section for bremsstrahlung is quite accurately expressed by $\sigma(E, \nu) d\nu = \text{const. } d\nu/\nu$ over a wide energy range.

6.1.4. Energy losses due to nuclear interaction.

It has been known for some time (George & Evans, 1950) that there is a significant cross-section for the inelastic collision of a muon with a nucleus, the interaction being regarded as being between the virtual photon cloud accompanying the muon, and the nucleus.

Following Fowler and Wolfendale (1958) the rate of energy loss due to nuclear interactions can be

$$\text{expressed by } - \left(\frac{dE}{dx} \right)_N = \frac{2\alpha}{\pi} N \sigma_\nu E$$

where σ_ν is the photonuclear cross-section assumed to be independent of energy and to equal $\sim 10^{-28}$ cm²/nucleon.

Recent work by Higashi et al on the interactions of muons at various depths underground have shown that the variation of muon cross-section with depth can be explained using the Williams-Weiszacker (W-W) method (1934-1935) and that for $E > 5$ GeV,

$$\sigma_\nu = (2.6 \pm 0.3) 10^{-28} \text{ cm}^2/\text{nucleon}.$$

Using this value for σ_ν , the energy loss by nuclear interactions is

$$- \left(\frac{dE}{dx} \right)_N = 7.3 \times 10^{-7} E \text{ MeV/gm.cm}^{-2}.$$

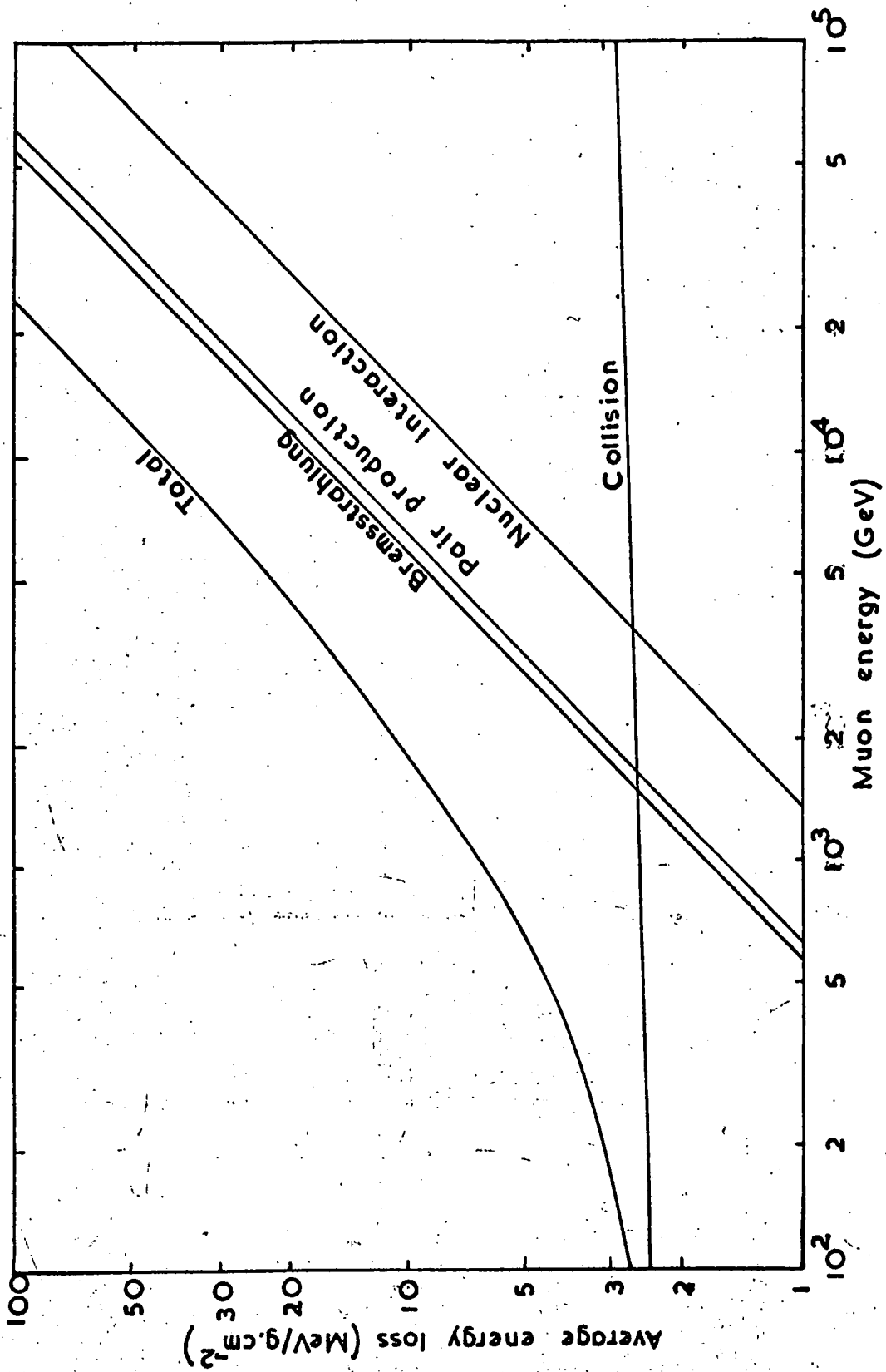


Fig.6.1 Average energy loss of muons in 'standard' rock.

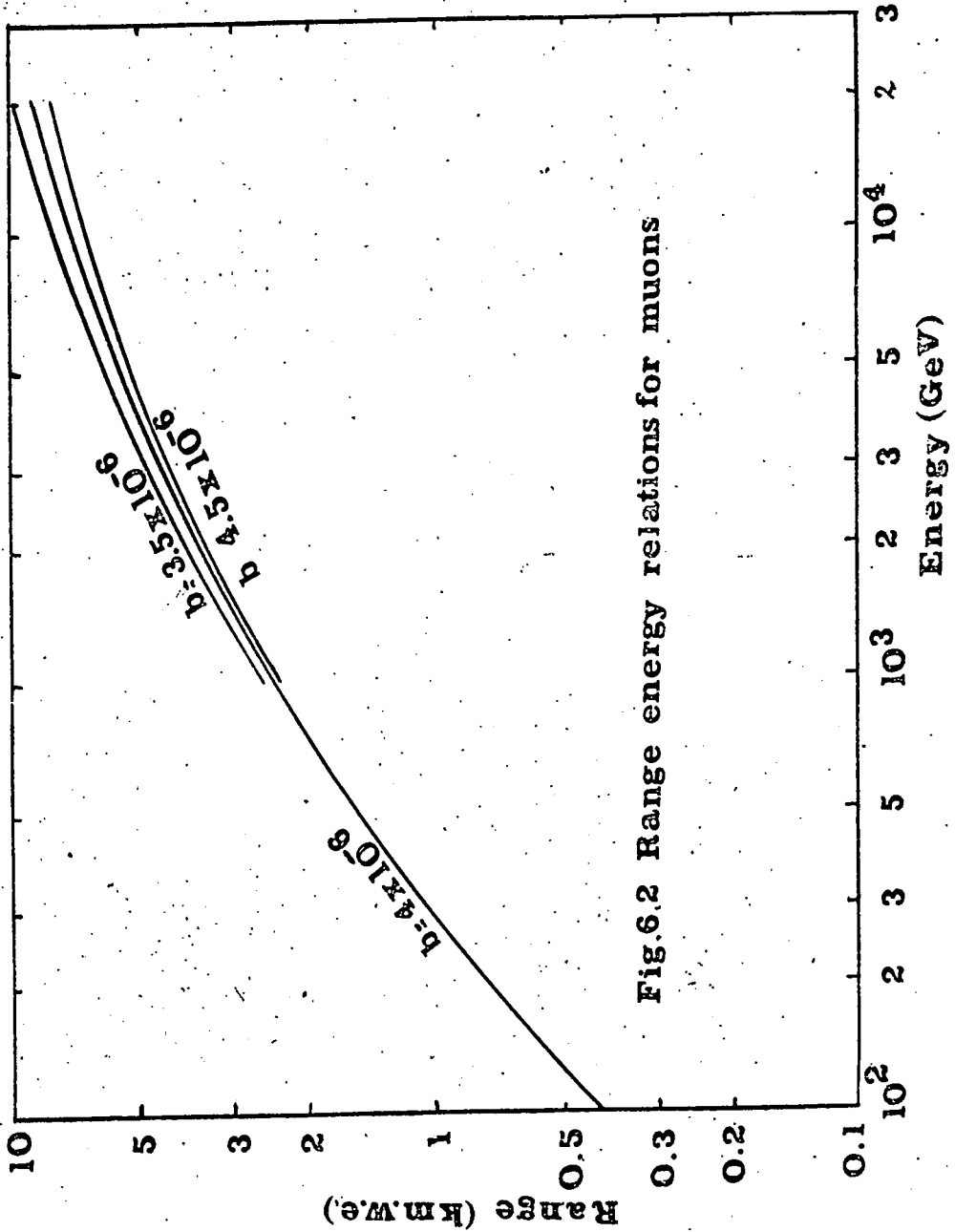


Fig.6.2 Range energy relations for muons

6.1.5. The total theoretical rate of energy loss. Summing the energy loss relations given in sections 6.1.1. - 6.1.4. the total theoretical rate of energy loss is

$$-\left(\frac{dE}{dx}\right)_{tot.} = 1.88 + 0.077 \ln\left(\frac{E_m'}{\mu c^2}\right) + bE \quad \text{MeV/gm.cm}^{-2}$$

(Fig.6.1) where the first two terms represent the contribution due to ionization and excitation, and the final term is due to the other three processes. The best estimate of b , which varies slightly with energy, is thought to be $(3.95 \pm 0.25) \times 10^{-6} \text{ gm}^{-1} \text{ cm}^2$. (Hayman et al 1963) over the muon energy range 500 to 10,000 GeV.

It can be seen from Fig. 6.1 that below 1000 GeV the dominant processes are ionization and excitation, but above 1000 GeV the other processes predominate.

The range-energy relation can be obtained by integrating the energy loss equation. On integration this becomes

$$E = a(e^{bx} - 1)/b \quad (6.1)$$

$$\text{where } a = 1.88 + 0.077 \ln\left(\frac{E_m'}{e\mu c^2}\right)$$

The range-energy relation is shown in Fig.6.2 for

$$b = 4.0 \times 10^{-6} \text{ gm}^{-1} \text{ cm}^2. \quad (\text{Curves are also shown for}$$

$$b = 3.5 \times 10^{-6} \text{ and } b = 4.5 \times 10^{-6} \text{ to show the dependence}$$

of the range on b).

6.2. Fluctuations in Energy Losses.

The average range-energy relationship is based on the assumption that the various types of energy loss are continuous processes. The continuous processes are in fact losses due to ionization and pair production whereas the discontinuous, or fluctuating, processes comprise bremsstrahlung and nuclear interactions. The essential difference is that the fluctuating processes have cross-sections which fall approximately as v^{-1} , whereas in the continuous processes they fall much more rapidly.

Hayman et al (1962-3) have examined the effect of fluctuations by means of a Monte Carlo calculation by computer, and the results of their analysis for two values of b are shown in Fig. 6.3a. Thus the vertical intensity at a depth d is given by
$$\bar{I}_m = \int_{E_0}^{\infty} N(E) dE$$
 neglecting straggling where E_0 is the energy corresponding to the range d , and $N(E) dE$ is the differential energy spectrum of vertical muons at sea-level, and

$$\bar{I}_s = \int_{E_{min}}^{\infty} P(d, E) \cdot N(E) dE$$

including straggling where $P(d, E)$ is the survival probability and E_{min} is the energy lost, due to continuous processes only, by a particle which just survives to the depth d .

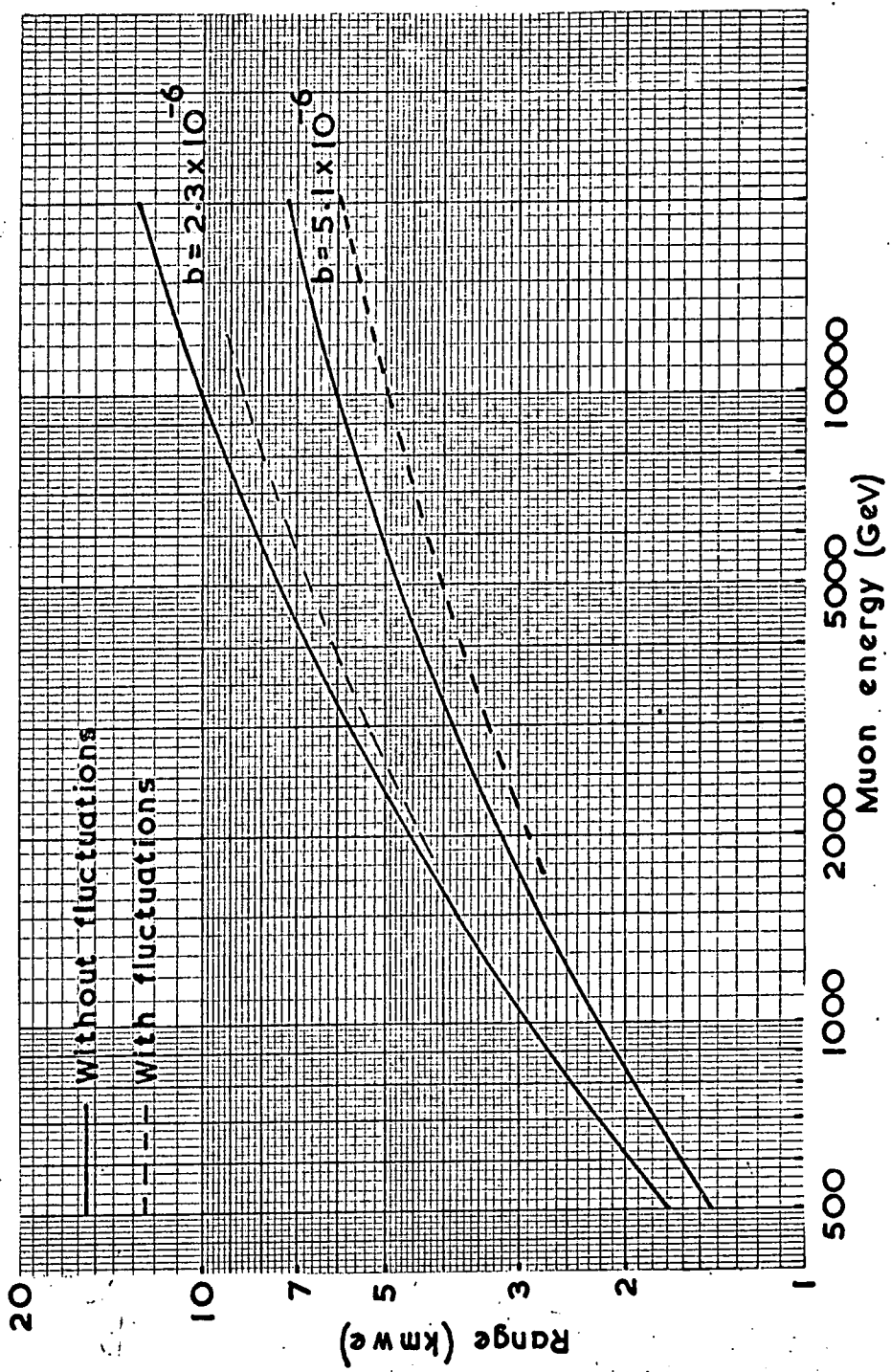


Fig.6.3a Mean range-energy curves for two values of b .

6.3. The Angular Distribution of Particles Underground.

It was seen (Section 4.3) that the exponent, n , of the angular distribution of particles underground is dependent on two factors: the logarithmic derivative, m , of the intensity-depth curve $\left(m = - \frac{\partial \ln I}{\partial \ln D} \right)$ and the enhancement factor, δ , concerning the contribution of particles other than pions to the production of muons, in particular K-mesons.

The variation of m with depth was derived from the best estimate of the depth-intensity curve for previous experiments relative to standard rock and was shown in Fig.4.8.

On the other hand the exponent n , and hence δ from the relation $m-n=\delta$, was seen to depend on the slope of the function $R \cos^m \theta$ where R is the ratio of the muon spectrum at production at a zenith angle θ to the vertical muon production spectrum. R was evaluated by using the measured sea-level muon vertical spectrum to obtain the muon vertical spectrum at production and the pion production spectrum. The muon production spectrum at a zenith angle θ was then obtained from the latter and hence R . The muon production spectra (and therefore R) were obtained in a similar fashion for various values

of the K/π ratio. It is seen from equation 4.4. that the function R is dependent on the decay probability of parent particles giving rise to muons at a zenith angle θ . This is strongly dependent on the nature of the parent particles. The decay characteristic energy of an unstable particle is defined as the energy at which its decay probability is just equal to its interaction probability at a depth equal to its interaction mean free path.

The observed values of n together with the predicted n versus depth relation were shown in Fig.4.9. It is seen that there is quite good agreement between experiment and 'theory' at 816 m.w.e. and 4110 m.w.e., but that there is some discrepancy at 1812 m.w.e. (Figs. 4.1 - 4.3.)

It is clear that the difference at 1812 m.w.e. is not due to any excess of muons at large zenith angles, but rather to a deficit in the near vertical direction. It is also interesting to note that the results of Bollinger and Barrett et al are in good agreement with the present experiment. It could be argued that the chi-squared test should be performed over a smaller zenith angular range than has been done here ($\theta_c = 60^\circ$).

However, examination of the chi-squared test data shows that even using $\theta_c = 45^\circ$, the best fit value of n is 2.90. Similarly for 4110 m.w.e. there is only a small contribution to χ^2 for $45^\circ \leq \theta \leq 60^\circ$, and thus there is little or no change in the best fit value of n for any angular range provided that $\theta_c \leq 60^\circ$. There is, on the other hand, a large contribution to chi-squared from the one event with zenith angle greater than 60° at this depth, yielding $n = 4.68$ for $\theta_c = 65^\circ$, but the statistics at 4110 m.w.e. are poor.

It is concluded that on the whole there is quite good agreement between the 'theoretical' and experimental values of the exponent of the angular distribution up to depths of ~ 5000 m.w.e., the observed differences at 1812 m.w.e. (three standard deviations) and 4110 m.w.e. being indicative of an increase in m , the logarithmic derivative of the depth-intensity curve of Osborne et al (1964) which was derived from experimental data. The statistics are not good enough to indicate the influence of the K/π ratio at production.

6.4. Implications of the Best Estimate Underground Spectrum.

It is clear from the preceding discussion that it is possible to make an attempt to resolve two problems.

Energy (GeV).	$I(\text{cm}^{-2}\text{sec}^{-1}\text{sr}^{-1})$	Energy (GeV).	$I(\text{cm}^{-2}\text{sec}^{-1}\text{sr}^{-1})$
20	2.62×10^{-4}	500	2.86×10^{-7}
30	1.29×10^{-4}	700	1.14×10^{-7}
50	4.81×10^{-5}	1000	4.56×10^{-8}
70	2.42×10^{-5}	1500	1.58×10^{-8}
100	1.19×10^{-5}	2000	7.28×10^{-9}
150	4.95×10^{-6}	3000	2.44×10^{-9}
200	2.64×10^{-6}	5000	4.80×10^{-10}
300	1.02×10^{-6}	7000	1.49×10^{-10}

TABLE 6.1. - COMPOSITE INTEGRAL SPECTRUM OF MUONS IN THE VERTICAL
DIRECTION AT SEA LEVEL (OSBORNE ET AL - 1964).

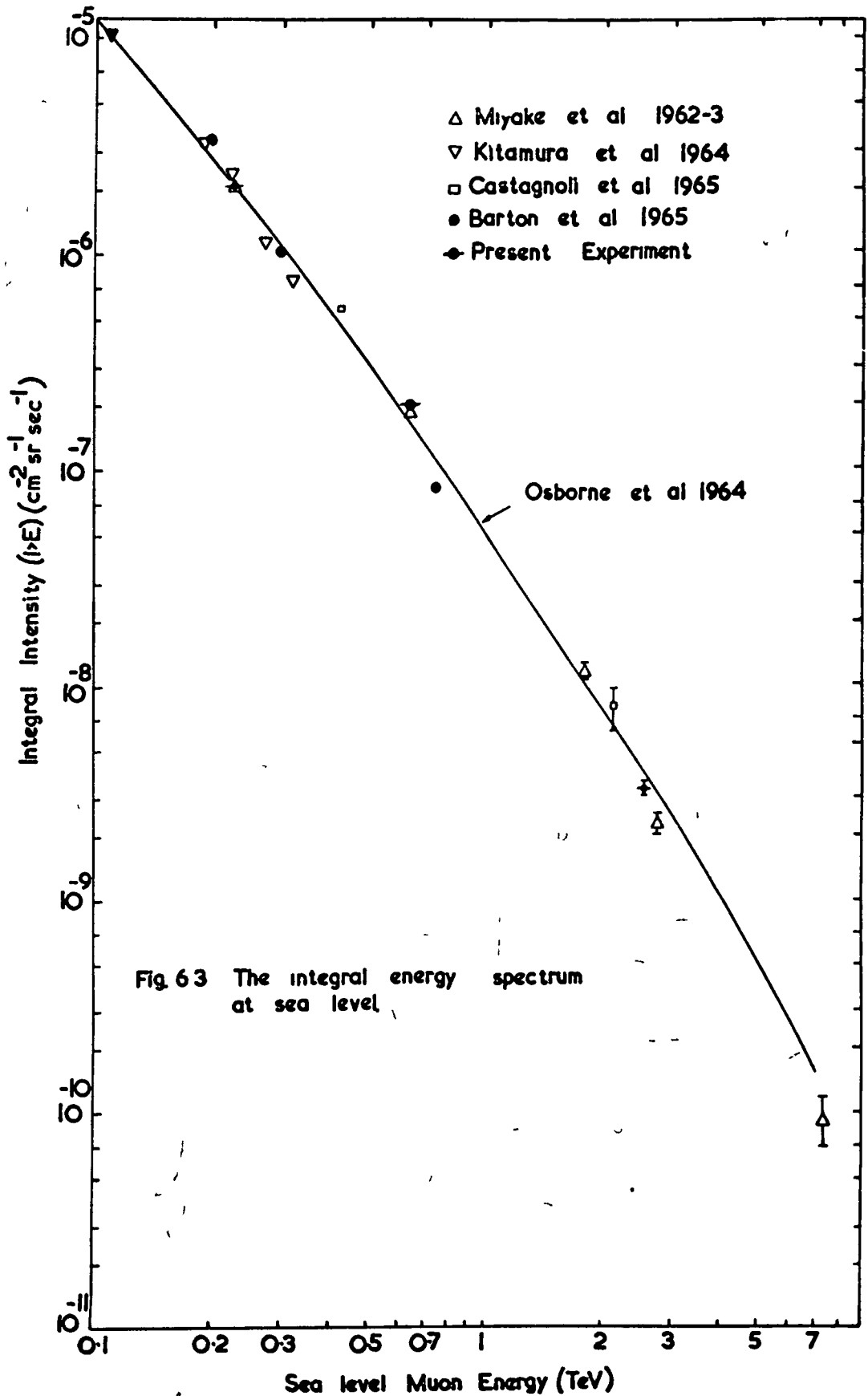


Fig 63 The integral energy spectrum at sea level

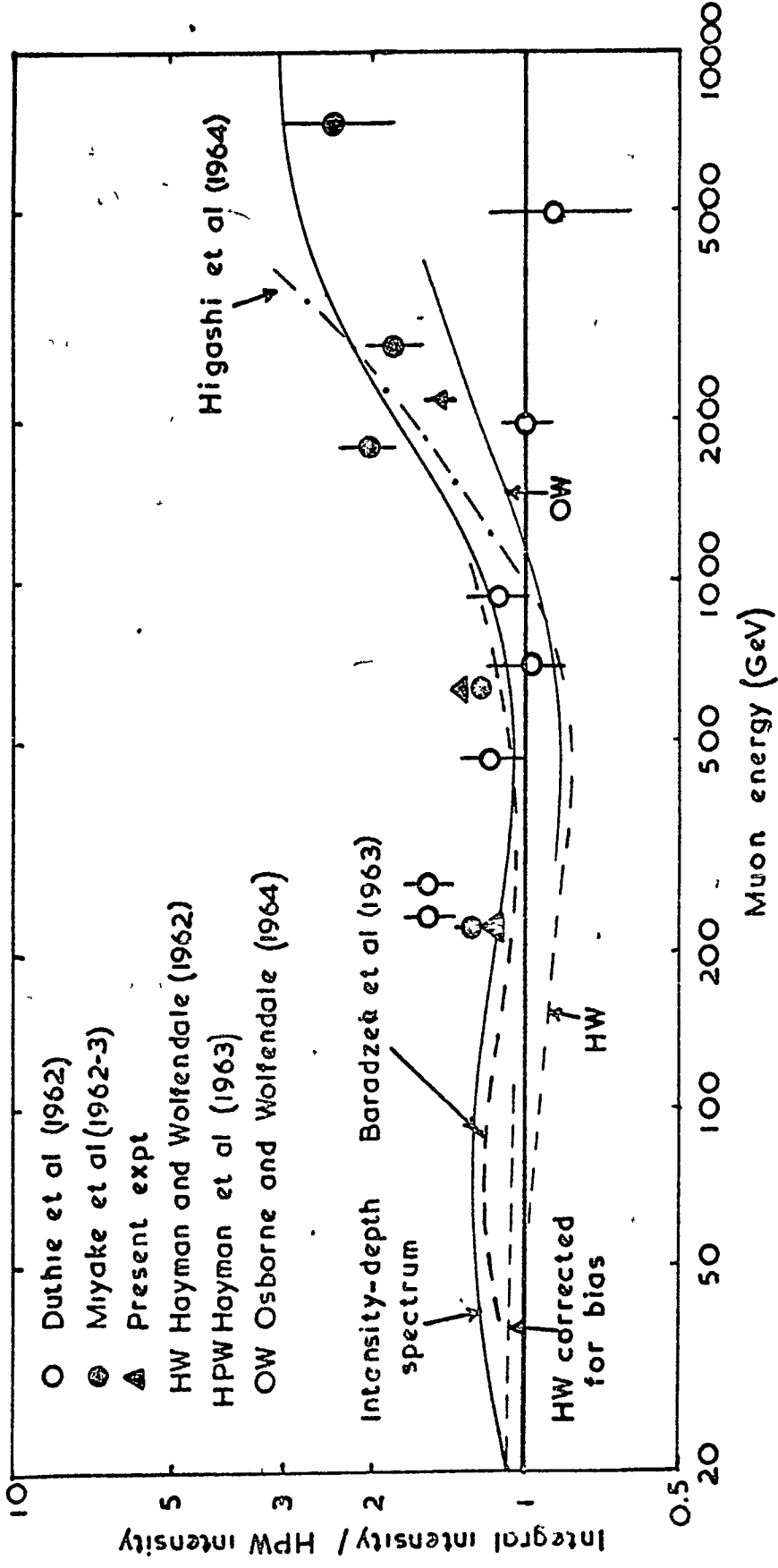


Fig 64 Comparison of recent determinations of the energy spectrum of muons at sea level (Osborne et al, 1964)

At shallow depths we can compare the depth-intensity spectrum with the sea-level integral energy spectrum and compare the observed and theoretical values of the quantity b in the energy loss equation. Secondly, at greater depths an estimate can be made of the nature of the parent particles (i.e. the K/π ratio).

6.4.1. The sea-level integral energy spectrum.

Osborne et al (1964) have summarized various measurements of the energy spectrum of cosmic ray muons. For energies greater than 1000 GeV indirect measurements have been used, whereas magnet spectrograph measurements are available up to energies of the order of 1000 GeV. Differences between various types of experiments have been resolved by Osborne et al (1964) and their resulting best estimate of the sea-level energy spectrum (OPW spectrum) in the range 20 - 7000 GeV is shown in Fig.6.3 and Table 6.1. They showed that the best estimate follows the corrected intensities of Hayman and Wolfendale (1962) up to 50 GeV, then to be 10% higher than the HPW estimate up to 200 GeV and to follow the intensity-depth spectrum to 7000 GeV. Comparison of various aspects of their analysis with the HPW spectrum is shown in Fig.6.4.

6.5. The Intensity-Depth Spectrum.

Comparison was made in Fig.5.2 of the results

of recent experiments with the OPW intensity-depth spectrum. However, that comparison was not strictly true since Miyake et al and Castagnoli et al adopted the only measurements of the exponent of the angular distribution available, i.e. the results of Randall and Hazen, Bollinger and Barrett et al. Not until the present experiment has the exponent been determined at depths greater than ~ 1500 m.w.e. Beyond 1500 m.w.e. Miyake et al and Castagnoli et al obtained values for η by an iteration process. It is clear from Fig. 4.9 that there are some differences between the observed and predicted values for η as a function of depth. Thus in order to compare recent experimental measurements of the vertical intensity with the OPW spectrum, corrections must be applied to allow for the effect of η . Since two depths of observation were common to the experiment of Miyake et al and the present experiment, the exponents found by the present experiment could be used for these two experiments. The results of doing this are shown in Table 6.2. It is seen that at 816 m.w.e. there is excellent agreement between the two experiments, and that at 1812 m.w.e. the agreement is within statistical errors. If it can be assumed that had the present experiment been conducted at 4280 m.w.e.

Depth (m.w.e)	Assumed nas	I _v /OPW (nas)	Theoretical		n observed in present experiment	I _v /OPW (nob)
			(K/π ± 20%)	(nth)		
MIYAKE ET AL.	2.3	1.19 ± 0.07	2.1	1.13 ± 0.07	1.92	1.09 ± 0.07
	3.1	1.18 ± 0.05	2.5	1.05 ± 0.04	3.26	1.22 ± 0.05
	4.5	1.42 ± 0.14	3.97	1.29 ± 0.13		
	5.2	1.12 ± 0.12	4.75	1.05 ± 0.11	5.55	1.07 ± 0.11
	6.6	1.00 ± 0.24				
CASTAGNOLI ET AL.	3	1.05 ± 0.01	2.35	1.04 ± 0.01		
	5-6	1.54 ± 0.35	4.23	1.56 ± 0.35		
PRESENT EXPERIMENT			2.1	1.42 ± 0.04	1.92	1.09 ± 0.04
			2.5	1.11 ± 0.03	3.26	1.32 ± 0.03
			4.55	1.05 ± 0.08	5.33	1.15 ± 0.09

TABLE 6.2. - COMPARISON OF RECENT UNDERGROUND RESULTS WITH THE OPW INTENSITY-DEPTH SPECTRUM.

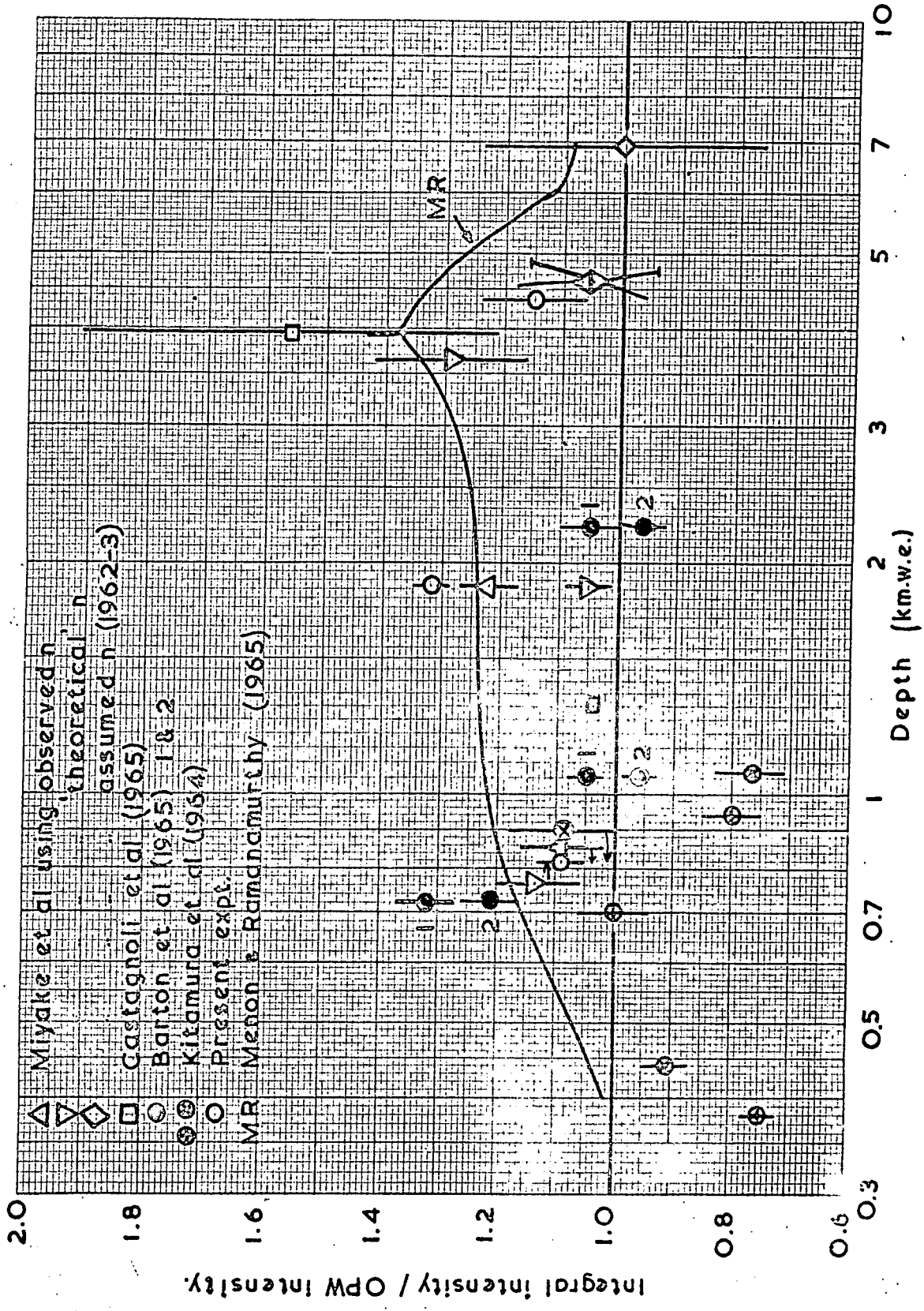


Fig.6.5 Comparison of recent intensity measurements with the OPW & MR spectra.

instead of 4110 m.w.e. the measured exponent of the angular distribution would have been 17% higher than the predicted value as was found at 4110 m.w.e., then the Miyake et al., 4280 m.w.e. intensity should be corrected for $n = 5.55$. It is seen that there is tolerable agreement between the two experiments in the region of 4500 m.w.e.

A similar correction can be made to the deepest intensity measured by Castagnoli et al since this is in the same depth region as the 4110 m.w.e. observation of the present experiment. Here the approximate angular distribution expected to have been measured would have $n = 4.95$. It is seen (Table 6.2) that there is little change from the figure quoted in Table 5.4, the reason for this being the slow variation of the acceptance of the Italian telescope with n . This was achieved by having the scintillators mounted at a separation of 2.5 m. The poor statistics of this measurement, however, give rise to tolerable agreement with the present experiment.

The Miyake et al and Castagnoli et al experimental results have also been corrected assuming that the 'theoretical' value of n is correct. These are summarized in Table 6.2 and displayed in Fig. 6.5.

For clarity the Miyake and Kitamura points in the region of 810 - 820 m.w.e. have been displaced from their correct depths as indicated by the arrows.

For purposes of discussion Fig. 6.5 can be conveniently divided into two depth bands, < 1500 m.w.e. and > 1500 m.w.e.

(a) 350 - 1500 m.w.e. It is seen that the agreement between the present experimental result at 816 m.w.e. is perfect with that of ~~the~~ Miyake et al at the same location, after correction to $n = 1.92$, and the underwater measurement of Kitamura et al at 812 m.w.e. It should not be forgotten that all the experimental results have also been corrected for the effect of Z^2/A equal to 5.5 (i.e. "standard rock"). These three measurements together with the Kitamura et al measurements at 439 and 705 m.w.e. and the Castagnoli et al intensity at 1315 m.w.e. are in fairly good agreement with the OPW spectrum. The same, however, cannot be said about the Kitamura intensities observed at the other three depths where the difference is some 25-35%. The reason for this is not known.

(b) 1500 - 5000 m.w.e. At 1812 m.w.e. there is quite good agreement within statistical errors between the

present experiment and that of Miyake et al after correction to $n = 3.26$ but these intensities are respectively 32% and 22% higher than the OPW spectrum. If the theoretical value of n were used, then the agreement between the OPW spectrum and the Miyake et al intensity would be better, but this treatment cannot surely be justified in view of the good agreement between the values of n measured by Bollinger, Barrett et al and the present experiment. At the same time the value of n derived by Miyake et al at 3625 m.w.e. gave a ratio of 1.42 ± 0.14 with the OPW spectrum, and this value of n is probably not too far removed from the value that would have been measured by the present experiment at the same depth, since it is some 13% higher than the predicted value in accord with similar higher values of n observed at 1812 and 4110 m.w.e. Indeed even if the 'theoretical' value of n were used the ratio with OPW spectrum would only reduce to 1.29 ± 0.13 . Comparison of the results of the present experiment at 4110 m.w.e. and the Miyake et al intensity at 4280 m.w.e. (corrected to $n = 5.55$) show good agreement both with each other and with the OPW spectrum.

It is therefore concluded that the OPW depth-intensity spectrum is probably correct below 1000 m.w.e. and in the region of 4000 - 5000 m.w.e. and that the

difference observed between the measured intensities and the OPW spectrum at 1812 m.w.e. (corresponding to a sea-level energy of ~ 600 GeV) might be due to inaccuracies in the Bollinger location II observations, which in the range 1000 - 3500 m.w.e. are consistently lower than would be expected by comparison with the Location I observations. An underestimate by about 50 - 100 m.w.e. in the effective depths at Location II would have the effect of giving an enhanced intensity depth spectrum sufficient to put the Location II observations in better agreement with those at Location I. It should be remembered that Location II was situated beneath Lake Cayuga which has a fairly steeply inclined bed.

Recently Menon and Ramanamurthy (1965) have also derived a best estimate fit to the intensity-depth spectrum (MR spectrum) and comparison of their spectrum is also shown in Fig.6.5. It is seen that in the range 700 - 7000 m.w.e. their spectrum is consistently higher than the OPW spectrum. In fact there is better agreement with the MR spectrum for the 1812 m.w.e. observation. It is found that the higher MR spectrum is due mainly to two causes, both related to the Bollinger observation:

- i) The effective depths at Location II are on average higher than those used by Osborne et al.

and ii) The intensities quoted for Location I in the range 1800 - 2500 m.w.e. are consistently higher than those used by Osborne et al by $\sim 7\frac{1}{2}\%$, then smaller by 7-19% between 2500 and 3100 m.w.e. and again higher by 13-21% between 3100 and 4500 m.w.e.

Finally it is noted that they did not correct the Bollinger depths for the effect of Z^2/A . (In the salt mine $Z^2/A = 5.0$ and not 5.5 as erroneously stated by Menon and Ramanamurthy). Correction for this effect would in fact reduce the depths quoted by these authors to give better agreement with the OPW figures thus obviating the difference due to i); the reasons for the different intensities quoted in ii) are not apparent, and one must conclude that one or other of the authors is in error.

It is, however, interesting to note the good agreement between the present experiment at 1812 m.w.e. and the Miyake observation at the same location and the Bollinger (1951) true vertical intensity at 1850 m.w.e. (Fig. 4.7). It would seem therefore that the derivation of vertical intensities from angular distribution measurements is not as straight forward as was believed. Following the argument of Menon and Ramanamurthy if it is assumed that the muons observed at various zenith angles

might have been produced in nuclear interactions directly or originated in the decays of extremely short lived parents (e.g. resonant states), then the Bollinger intensities would not have needed to be corrected for the enhanced decay probability of pions and K-mesons, their normally assumed source. In such a case the intensities due to the angular distribution would in fact be higher than as shown in Fig.4.7, correspondingly enhancing the OPW best estimate intensity-depth spectrum. It is suggested that further accurate experiments on the angular distribution and intensity of muons should be carried out at various depths in the same mines to clarify this situation (Rodgers (1961) and Dmitriev et al (1963)).

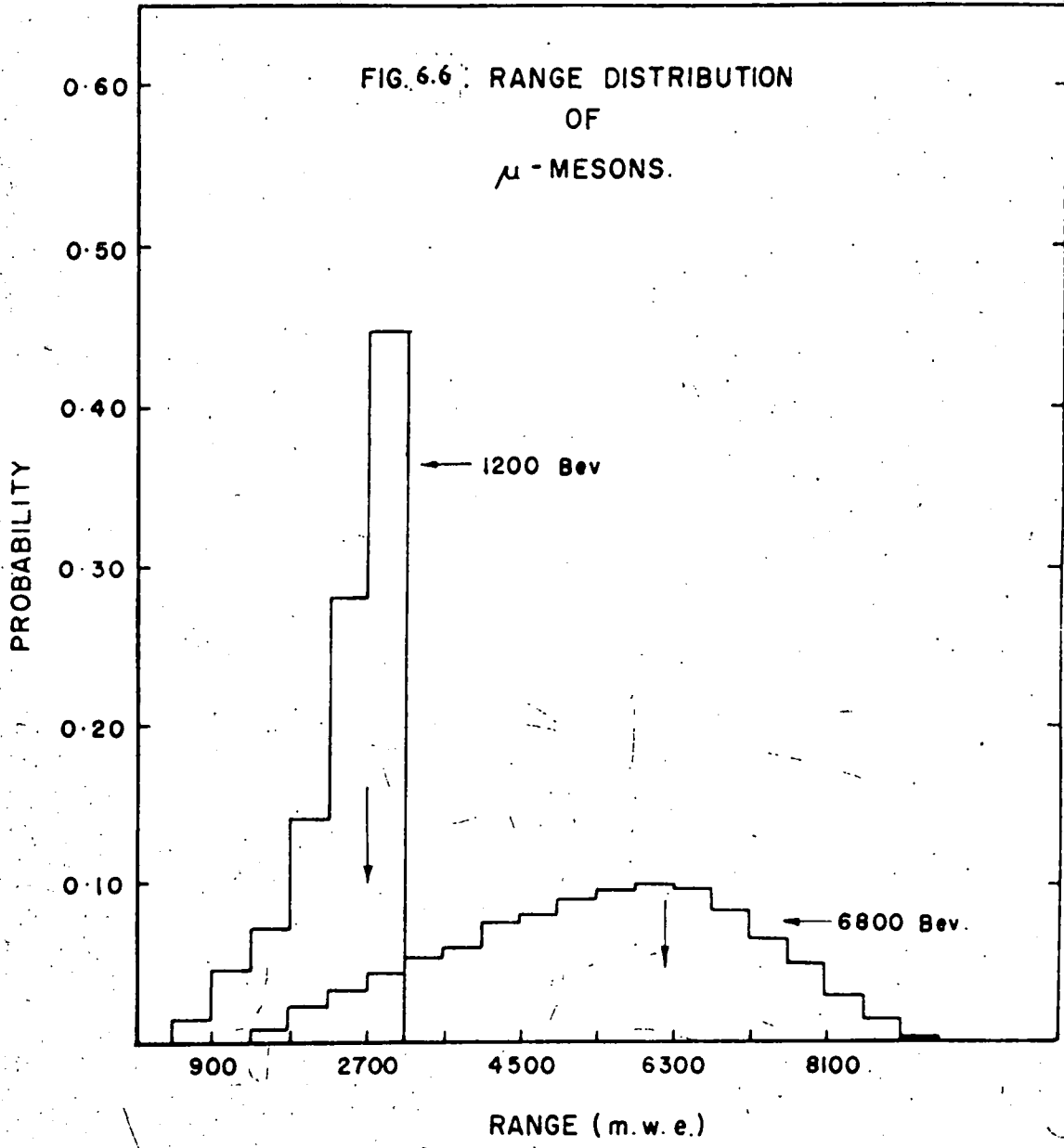
6.6. The Sea-Level Energy Spectrum.

It was pointed out in section 6.1 that the sources of energy loss by muons in their propagation underground are :-

- i) ionization and excitation;
- ii) direct pair production;
- iii) bremsstrahlung;
- and iv) nuclear interaction.

Collision losses by ionization and excitation were seen (Fig.6.1) to predominate for sea-level muon

FIG. 6.6 RANGE DISTRIBUTION OF μ -MESONS.



energies less than 1000 GeV when losses due to direct pair production and bremsstrahlung become comparable and in fact predominate for $E_{\mu} > 2000 \text{ GeV}$

Thus at shallow depths ($\leq 2000 \text{ m.w.e.}$ corresponding to $E_{\mu} \lesssim 700 \text{ GeV}$) the range-energy relation (Fig.6.2) may be considered to be unique, since the rate of energy loss for muons is of the order of 250 - 300 MeV/gm.cm⁻². It can no longer be considered unique for greater depths (or higher energies) because of the other three processes in which the muons lose large amounts of energy in a few catastrophic encounters giving rise to the fluctuation problem. It was mentioned in section 6.2 that the fluctuating processes have cross-sections which fall as v^{-1} , whereas the continuous processes fall more rapidly. The effect of fluctuations on the range-energy relation was strikingly illustrated by Miyake et al (1964) reproduced here in Fig. 6.6. This shows the range distributions to be expected for muons with sea-level energies of 1200 and 6800 GeV. The arrows indicate the ranges expected from a unique range-energy relation. It is therefore obvious that the sea-level energy spectrum cannot be simply derived using equation 6.1.

It was shown earlier (section 6.2) that the vertical intensities at a depth d is given by:

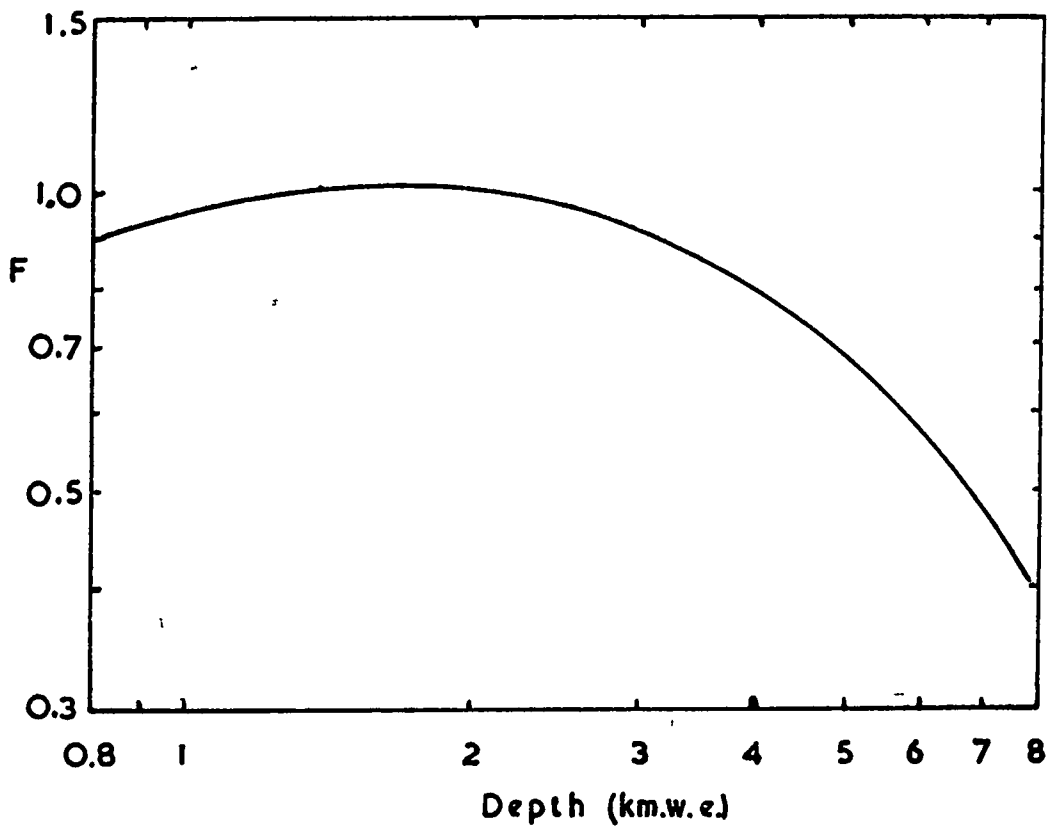


Fig. 67 Variation of the correction factor, F.

$$I_m = \int_{E_0}^{\infty} N(E) dE \quad \text{neglecting straggling}$$

$$\text{and } I_s = \int_{E_{min}}^{\infty} P(d, E) \cdot N(E) dE \quad \text{including range}$$

straggling where the variables have the same definition as before. A correction factor F_c is defined as the ratio I_m/I_s of these intensities and it is by this ratio that the intensity measured at a given depth should be multiplied and plotted against the muon energy corresponding to that depth as given by equation 6.1 (the average range-energy relation). The correction factor as a function of depth derived by Hayman et al for standard rock is shown in Fig.6.7.

The correction factor is applied to the results of the experiments of Miyake et al, Castagnoli et al, (both corrected for n), Kitamura et al and the present experiment, and the sea-level intensities are shown in Table 6.3 and plotted in Fig. 6.3 together with the best estimate sea-level energy spectrum of Osborne et al (1964). Comparison of the deduced sea-level intensities with the OPW spectrum is more clearly shown in Fig.6.8 where the horizontal line with ordinate equal to unity represents the OPW spectrum.

Since the Kitamura measurements were made at fairly shallow depths, no correction for range straggling

<u>Experiment</u>	<u>Corrected depth (m.w.e.)</u>	<u>I(d)</u>	<u>Correct- ion Fac- tor, F.</u>	<u>F x I(d) = I(> E).</u>	<u>I_v/OPW</u>	<u>Sea-level Muon Ener- gy (GeV).</u>
MIYAKE ET AL.	818	(2.29 [±] 0.15) 10 ⁻⁶	0.905	(2.07 [±] 0.14) 10 ⁻⁶	0.995 [±] 0.067	225
	1870	(1.83 [±] 0.08) 10 ⁻⁷	1.011	(1.85 [±] 0.08) 10 ⁻⁷	1.20 [±] 0.05	635
	φ 3625	(1.42 [±] 0.14) 10 ⁻⁸	0.816	(1.16 [±] 0.11) 10 ⁻⁸	1.20 [±] 0.11	1800
	4600	(3.10 [±] 0.33) 10 ⁻⁹	0.744	(2.31 [±] 0.25) 10 ⁻⁹	0.77 [±] 0.08	2800
	φ 6900	(1.92 [±] 0.47) 10 ⁻¹⁰	0.479	(9.19 [±] 2.25) 10 ⁻¹¹	0.78 [±] 0.19	7400

CASTAGNOLI ET AL.	1315	(5.60 [±] 0.07) 10 ⁻⁷	1.00	(5.60 [±] 0.07) 10 ⁻⁷	1.23 [±] 0.02	420
	φ 3950-100	(1.00 [±] 0.23) 10 ⁻⁸	0.79	(7.90 [±] 1.82) 10 ⁻⁹	1.23 [±] 0.28	2100

KITAMURA ET AL.	439	(1.04 [±] 0.04) 10 ⁻⁵	1.00	(1.04 [±] 0.04) 10 ⁻⁵	1.07 [±] 0.04	110
	705	(3.20 [±] 0.20) 10 ⁻⁶	1.00	(3.20 [±] 0.20) 10 ⁻⁶	1.05 [±] 0.07	188
	812	(2.29 [±] 0.19) 10 ⁻⁶	1.00	(2.29 [±] 0.19) 10 ⁻⁶	1.10 [±] 0.09	223
	940	(1.12 [±] 0.07) 10 ⁻⁶	1.00	(1.12 [±] 0.07) 10 ⁻⁶	0.85 [±] 0.05	270
	1072	(7.50 [±] 0.60) 10 ⁻⁷	1.00	(7.50 [±] 0.60) 10 ⁻⁷	0.83 [±] 0.07	318

PRESENT EXPERIMENT	818	(2.29 [±] 0.09) 10 ⁻⁶	0.905	(2.07 [±] 0.08) 10 ⁻⁶	0.995 [±] 0.038	225
	1870	(1.98 [±] 0.05) 10 ⁻⁷	1.011	(2.00 [±] 0.05) 10 ⁻⁷	1.30 [±] 0.03	635
	4360	(4.47 [±] 0.34) 10 ⁻⁹	0.748	(3.32 [±] 0.25) 10 ⁻⁹	0.83 [±] 0.06	2530

φ No correction for n.

TABLE 6.3. - THE INFERRED INTEGRAL SEA-LEVEL VERTICAL MUON INTENSITIES FROM RECENT UNDERGROUND EXPERIMENTS AND COMPARISON WITH THE OPW SEA-LEVEL SPECTRUM.

The differences between these ratios and the corresponding ratios (with respect to depth) in figure 6.5 are due to the differing fluctuation corrections of Kanamitsu and Osborne et al (1964).

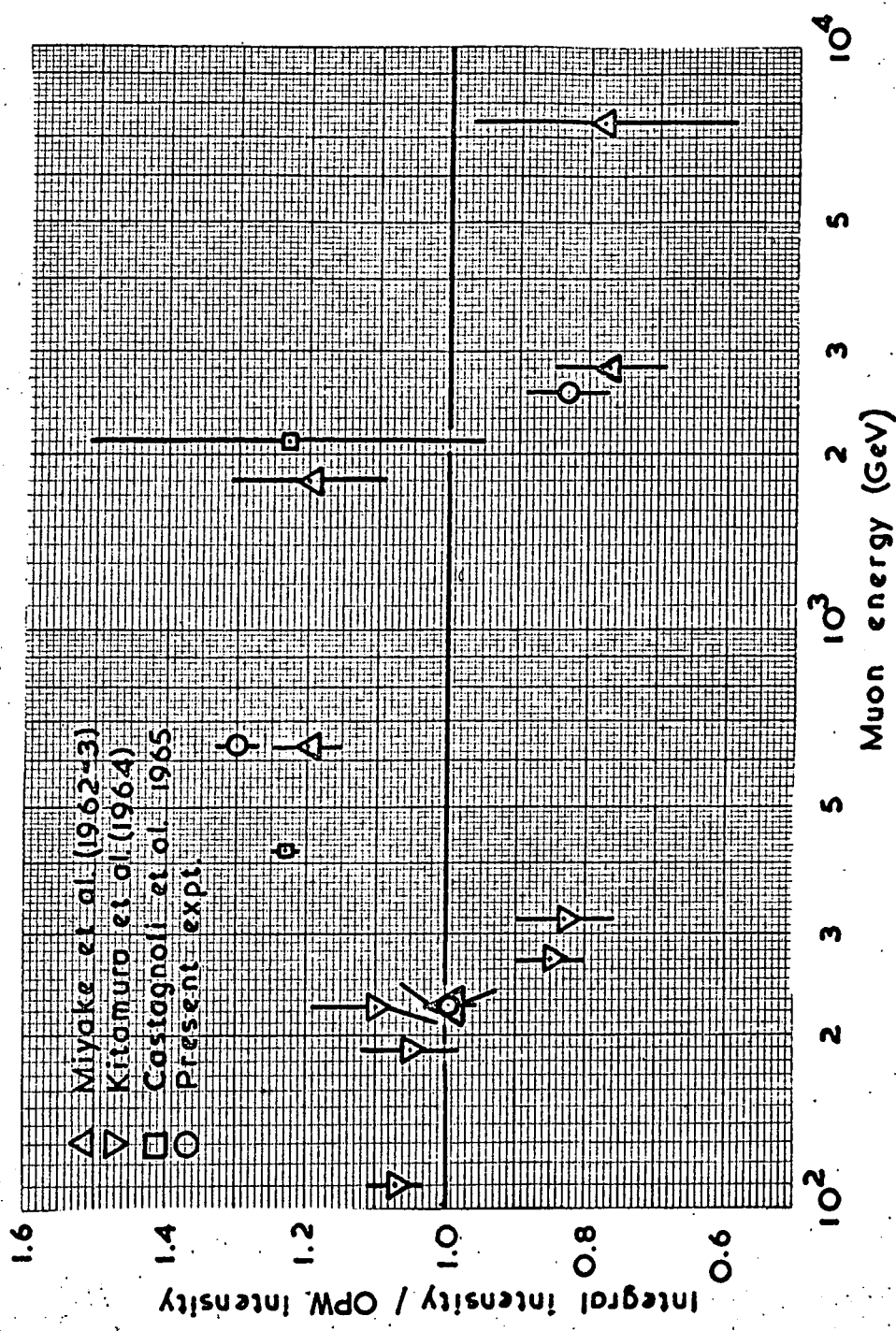


Fig. 6.8 Comparison of inferred sea level intensities with the OPW spectrum.

has been applied. The Miyake et al intensities refer to the underground intensities corrected for observed n , except the 1800 and 7400 GeV intensities. These two intensities refer to the theoretical n and Miyake et al assumed n . If the values of n observed in the present experiment are any criterion, then it is likely that direct measurements with the apparatus at these two depths (3625 and 6900 m.w.e.) would have shown n to be greater than the theoretical values shown in Fig. 4.9 giving correspondingly higher vertical intensities on correction of the Miyake et al points. However, it is thought that the value of n assumed at 3625 m.w.e. by Miyake et al is not too far removed from the value that might have been observed with the present apparatus and the intensity can be regarded as fairly close to the truth.

It is seen from Fig. 6.8 that there is good agreement at energies less than about 300 GeV between the OPW spectrum and various measurements. In the energy range 400 - 1000 GeV the comparison is not so good ($\sim 20-30\%$ higher than OPW spectrum). This is not surprising when it is remembered that this range corresponds to a depth range 1300 - 2500 m.w.e. where a similar

discrepancy was apparent (Fig.6.5) for the two Kolar Gold Field experiments. At high energies (> 1500 GeV) the agreement is tolerably good within statistical variations, the greatest experimental deviation from the OPW spectrum being three standard deviations.

It is concluded therefore that the best estimate depth-intensity spectrum of Osborne et al (1964) is quite accurate to 7000 m.w.e. except in the range 1300 - 2500 m.w.e. where it underestimates the vertical intensity by some 25%. This underestimation is of course reflected in the sea-level energy spectrum derived from the depth-intensity spectrum. A close look at the OPW sea-level energy spectrum in fact reveals a curious 'dip' in the region of 500 - 2000 GeV, and it is considered that this dip has originated from some inaccuracy in the analysis of Bollinger's Location II measurements which were noted earlier (section 6.5) as being consistently lower than his Location I measurements at about the same effective depths.

6.7. The K/π Ratio.

Osborne and Wolfendale (1964) derived the K/π ratio at production from the energy spectra of electromagnetic cascades in the cosmic radiation by predicting the sea-level muon spectra at sea-level on the basis of

pions only or K-mesons only being the parents of muons and comparing these spectra with the sea-level muon spectrum measured directly by magnet spectrographs and, at higher energies, inferred from the underground depth-intensity measurements. They found that, assuming that the energy spectra of pions and kaons have the same form, the K/π ratio varies from $20 \pm 20\%$ at 10^4 GeV primary energy, through $10 \pm 15\%$ at 7×10^4 GeV to $40 \pm 30\%$ at 6×10^5 GeV (Fig.6.9). This corresponds to a range of pion and K-meson energies from about 300 to 5000 GeV. Also shown in Fig. 6.9 are the K/π ratios derived from other experiments. It is seen that there is no marked inconsistency between the various determinations above 2×10^4 GeV primary energy. It seems apparent that the trough in the K/π ratio derived by the γ -e cascade analysis is partially due to the variation in gradient of the OPW spectrum. The present work has shown that the measured underground intensity at 1812 m.w.e. is in fact higher than the OPW spectrum by some 25%. This depth corresponds to an approximate pion energy of some 800 GeV at production or some 6×10^4 GeV primary energy. There is somewhat better agreement between the observed intensity at 4110 m.w.e. and the OPW spectrum, and it is concluded that the OPW spectrum underestimates the

intensity at depths of the order of 2000 m.w.e. and consequently the K/π ratio at primary energies of 6×10^4 GeV to $\sim 2 \times 10^5$ GeV by perhaps 10-20%.

It is clear, therefore, that the present measurements (and summary) suggest that the K/π ratio is sensibly constant, at $\sim 25\%$, over the whole range of primary energy $10^2 - 10^6$ GeV.

---00o---

CHAPTER 7.

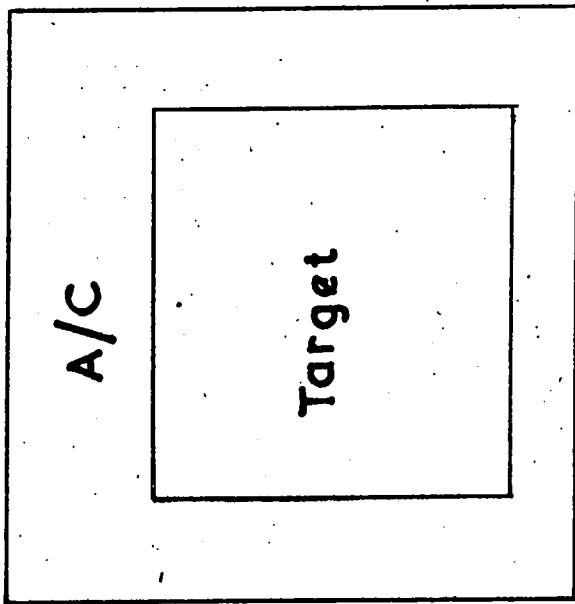
THE DISTRIBUTION IN ARRIVAL TIMES OF COSMIC RAYS FAR UNDERGROUND.

7.1. Introduction.

Many studies have shown that there is no significant variation with time of the flux of cosmic ray primaries of energy above some few hundred GeV outside the well known variations due to changes in atmospheric parameters. A recent experiment by Cowan et al (1964) has, however, suggested that there are significant variations in the muon component underground. The muons in question are produced by neutral particles, presumed to be neutrinos, and the main feature of the variation is the occurrence of bursts of particles in time intervals ranging from a few seconds to about five minutes.

7.2. The Experiment of Cowan et al (1964).

The apparatus (Fig. 7.1) comprised a 6 ft. long plexiglass parallelepiped 2'8" x 2'6", containing activated decalin which served as a target, surrounded by an anti-coincidence liquid scintillator. The target and anti-coincidence signals were displayed on the upper and lower beams of a double beam oscilloscope respectively after a 10 μ s delay. The gain of the anticoincidence system was



l'

Fig.7.1 The apparatus of Cowan et al.

twenty times that of the target system. Triggering signals for the oscilloscope sweep were obtained from a delayed coincidence unit which accepted all signals from the target larger than 5 MeV, waited for 2 μ S, then opened a 10 μ S long gate in anticipation of a possible decay electron pulse. Thus all decaying muon events were recorded on film, i.e. the stopping cosmic ray muons as well as those produced in the system by neutral particles. Identification of the latter was made by the absence of an anticoincidence pulse on the lower trace. About four stopping and decaying cosmic ray muons were observed per hour, providing a running check on the performance of the apparatus. The data were collected between 9th September 1963 and 11th January 1964. The apparatus was operated at a depth of about 200 m.w.e.

A prototype apparatus had been operated earlier in 1963 and it was found that the occurrence of events was not randomly distributed in time throughout the day. The effect was more apparent in the second run because of the increased target size and was most noticeable in the appearance of pairs, triplets and higher order multiplets with time spacings of the order of seconds and minutes. The departure of these data from a uniform distribution can be tested by an analysis of the spectrum

of elapsed times between successive events. If m is the mean rate of occurrence of a Poisson distribution of events per unit time then the spectrum of waiting times is given by

$$F(t) = 1 - \exp(-mt)$$

where $F(t)$ is the number of intervals expected which are less than or equal to t . This function is plotted for the experimental data as the solid curve in Fig. 7.2 for $m = 9.3 \times 10^{-5} \text{ sec}^{-1}$, normalized to 633 intervals. The corresponding observed spectrum of waiting times is plotted as points in the figure.

It is seen that there is good agreement between the observed and expected distributions for intervals in excess of 30 minutes, but the observed distribution departs radically from the expectation for shorter intervals. This was interpreted as the results of bursts or periods of large increases in intensity of the neutral radiation producing the signals seen against a uniform background. These bursts are seen to have durations extending from seconds to many minutes and are unlike any previous cosmic ray phenomena reported from underground observations.

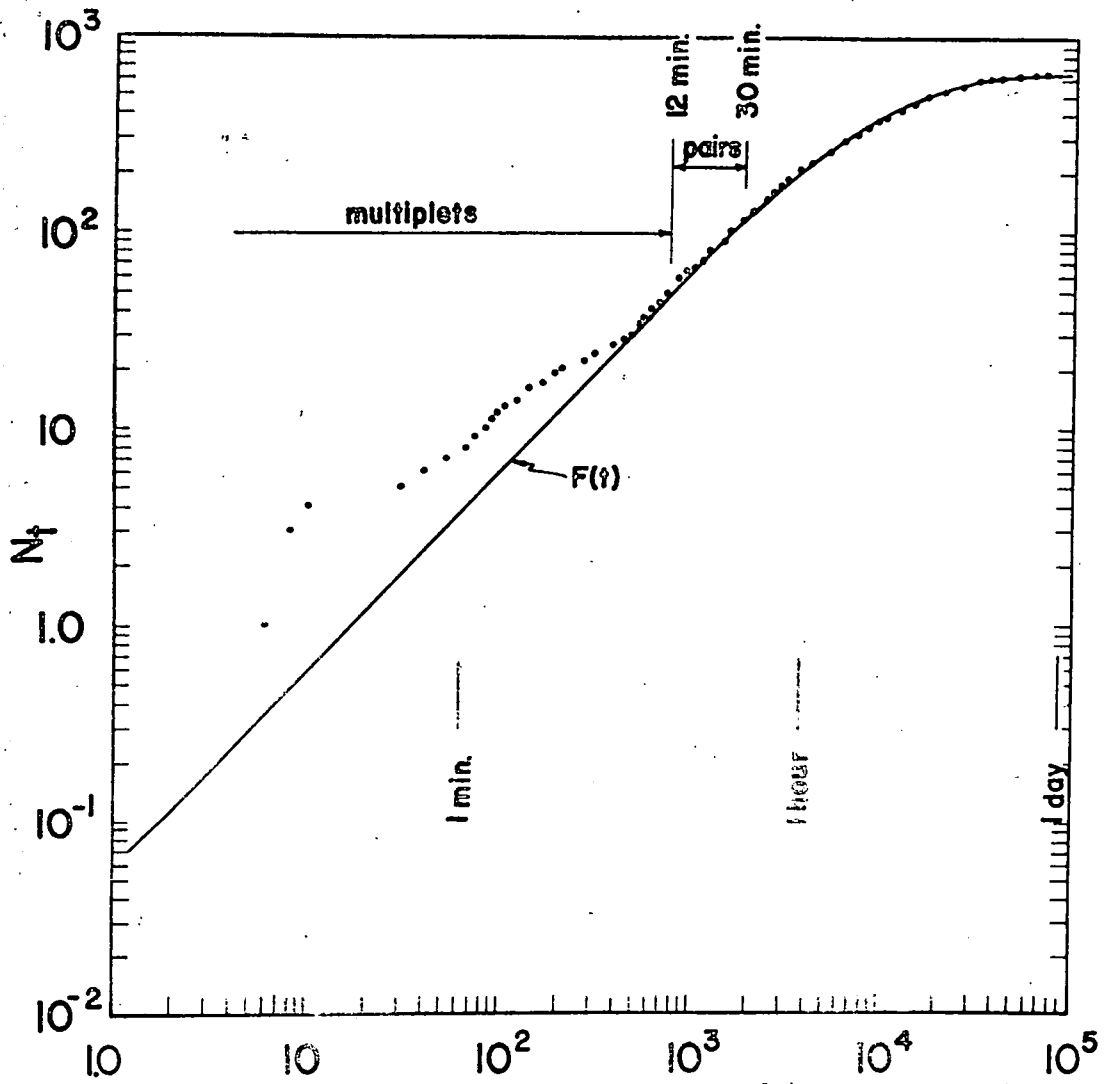


Fig.7.2 Waiting Time, t (sec.) (Cowan et al.)

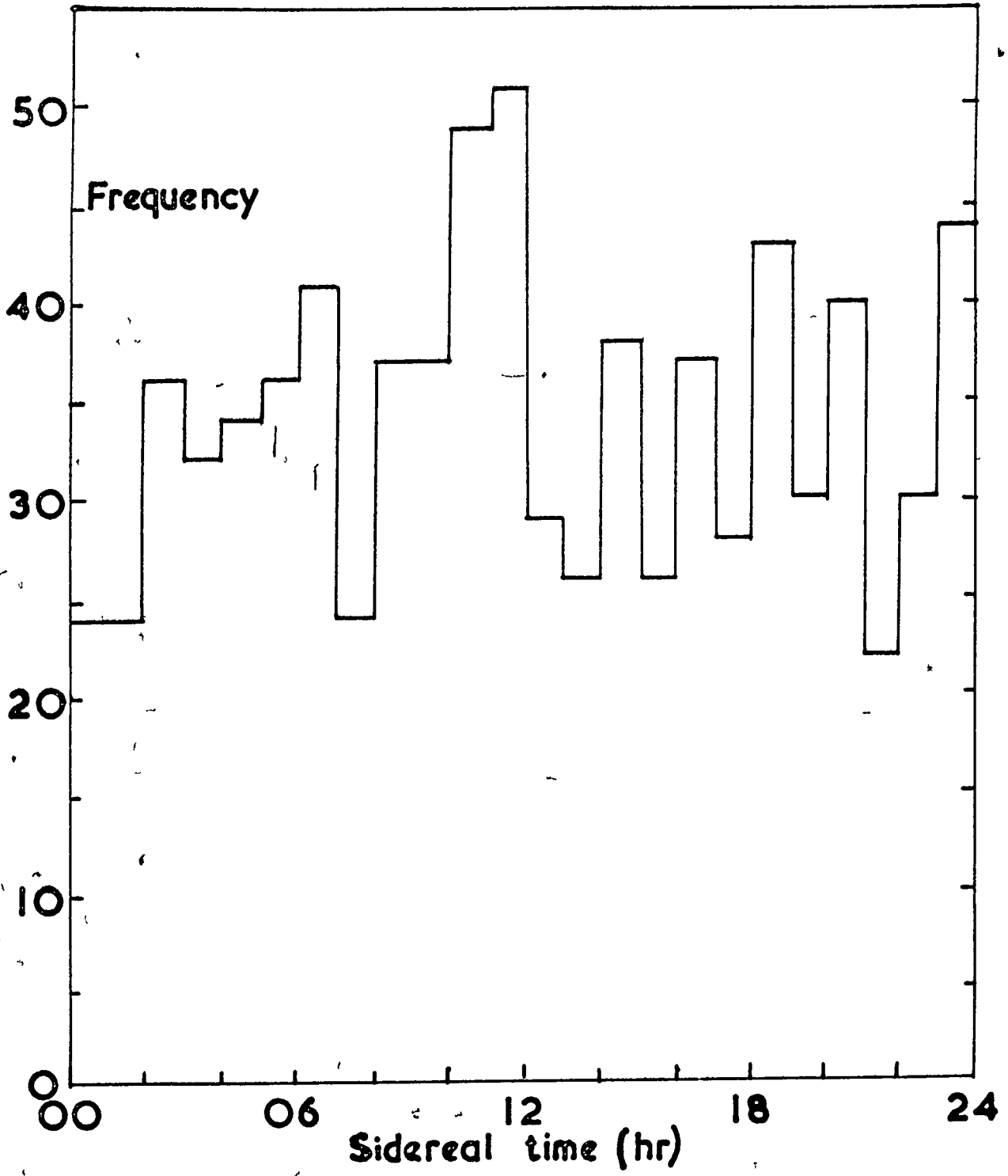
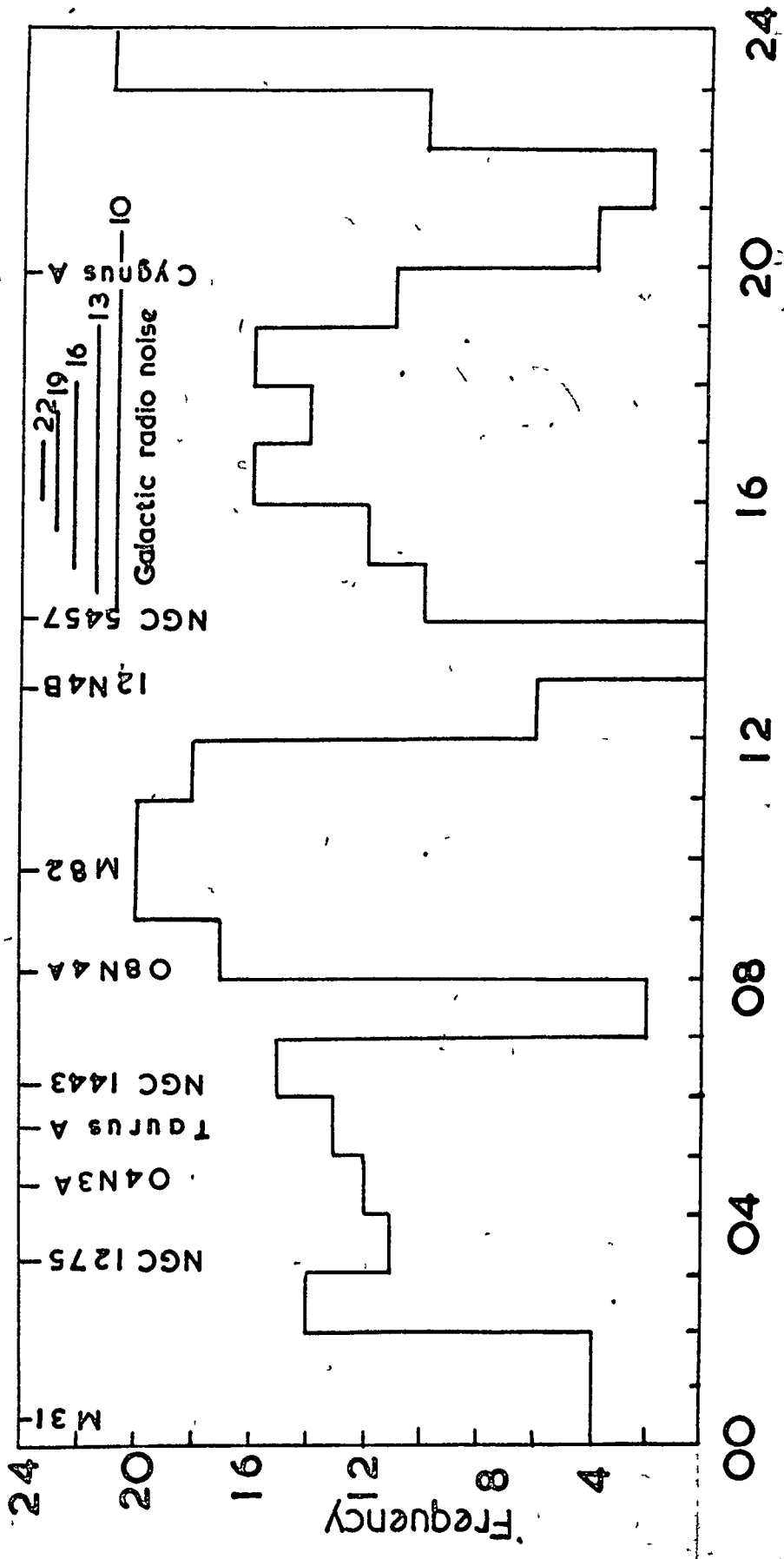


Fig. 7.3 Sidereal time distribution (Cowan et al)

An analysis of the data with respect to sidereal time was also made by computing the sidereal times for each event and accumulating them in 24 bins of one sidereal hour each for the entire interval. The results are displayed in Fig. 7.3. The mean rate of events per sidereal hour was (34.0 ± 8.0) , and it is seen that all bins are within two standard deviations of the mean. Analysis of the occurrence of the bursts was made in a search for a diurnal effect. Associated pairs with intervals equal to or less than half an hour but greater than twelve minutes were plotted in sidereal time as shown in Fig. 7.4. Also shown on this distribution are the right ascensions of strong radio sources on or near the zenith ($\pm 15^\circ$) at Washington, D.C. If the actual sidereal times of the bursts are plotted, two totally clear lanes are seen, one of about 50 minutes duration at about 0730 hours and the other of almost 2 hours duration around 1300 hours. Two others are almost empty: one of about a one hour duration centred on 0130 hours and containing only two associated pairs, and the other of about 1-1/2 hours duration centred on 2100 hours containing one associated pair. It is interesting to note that only one of the discrete sources (12N4B) falls within the clear lanes which are constant in time.



Sidereal time variation of associated events (Cowan et al)

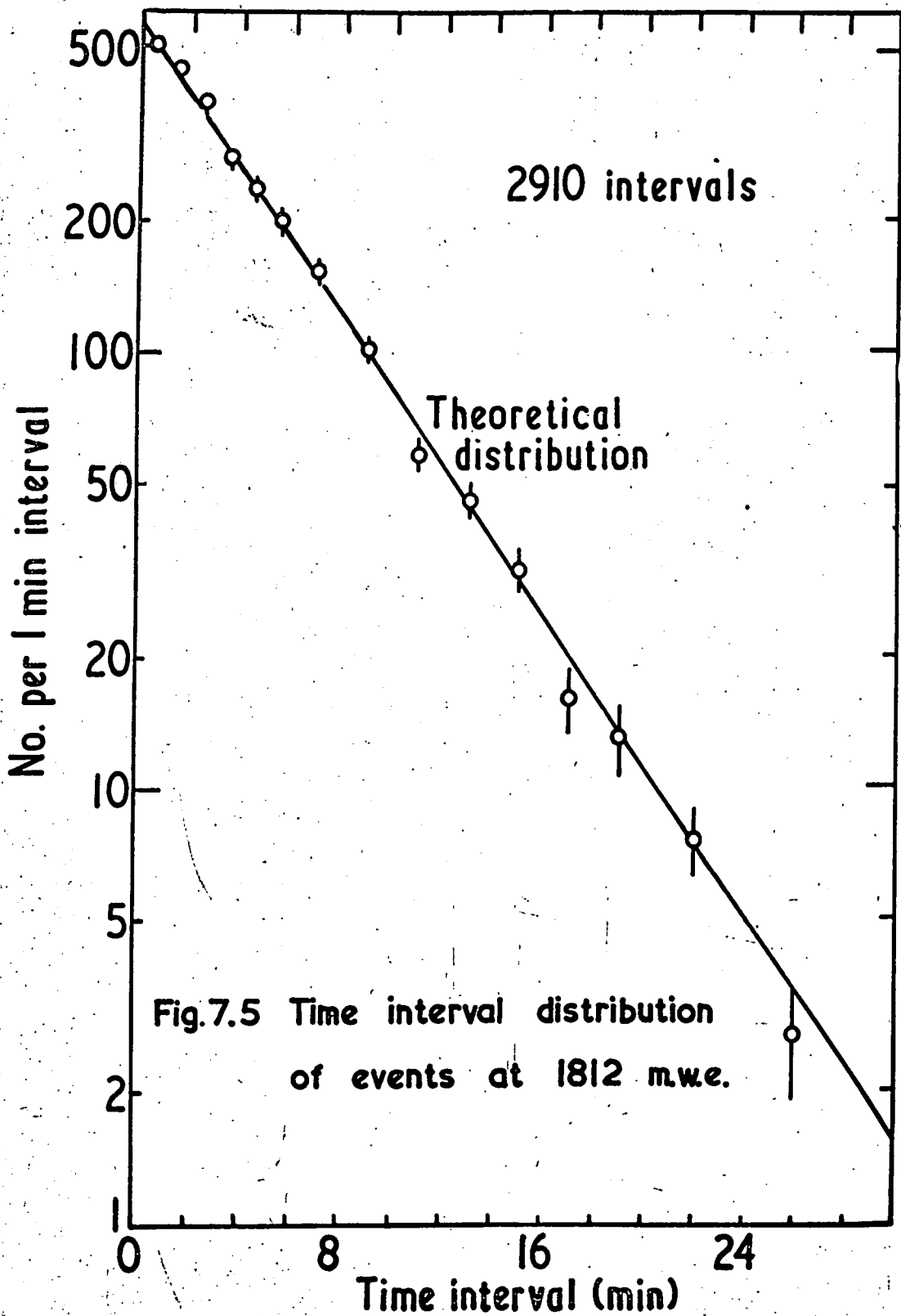
Fig.7.4 Sidereal time variation of associated events (Cowan et al)

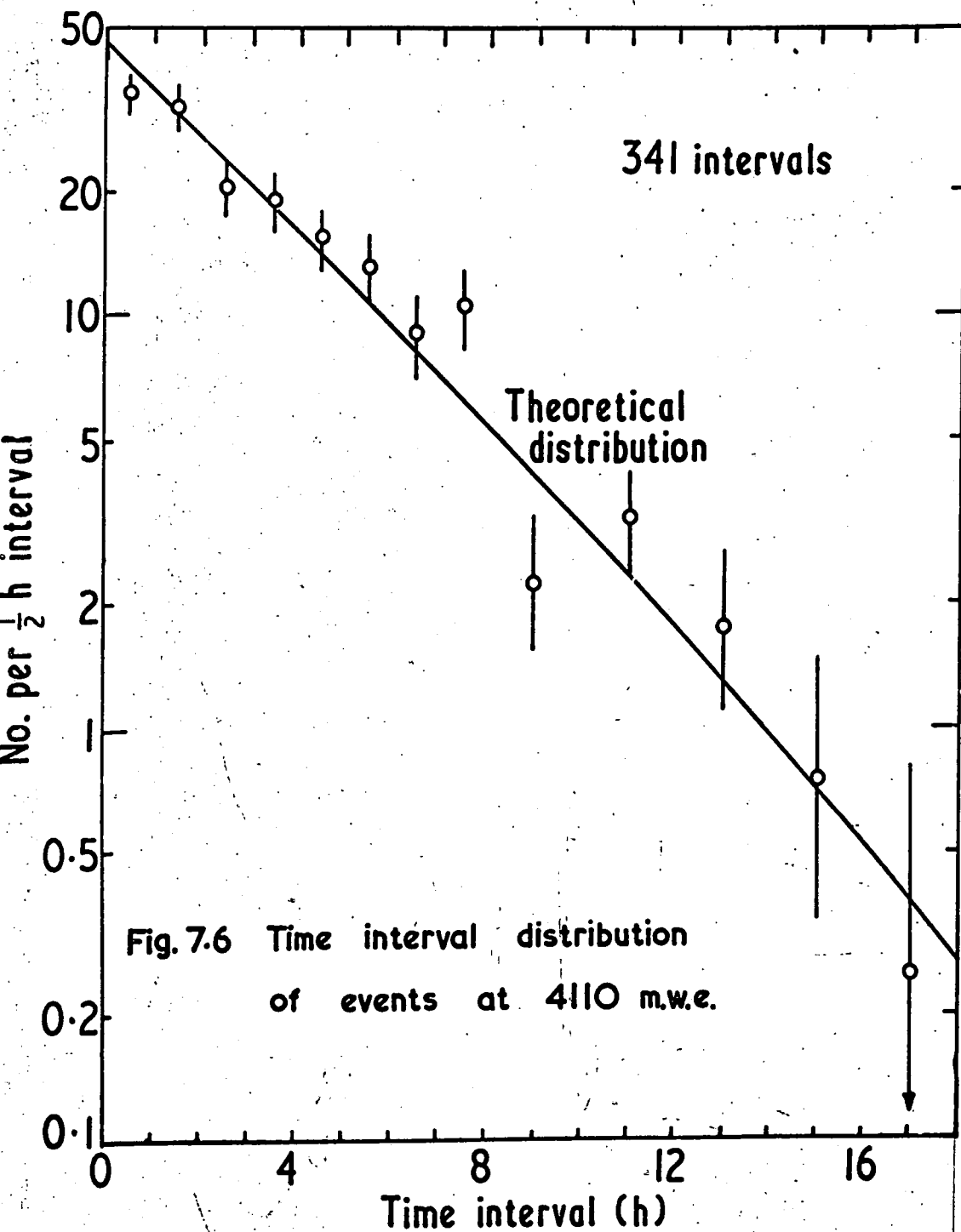
The conclusions of Cowan et al were that cosmic neutrinos were being detected by means of a very narrow resonance in the cross-section function with a maximum value of the order 10^{-28} cm^2 , and that the neutrino flux is estimated to be about $10^{-3} \text{ cm}^{-2} \cdot \text{sec}^{-1} \cdot \text{MeV}^{-1}$ in the region of 170 MeV from sources distributed on the celestial sphere from $+ 15^\circ$ to $+ 45^\circ$.

7.3. The Present Experiment.

In view of the results of Cowan et al it was deemed necessary to make a study of the arrival times of the events detected in the Kolar Gold Field. This was possible at only the two greater depths, since the arrival times of particles at 816 m.w.e. were not recorded.

It is to be noted that should no variations be found this would not necessarily be in conflict with the results of Cowan et al, since the present work refers to all particles, and the depths are considerably greater. A similar analysis is desirable, however, since there does not seem to have been such an examination in the past. The observations of a non-Poissonian distribution in time intervals between successive underground events would not be inconsistent with the ground level observation of a lack of long term time variations if the average rate of bursts were constant.





The results of the present experiment are shown in Figs. 7.5 and 7.6 where the abscissa is the time interval between successive events. The data were taken at the depths of 1812 and 4110 m.w.e., where the minimum muon energies required for penetration were ~ 600 and 2500 GeV respectively. The distributions refer to sea-level muon energies above these values if, as seems very likely, the vast majority of the underground muons are of atmospheric origin as distinct from muon production by neutrinos in the earth. The theoretical distributions shown in Figs. 7.5 and 7.6 were derived from the Poissonian distribution, modified at longer times to allow for the finite lengths in time of the sets of photographic records (e.g. in an 18-hour film only the first hour is effective for events with time interval ≥ 17 hours). At short times a correction was applied to the observed numbers for the events lost in the seven seconds dead time of the apparatus.

It is clear that there is no marked divergence from expectation. In particular the number of particles arriving within 1 minute at 1812 m.w.e. and within 1 hour at 4110 m.w.e. is not in excess of expectation.

The data collected at 4110 m.w.e. were analysed with respect to sidereal time, and the results are shown

in Fig. 7.7, where N_o/N_m is the ratio of the observed number to the number expected isotropy. The results of Hasegawa et al. (1963) concerning μ -rich extensive air showers produced by primaries of energy greater than about 4×10^{15} eV are also shown in this figure. The mean primary energy corresponding to the underground muons at 4110 m.w.e. is $\sim 7 \times 10^{14}$ eV. The lack of variation found in the present experiment indicates that either the underground muons are produced by cosmic ray primaries different from those producing μ -rich showers, or that the variation ceases below $\sim 10^{15}$ eV primary energy.

It is concluded that there is no significant non-Poissonian contribution to the distribution of time intervals between the arrival of successive events underground, and that the phenomena reported by Cowan et al at shallower depths has not been observed with the present apparatus.

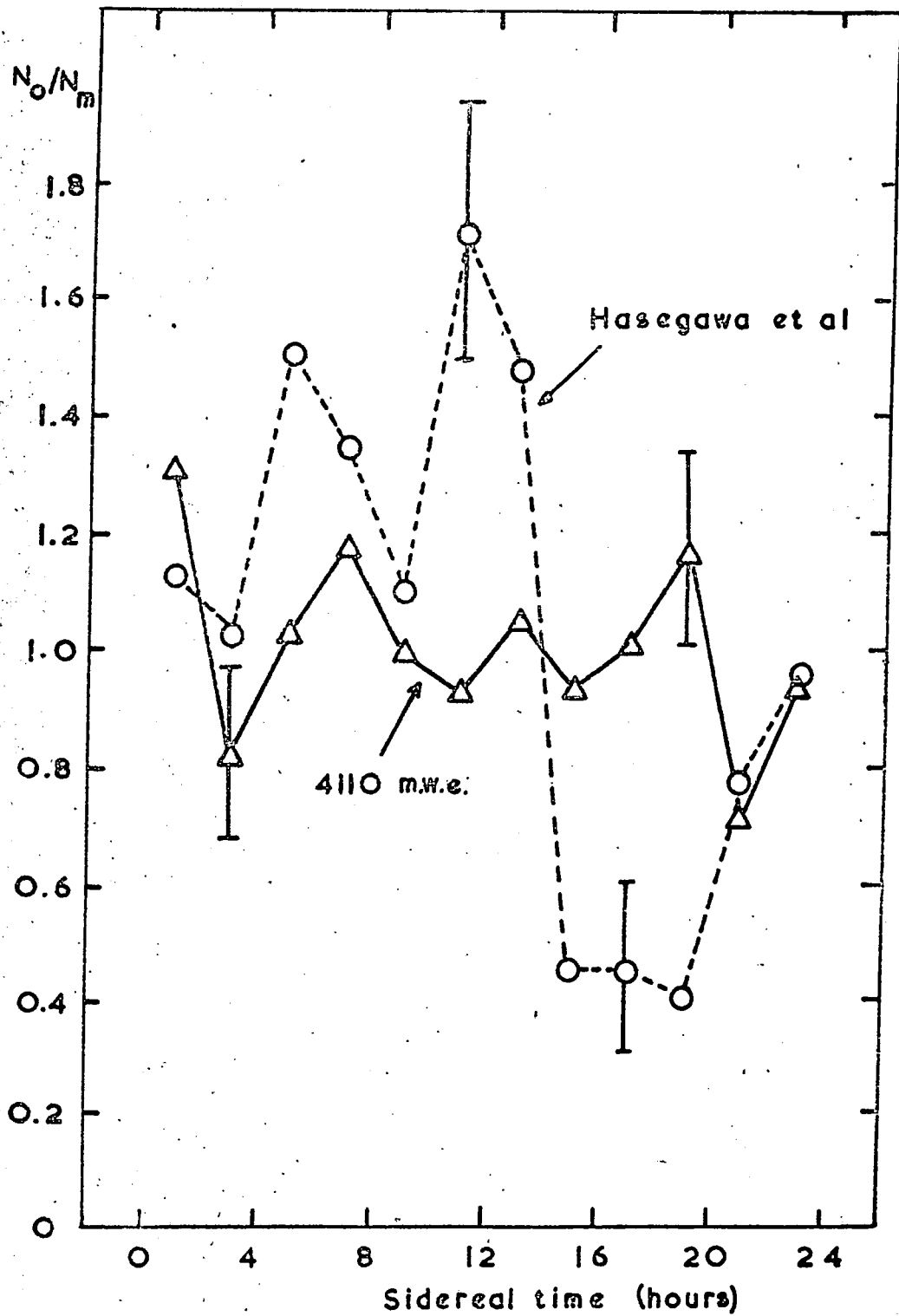


Fig.7.7 The distribution in sidereal time of events at 4110 m.w.e.

CHAPTER 8.

ELECTROMAGNETIC INTERACTIONS.

8.1. Introduction.

Studies of the interactions of muons deep underground are of interest in that they enable an examination to be made of electromagnetic phenomena occurring at very high energies. Comparison of the frequencies of interactions at various depths allows the energy dependence to be studied. The events to be described are those which showed evidence of muons accompanied by a soft component generated locally in the surrounding rock or in the apparatus.

8.2. Classification of Events.

The types of interaction seen from the flash tube records can be classified as follows :-

- (a) Secondaries visible above the lead absorber, i.e.
 - (i) single electrons incident from the rock above the apparatus,
 - (ii) electron showers incident from the rock,
 - (iii) single, low energy electrons (δ -rays) generated within the top flash tube tray.
- (b) Secondaries visible below the lead absorber, i.e.
 - (i) single electrons generated in the lead,

<u>Type of interaction</u>	816 m.w.e.	1812 m.w.e.	4110 m.w.e.
Total events	3643	5965	476
Single electron from rock	148	340	38
Single electron from lead	157	258	32
Electron shower from rock	97	196	17
Electron shower from lead	140	233	30
Single electron in top flash tube tray	46	69	5
Single electron in lower flash tube tray	74	86	9

Table 8.1 Frequencies of electromagnetic interactions.

	%	%	%
Single electron from rock	4.06±0.33	5.70±0.31	7.98±1.29
Single electron from lead	4.31±0.34	4.33±0.27	6.72±1.19
Electron shower from rock	2.66±0.27	3.29±0.24	3.57±0.87
Electron shower from lead	3.84±0.32	3.91±0.26	6.30±1.15 +0.71
Single electron in top flash tube tray	1.26±0.19	1.16±0.14	1.05±0.45
Single electron in lower flash tube tray	2.03±0.24	1.44±0.16	1.89±0.87 -0.61

Table 8.2 Probabilities of occurrence of e.m. interactions.

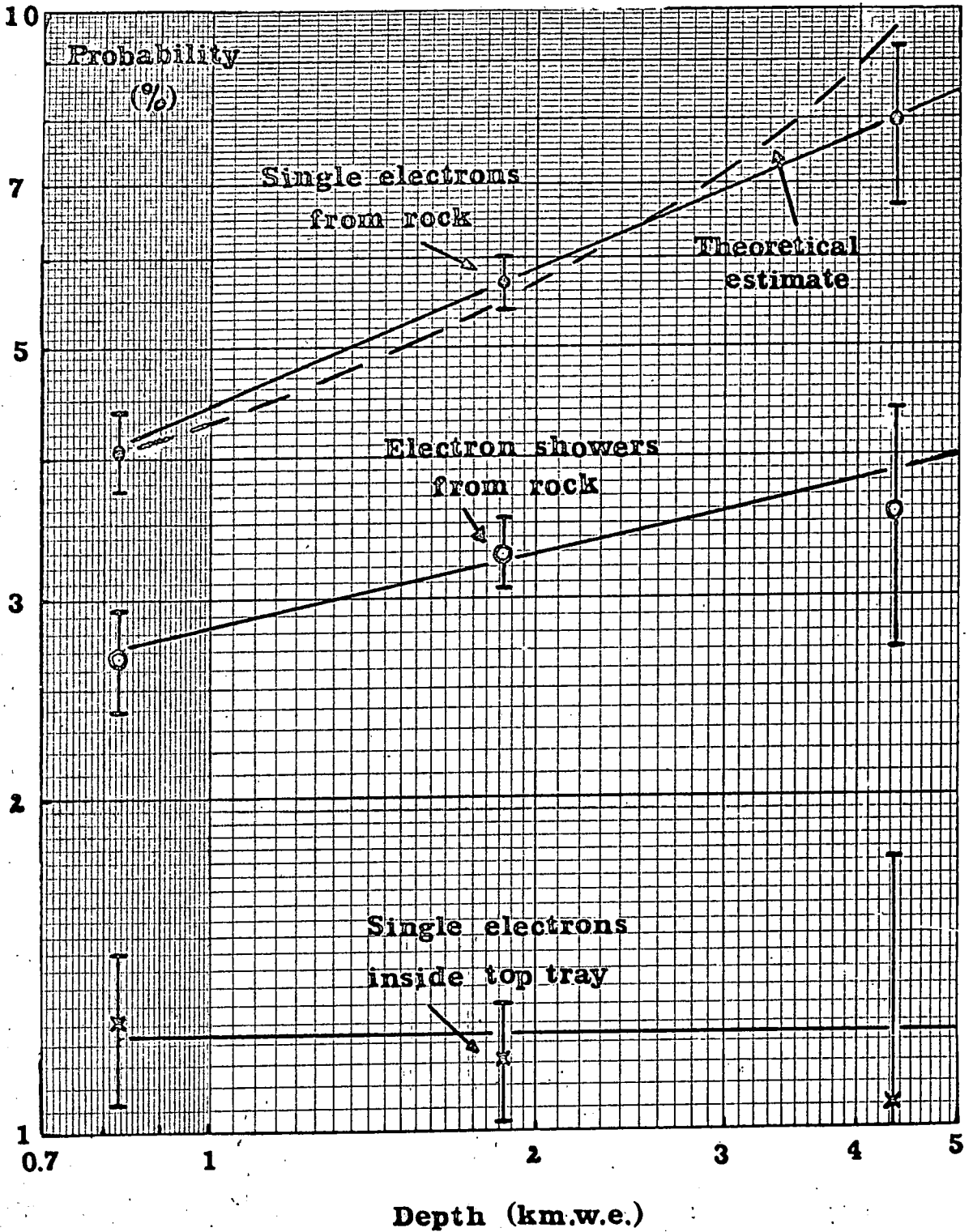


Fig. 8.1 Probabilities of accompaniment above the lead.

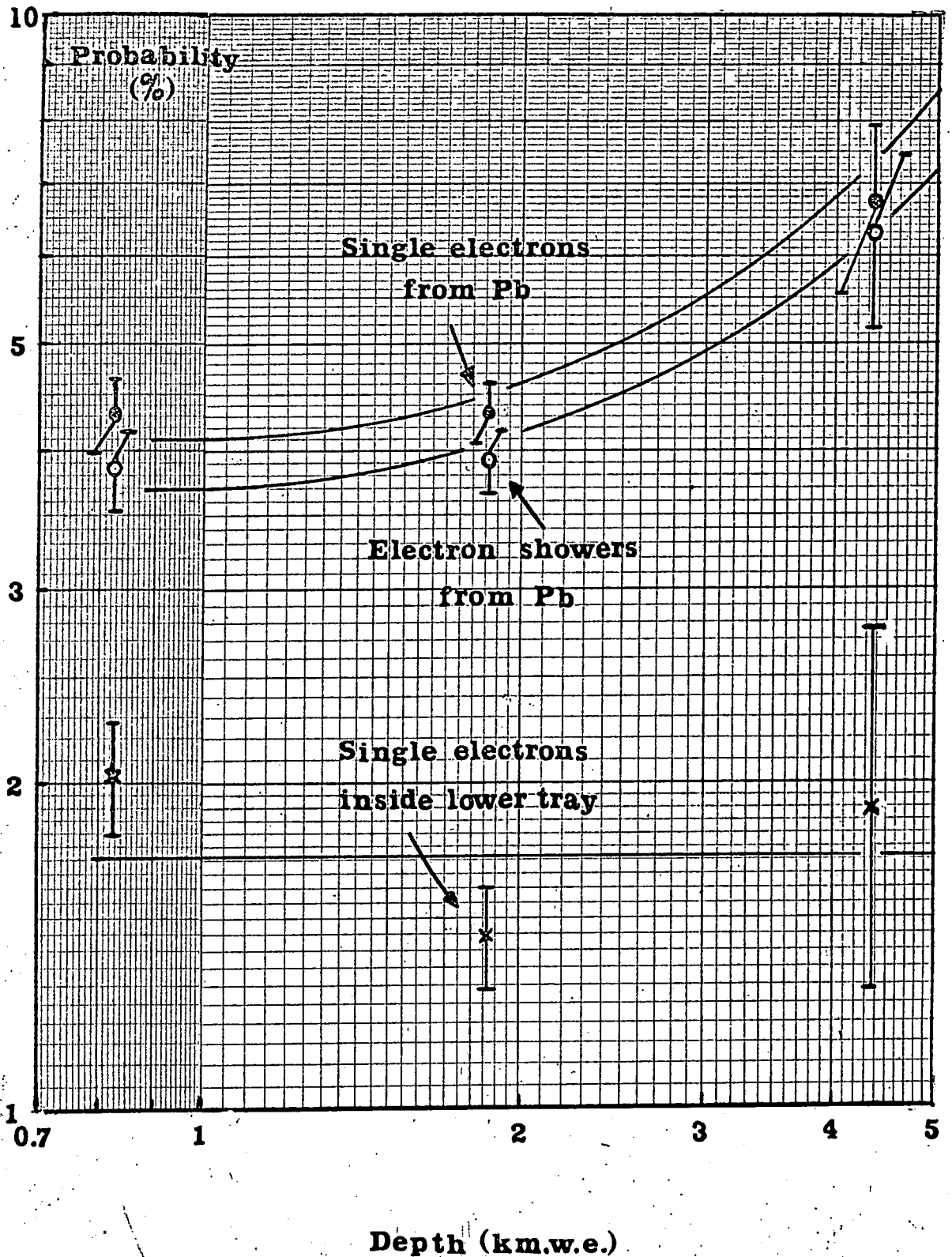


Fig.8.2 Probabilities of accompaniment below the lead.

- (ii) electron showers produced in the lead,
- (iii) single, low energy electrons (δ -rays)
generated within the lower flash tube tray.

The frequencies and probabilities of occurrence of each type of event for the three depths of observation (816, 1812 and 4110 m.w.e. respectively, the corresponding mean muon energies underground being 170, 470 and 1470 GeV) are shown in Tables 8.1 and 8.2 respectively. The probabilities of occurrence are plotted as a function of depth for rock and lead in Figs. 8.1 and 8.2.

8.3. Interpretation of the Electromagnetic Interactions.

Those events where single electrons were generated in the flash tube trays correspond to the lowest energy transfers. The near constancy of the probabilities of their occurrence as a function of depth can be understood since the cross-section for production of very low energy electrons through μ -e collisions is virtually independent of energy. The somewhat higher values for the lower tray are probably due to enhancement by low energy electrons which were actually produced in the lead, but were so scattered as to appear to have been produced in the lower tray.

The increase in the other probabilities with increasing depth confirm, qualitatively, the increase with

increasing energy predicted from the theory of electromagnetic interactions (Hayman et al. 1963). This increase is due to the growing importance of bremsstrahlung and direct pair production. The increase in cross-section for direct pair production is largely responsible for the increase in probability for the observation of single electrons. The reason for this is that one electron usually receives the majority of the energy and the cross-section favours low energy transfers since for a given muon energy $\sigma \propto E_t^{-3}$ where E_t is the energy transferred to the electron.

An attempt has been made to make a quantitative estimate for the production of single electrons in rock using the data of Hayman et al (1963). It was assumed that only half the ionization loss is efficient in producing potentially observable electrons, the remainder going in distant collisions, and adding the contribution from pair production (cf. Fig.6.1). The resulting variation is shown as a dotted curve, normalized to the shallowest depth, in Fig.8.1. The agreement between prediction and observation is satisfactory, but cannot be regarded as positive evidence for this type of interaction.

Similarly it is difficult to predict a theoretical

estimate for shower production because of the complexities of shower multiplication. However, the increase in shower probabilities with depth is thought to be due to the growing importance of the energy losses due to bremsstrahlung. The increased probability for shower production in lead compared with rock is presumably due to the effect of the Z^2/A dependence of the rate of energy loss factor ($Z^2/A = 6.3$ for K.G.F. rock and 32.5 for lead) offset largely, but not completely, by the reduction in target thickness since the radiation length, X_0 , is shorter in lead (5.8 gm.cm^{-2}) than rock (24 gm.cm^{-2}).

8.4. Extrapolation to very great depths.

Of contemporary interest is an extrapolation of the observed probabilities to predict the expected values at 7600 m.w.e. (the location of the K.G.F. neutrino experiment).

The extrapolated values are as follows :-

- i) the probability of an incident muon being accompanied by one or more secondaries is 13-20%,
and
- ii) the probability of an incident muon generating one or more electrons in the lead absorber is 16-30%.

Thus the total probability of observing a

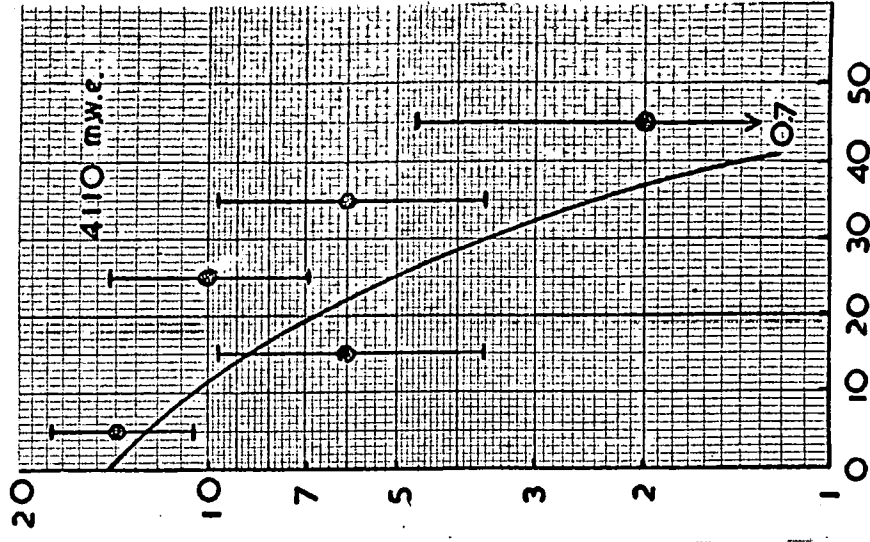
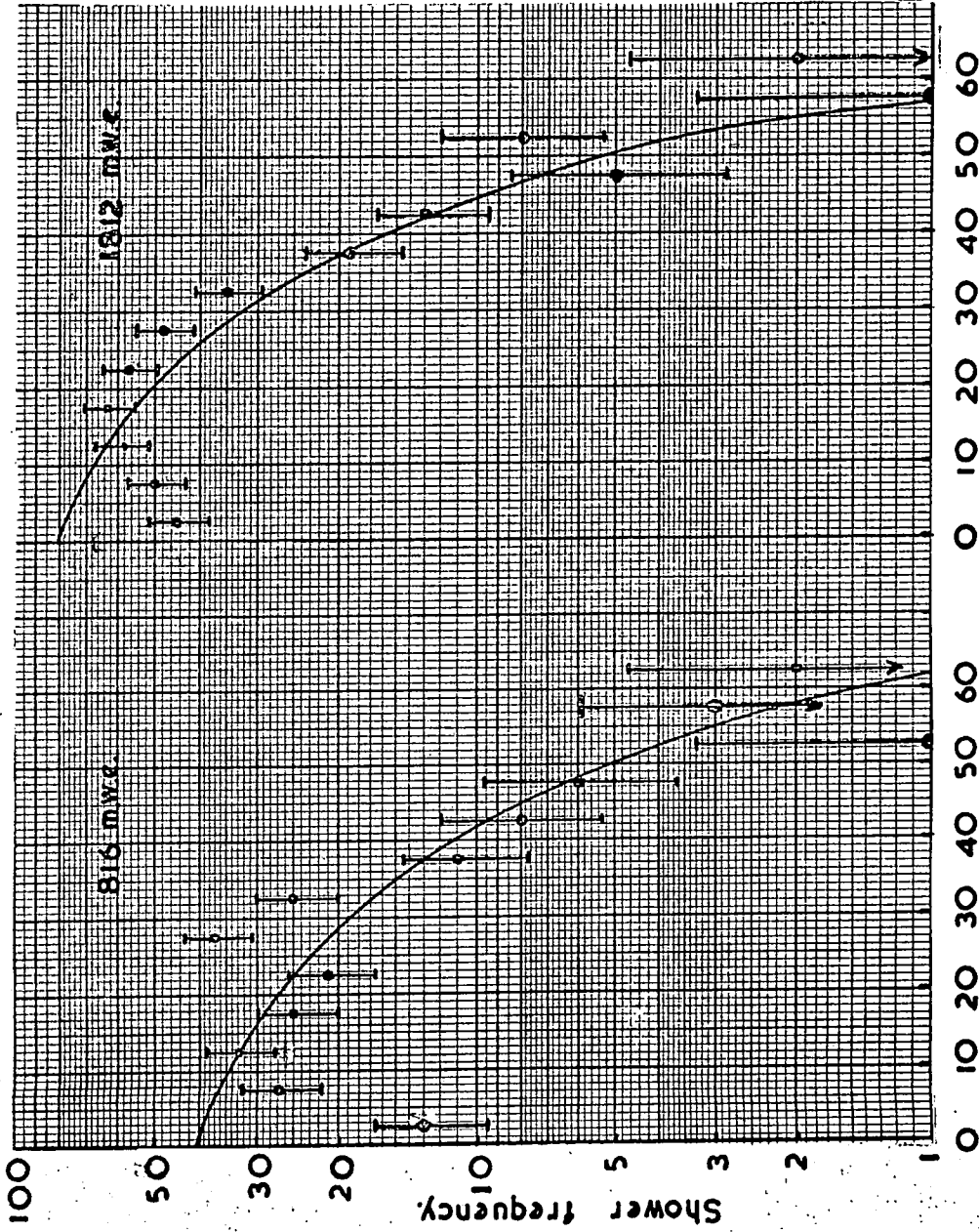


Fig. 8.3. The angular distributions of single muons accompanied by showers.

secondary associated with a muon of atmospheric origin at 7600 m.w.e. is 30-50%. This is much higher than expected for muons produced in neutrino interactions since these are expected to have energies in the region of tens of GeV and for which the probability is thought to be less than 10%. Such information can be of value in distinguishing, on a statistical basis, between the muons of the two different origins deep underground.

8.5. Muons Accompanied by Electron Showers.

A more detailed analysis was made of this class of event with respect to the angular distributions of single muons accompanied by electron showers. The angular distributions at the three depths are shown in Fig.8.3. Also shown are the observed angular distributions determined in Section 4.2 normalized to the total number of shower events at each depth.

The distributions at the two shallowest depths are clearly flatter than those for single particle events, as would be expected. The probability distributions as a function of projected zenith angle ^{at 1812 m.w.e.} show a steady increase between 0° and about 30° (equivalent to a depth of about 2100 m.w.e.) and then a decrease to about 50° (2800 m.w.e.) A slow increase with zenith angle would be expected because

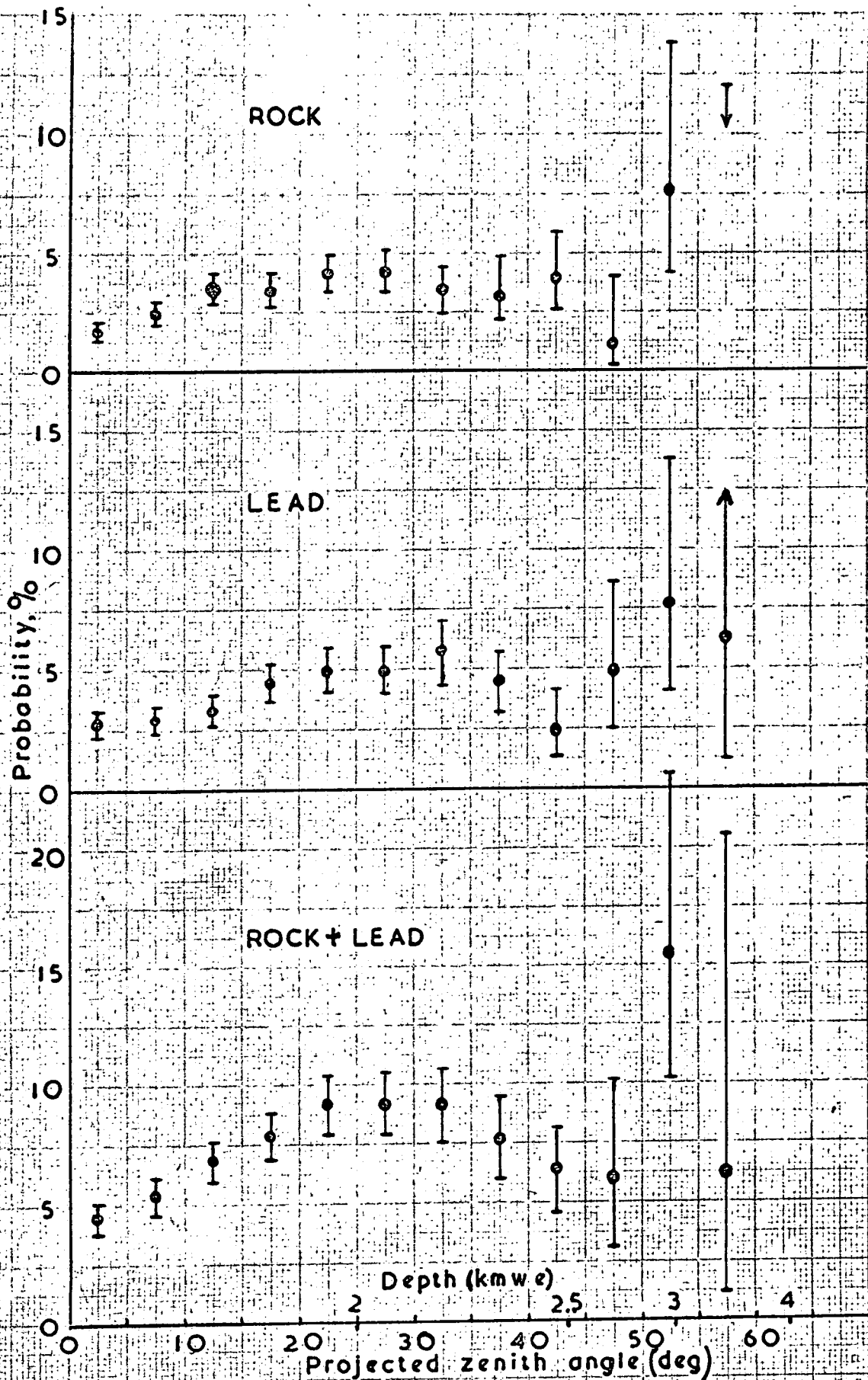


Fig.84 Probabilities of shower occurrence at 1812 m.w.e.

of increasing muon energy, but not as rapid as displayed in the distribution for rock + lead in Fig.8.4. (The probability distribution at 816 m.w.e. also shows the same trend). In an attempt to determine the reason for this the probability distributions of shower events from the rock and from the lead are also shown in Fig.8.4. There is some indication of a slightly faster increase in probability with zenith angle for rock showers than those from the lead absorber. There is no obvious physical reason why the shower distributions are as shown; a possible explanation is the presence of errors in track location where very dense showers are concerned and the muon path is defined by only four flash tubes. In order to make more accurate measurements of the zenith angles of muons initiating such events it would be necessary to increase the number of layers of flash tubes.

The angular distributions shown in Figs.4.1 - 4.3 were divided into two parts, above and below the median angle. The shower distributions were similarly divided, and the probability of occurrence of showers above and below the median angles were found. The results are shown in Table 8.3. At each depth the probability of shower occurrence at angles greater than the median is larger

	816	1812	4110
	m.w.e.	m.w.e.	m.w.e.
	%	%	%
P(<median)	4.5±0.5	5.5±0.4	8.0±1.9
P(>median)	6.6±0.6	9.2±0.6	13.2±2.5

Table 8.3 Probabilities of shower accompaniment of muons with respect to the median zenith angle.

than that below. Thus experiments in which shower events are rejected will give values of n which are too large.

CHAPTER 9.

MULTIPLE PENETRATING PARTICLES.

9.1. Introduction.

Several workers have reported the simultaneous occurrence of two or more penetrating particles at various depths (≤ 1600 m.w.e.) underground. (Higashi et al (1957, 1960, 1962,A), Kessler and Maze (1957), Barrett et al (1952) and Vernov et al (1960, 1962)). Such events have been referred to in the past as beams of muons or muon bundles. Vernov et al recorded bundles underground simultaneously with the detection of quite large extensive air showers at ground level and found that the bundles were not connected with local showers from individual muons, but occurred in the composition of extensive air showers. This has been confirmed in similar experiments by Higashi et al who observed muon beams in cloud chambers operated at 50 m.w.e. in conjunction with a large size air shower detector at ground level. More recently Chaudhuri and Sinha (1963) have also reported the existence of muon bundles at a depth of 148 m.w.e. in a cloud chamber experiment. In 4,531 hours of operation, 20 double events, 4 triple and 3 quadruple events were detected. The individual particles in these events penetrated all the

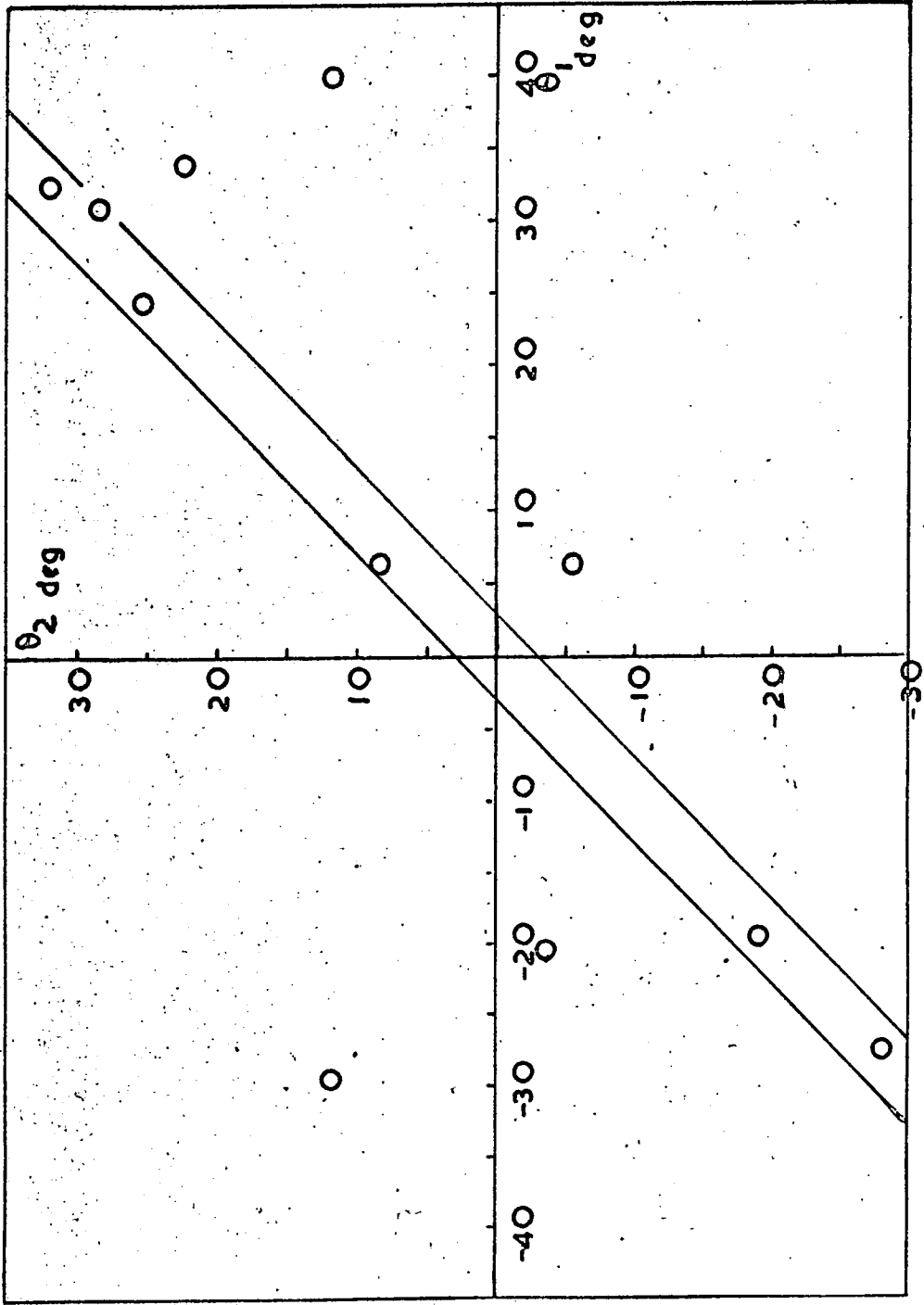


Fig.9.1 The angular distribution of double muon events at 816 m.w.e.

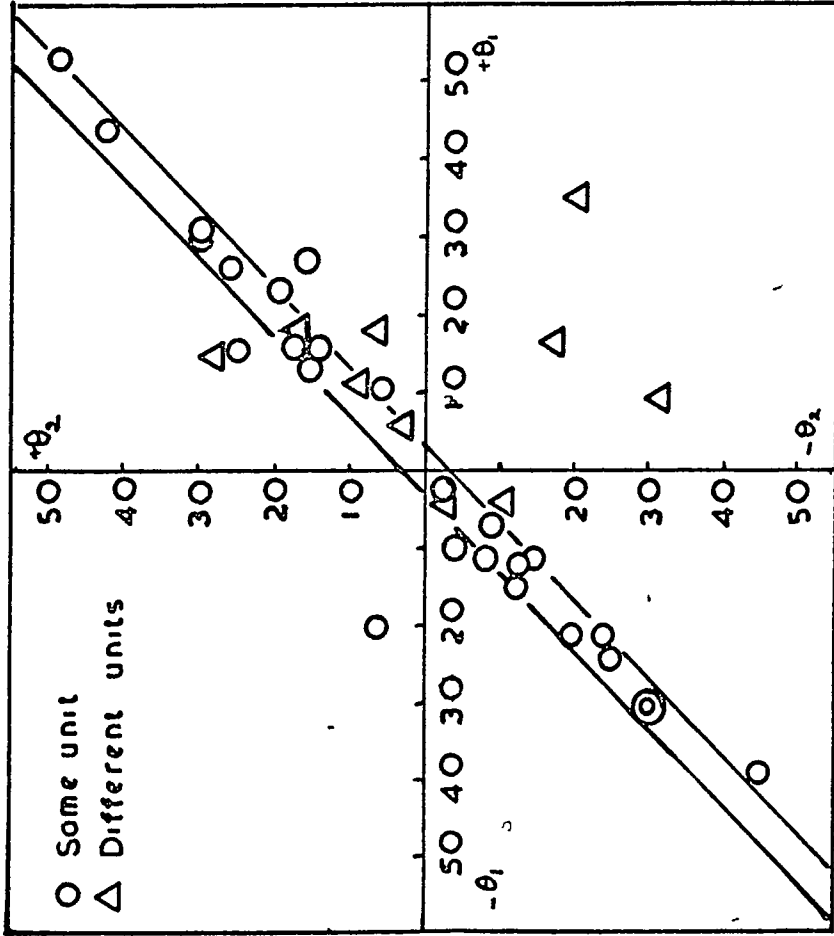


Fig.9.2 The angular distribution of double particle events at 1812 mwe

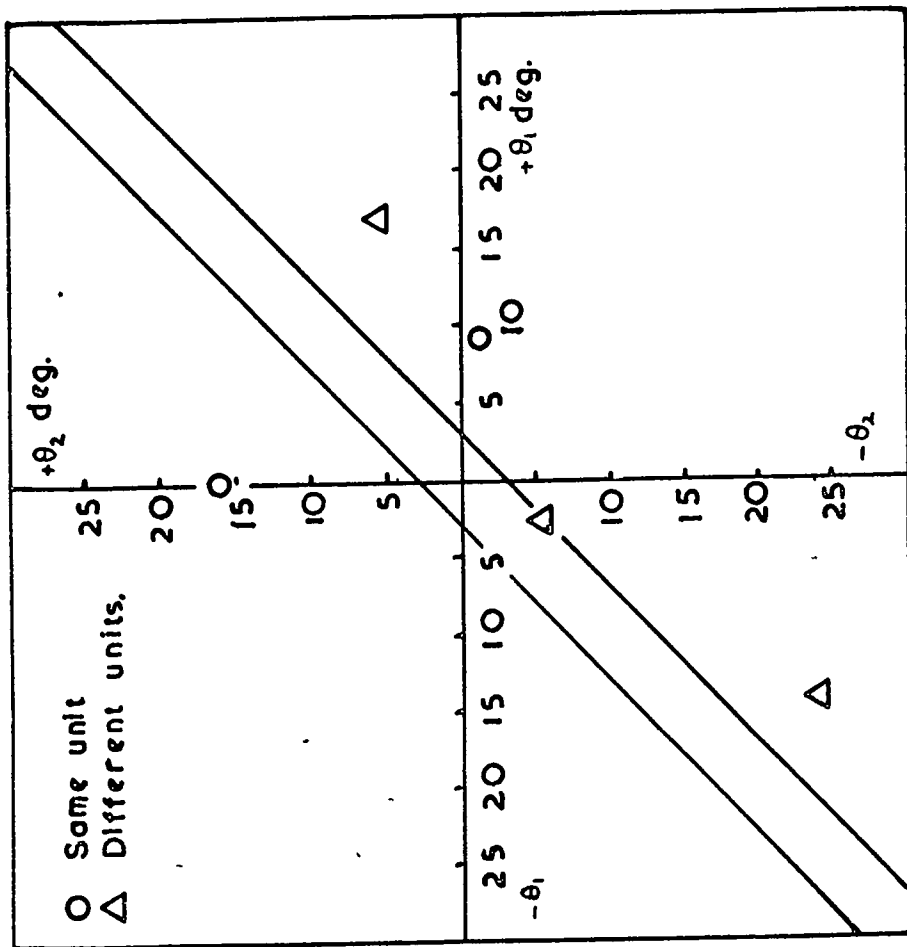


Fig.93 The angular distribution of double particle events at 4110 m.w.e.

cloud chamber plates (0.3 and 0.9 radiation lengths at various stages of the experiment) in addition to 20 cm.Pb. placed above the chamber, and were found parallel within 2° over their entire track lengths inside the chamber. The separation between any two particle tracks in the events ranged between 5 and 30 cm.

9.2. The Present Experiment.

The multiple penetrating particle events (MPP) detected in the present experiment can be classified as follows :-

- i) Events where two or more particle tracks can be resolved, and
 - ii) Events where a core of very close particles were seen.
- Of the former category there were 11, 41 and 5 events at the three depths of observation, 816, 1812 and 4110 m.w.e. respectively, and 7, 16 and 2 close cores.

The events in category (i) containing two penetrating particles can be seen plotted on the scatter diagrams (Figs. 9.1 - 9.3) for the three depths, where the axes θ_1, θ_2 are the projected zenith angles of the muons (particles from the north have positive zenith angles and those from the south negative). At 1812 m.w.e., 5 of the events were triplets (Table 9.1). A channel 6° in width

θ_1	θ_2	θ_3
+3.5°	+3.0°	+2.5°
-20.5°	-20.5°	-19.0°
-24.0°	-24.0°	-26.0°
-13.0°	-23.0°	-24.0°
+6.5°	+7.0°	+6.5°

Table 9.1 Events at 1812 m.w.e. showing more than two penetrating particles.

has been plotted on the scatter diagrams, and events falling within this channel are defined as associated parallel pairs of penetrating particles.

9.2.1. MPP's at 816 m.w.e.

The scatter diagram (Fig.9.1) shows that of the eleven photographs where two particles were seen to penetrate the apparatus, only six pairs lie within the 6° channel. Of the remaining five all but one pair (that plotted at $+6.5^\circ, -5.5^\circ$) are diverging from above. It will be remembered that the two telescopes were operated consecutively at 816 m.w.e. and therefore all eleven pairs of particles are contained in an area of one square metre. It is interesting to note that only one parallel pair is near the zenith, the remaining five pairs being $> 20^\circ$ to the zenith. The rate of occurrence of parallel pairs at 816 m.w.e. is $(4.0 \pm \frac{2.4}{1.6}) 10^{-5} \text{ Sec}^{-1}$. Electromagnetic interactions were seen associated with five of the parallel events. (2 secondary electrons from the rock, one in the lower flash tube tray and three showers from the lead).

9.2.2. MPP's at 1812 m.w.e.

At this depth both telescopes were operated

simultaneously at a separation of about 1.5 m. It was therefore possible to search for the existence of associated penetrating particles more widely separated than at 816 m.w.e.

19 pairs of parallel particles were observed in the same telescope, and 4 parallel pairs with one particle in each telescope. In addition there were five triple events (Table 9.1). The first two of the triple events each show three parallel penetrating particles, but in both cases two particles are in one telescope and the third is in the other. This type of event would have ^{of} course been analyzed as a pair of particles at 816 m.w.e. The third event shows three parallel particles passing through the same telescope at zenith angles of -24° , -24° and -26° . The fourth triplet again shows three particles passing through one telescope, but only two are parallel, the third particle diverging from the parallel tracks by about 11° . The fifth triplet event shows three parallel particles penetrating a single telescope. In addition there are two secondary electrons from the rock which stopped in the lead, and one of the penetrating particles has produced a small cascade shower from the lead. The rate of occurrence of parallel pairs in 1 detector at this

depth was $(7.2 \pm 1.7) 10^{-6} \text{ sec.}^{-1}$.

The angular distribution of particle bundles is shown in Fig.9.4. The horizontal separation (projected view) between the particles in doublet events was measured for those cases where the two muons passed through the same telescope. This distribution is shown in Fig.9.5 where comparison is made with the distribution for single muons taking arrival direction into account. In order to obtain this latter distribution, various angular ranges were selected (i.e. 0° - 10° , 10° - 20° , etc.) and the separation between consecutive particles in the same angular range was measured and a histogram plotted for each range. Finally, these histograms were added together to give the histogram shown in Fig.9.5. The mean value of the MPP separation distribution was found to be $(14.69 \pm 2.82)\text{cm}$ and that for single muons was $(28.50 \pm 0.91)\text{cm}$. The curve shown for the single particle distribution is an approximate fit and has been normalized to the MPP distribution.

In view of the flatness of the angular distribution of MPP's and the difference in the separation of pairs from that of single muons it is concluded that the

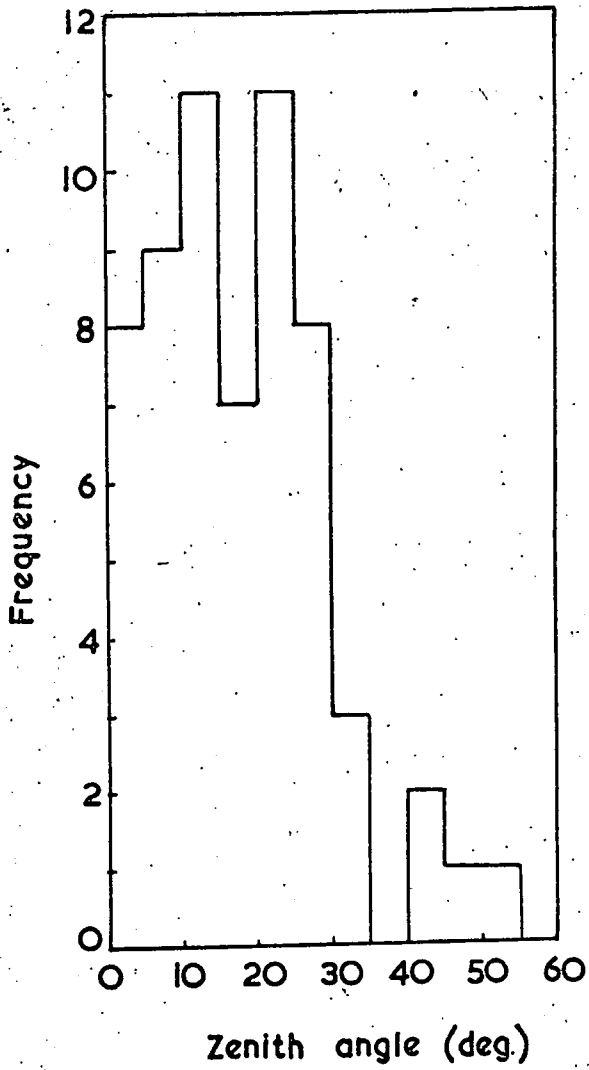


Fig. 9.4 The angular distribution of double particle events (1812 m.w.e.)

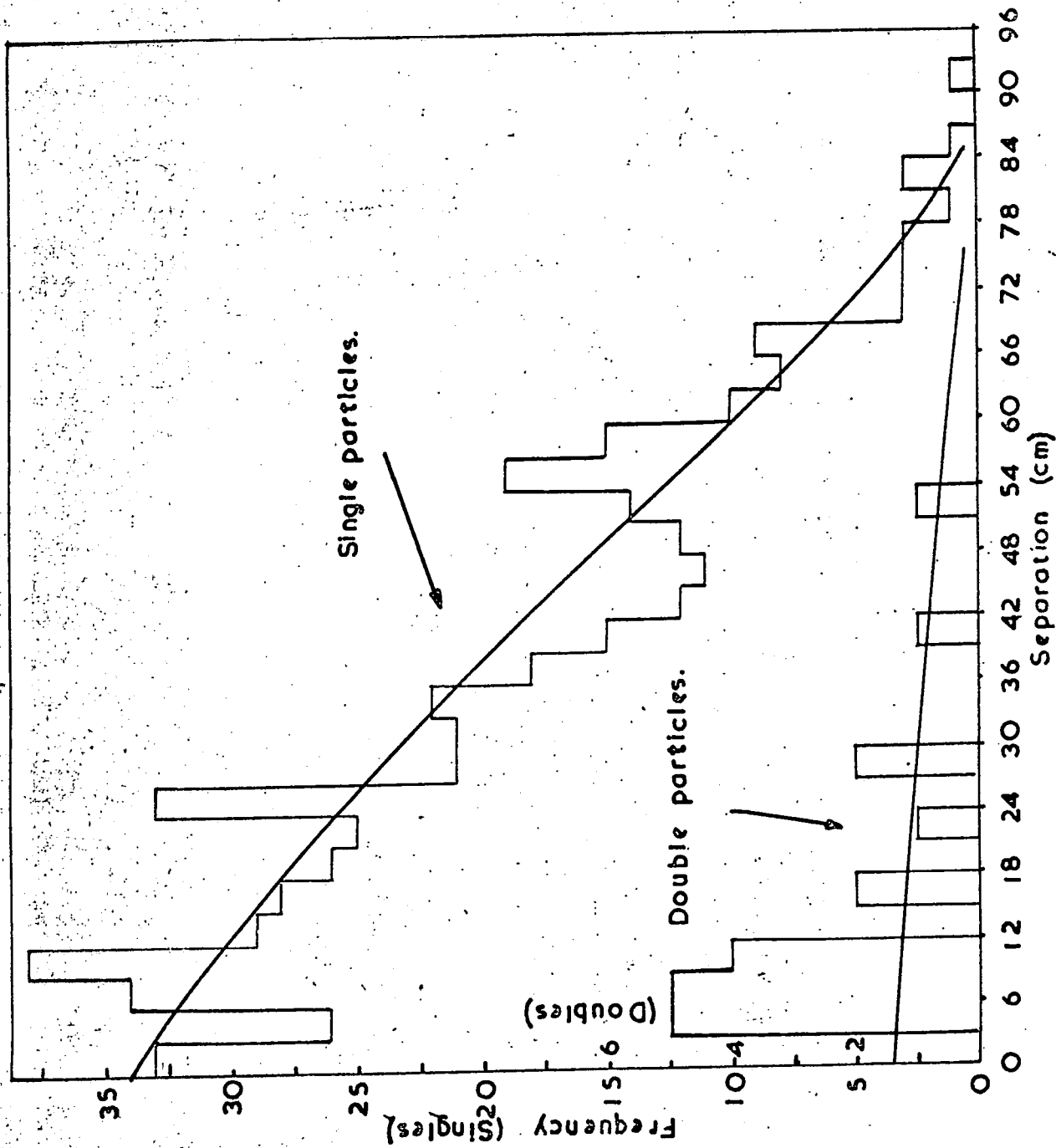


Fig.9.5 Separation of single & double events at 1812 m.w.e.

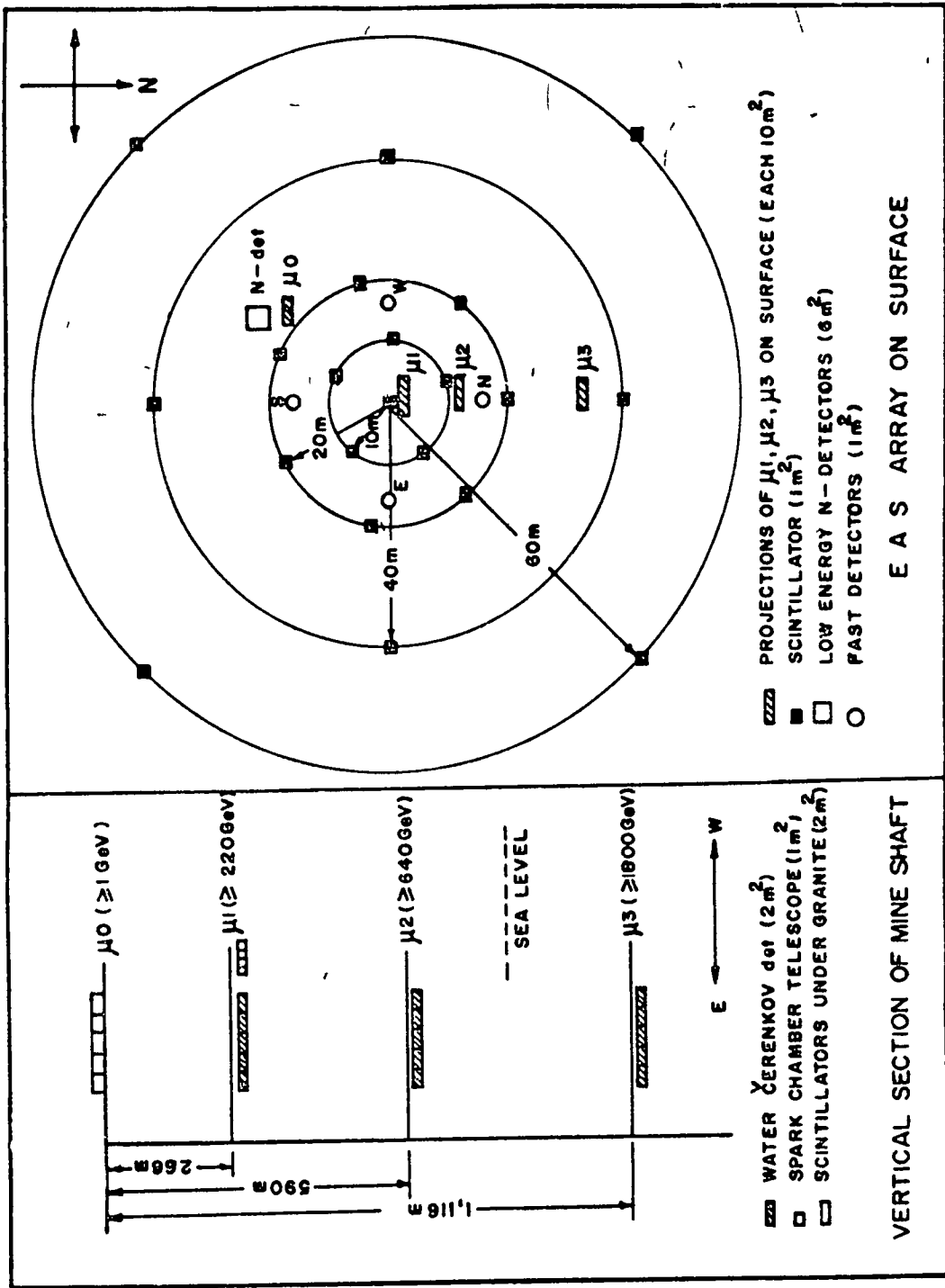


Fig 96 The E A S and underground arrangement at KGF

MPP's and the single particle events are not of the same origin. It is probable that the MPP's originate in extensive air showers as reported by the various authors mentioned in Section 9.1.

Confirmation of this can be made by operating an air shower array of detectors on the surface in conjunction with underground detectors. Such an experiment has in fact been started at the Kolar Gold Fields by the EAS Group from Tata Institute, Bombay. The proposed experimental arrangement is shown in Fig.9.6. It comprises on surface 20 m^2 plastic scintillator to measure the shower size, 4 fast timing scintillators to determine the arrival direction, 15 N-particle detectors and 10 m^2 of scintillator situated beneath a granite stack to measure muon density ($\geq 1 \text{ GeV}$). 30 m^2 of water Cerenkov detectors will eventually be distributed at depths of 816, 1812 and $\sim 3400 \text{ m.w.e.}$ It is envisaged that spark chambers will also be operated at 816 m.w.e. to determine the arrival direction of muons and investigate close cores of muons. At the time of writing the shower size detector at surface and the water Cerenkov tanks at 816 and 1812 m.w.e. have been in operation for about 8 months. The rate of occurrence underground of events in coincidence with air

showers at the surface is $\sim 5.6 \times 10^{-5} \text{ sec}^{-1} \text{ m}^{-2}$ at 816 m.w.e. and $\sim 4.2 \times 10^{-6} \text{ sec}^{-1} \text{ m}^{-2}$ at 1812 m.w.e. Comparing these rates with the rates of multiple events observed in the experiment being reported here $\left[(4.0^{+2.4}_{-1.6}) 10^{-5} \text{ sec}^{-1} \right]$ and $(7.2 \pm 1.7) 10^{-6} \text{ sec}^{-1}$ it is reasonable to suppose that the multiple penetrating particles are part of the composition of extensive air showers.

9.2.3. MPP's at 4110 m.w.e.

In addition to the two telescopes a "wing" array of flash tubes was also operated at this depth. The "wing" flash tubes were pulsed by the UHT for every event recorded by either telescope. Of the five double particle events only one is seen to lie within the 6° band (Fig.9.3), the particles arriving at projected zenith angles of -2.5° and -5.5° . The horizontal separation of the two particles was more than 1.5 m. and less than 3.5 m. since they occurred in separate telescopes. Examination of the five events shows, however, that in each case the point of interaction is in the last two or three metres of the overlying rock. Thus the rate of particle bundles from air showers is $< 1.3 \times 10^{-7} \text{ sec}^{-1}$.

It is of interest to note that all the double events at this depth have vertices in the overlying rock, and that none come from below. Nor was there any indication, by secondary electrons, of single muons travelling upwards. The implication of this is that no obvious neutrino induced muons were detected at this depth.

9.3. Origin of Particle Bundles.

An attempt has been made to account for the observed number of parallel double particle events on the assumption that they originated in extensive air showers as double muons (via intermediate pions) and as pion-muon pairs from nuclear interactions of muons in rock. (These calculations were carried out by D.R. Creed and J. Wdowczyk).

Using the best estimate primary spectrum of Brooke et al (1964) the primary protons were allowed to interact at intervals of 80 gm.cm^{-2} and the resulting energy spectrum of muons at ground level was determined. Knowing the heights of the origin of the muons and the transverse momentum distribution of the parent pions (Pinkau, 1964), the radial distribution of muons was found. Only vertical showers were considered, typical initial primary proton energies required to produce showers of muons at the three depths being 7×10^4 , 2×10^5 and 5×10^5 GeV respectively.

Depth (m.w.e.)	816	1812	4110
Number of parallel double tracks in the same unit.	6	19	0
Number of parallel single tracks, one in each unit.	0	4	1
Number of parallel triple tracks, one in one unit & two in the other.	0	2	0
Number of parallel triple tracks in the same unit.	0	3	0
Observed rate of double particle events.(/sec.)	$(4.0^{+2.4}_{-1.6}) \cdot 10^{-5}$	$(7.2 \pm 1.7) \cdot 10^{-6}$	$< 1.3 \times 10^{-7}$
Rate expected from E.A.S.(/sec)	4.8×10^{-5}	5×10^{-6}	$(3 \pm 1.5) \cdot 10^{-7}$
Rate expected from pion production(/sec)	1.2×10^{-5}	1.3×10^{-6}	0.7×10^{-7}

Table 9.2 Rates of multiple penetrating particles. (At 1812 & 4110 m.w.e. the two units were operated concurrently.)

The rate of two muons falling within the detecting area at each of the three depths is shown in Table 9.2. In order to check the analysis the intensities of single muons were computed and found to be very close to observation. The ratios of the observed to calculated intensities are 1.00, 1.03 and 1.04 at 816, 1812 and 4110 m.w.e. respectively.

The contribution from the nuclear interactions of muons was similarly calculated using the cross sections for shower production given by Fowler and Wolfendale (1958). It was assumed that most of the energy lost went into the production of a single pion. The total flux of pions and their radial distribution round the original muons were estimated and the rate of observing a muon-pion pair was found for each depth (Table 9.2). The pions were found to fall almost entirely within 30 cm. of their parent muons, the separation taking place in the air gap above the apparatus.

The effect of scattering was taken into account in both treatments, but this only affected the radial distribution, not the total number of double particle events.

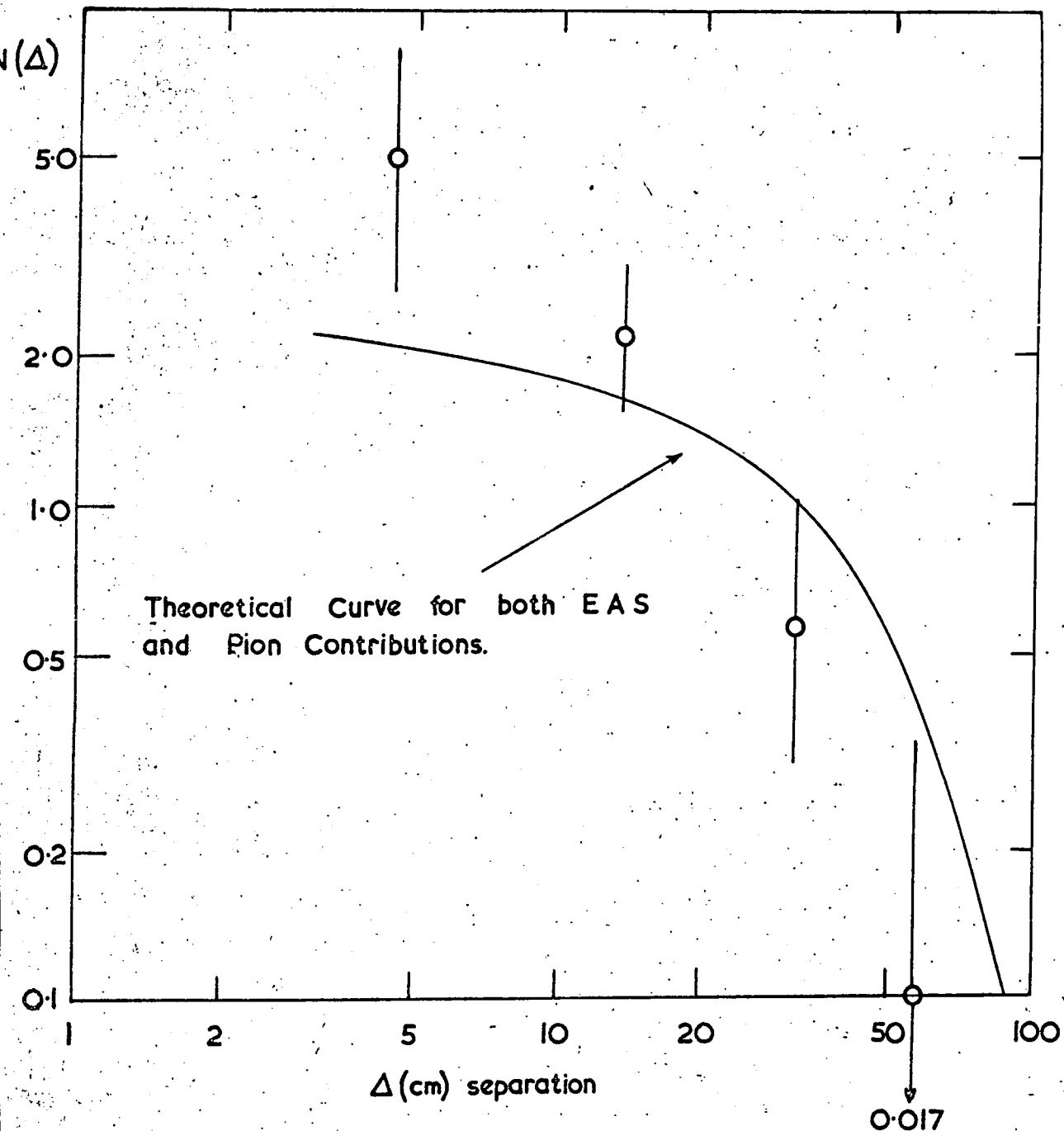


Fig. 9-7 Separation frequency of double particles at 1812 mwe.

There is seen to be reasonable agreement between the sum of these two processes and the observed rates.

The approximate projected lateral separation distributions were calculated from the radial distributions, and it was found that the pion contribution was mainly confined to small separations whereas the theoretical double muon contribution was dominant at larger separations. The experimental and theoretical results are compared in Fig.9.7 for the depth 1812 m.w.e. where most of the events were recorded. For such a simple approach the agreement is satisfactory although there is a possible excess of observed events at very small separations (< 10 cm).

The theoretical number of events (EAS model, the muon interaction contribution being negligible) with one particle in each unit is between five and eight, comparing quite well with the observed pairs (six).

It therefore seems that the multiple penetrating particles observed at these depths can be adequately explained by the production (by way of intermediate pions) of more than one muon by the same primary nucleon in the atmosphere, and by the local nuclear interactions of muons, except for a possible excess at small separations. Further

observations with a detector not limited to a minimum separation of 3 cm. (e.g. spark chambers) would help to clarify this point.

9.4 Comparison with other workers

The only results available at comparable depths with well defined geometry are those of Barrett et al (1952) at 1574 m.w.e. These workers observed 39 parallel double particle events and 4 triplets in 21,070 single muon counts. This gives an observed rate of $(6.0^{+1.2}_{-1.0})10^{-6}\text{sec}^{-1}$ for double events and $(6.2^{+4.9}_{-3.0})10^{-7}\text{sec}^{-1}$ for triplets, compared with $7.2 \times 10^{-6}\text{sec}^{-1}$ and $3.5 \times 10^{-7}\text{sec}^{-1}$ expected on the basis of the EAS Model. In their experiment the contribution of muon-pion pairs must have been negligible since the penetrating particles traversed ~ 1 m. of lead and iron.

Mention has already been made (Section 9.2.3) of the Tata Institute extensive air shower and simultaneous underground experiments at 816 and 1812 m.w.e. where the rates were in quite good agreement with the present experiment.

The agreement between these experiments further confirms the hypothesis that at these depths the main contribution to multiple penetrating particles is from muons associated with extensive air showers.

CHAPTER 10.

NEUTRINO EXPERIMENTS AND MUON INTENSITIES AT THE GREATEST DEPTHS.

10.1. Introduction.

The experiment of Miyake et al (1962, 1963) at a depth of 8400 m.w.e. has indicated the great advantages to be gained by carrying out experiments at great depths in a search for neutrino induced interactions. The major advantage is that the remanent atmospheric muon component at great depths is extremely small. Miyake et al operated two scintillator and geiger counter telescopes (total area 3.11 m^2) for a total of 60 days. In this time no counts were recorded and it was estimated that the vertical muon intensity was $< 10^{-11} \text{ cm}^{-2} \text{ sr}^{-1} \text{ sec}^{-1}$.

The significance of this result was discussed by Menon et al (1963) who concluded that the cross-section for the elastic scattering of muon neutrinos by nucleons is $\leq 1.5 \times 10^{-36} \text{ cm}^2$., and, if the intermediate boson exists, it should have a mass, M_w , greater than that of the K-meson (i.e. $> 494 \text{ MeV}$). Recent experiments at accelerators have shown that the cross-section for elastic

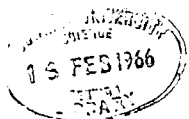
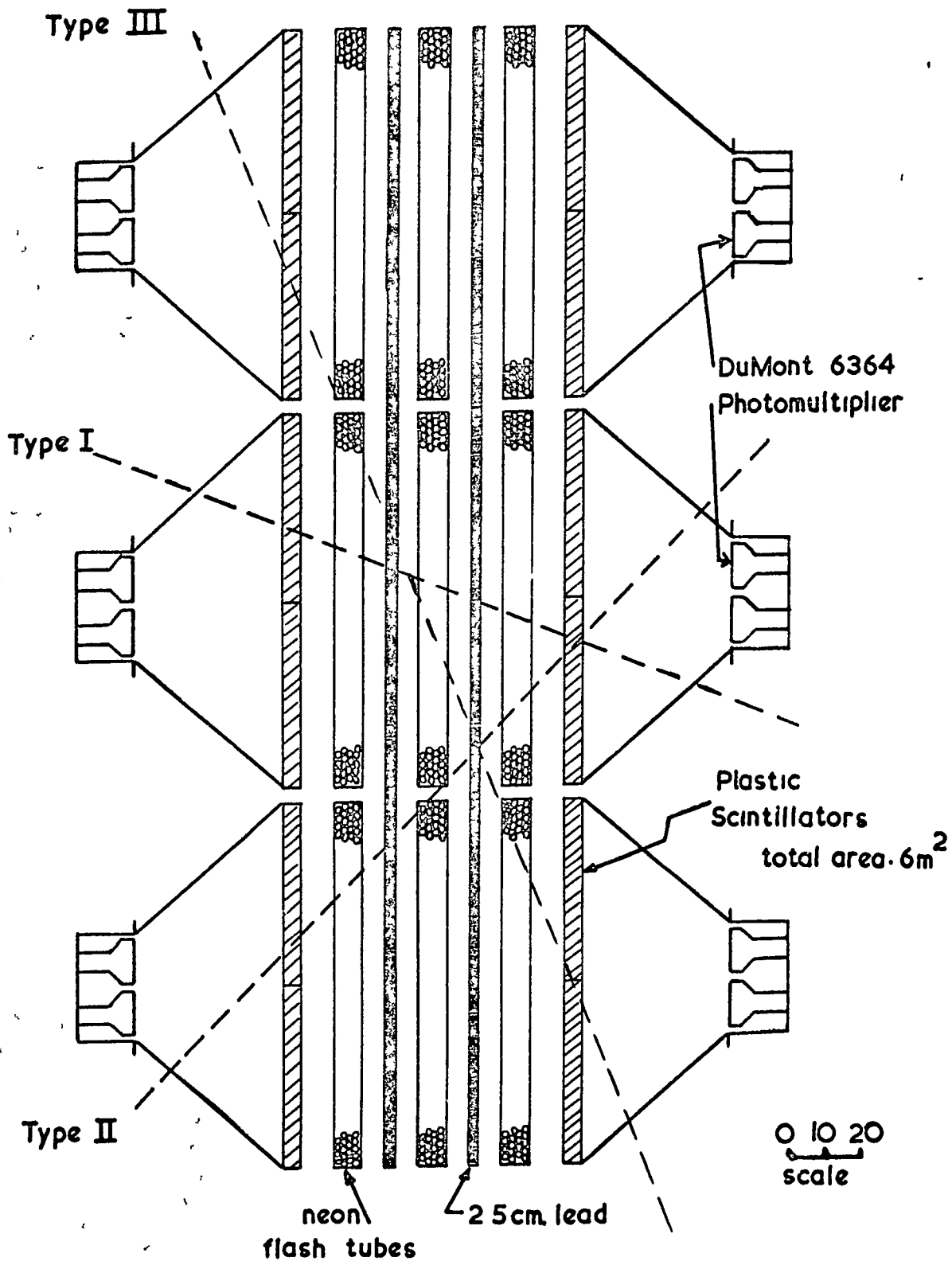


Fig IO I The KGF. Neutrino Telescope



scattering of muon neutrinos is $\sim 10^{-38} \text{ cm}^2/\text{nucleon}$ and that $Mw > 1.8 \text{ GeV}$ (Danby et al, 1962).

In view of these results an experiment has been commenced jointly by the Tata Institute of Fundamental Research, Bombay, Osaka City University, Japan and Durham University, U.K., in the Kolar Gold Mines at a depth of 7600 m.w.e. (standard rock). In so far as the results are relevant to the derivation of vertical intensities and exponents deep underground, some description of the experiment will be given.

10.2. The Apparatus.

The apparatus comprises two telescopes, each consisting of two vertical walls of plastic scintillators 2 m. long and 3 m. high separated by 84.5 cm. (Fig.10.1 and Plate No. 4). The scintillators on each wall consisted of six elements, each one square metre in area and composed of four scintillator blocks. Each scintillator element is viewed by two adjacent 5" Dumont 6364 photomultipliers; four-fold coincidences are recorded between a pair of photomultipliers on one wall and any pair on the other wall. Between the scintillator walls there are

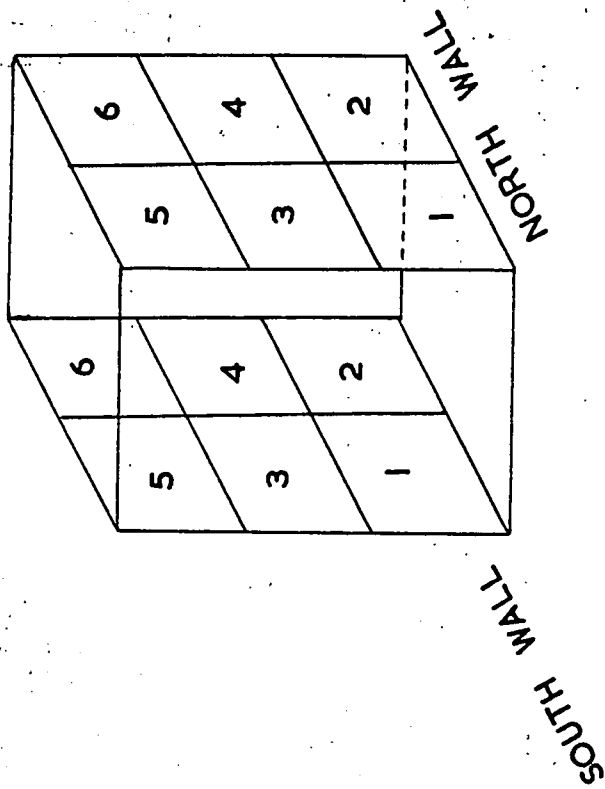


Plate 4 A 'neutrino' telescope at 7600 m.w.e.

three arrays of neon flash tubes, covering the whole scintillator area, fitted with four columns of flash tubes in each array. The flash tubes are identical to those described earlier (Section 2.4) except that they are 2 m. long. The flash tubes in each telescope are viewed directly by two open shutter cameras from a distance of 6 m., one camera viewing the top half of the telescope and the other the lower half with some overlapping in the centre. Two walls of lead absorber, each 2.5 cm. in thickness are placed between the flash tube arrays. When four-fold coincidences occur, the photomultiplier pulses are suitably delayed and displayed on oscilloscopes and photographed, and, after a delay of $30\ \mu$ s, a high voltage pulse is applied to the electrodes of the flash tube arrays in both telescopes. A cycling system is then brought into operation and serves two functions: fiducial marking lights and clocks are illuminated and recorded on the film, and the film advanced. From the instant the coincidence occurred the apparatus is made insensitive to any further events for a period of 12 seconds.

The camera films are advanced automatically every 4 hours 25 minutes by a timing device. During this

Fig. 10-2. Types of coincidences detected by the KGF "neutrino" apparatus



TYPE I EVENTS: $(N_{1OR2} + S_{1OR2})$ OR $(N_{3OR4} + S_{3OR4})$
 OR $(N_{5OR6} + S_{5OR6})$

TYPE II EVENTS: $(N_{3OR4} + S_{1OR2})$ OR $(N_{3OR4} + S_{5OR6})$
 OR $(N_{5OR6} + S_{3OR4})$ OR $(N_{1OR2} + S_{3OR4})$

TYPE III EVENTS: $(N_{1OR2} + S_{5OR6})$ OR $(N_{5OR6} + S_{1OR2})$

N MEANS NORTH ; S MEANS SOUTH

period a continuous check on the stability of the photomultipliers and coincidence circuits is made by a counter and printing register. The two-fold coincidences for each pair of photomultipliers are monitored in turn for about 9-1/2 minutes each and printed out on paper at the end of this time. When all twentyfour channels have been monitored, the total two-fold rates for each side of each telescope are monitored in turn for the same length of time. The counting rate of each pair of photomultipliers was adjusted to be ~ 20 /hour, almost all of which was due to background gamma rays of radioactive origin. The resolving time of the apparatus is $2 \mu s$, and thus the 4-fold chance coincidence rate is 1 per 7 years for each telescope. It is estimated that the chance rate due to double Compton effect of γ -rays is less than 1 per 10 years per telescope.

Since the amplitudes of the pulses from all the scintillator elements are displayed on oscilloscopes, it is possible to classify the events into three types, I, II, III, as shown in Figs.10.1 and 10.2, and thus some crude information is available about the azimuth angle of the particle track.

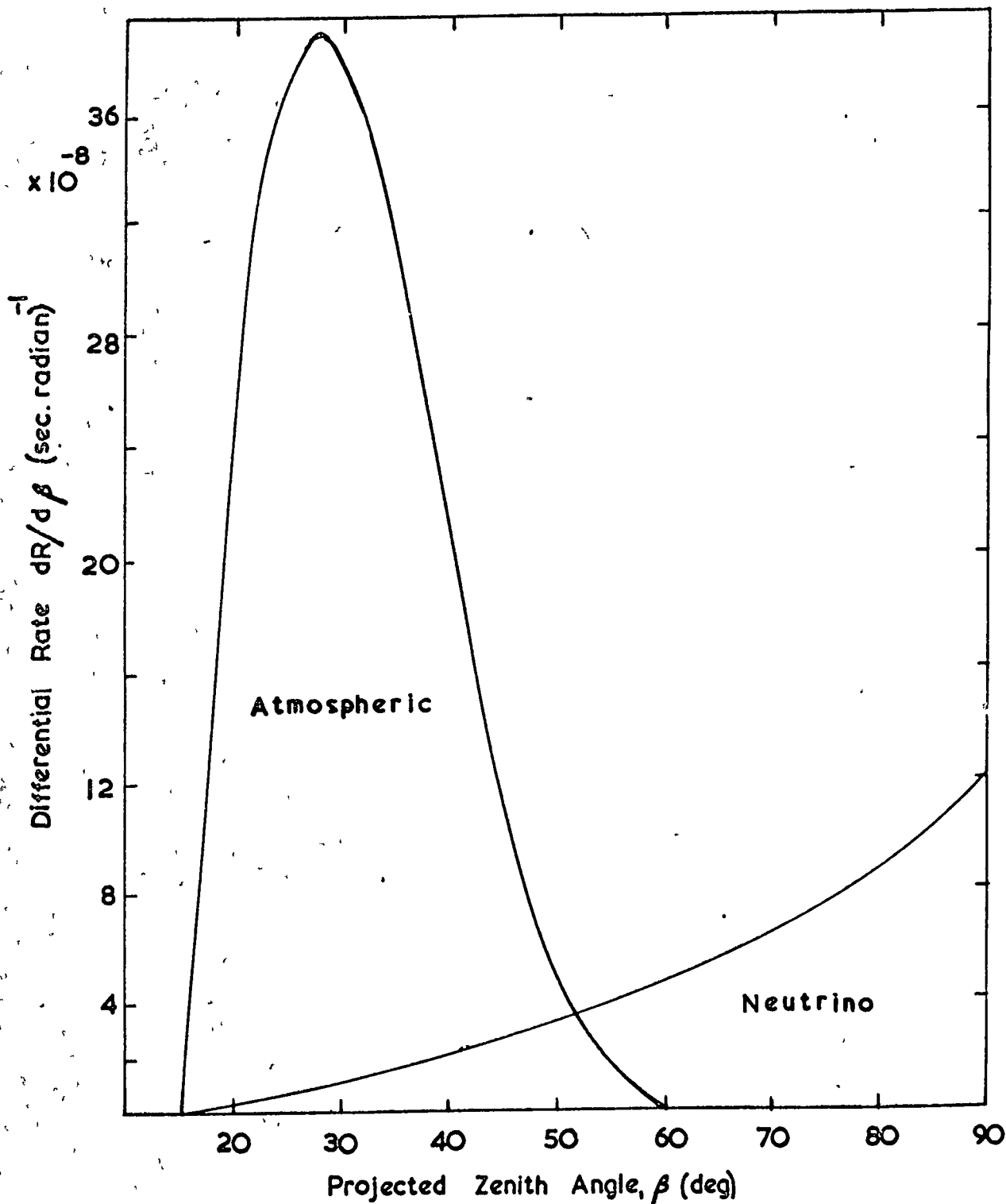


Fig. 10.3. The differential aperture of the KGF neutrino apparatus

The flash tube photographs of the events are analyzed in the same fashion as described earlier (Section 3.2). It will be remembered that the angles measured from the photographs are the projected zenith angles. With the present apparatus it is not possible to define the direction of motion of the particle except where knock-on electrons accompany the penetrating particle. It is assumed that these electrons are preferentially knocked-on in the forward direction.

Each telescope has an aperture of $19.5 \text{ m}^2 \text{ sr}$. and can accept particles in the zenith angular range 15° - 90° from both upper and lower hemispheres. It is seen therefore that the apparatus can detect penetrating particles of two origins :-

- i) atmospheric muons having zenith angles greater than 15° , and
- ii) muons produced in the interactions of neutrinos with nucleons in the surrounding rock.

The differential rate of these two types of events is shown in Fig. 10.3 as a function of projected zenith angle (Achar et al 1965 a). The distribution

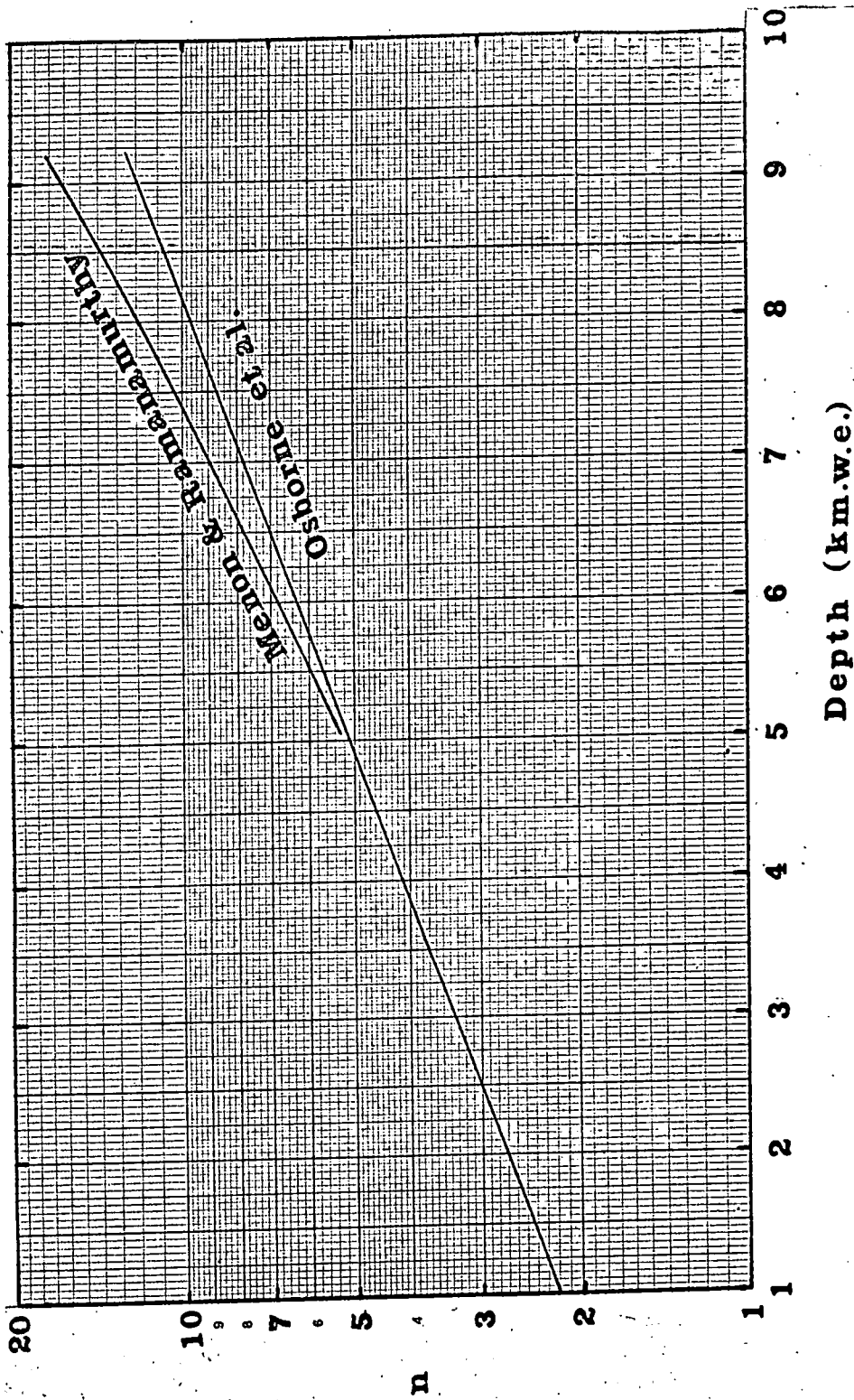
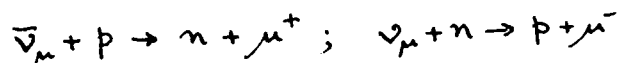


Fig.10.4 The variation of n with depth.

for atmospheric muons is based on a distribution of the form $I(\theta) = k \cos^n \theta$. This distribution is the mean of the distributions obtained by Menon and Ramanamurthy $[I(\theta) = 8.4 \times 10^{-7} \cos^{10.2} \theta]$, and Osborne and Wolfendale $[I(\theta) = 8.7 \times 10^{-7} \cos^{8.9} \theta]$ from the OPW best estimate intensity-depth spectrum. The variation of n with depth is shown in Fig.10.4. The effective apertures of the telescopes for these distributions are 0.155 and $0.20 \text{ m}^2 \text{ sr}$. respectively.

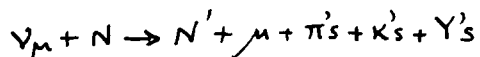
Osborne and Wolfendale have considered the following types of neutrino interactions to derive the rate of events for neutrino induced muons :-

i) Elastic Interactions.



Close to the threshold the cross-section increases linearly with the neutrino energy, but for $E_\nu \gtrsim 1 \text{ GeV}$ the total cross-section is constant ($0.75 \times 10^{-38} \text{ cm}^2/\text{np pair}$).

ii) Inelastic Interactions.



Up to 10 GeV the cross-section increases linearly with

neutrino energy (Bloch et al. 1964) although a more rapid increase cannot be excluded. Three types of behaviour have therefore been considered -

- a) Inelastic (1) $\sigma_{inel} = 0.45 \times 10^{-38} E_{\nu} \text{ cm}^2/\text{nucleon}$ with a cut-off at 10 GeV;
- b) Inelastic (2) $\sigma_{inel} = 0.45 \times 10^{-38} E_{\nu}^2 \text{ cm}^2/\text{nucleon}$ with a cut-off $\gg 10$ GeV; and
- c) Inelastic (3) $\sigma_{inel} = 0.19 \times 10^{-38} E_{\nu}^2 \text{ cm}^2/\text{nucleon}$ with a cut-off at 40 GeV.

Below the cut-off energy the mean muon energy was assumed to be half that of the neutrino and above it the cross-section is taken as constant and $E_{\mu} = E_{\nu}$.

iii) Production of an Intermediate Boson (W).

Accelerator experiments have shown that this boson, if it exists, has mass > 1.8 GeV. The type of interaction considered is $\nu_{\mu} + \bar{z} \rightarrow \bar{z}' + \mu + W$

the W promptly decaying to a muon and neutrino. The W production cross-section used was that of Wu et al (1964) for neutrino energies up to 20 GeV together with the asymptotic expression of Von Gehlen (1963) which is valid above 100 GeV.

Table 10.1

Predicted numbers of events in 263 telescope-days.

Interaction.	Number of events (Double events in brackets)	Approx. median energy (GeV).
(a) Elastic	0.29	2.5
(b) Inelastic (1)	0.76 (0.07)	10
(c) Inelastic (2)	1.29 (0.07)	25
(d) Inelastic (3)	8.68 (0.09)	45
(e) Intermediate Boson, W $m_W=1.8$ GeV	1.28 (0.20)	100
(f) Intermediate Boson, W $m_W=2.5$ GeV	0.58 (0.08)	200
(g) Glashow Resonance $m_W=1.8$ GeV	0.38	3000
(h) Glashow Resonance $m_W=2.5$ GeV	0.08	6000
Lower limit (a+b)	1.05	
Atmospheric muons	3.4 ± 0.5	

Table 10.2

Predicted Angular Distribution.

Type of events	I	II	III
Neutrino initiated muons	72.6%	25.9%	1.5%
Atmospheric muons	5.5%	61.3%	33.2%

iv) Glashow Resonance.

If the W-boson exists then there will be a resonance in the interaction of $\bar{\nu}_e$ with atomic electrons at a neutrino energy of $m_W^2/2 m_e$. The W will then decay by the muon mode, the complete reaction being -



The flux of muons underground from this interaction has been calculated by Zagrebin and Zheleznykh (1964).

The predicted number of events from both atmospheric muons and neutrino initiated muons are shown in Table 10.1, and the expected division into events of types I, II and III is shown in Table 10.2.

10.3. The Experimental Results.

The apparatus has been in operation since March 1965, and 15 events have been recorded in 263 telescope-days. The events are listed in Table 10.3. In three of the events, the penetrating particle did not pass through the scintillators on both sides of the apparatus, the necessary coincidence being made by an accompanying particle or shower. In two of these events the track of the accompanying particle can be seen on the flash tube records; these tracks are seen to pass through the

Event No.	Date & time (Hr.Min.)	Coincidence & telescope	Event type	Projected zenith angle(deg)	Remarks
1	5.4.65 20-04	S4+N4 (2)	I	>37	Flash tubes not present
2	27.4.65 18-26	S1+N1 (1)	I	48±1	Two extreme nft trays present
3	25.5.65 20-03	S6+N6 (2)	I	75 ± 10	Central nft tray present
4	3.7.65 12-30	S1+N1 (2)	I	96.2 ± 0.8 99.2 ± 0.3	Double track event
5	13.7.65 16-13	S3,5,6+N4 (2)	II	45 ± 1	
6	18.7.65 02-52	S1,2+N3,6 (1)	-	8.5 ± 1	Out of geometry
7	24.7.65 11-47	S3+N6 (1)	II	37.5 ± 1	
8	27.7.65 03-24	S3+N6 (1)	II	29.5 ± 1	Muon. + e.m. shower from lead
9	29.7.65 19-07	S3+N1 (2)	II	32.5 ± 2.5	ditto.
10	1.8.65 21-00	? (1)	-	25± 1	Out of geometry, no 'scope data
11	2.8.65 03-38	S4+N6 (1)	II	47 ± 1	Muon. + e.m. shower from lead
12	11.8.65 17-37	S5+N4 (1)	-	33 ± 1	Out of geom.
13	12.8.65 11-38	S1,2,4,6+N2,4,6 (1) S1-6+N2,4 (2)		? ?	Dense shower No tracks
14	19.9.65 02-22	S1,3+N5 (2)	III	26.5 ± 1	
15	10.9.65 08-20	S3+N5 (1)	II	40 ± 1	

Table 10.3 Observed events at 7600 m.w.e. up to 11.9.65

scintillator elements which made the coincidence. It will be noted that the projected zenith angles of these three events are small and they are considered to be muons of atmospheric origin.

The 13th event was observed in telescope 2. All scintillator elements on the southern side showed large pulses as also did one on the north side (N4); other scintillator elements on the north showed pulses but these were much smaller. Telescope 1 also showed pulses in coincidence (N2,4,6; S1,2,6) the southern pulses being much larger than the northern. The flash tube photographs of telescope 2 are unfortunately incomplete; because of a fault in the film winding system for telescope 2 only the lower 2m of flash tubes are visible, the top-most section overlapping with the previous photograph thus losing some of the relevant details. However, it is seen that practically all the flash tubes in the southern side had discharged; in the central array a few well separated large clusters of tubes which had discharged can be seen, whilst a few tubes (showing some clustering) had discharged in the northern array. The flash tube photographs of telescope 1 show no evidence of the event. The UHT pulse was in fact

applied to telescope 1 during this event as was seen from the few widely separated tubes which did fire. The number of flashed tubes in telescope 1 is not inconsistent with the frequency of spurious flashed tubes (~ 1 per pulse per 2m^2). Apart from the defect in the winding of the telescope 2 cameras there were no other instrumental faults and the event is therefore genuine. The most probable explanation of the event is that it was due to an electromagnetic shower arriving from the southern rock wall and travelling at a small angle to the plane of the rock wall. It is difficult to assign an exact value to the zenith angle since there is no clear unambiguous track of a penetrating particle. It would seem that the zenith angle was large, and the event would therefore correspond to a neutrino interaction.

Two other events (Nos.3 & 4) are clearly due to the results of neutrino interactions because of their large zenith angles. The 4th event is of particular interest in that there are two penetrating particles diverging from a point below the horizontal. An analysis of this event has already been reported (Achar et al, 1965 a,b) and it is sufficient to mention here only the

main conclusions. Both particles penetrated ≥ 9 radiation lengths without multiplication or large angle scattering and are therefore heavier than electrons. The meeting point of the two tracks could be close to the rock surface or up to a projected depth of one metre inside the rock. This range of possibilities is due to the errors in determining the zenith angles of the particles. The maximum actual distance traversed through rock is 1.7 metres. The uncertainty in the traversal of the rock does not allow any definite conclusion to be made concerning the nature of the particles, (i.e. they could both be muons or one muon accompanied by a pion). If both were muons then there is a high probability that the event corresponds to the production of an intermediate boson. However, there is no doubt that the event is due to the inelastic interaction of a neutrino.

Of the remaining 9 events, 8 have projected ^{zenith} angles in the range 21° to 48° , and in one case it is only possible to state that the angle is greater than 37° since the flash tubes were not installed at that time. It is not easy to determine whether events with zenith angles smaller than $\sim 60^\circ$ are due to atmospheric muons remanent

at this depth or to neutrino interactions (cf. Fig.10.3). However, consideration of the individual zenith angles suggests that five or six of the total events are due to neutrino interaction, the remainder being due to atmospheric muons, (i.e. those events having a projected zenith angle greater than 45° are considered to be neutrino initiated).

10.4. The Vertical Intensity of Atmospheric Muons at 7600 m.w.e.

Only a lower limit can be put to the projected zenith angle of the first event, but since it is a type I event and the other three events of this type are considered to be neutrino induced it will also be assumed to fall into this category. The observed number of atmospheric muons passing through both sides of either telescope is therefore 5 in 262.5 telescope-days. The observed rate of atmospheric muons is thus $(1.90_{-0.81}^{+1.30})$ per 100 telescope-days. The corresponding vertical intensity of muons at 7600 m.w.e. is :-

$$(1.10_{-0.47}^{+0.74}) \times 10^{-10} \text{ cm.}^{-2} \text{ sr.}^{-1} \text{ sec.}^{-1} \text{ for } n = 8.9$$

or

$$(1.42_{-0.60}^{+0.98}) \times 10^{-10} \text{ cm.}^{-2} \text{ sr.}^{-1} \text{ sec.}^{-1} \text{ for } n = 10.2$$

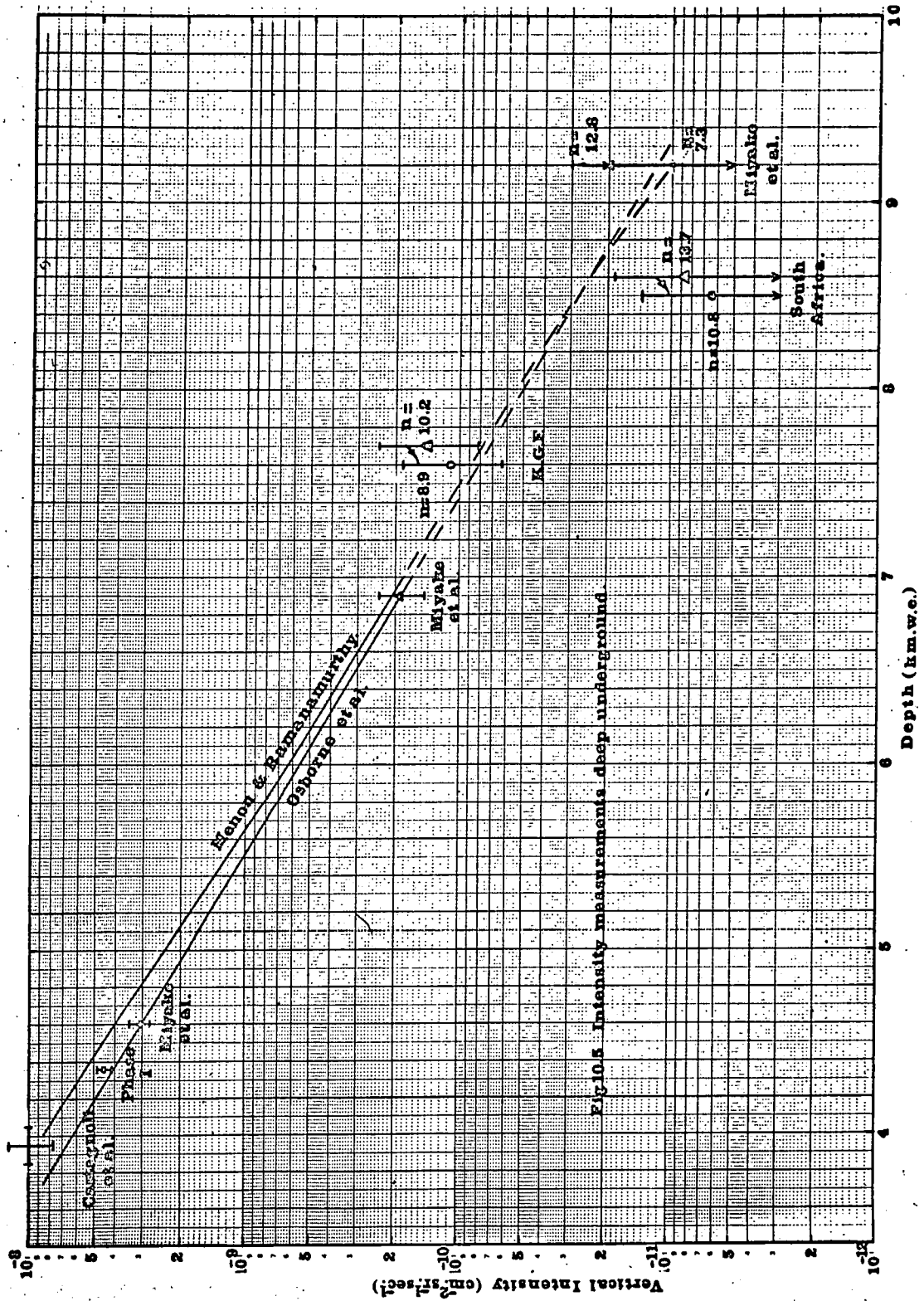
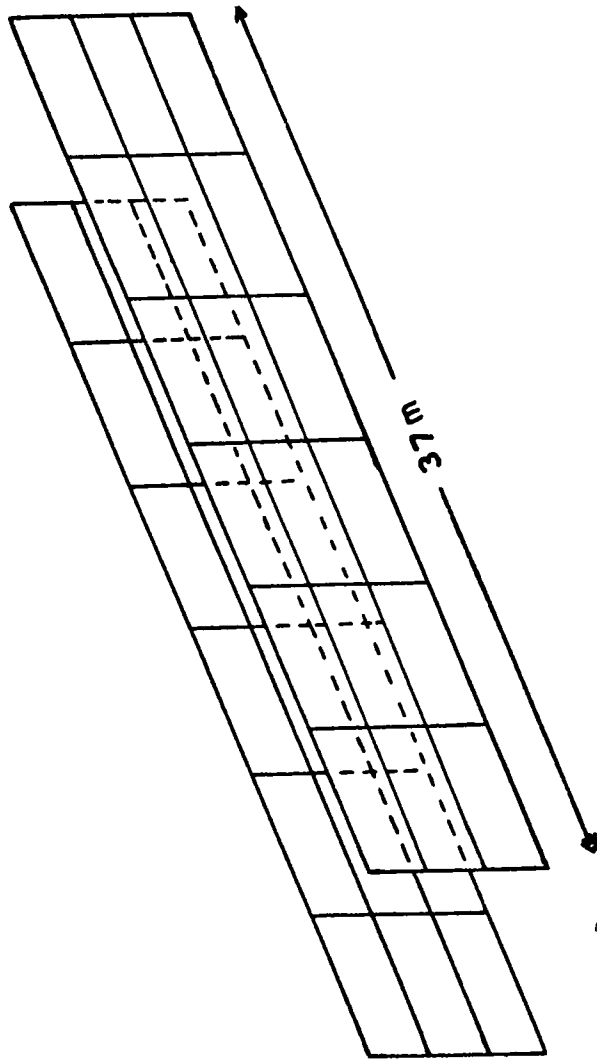


Fig.10.5 Intensity measurements deep underground

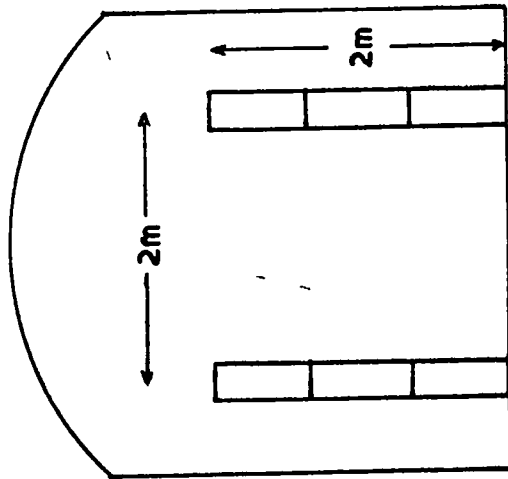
These intensities are plotted on the intensity-depth spectrum shown in Fig.10.5 together with the best estimate distributions of Osborne et al (1964) and Menon and Ramanamurthy (1965). These distributions are shown as broken lines for depths greater than 7000 m.w.e. since the only previous measurement is that of Miyake et al (1962-3) at 9200 m.w.e. when no counts were recorded in 120 telescope-days with a total area of 3.2 m^2 . Using an exponent of 7.3 Miyake et al deduced that the vertical intensity at 9200 m.w.e. was $< 10^{-11} \text{ cm}^{-2} \text{ sr}^{-1} \text{ sec}^{-1}$ (The limit corresponds to one event, see section 10.6). Thus the Menon and Ramanamurthy spectrum is regarded an upper limit over this range. On the other hand the distribution of Osborne et al is linear on this plot over the range 4000-7000 m.w.e. It has therefore been extrapolated linearly to 9200 m.w.e. Also shown in Fig.10.5 are the intensities measured by Castagnoli et al (1965) at 3950 m.w.e., by Miyake et al (1962-3) at 4600 and 6900 m.w.e., and in phase I of the experiment being reported at 4360 m.w.e.

10.5. The South African Neutrino Experiment.

The Case Institute, Cleveland, Ohio, and the



Rail geometry in perspective



End view

Fig. 106 The South African experimental arrangement at 8500 m w e

University of Witwatersrand, Johannesburg, South Africa, have set up a laboratory at 10,492 feet below surface in the East Rand Proprietary Mine, Johannesburg, ($\rho = 2.75 \text{ gm.cm.}^{-3}$, $Z^2/A = 5.0$). This corresponds to a depth of 8500 m.w.e. standard rock.

The detector array, shown schematically in Fig.10.6, consists of two parallel vertical walls of liquid scintillator made up of 36 elements. The array is grouped into 6 "bays" of 6 elements each. Each detector element is a rectangular box of lucite of wall area 3.07 m^2 containing 380 litres of liquid paraffin, and is viewed at each end by two 5" photomultipliers. The array consists of a hodoscope which gives a rough measurement of the zenith angle of a charged particle passing through it. In addition the event is located along the detector axis by the ratio of the photomultiplier responses at the two ends. The sum of the responses then provides a measure of the energy deposited and hence the track length in the detector. For minimum ionizing particles the scintillator is 20 MeV in thickness. This is well above the energies characteristic of radioactively emitted particles. The triggering requirements are a four-fold coincidence of any

Date	Time (Greenwich)	Tank	Location of event (m) from north end	Energy deposited in detector (MeV)
23.2.65	21-48	E4L	2.1	29
		W4L	2.8	18
1.3.65	00-20	E5M	0.03	55
		W5U	4.9	118
17.3.65	18-52	E4L	3.6	19.4
		W4L	1.7	16.0
20.4.65	14-16	E2M	4.6	23.5
		W2M	3.4	24.5
1.6.65	22-37	E1L	5.5	18.5
		W2L	0.55	18.0
3.6.65	01-42	E4U	2.4	5.0
		W4M	3.7	18.0
1.7.65	15-21	E3M	1.3	21.0
		W3U	3.0	30.0

Table 10.4 Eight-fold events (coincidences involving one element of each side) observed in 563 bay-days in the South African neutrino experiment.

Date	Time (Greenwich)	Tank	Location of event (m) from north end	Energy deposited in detector (MeV)
27.10.64	19-39	E1M	3.6	58
		E1L	?	10
		W1U	1.1	158
		W1M	2.3	116
		W1L	2.4	37
13.12.64	10-31	E2M	3.4	75
		E2L	2.1	59
22.12.64	11-03	E1U	3.7	37
		E1M	4.3	51
		E1L	4.6	16
11.2.65	02-20	E1U	1.7	84
		E1M	1.6	78
		E1L	1.8	21
14.2.65	22-35	E4M	3.9	85
		E4L	?	?
		E5M	0.09	51
		W4M	2.9	49
		W4L	4.2	34
7.5.65	02-10	W5M	1.8	65
		W5L	1.4	97
12.6.65	13-40	E3U	3.9	60
		E3M	3.4	122
		E3L	1.7	19

Table 10.5 Miscellaneous multi-tank events observed in 563 bay-days in the South African experiment.

Date	Time (Greenwich)	Tank	Energy deposited in detector (MeV)
9.11.64	00-48	E1L	45
23.11.64	16-05	E1L	48
25.11.64	15-09	E1L	63
14.2.65	02-52	W5M	26
24.2.65	15-04	W2M	39
11.3.65	11-03	E4L	54
11.3.65	21-40	W5M	51
12.3.65	15-38	E2L	26

Table 10.6 Single tank events with energy deposition
> 18 MeV observed in 265 bay-days (until 18.3.65)
in the South African Neutrino Experiment.

four photomultiplier tubes viewing either the east or the west scintillators. The photomultiplier pulses were suitably delayed and displayed on oscilloscopes for photography.

The experiment was started in September 1964 and all six bays have been in operation since June 1965. The total running time to date is 563 bay-days. Details of the observed events are shown in Tables 10.4 - 10.6. It will be noted that the events shown in Table 10.4 are 8-fold coincidences involving one scintillator on each side of the array (i.e. K.G.F. types I and II). Such events have a minimum projected zenith angle of $\sim 54^\circ$. It is estimated that about one atmospheric muon per year produces a coincidence of this type. The contribution from stars produced by muons is thought to be much less than 3 per year. A more important source of contamination in events of this type are pairs of associated high energy near vertical muons. However, one would expect that the energy deposition would be much larger than that observed in Table 10.4. Two events listed in Table 10.5 (27th October 1964 and 14th February 1965) are consistent with this multiple muon hypothesis. It is therefore plausible

to assume that the events listed in Table 10.4 are due to neutrino interactions.

The single tank events listed in Table 10.6 are thought to be due to atmospheric muons with an admixture of neutrino induced muons. Events number 2, 3, 4, 6 and 7 listed in Table 10.5 are similarly considered to be due to the passage of near vertical particles through the apparatus. It will be noted that in each event only the scintillators on one side of a bay were triggered. The events of 27th October 1964 and 14th February 1965 are more complex, but in view of the large amounts of energy deposited in some of the scintillators it is thought that the events are due to either pairs of associated near vertical muons or are complex events similar to event number 13 observed in K.G.F.

For the purpose of deriving the intensity of atmospheric muons at 8500 m.w.e. the events shown in Tables 10.5 and 10.6 can be lumped together and assumed to be due to atmospheric muons with an admixture of neutrino induced muons.

Osborne (private communication) has determined

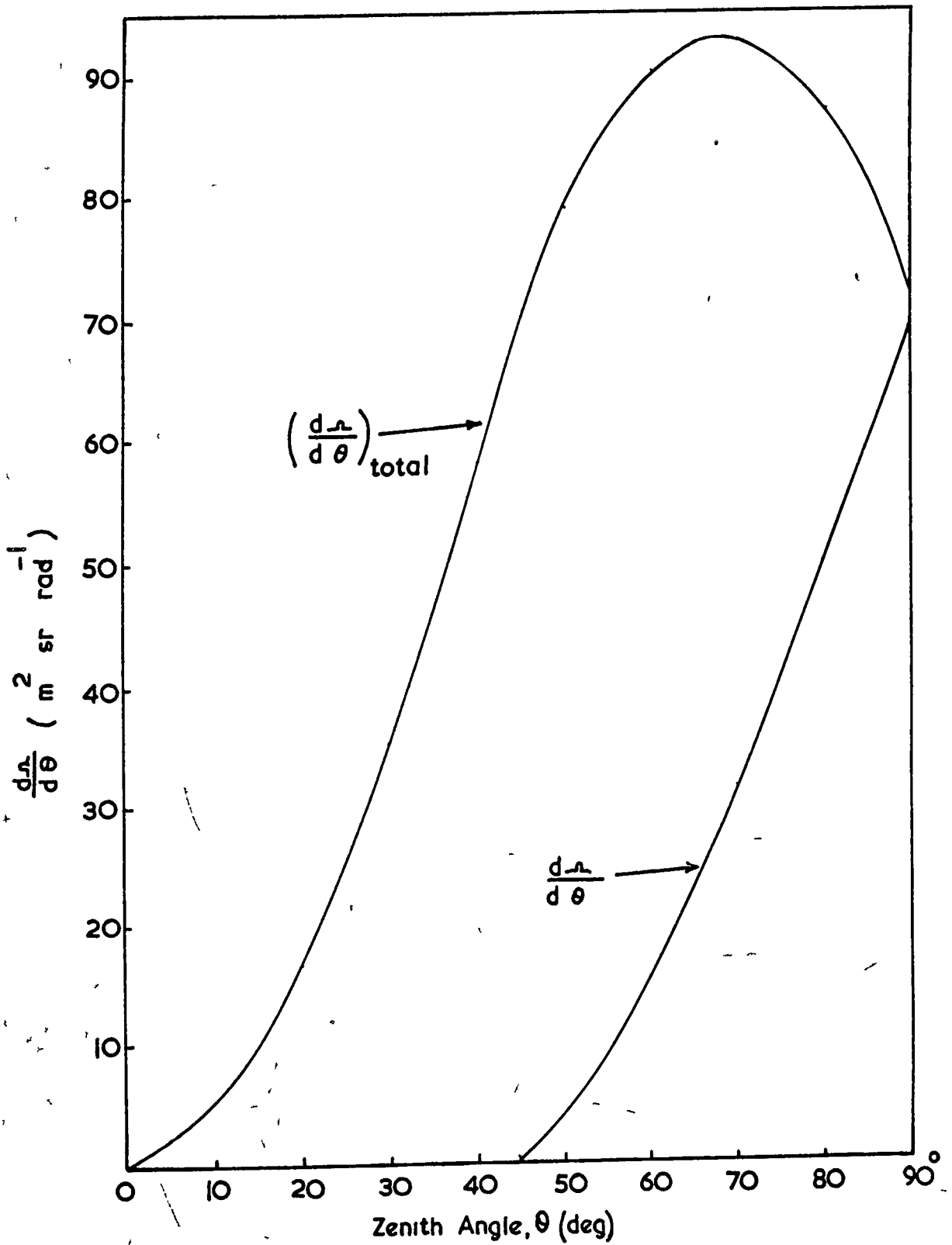


Fig. 10.7 Differential aperture of the South African arrangement

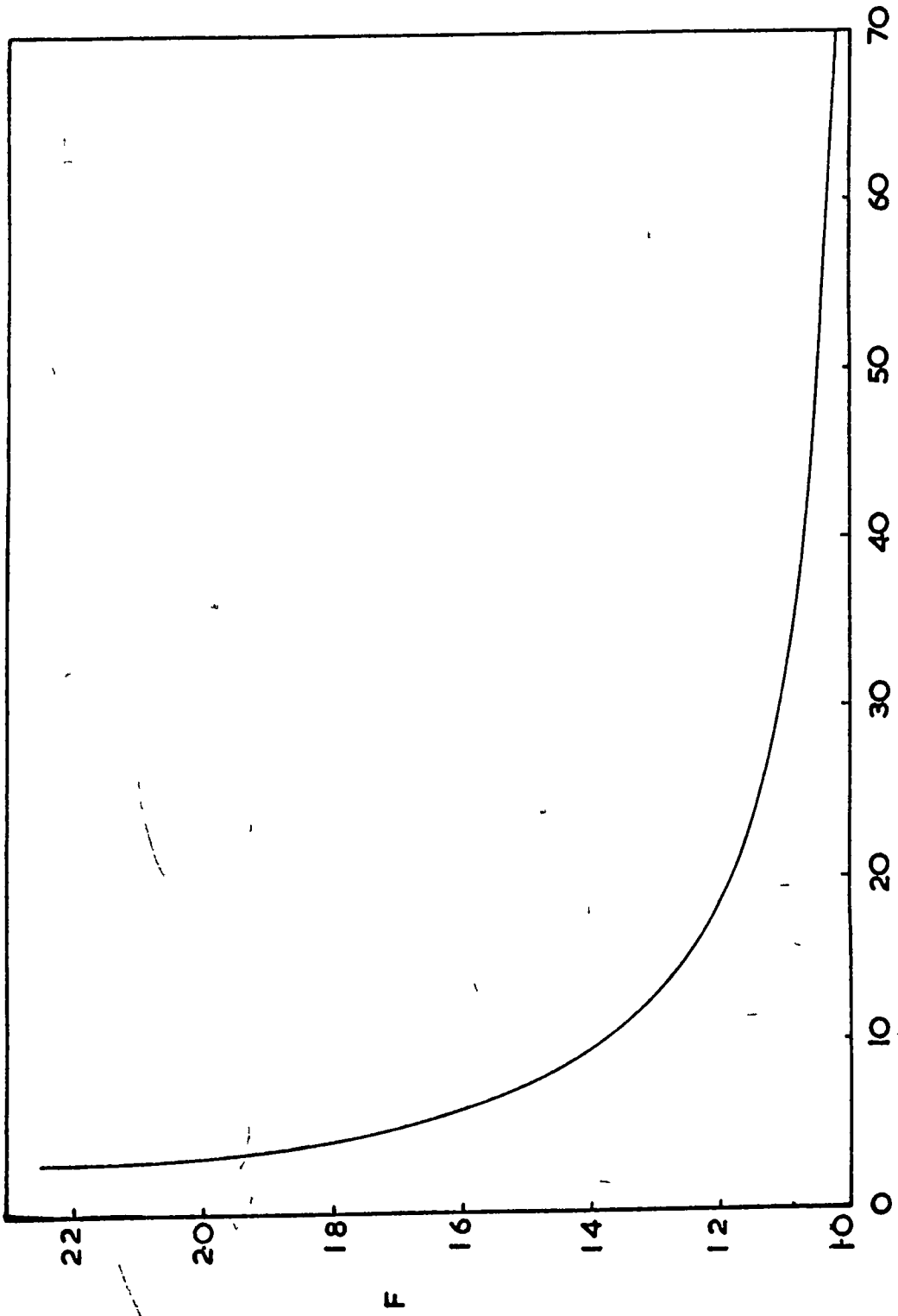


Fig 10 8 Correction factor for South African telescope

the differential aperture of the South African array (Fig.10.7), where the curve $\frac{dn}{d\theta}$ represents the differential aperture for 8-fold coincidences and $(\frac{dn}{d\theta})_{total}$ is the total differential aperture taking single tank events into account as well as 8-fold coincidences. The apertures for one quadrant are simply the area under the curves and are 23.2 and 87.5 m²sr. respectively. The total apertures for all quadrants and allowing for particles travelling from both above and below the horizontal are 8 times these values (i.e. 185.5 and 700.3 m²sr.) However, since these apertures have been found assuming that the detectors have no thickness, a correction factor, F, (Fig.10.8) must be applied to $(\frac{dn}{d\theta})_{total}$.

If an angular distribution of the form $I(\theta) = I_v \cos^n \theta$ is assumed, the vertical intensity, I_v , is given by -

$$I_v = \frac{1.12 R}{\int 4F \frac{dn}{d\theta} \cos^n \theta d\theta} \text{ m}^{-2} \text{ sr}^{-1} \text{ sec}^{-1}$$

where 1.12 is the correction factor to allow for gaps between the detectors and R is the observed rate of atmospheric muons/second. Two angular distributions have been

used to estimate I_ν . For $n = 10.8$ (Osborne et al. 1964) the denominator of the above equation is $19.24 \text{ m}^2 \text{ sr}$. whilst for $n = 13.7$ (Menon and Ramanamurthy, 1965) it is $14.25 \text{ m}^2 \text{ sr}$.

From Table 10.4 it is seen that the rate of neutrino induced events is $(8.63 \begin{smallmatrix} +4.68 \\ -3.14 \end{smallmatrix}) 10^{-7} \text{ sec}^{-1}$ and from Tables 10.5, 10.6 the rate of atmospheric muon events plus the admixture of neutrino induced events is $(2.96 \pm 0.76) 10^{-6} \text{ sec}^{-1}$. An estimate can be made of this admixture by multiplying the neutrino induced rate of events by the ratio of the aperture of single tank events for atmospheric muons to the aperture for 8-fold coincidences. This ratio is 2.78, leading to an admixture of neutrino induced events in single tank events of $(2.40 \begin{smallmatrix} +1.30 \\ -0.87 \end{smallmatrix}) 10^{-6} \text{ sec}^{-1}$. The atmospheric muon rate is therefore $(0.56 \begin{smallmatrix} +1.63 \\ -0.56 \end{smallmatrix}) 10^{-6} \text{ sec}^{-1}$. It should be remembered at this stage that the aperture for neutrino events has been found assuming an isotropic distribution of neutrino events. This is not exactly the case, and Osborne (private communication) has concluded that the ratio quoted above (2.78) should be ~ 2 . Using this value the atmospheric muon rate is $(1.23 \begin{smallmatrix} +1.40 \\ -1.23 \end{smallmatrix}) 10^{-6} \text{ sec}^{-1}$.

Thus for $n = 10.8$, $I_v = (6.4_{-6.4}^{+7.3})10^{-8} \text{ m.}^{-2} \text{ sr.}^{-1} \text{ sec.}^{-1}$

and for $n = 13.7$, $I_v = (8.6_{-8.6}^{+9.9})10^{-8} \text{ m.}^{-2} \text{ sr.}^{-1} \text{ sec.}^{-1}$

at 8500 m.w.e. These intensities are plotted on Fig.10.5.

10.6 The Experiment of Miyake et al (1962-3) at 8400 m.w.e.

The no-count observation of Miyake et al at 8400 m.w.e. (9200 m.w.e. of standard rock) indicated that the vertical muon intensity is $< 10^{-11} \text{ cm.}^{-2} \text{ sr.}^{-1} \text{ sec.}^{-1}$. This was based on an assumed exponent of the angular distribution of 7.3 which is clearly an underestimate. The upper limit to the intensity quoted by Miyake et al corresponds to one event. The Regener (1951) upper limit of zero (corresponding to 1.83 events) should have been used, which immediately gives

$$I_v < 1.93 \times 10^{-11} \text{ cm.}^{-2} \text{ sr.}^{-1} \text{ sec.}^{-1} \text{ for } n = 7.3.$$

From Fig.10.4 it is seen that $n = 12.7$ at 9200 m.w.e., using the OPW spectrum, giving $I_v < 3 \times 10^{-11} \text{ cm.}^{-2} \text{ sr.}^{-1} \text{ sec.}^{-1}$. If the Menon and Ramanamurthy spectrum is used (when $n = 17.5$) this upper limit is still higher ($I_v < 4 \times 10^{-11} \text{ cm.}^{-2} \text{ sr.}^{-1} \text{ sec.}^{-1}$). Thus at this extreme depth the vertical intensity would appear to vary quite slowly for large changes in n .

10.7. The Experiment of Barton (1961) at 5050 m.w.e.

A no-count observation in 21 days at 5050 m.w.e. (5150 m.w.e. of standard rock) gives $I_V < 1.64 \times 10^{-9}$ cm.⁻² sr.⁻¹ sec.⁻¹ It is not known how sensitive the telescope was to variations in n or what value of n was used to derive this upper limit. However, in a private communication to Menon and Ramanamurthy (1965) the author believes that the uncertainties due to n in the flux values observed are small compared with the statistical errors. The upper limit was chosen such that the probability of the true rate being greater was 16% (Regener, 1951).

10.8. Conclusion: the variation of I_V and n at great depths.

The recent experimental results at depths greater than ~4000 m.w.e. are shown in Fig.10.5 together with the best estimate depth-intensity relations of Menon and Ramanamurthy (1965) (MR-spectrum) and Osborne et al (1964) (OPW spectrum). As mentioned earlier the latter distribution is linear over the range 4000-7000 m.w.e. and has been extended linearly to 9000 m.w.e. The relation due to Menon and Ramanamurthy should be regarded as an upper limit near 9000 m.w.e. and is based on the analysis of

Miyake et al (1962-3) who indicated $I_V < 10^{-11} \text{ cm.}^{-2} \text{ sr.}^{-1} \text{ sec.}^{-1}$ based on one event. It was seen (Section 10.6) that this upper limit should be $1.93 \times 10^{-11} \text{ cm.}^{-2} \text{ sr.}^{-1} \text{ sec.}^{-1}$ for no events and using their assumed angular distribution. Using the angular distribution expected from the OPW spectrum, $I_V < 3 \times 10^{-11} \text{ cm.}^{-2} \text{ sr.}^{-1} \text{ sec.}^{-1}$

It is seen that with this in mind there are no gross disagreements between recent experimental results at depths > 4000 m.w.e. with either the MR or OPW spectra, the greatest discrepancy being the South African result (< 2 standard deviations). It is not clear how the spectrum varies at depths greater than 8000 m.w.e. but should it become steeper (i.e. n increases) then it must be remembered that the South African and Miyake et al intensities will increase, bringing closer agreement between prediction and observation.

At this stage it is useful to consider the variation of n with depth (Figs. 4.9 and 10.4). It will be remembered that the predicted variation was obtained from the OPW spectrum and compared with the observed variation to 4360 m.w.e. In the region of 1500-2000 m.w.e. it was seen that the various experimental observations were

consistently higher than the predicted values and that there was no inconsistency between the various results. Again at 4360 m.w.e. the observed value of n was higher than predicted. It is true that whilst there is statistical agreement between all these observations and the predicted values, it is possible that the observed value of n at a particular depth is really the value at a somewhat greater depth, and better agreement can then be obtained by shifting the "theoretical" curve to shallower depths. If this is really the case, then the values of n used to derive the vertical intensities for the three experiments > 7000 m.w.e. are an underestimate leading to a consequential increase in I_v .

CHAPTER 11.

CONCLUSIONS.

The results of the two experiments underground show that there are definite advantages to be gained by using visual detectors in conjunction with conventional counter telescopes. Not only can the tracks of the underground cosmic ray component be seen, but their angular distribution and interaction probabilities at various depths can be easily determined.

The previous greatest depth at which the angular distribution was measured directly was at 1800 m.w.e. ('standard' rock) by Bollinger, (1951-2), using a counter telescope. His results have been confirmed in the first experiment reported here, and the direct measurement of n has been extended to 4360 m.w.e. ('standard' rock). The experimental values of n have been compared with those expected from an analysis of the intensity-depth relation of Osborne et al. (1964) - the OPW spectrum - assuming a K/π ratio of 20%. It was seen (figure 4.9) that the experimental values of n are consistently higher than expected at depths greater than ~ 1000 m.w.e. (even if the cut-off zenith angle is reduced to 45° then the change in n at 1870 m.w.e. ('standard' rock) is only -0.3, and insufficient to restore agreement.). Further, it was shown that experiments in which 'shower' events are rejected tend to give

Experiment	Depth (m.w.e.) ('standard' rock)	Vertical Intensity (cm ⁻² sr ⁻¹ sec ⁻¹)
M	818	(2.31 ± 0.14)x10 ⁻⁶
P	818	(2.29 ± 0.09)x10 ⁻⁶
C	1315	(5.55 ± 0.07)x10 ⁻⁷
M	1870	(1.84 ± 0.07)x10 ⁻⁷
P	1870	(1.98 ± 0.05)x10 ⁻⁷
M	3625	(1.29 ± 0.13)x10 ⁻⁸
C	3950	(1.00 ± 0.23)x10 ⁻⁸
P	4360	(4.47 ± 0.34)x10 ⁻⁹
M	4600	(3.10 ± 0.33)x10 ⁻⁹
M	6900	(1.92 ± 0.45)x10 ⁻¹⁰
P	7600	(1.26 $\begin{smallmatrix} + 0.86 \\ - 0.54 \end{smallmatrix}$)x10 ⁻¹⁰
S	8500	(7.5 $\begin{smallmatrix} + 8.6 \\ - 7.5 \end{smallmatrix}$)x10 ⁻¹²
M	9200	<3x10 ⁻¹¹

M Miyake et al. (1962-3)

C Castagnoli et al. (1965)

S South African neutrino experiment.

P Present experiments.

Table 11.1 Adopted intensities of recent underground expts.

values of n which are too high. A possible explanation of the discrepancy between the predicted and measured values of n is that the predicted value at a particular depth in fact corresponds to the value at a somewhat shallower depth because of the shape of the intensity-depth relation.

The vertical muon intensities were derived for the three depths of observation and compared with the results of other workers. Corrections were applied to the observations of Miyake et al. (1962-3) and Castagnoli et al. (1965) to allow for the effect of a change in n from the values used by these workers. The results of this were summarized in table 6.2, and displayed in figure 6.5 where a comparison was made with the OPW and Menon and Ramanamurthy (MR) intensity-depth relations. The final adopted intensities are shown in table 11.1. (Also included in this table are the vertical intensities derived from the neutrino experiments described in Chapter 10.). These intensities were compared with the OPW spectrum in figure 6.5.

It was seen that the intensities observed in the present experiment agreed perfectly at 818 m.w.e., and were within statistical errors at 1870 m.w.e. with those observed by Miyake et al. (1962-3), at the same locations, after correcting for n . Again there is statistical agreement between the intensities observed at 4360 and 4600 m.w.e. in

the respective experiments. Comparison with the OPW spectrum shows that there is quite good agreement with the intensities observed in these experiments at 818 m.w.e. and in the region of 4000-5000 m.w.e., but those observed at 1870 m.w.e. are more consistent with the MR spectrum which is ~24% higher than the OPW spectrum at this depth. It was shown (section 6.5) that the MR spectrum is in fact an overestimate since the Bollinger (1951) depths were not corrected for the effect of Z^2/A , and the intensities derived by Menon and Ramana-murthy from Bollinger's angular distribution at location I differ from those derived by Hayman et al. (1963).

Comparison of the intensities observed by Kitamura et al. (1964), showed that there was reasonable agreement with the OPW spectrum at 439, 705 and 812 m.w.e., but those observed at the other depths differed by 25-35%. There is no obvious reason for the discrepancies, but possibilities include an inaccurate range-energy relation and experimental difficulties concerned with keeping the apparatus in a stable position at great depths. In so far as the discussion here refers to measurements made under rock, the results of Kitamura et al. will not be included in the derivation of the best estimate.

Similarly, because of normalization problems, coupled with the possibility of the measurements including

Depth (m.w.e.) ('standard' rock)	Vertical Intensity ($\text{cm}^{-2}\text{sr}^{-1}\text{sec}^{-1}$)
400	1.48×10^{-5}
500	8.38×10^{-6}
600	5.24×10^{-6}
700	3.43×10^{-6}
800	2.40×10^{-6}
900	1.71×10^{-6}
1000	1.29×10^{-6}
1500	3.73×10^{-7}
2000	1.31×10^{-7}
2500	5.88×10^{-8}
3000	2.62×10^{-8}
4000	6.96×10^{-9}
5000	2.01×10^{-9}
6000	5.91×10^{-10}
7000	1.70×10^{-10}
8000	5.00×10^{-11}
9000	1.45×10^{-11}

Table 11.2 The best estimate intensity-depth relation.

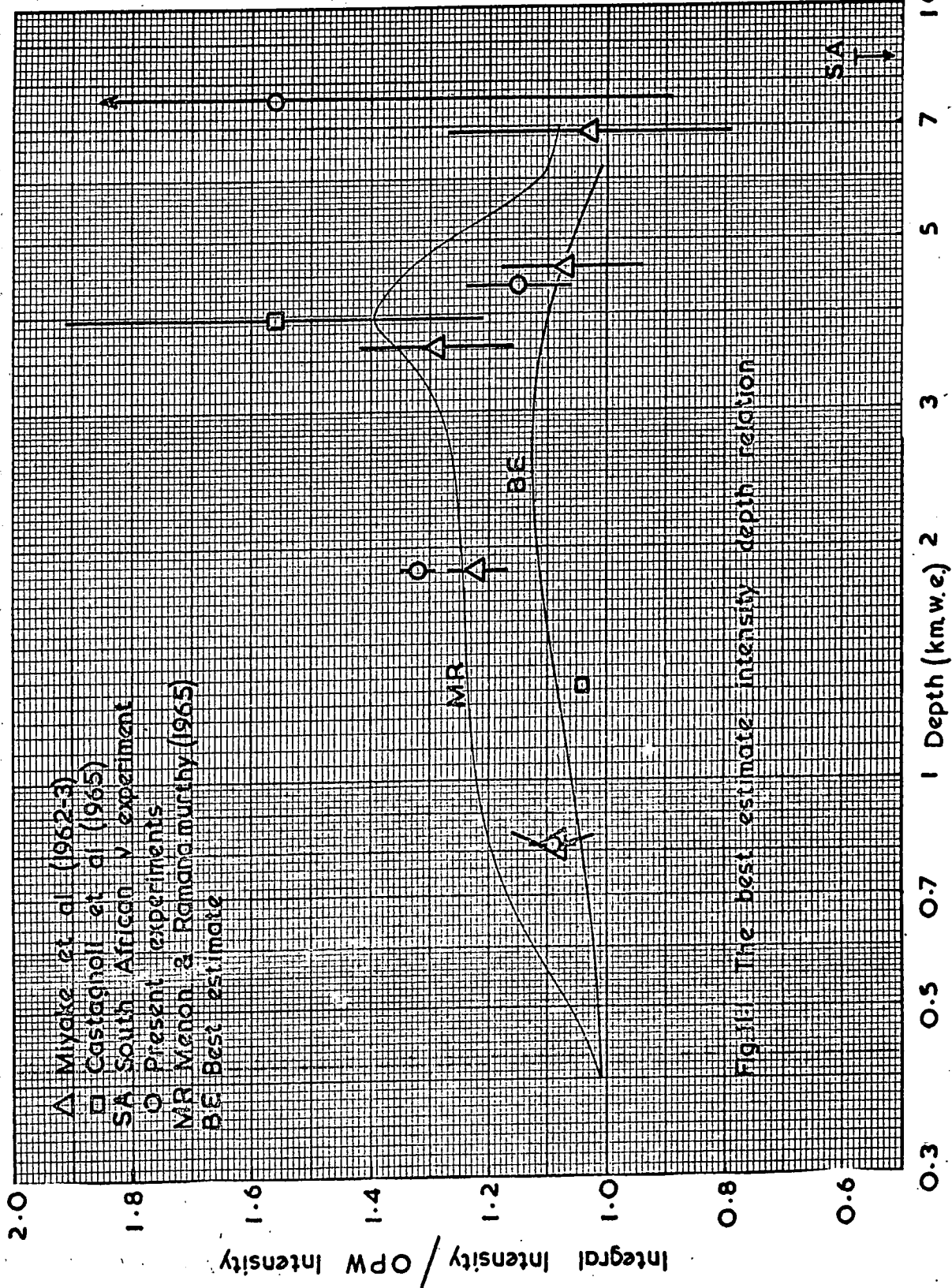


Fig. 11. The best estimate intensity depth relation

side showers etc., the results of Barton et al. (1965) will not be used.

The measurement of Castagnoli et al. (1965) at 1315 m.w.e. has high statistical accuracy, whilst that at 3950 m.w.e. is not as accurate, but nevertheless both will be used since they are absolute measurements.

At the greatest depths (≥ 6900 m.w.e.), the two measurements of Miyake et al. (1962-3) and those from the current neutrino experiments can be utilized. Since there is some doubt as to which values of the exponent of the angular distribution should be used for the latter experiments, the mean intensity at each depth will be adopted (i.e. $(7.5^{+8.6}_{-7.5}) \times 10^{-12} \text{ cm}^{-2} \text{ sr}^{-1} \text{ sec}^{-1}$ for the South African experiment, and $(1.26^{+0.86}_{-0.54}) \times 10^{-10} \text{ cm}^{-2} \text{ sr}^{-1} \text{ sec}^{-1}$ for the K.G.F. experiment.).

The resulting best estimate of the intensity-depth relation given in table 11.2 was derived by adjusting the OPW spectrum, (figure 11.1), allowing suitable weighting for the above experimental observations. Comparison with the OPW and MR relations shows that, in the depth interval 400-7000 m.w.e., the resulting best estimate lies between these two relations. Since no new direct measurements have been made at depths shallower than 400m.w.e., the OPW spectrum will be assumed correct in this region. A plot of $\log I$ vs. D

shows that the best estimate intensity-depth relation is linear over the range 4000-7000 m.w.e. The vertical muon intensities derived from the neutrino experiments at 7600 and 8500 m.w.e., together with the upper limit from the experiment of Miyake et al (1962-3) at 9200 m.w.e. suggest that the linear dependence probably extends to 9000 m.w.e. Further observations of muon intensities at very great depths are clearly necessary.

The results of Barton et al. (1965) were treated in two ways giving the intensities $I_V(1)$ and $I_V(2)$ (table 5.5). At the three depths of observation (724, 1058 and 2225 m.w.e.) the ratios of the best estimate to the OPW spectrum are respectively 1.03, 1.06 and 1.12. Comparing $I_V(1)$ and $I_V(2)$ with the best estimate relation gives the following ratios for the three depths:

for $I_V(1)$: 1.28 ± 0.05 , 0.99 ± 0.03 and 0.94 ± 0.04 , and
 for $I_V(2)$: 1.17 ± 0.05 , 0.91 ± 0.03 and 0.91 ± 0.04 ,
 with a possible reduction to allow for side showers etc.

An empirical relation between the vertical cosmic ray intensity, I , and depth, D (m.w.e.), has been given by Miyake (1963), of the form:

$$I(>D) = \frac{K \exp(-\beta D)}{(D+a)^\alpha (D+H)} \text{ cm}^{-2} \text{ sr}^{-1} \text{ sec}^{-1}$$

where H, K, a, α, β are constants. The intensities derived from the present work are consistent with this relation if $H=400$,

Depth (m.w.e.)	$\beta \times 10^4$
400	7.67
500	7.92
700	8.05
1000	8.08
2000	7.40
3000	7.16
4000	6.94
5000	6.94
6000	7.08
7000	7.30
8000	7.51
9000	7.72

Table 11.3 The variation of β with depth.

Energy (GeV)	Vertical Intensity ($\text{cm}^{-2}\text{sr}^{-1}\text{sec}^{-1}$)
20	2.62×10^{-4}
30	1.29×10^{-4}
50	4.81×10^{-5}
70	2.42×10^{-5}
100	1.19×10^{-5}
150	5.02×10^{-6}
200	2.73×10^{-6}
300	1.08×10^{-6}
500	3.14×10^{-7}
700	1.27×10^{-7}
1000	5.15×10^{-8}
1500	1.78×10^{-8}
2000	8.15×10^{-9}
3000	2.64×10^{-9}
5000	4.97×10^{-10}
7000	1.50×10^{-10}

Table 11.4 The integral energy spectrum of muons in the vertical direction at sea-level.

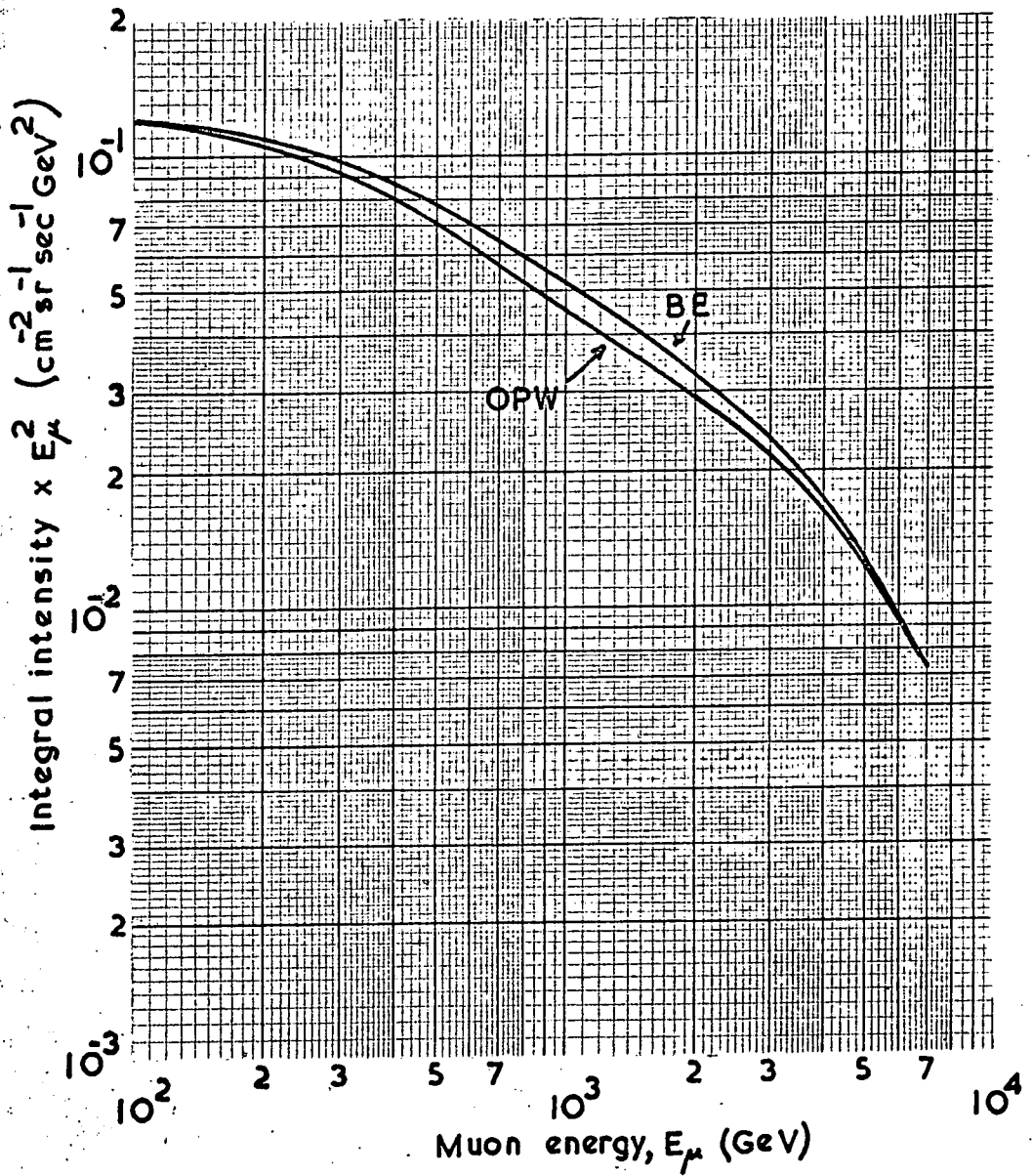


Fig.11.2 The best estimate (BE) & Osborne et al. (OPW) integral energy spectra at sea-level.

$K=160$, $a=10$, $\alpha=1.53$ and if β is taken to be a slowly varying function of depth. (values of β are given in table 11.3).

The sea-level energy spectrum of Osborne et al. (1964) has been corrected to allow for the new best estimate underground spectrum, and the results are given in table 11.4. A plot of this spectrum (figure 11.2, where the intensity has been multiplied by E^2) shows that the 'dip' observed in the OPW spectrum in the energy range 500-2000 GeV is not now as prominent, and in fact has no statistical foundation. As a consequence of the increase in muon intensity, the K/π ratio derived by Osborne and Wolfendale (1964) is an underestimate.

It has been shown by Osborne (private communication) that the ratio of all kaons to all pions giving rise to muons from γ -e cascades is represented by

$$\frac{K^{\pm 0}}{\pi^{\pm 0}} = \frac{2}{3} \cdot \frac{1 - A(E_K/1.47) \cdot F_K}{A(E_\pi/1.16) \cdot F_\pi}$$

where F_K , F_π are the kaon and pion spectra at production, and the functions $A(E_K/1.47)$ and $A(E_\pi/1.16)$ are obtained from the relation: $A = (N_K - N_M) / (N_K - N_\pi)$, where N_K , N_π are the muon spectra at production from all kaons or all pions as parents respectively, and N_M is the observed muon spectrum at production. The energy spectra F_K , F_π , N_K , N_π are shown in table 11.5. Evaluation of the K/π ratio for best estimate energy spectrum shows that Osborne and Wolfendale underestimated the K/π

Energy ($E_{\pi/K}$, GeV)	$N_K E_{\mu}^2$ ($\text{cm}^{-2}\text{sr}^{-1}\text{sec}^{-1}\text{GeV}^2$)	$N_{\pi} E_{\mu}^2$ ($\text{cm}^{-2}\text{sr}^{-1}\text{sec}^{-1}\text{GeV}^2$)	$F_K \pm E_K^3$ ($\text{cm}^{-2}\text{sr}^{-1}\text{sec}^{-1}\text{GeV}^3$)	$F_{\pi} \pm E_{\pi}^3$ ($\text{cm}^{-2}\text{sr}^{-1}\text{sec}^{-1}\text{GeV}^3$)
300	1.93×10^{-3}	6.36×10^{-4}	2.45	0.575
400	1.47×10^{-3}	4.22×10^{-4}	2.92	0.637
500	1.18×10^{-3}	3.04×10^{-4}	3.32	0.69
700	8.34×10^{-4}	1.81×10^{-4}	4.00	0.77
1000	5.64×10^{-4}	1.01×10^{-4}	4.83	0.86
1500	3.42×10^{-4}	5.08×10^{-5}	5.95	0.945
2000	2.33×10^{-4}	3.03×10^{-5}	6.75	1.02
3000	1.31×10^{-4}	1.39×10^{-5}	7.96	1.06
5000	5.87×10^{-5}	2.80×10^{-5}	9.32	1.01

Table 11.5 The energy spectra N_K , N_{π} , F_K and F_{π} .

Primary energy (TeV)	$(K/\pi)_{\text{all}}$ %
20	35.5±15
30	31 ± 14
50	26 ± 12
70	23.8±12
100	25 ± 12
200	32 ± 12
300	37 ± 14
500	42 ± 18
600	44 ± 25

Table 11.6 The K/π ratio as a function of primary energy.

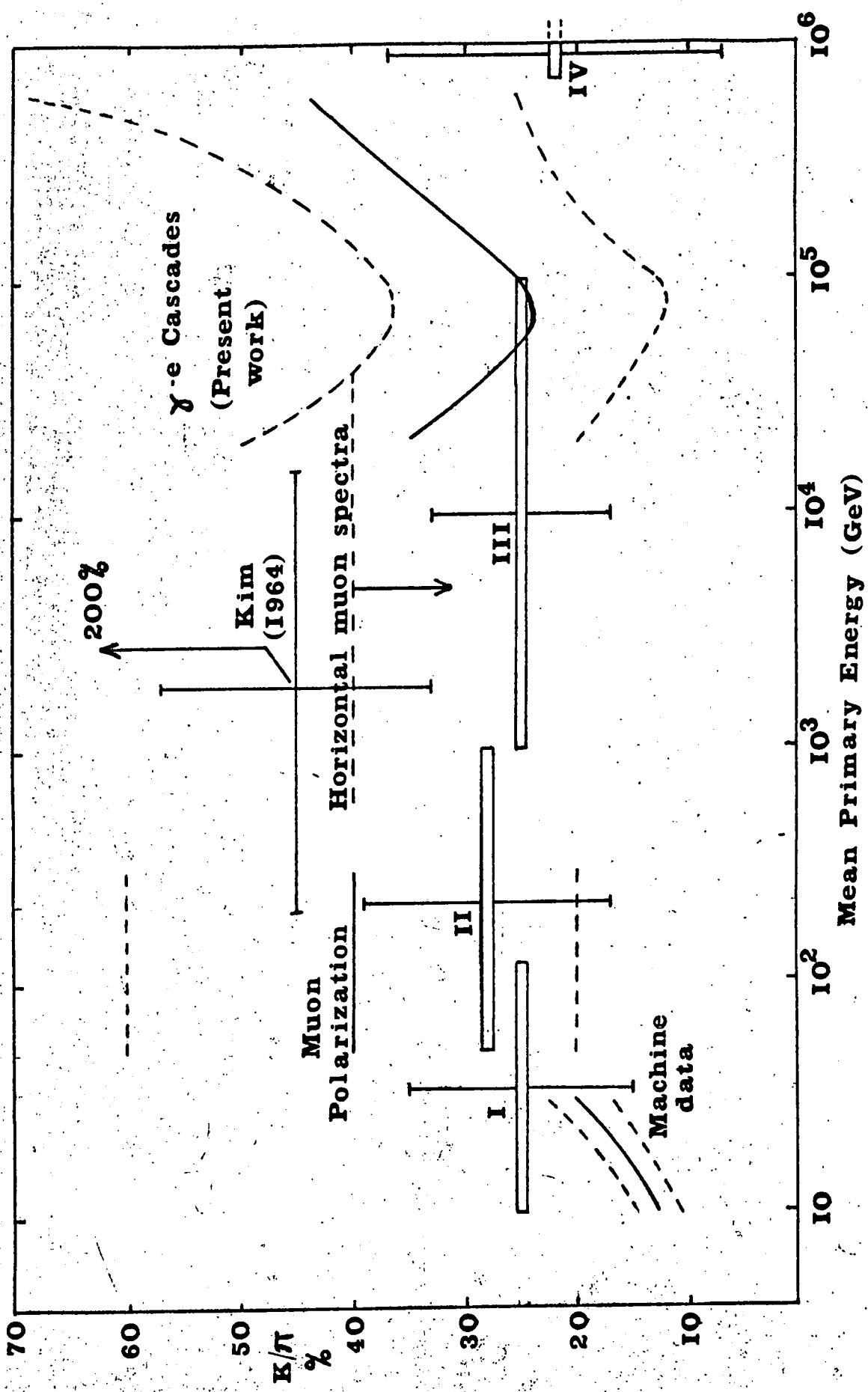


Fig. II.3 The variation of the K/π ratio with mean primary energy.

ratio by 10-15%. The resulting best estimate of the K/π ratio is shown in table 11.6 as a function of primary energy. These results are compared with those of other workers summarized by Osborne and Wolfendale (1964) in figure 11.3, where the points I-IV are from the review by Perkins (1961). The upper limit of the K/π ratio from inclined muon spectra was 10% when the results of Osborne and Wolfendale were published, but Ashton et al. (1965, pre-print, Proc. Phys. Soc.) have given a new upper limit of 40%. It is seen in figure 11.3 that there is no marked inconsistency between the various determinations in the energy range studied in the present work, $2 \times 10^4 - 6 \times 10^5$ GeV. At low energies (10-200) GeV, there is rough consistency between the various determinations, but large discrepancies appear in the range 200- 2×10^4 , where Kim (1964, pre-print, University of Chicago) gives a very high ratio. The results shown in figure 11.3 indicate that the K/π ratio is constant at about 30% over the primary energy range $10^2 - 10^6$ GeV.

The distributions in arrival times were studied at 1870 and 4360 m.w.e. ('standard' rock), but no significant non-Poissonian contribution was observed, indicating that the phenomenon of bursts of particles at small time intervals reported by Cowan et al. (1964) has not been detected at these depths.

Electromagnetic interactions of muons in lead and rock were observed, and it was found that the probability of a muon producing a secondary electron or electron shower increases with depth (and therefore energy), thus demonstrating the growing importance of energy losses by bremsstrahlung and direct pair-production. The result of extrapolating the observations to 7600 m.w.e. shows that the probability of observing a secondary associated with a muon of atmospheric origin should be in the range 30-50%. This high value finds support from the experimental results at 7600 m.w.e., in which it was found that out of 8 atmospheric muons (including the three 'out of geometry' events), 6 had secondaries in association. This value is even higher than expected, probably because of various bias effects.

The occurrence of more than one particle passing simultaneously through the apparatus was also observed at each depth. It was shown that such events can be explained by the production of more than one muon (via intermediate pion decay) by the same primary nucleon initiating extensive air showers in the atmosphere, and by the local nuclear interactions of muons in the surrounding rock. The agreement with the results of other workers was quite good.

Turning to neutrino observations, five or six neutrino induced events have been detected at 7600 m.w.e. ('standard' rock) together with five 'in geometry' atmospher-

eric muons in 262.5 telescope days. One of the neutrino events observed comprised two particles penetrating the apparatus diverging from a point below the horizontal. Due to inaccuracies in track location, it was not possible to determine whether the event was due to the production of a muon plus an intermediate boson which decays promptly to give a muon, or to a simple inelastic neutrino interaction in which a muon and a pion were produced. The experiment is still in operation, and the apparatus will soon be increased by a further three telescopes each 2m^2 in area. In addition, two more arrays of neon flash tubes will be included in these telescopes, in order that the azimuth angle may be determined, together with an increased thickness of absorber. This will comprise 2.5 interaction lengths of iron to reduce doubts as to the nature of particles produced in neutrino interactions. It is hoped that more double particle events at large zenith angles and events similar to the 13th. event (table 10.3) will soon be detected.

It is clear that, until particle accelerators are built having much higher energies available than exist at the present time, cosmic ray experiments underground will continue to play an extremely important role in the field of fundamental research.

APPENDIX I.

GEOLOGICAL DESCRIPTION OF THE GOLD MINES AND CHEMICAL COMPOSITION AND DENSITIES OF VARIOUS ROCK SAMPLES.

The Kolar Gold Fields in which the present experiment has been performed are situated in latitude $12^{\circ}57'N$, longitude $78^{\circ}18'E$ in Mysore State, Southern India at a distance of about 90 km from Bangalore.

Geological Description.

The geology of the gold mines has been described by T. Pryor in the following terms:

"The mines occur towards the southern end of a narrow strip of pre-Cambrian hornblende schist which is surrounded by the complex of gneissic and granitic rocks which covers the greater part of Southern India. The Kolar schist belt is composed of metamorphosed igneous rocks, probably originally mainly basalts and dolerites, which on their western edge, are bounded by a discontinuous band of ferruginous quartzite, and on the eastern edge a crust conglomerate is locally developed. Numerous dykes of much later age (though, still pre-Cambrian), traverse all the other rocks of the district. These dykes run in two directions roughly at right angles to each other, viz. north and south, and east and west".

Chemical Composition.

Most (>90%) of the rock encountered in the mines consists of hornblende schists with pegmatites and quartz making up the rest. The average chemical composition of the rock samples of each category has been determined by the Analytical Division of the Atomic Energy Establishment, Trombay, and is given in the table below:

Chemical Composition of Rocks at K.G.F.

Type of rock sample	Hornblende Schist %	Pegmatite %	Quartz %
SiO ₂	49.24	29.56	70.18
Al ₂ O ₃	13.50	19.51	11.43
Total Iron as Fe ₂ O ₃	13.70	12.59	6.03
MnO	0.19	0.11	0.11
TiO ₂	0.70	0.52	0.13
CaO	11.41	17.58	4.44
MgO	9.10	8.30	1.43
Alkalies as Na ₂ O + K ₂ O	2.13	2.44	4.47
Loss on ignition	0.56	9.04	1.46

Densities of Rock Samples.

The densities of rock samples from various depths are given in the table on next page. Hornblende schist being the most abundant rock (believed to be certainly $> 90\%$ and probably $\sim 98\%$ by volume), the average density, viz. 3.02 gm.cm^{-3} of only this type of rock has been considered in estimating the depths in the present work. The admixture of other types of rocks ($< 10\%$) whose densities are all $> 2.6 \text{ gm.cm}^{-3}$ may lead to a correction to depths expressed in units of m.w.e. by -2% .

---o0o---

Densities of Rocks at K.G.F.

Sample No.	Level	Density gm.cm ⁻³	Rock Specimen	
1	4	2.98	H.S.	
2	10	3.00	H.S.	
3	20	3.01	H.S.	
4	20	2.97	Q	
5	28	2.98	H.S.	
6	28	3.08	Q	
7	34	2.99	H.S.	
8	42	3.04	H.S.	
9	47	3.16	H.S.	
10	52	3.07	H.S.	H.S. = Hornblende Schist
11	57	3.07	H.S.	Q = Quartz
12	58	2.65	P	P = Pegmatite
13	58	2.70	P	Approximate } = level No.x depth from } 100 ft. surface }
14	58	2.66	P	
15	62	3.06	H.S.	
16	62	2.67	Q	
17	67	3.00	H.S.	
18	73	2.98	H.S.	
19	79	3.28	H.S.	
20	79	2.65	P	
21	79	2.60	P	
22	82	3.07	H.S.	
23	88	2.64	P	
24	88	2.62	P	
25	88	3.00	H.S.	

ACKNOWLEDGEMENTS.

Professor G.D. Rochester, F.R.S., is thanked for his interest and encouragement at all stages of the work.

The author is immensely grateful to his supervisor, Professor A.W. Wolfendale, for his continuous advice and guidance over the past two years and to his 'local' supervisors in India, Professor B.V. Sreekantan, Dr. P.V. Ramanamurthy and Professor K. Hinotani for their guidance and useful discussions.

The present work would not have been possible without the invaluable collaboration of the experimental teams in the two experiments (Dr. P.V. Ramanamurthy, Mr. V.S. Narasimhan and Mr. C.V. Achar of the Tata Institute and Mr. D.R. Creed (Durham) in Phase I of the experiments and these together with Professor K. Hinotani of Osaka City University in Phase II) and the numerous technicians and scanners (in particular Messrs M.S. Borkar and A.M. Vinze of the Tata Institute and Miss C. Gyll, Miss F. Coates, Messrs E.W. Lincoln, W. Leslie, R. Stark, P.J. Finley and J. Hooke of Durham). Mr. J.L. Osborne is thanked for many useful discussions.

It is a pleasure to acknowledge the facilities afforded to the team by the Managing Director of the

Kolar Gold Mining Undertakings, Mr. M.H. Parthasarathy, I.A.S., to Mr. A. Cave, M.B.E., and Mr. V.V.R. Rao, successive superintendents of the Champion Reef Mine, Mr. E. Krishnaswamy, Assistant Superintendent, Mr. P.L. Bhasin, Chief Surveyor, Mr. B.R. Garuda Char, Chief Electrical Engineer, and Mr. B. Srinivasan, Assistant Electrical Engineer and many other officers and men of the Undertakings, who all so willingly gave assistance, at various stages of the work, and helped to make the stay in Kolar Gold Field a memorable and happy one.

Mr. C.E. Jacobs of Bharat Earth Movers Ltd., Kolar Gold Fields, is thanked for his painstaking and accurate typing of this thesis.

Finally, the Tata Institute of Fundamental Research, Bombay, is thanked for inviting the author as a Visiting Member at the Institute during the past two years, and the Higher Degrees Committee of the University of Durham is thanked by the author for allowing him to accept this invitation.

-----oOo-----

REFERENCES.

- Achar, C.V., Narasimhan, V.S., Ramanamurthy, P.V., Creed, D.R., Pattison, J.B.M., & Wolfendale, A.W., Proceedings of the 9th International Conference on Cosmic Rays, London, 1965. (In the Press).
- Achar, C.V., ^{Menon, M.G.K.,} Narasimhan, V.S., Ramanamurthy, P.V., ^{Sreekantan, B.V.,} Hinotani, K., Miyake, S., Creed, D.R., Osborne, J.L., Pattison, J.B.M., & Wolfendale, A.W., Proceedings 9th. Int. Conf. on Cosmic Rays, London, 1965a. (In the Press).
- Physics Letters, 18, 196, 1965c.
Physics Letters, 19, 78, 1965 b.
- Ashton, F., Proc. Phys. Soc., 77, 587, 1961.
- Avan, L., & Avan, M., C.R. Acad. Sci., Paris, 241, 1122, 1955.
- Baradzei, L.T., Rubtsov, V.I., Smorodin, Y.A., Solov'ev, M.V., Tolkachev, B.V., Trud. Fiz. P.N. Lebedev Inst. Acad. Nauk., Moscow, 26, 224, 1964.
- Barnóthy, J. & Forró, M., Z. Physik, 104, 744, 1937.
Phys. Rev. 55, 870, 1939.
Phys. Rev. 58, 844, 1940.
Phys. Rev. 74, 1300, 1948.
- Barrett, P.H., Bollinger, L.M., Cocconi, G., Eisenburg, Y., & Greisen, K., Rev. Mod. Phys. 24, 133, 1952.
- Barton, J.C., Phys. Rev. Letters, 5, 514, 1960.
- Barton, J.C., Phil. Mag., 6, 1271, 1961.
- Barton, J.C. & Michaelis, E.G., Proc. Phys. Soc., 77, 377, 1961.
- Barton, J.C. & Stockel, C.T., Proc. 9th Int. Conf. on Cosmic Rays, London, 1965. (In the Press).
- Bhabha, H.J., Proc. Roy. Soc., A152, 559, 1935.
Proc. Camb. Phil. Soc., 31, 394, 1935.
- Bloch, M.M. et al., Phys. Letters, 12, 281, 1964.
- Bollinger, L.M., Phys. Rev., 79, 207, 1950.
Ph.D. Thesis, Cornell University, 1951.

- Brooke, G., Hayman, P.J., Kamiya, Y., & Wolfendale, A.W.,
Proc. Phys. Soc., 83, 853, 1964.
- Castagnoli, C., De Marco, A., Longhetto, A. & Penengo, P.,
Nuovo Cimento, 33, 722, 1964.
Nuclear Physics, 63, 1, 79, 1964.
Nuovo Cimento, 35, 969, 1965.
- Chaudhuri, N. & Sinha, M.S., Proc. 8th. Int. Conf. on
Cosmic Rays, Jaipur, 6, 106, 1963.
- Clark, G.W., Scherb, F. & Smith, W., Rev. Sci. Inst.,
28, 433, 1957.
- Cowan, C.L., Ryan, D.F. & Szydluk, P.P., Catholic University
of America, Washington, D.C., 1964.
- Coxell, H., Ph.D. Thesis, Durham University, 1961.
- Danby, G., Gaillard, J.M., Goulianos, K., Lederman, L.M.,
Mistry, N., Schartz, M. & Steinberger, J., Phys. Rev.
Letters, 9, 36, 1962.
- Dmitriev, V.A. & Khristiansen, G.B., Soviet Physics,
J.E.T.P., 17, 276, 1963.
- Duthie, J., Fowler, P.H., Kaddoura, A., Perkins, D.H.,
& Pinkau, K., Nuovo Cimento, 24, 122, 1962.
- Fermi, E., Phys. Rev., 56, 1242, 1939, & 57, 485, 1940.
- Fowler, G.N. & Wolfendale, A.W., Prog. Cos. Ray Phys.,
Vol. IV, 1958.
- von Gehlen, G., Nuovo Cimento, 30, 859, 1963.
- George, E.P., Prog. Cos. Ray Phys., Vol. I, 1952.
- George, E.P. & Evans, J., Proc. Phys. Soc., A63, 1248, 1950.
- Halpern, O. & Hall, H., Phys. Rev., 57, 459, 1940, &
73, 477, 1948.
HASEGAWA, H. et al., Proc. 8th. Int. Conf. on Cos. Rays, Jaipur, Vol. 4, 248, 1963.
- Hayakawa, S. & Tomonago, S., Prog. Theor. Phys.,
4, 496, 1949.
- Hayman, P.J., Palmer, N.S. & Wolfendale, A.W.,
Proc. Phys. Soc., 80, 800, 1962.
Proc. Roy. Soc., A275, 391, 1963.
- Hayman, P.J. & Wolfendale, A.W., Proc. Phys. Soc.,
80, 710, 1962.

- Higashi, S., Kitamura, T., Mishima, Y., Mitani, S., Miyamoto, S., Oshio, T., Shibata, H., Watanabe, K., & Watase, Y., Proc. Int. Conf. Cos. Rays & Earth Storm, Kyoto, J. Phys. Soc. Japan, (Suppl. A III), 17, 362, 1962.
- Higashi, S., Kitamura, T., Mishima, Y., Miyamoto, S., Oshio, T., Shibata, H. & Watase, Y., Proc. Int. Conf. Cos. Rays & Earth Storm, Kyoto, J. Phys. Soc. Japan, (Suppl. A.III), 17, 209, 1962A.
- Higashi, S., Oshio, T., Shibata, H., Watanabe, K. & Watase, Y., Nuovo Cimento, 5, 597, 1957.
- Higashi, S., Mitani, S., Oshio, T., Shibata, H., Watanabe, K. & Watase, Y., Proc. Moscow Cos. Ray Conf., II, 17, 1960.
- Higashi, S., Kitamura, T., Watase, Y., Oda, M. & Tanaka, Y., Nuovo Cimento, 32, 1, 1964.
- Kessler, D. & Maze, R., Nuovo Cimento, 5, 1, 1957.
KIM, CO., PRE-PRINT, UNIV. OF CHICAGO, 1964. (PHYS. REV., 136, 2B, 515, 1964.)
- Kitamura et al., Private Communication, 1964.
- Lovati, A., Mura, A., Succi, C. & Tagliaferri, G., Nuovo Cimento, 12, 526, 1954.
- Mando, M. & Ronchi, L., Nuovo Cimento, 9, 517, 1952.
- Menon, M.G.K. & Ramanamurthy, P.V., Prog. Cos. Ray & Elem. Particle Physics, Vol. IX, (In the Press).
- Menon, M.G.K., Ramanamurthy, P.V., Sreekantan, B.V. & Miyake, S., Physics Letters, 5, 272, 1963.
 Nuovo Cimento, 30, 1208, 1963.
MIYAKE, S., J. PHYS. SOC. JAPAN, 18, 1093, 1963.
- Miyake, S., Narasimhan, V.S., & Ramanamurthy, P.V., Proc. Int. Conf. Cos. Rays & Earth Storm, Kyoto, J. Phys. Soc., Japan, (Suppl. A III), 17, 318, 1962.
 Proc. 8th. Int. Conf. on Cos. Rays, Jaipur, Vol.6, 249/250, 1963.
- Osborne, J.L., Palmer, N.S., & Wolfendale, A.W., Proc. Phys. Soc., 84, 911, 1964.
- Osborne, J.L. & Wolfendale, A.W., Proc. Phys. Soc., 84, 901, 1964.
- Ozaki, S., Proc. Int. Conf. on Cos. Rays & Earth Storm, Kyoto, J. Phys. Soc., Japan, (Suppl. A III) 17, 330, 1962.
- Pattison, J.B.M., M.Sc. Thesis, Durham University, 1963.

- Perkins, D.H., CERN Conf. on Very High Energy Phenomena, Geneva, 99, 1961.
- Pine, J., Davisson, R.J. & Greisen, K., Nuovo Cimento, 14, 1181, 1959.
- Pinkau, K., Fort. der Phys., 12, 139, 1964.
- Racah, G., Nuovo Cimento, 14, 93, 1937.
- Ramanamurthy, P.V., Ph.D. Thesis, Bombay University, 1962.
Proc. 8th. Int. Conf. on Cos. Rays, Jaipur, Vol. 6, 22, 1963.
- Randall, C.A. & Hazen, W.E., Phys. Rev., 81, 144, 1951.
Nuovo Cimento, 8, 878, 1958.
- Regener, V.H., Phys. Rev., 84, 161, 1951.
- Rodgers, A.L., Proc. Phys. Soc., 78, 918, 1961.
- Rossi, B., High Energy Particles (Prentice Hall, New York), 1952.
- Rozental, I.L. & Streltsov, V.N., Soviet Physics, J.E.T.P., 8, 1007, 1959.
- Sitte, K., Handbuch der Physik, 46/1, 157, 1961.
- Sreekantan, B.V. & Naranan, S., Proc. Ind. Acad. Sci., 36, 97, 1952.
- Sreekantan, B.V., Naranan, S. & Ramanamurthy, P.V., Proc. Ind. Acad. Sci., 43, 113, 1956.
- Sternheimer, R.M., Phys. Rev., 88, 851, 1952, & 115, 137, 1959.
- Vernov, S.N., Khva, L.D., Khrenov, B.A. & Khristiansen, G.B., Proc. Moscow Cos. Ray Conf., II, 1960.
Proc. Int. Conf. Cos. Rays & Earth Storm, Kyoto, J. Phys. Soc., Japan, (Suppl. A III), 17, 213, 1962.
- V. Weiszacker, C.F., Z. Phys. 88, 612, 1934.
- Williams, E.J., Mat. Fys. Medd. Dan. Vid. Selak, 13, 4, 1935.
- Wu, A., Yang, C.P., Fuchel, K. & Heller, S., Phys. Rev. Letters, 12, 57, 1964.
- Zagrebin, V.A. & Zheleznykh, I.M., Preprint, P.N. Lebedev Institute, Moscow, 1964.

